VORTICAL STRUCTURES IN TURBOMACHINERY TIP CLEARANCE FLOWS

by

Gwo-Tung Chen

B.S., National Taiwan University (1982)
S.M., Massachusetts Institute of Technology (1987)

Submitted to the Department of Aeronautics and Astronautics
in partial fulfillment of the requirements for the degree of

Doctor of Philosophy

at the

MASSACHUSETTS INSTITUTE OF TECHNOLOGY

February 1991

Signature of Author .....
Department of Aeronautics and Astronautics
February, 1991

Certified by .....
Dr. Edward M. Greitzer
Thesis Supervisor, Director of Gas Turbine Laboratory
Professor of Aeronautics and Astronautics

Certified by .....
Dr. Choon S. Tan
Principal Research Engineer of Aeronautics and Astronautics

Certified by .....
Dr. Michael B. Giles
Associate Professor of Aeronautics and Astronautics

Accepted by .....
Professor Harold Y. Wachman
Chairman, Department Graduate Committee

VORTICAL STRUCTURES IN TURBOMACHINERY TIP CLEARANCE FLOWS

by

GWO-TUNG CHEN

Submitted to the Department of Aeronautics and Astronautics in February, 1991 in partial fulfillment of the requirements for the Degree of Doctor of Philosophy

Abstract

A new approach is presented for analyzing compressor tip clearance flow. The basic idea is that the clearance velocity field can be (approximately) decomposed into independent through-flow and cross-flow, since chordwise pressure gradients are much smaller than normal pressure gradients in the clearance region. As in the slender body approximation in external aerodynamics, this description implies that the three-dimensional, steady, clearance flow can be view as a two-dimensional, unsteady flow. Using this approach, a similarity scaling for the cross-flow in the clearance region is developed and a generalized description of the clearance vortex is derived. Calculations based on the similarity scaling agree well with a wide range of experimental data in regard to flow features such as cross-flow velocity field, static pressure field, and tip clearance vortex trajectory. The scaling rules also provide a useful way of exploring the parametric dependence of the vortex trajectory and strength for a given blade row. The emphasis of the approach is on the vortical structures associated with the tip clearance because this appears to be a dominant feature of the endwall flow; it is also shown that this emphasis gives considerable physical insight into overall features seen in the data.

Based on the flow model, analytical expressions are derived for the decrease in overall performance (efficiency, pressure rise, and torque) of a compressor due to clearance. Similar expressions are also derived for a turbine. Calculations carried out agree well with compressor and turbine data covering a broad range of flow coefficients, stage loadings, and clearances.

Thesis Supervisor:	Dr. Edward M. Greitzer
Title:	Professor of Aeronautics and Astronautics and Director of Gas Turbine Laboratory

Acknowledgements

To Prof. E.M. Greitzer, for his continual support, guidance, and many excellent suggestions during this research. I have learned a lot from him during my stay at MIT. However, his incredible ability to digest and process data at the *speed of light* is still a mystery to me.

To Dr. C.S. Tan, for his continuous advice, help, and support throughout this work.

To Prof. M.B. Giles, for his helpful comments on the modelling and many valuable discussions.

To Prof. F.E. Marble, for his idea on the modelling and many insightful questions.

To my wife, May, for her understanding, patience and emotional support, without which successful completion of this thesis work would not have been possible.

To my parents and sisters, for their encouragement, support, and love throughout my life.

I would also like to thank Prof. A.H. Epstein, Prof. Martinez-Sanchez, and Prof. Landahl, for their helpful advice and comments. In addition, the suggestions and comments of Mr. A.J. Crook and Dr. N.K.W. Lee were very helpful. I must also thank Prof. N.A. Cumpsty for his constructive critical comments and Dr. S. Tarares and Mr. Y. Qui for useful discussions concerning the vortex method computations. I would also like to thank Mr. W.C. Au for his help running my panel method code on the Cray. The assistance of Mrs. H.E. Rathbun and Mr. R. Haimes during my stay at MIT are greatly appreciated. Finally, primary support for this work is from the NASA Lewis Research Center under Grant NSG-3208, Mr. F.A. Newman, Program Monitor. Partial support

has also been furnished by the General Electric Aircraft Engine Business Group. Both these sources are gratefully acknowledged.

Contents

List of Figures

List of Tables

Nomenclature

a = speed of sound

b = span

b_{eff} = effective span, see Eq. (5.19)

b_{un} = $b - b_{eff}$

c = chord

C_p = specific heat or pressure coefficient

C_p^* = pressure coefficient across blade row, see Eq. (G.9)

C_x = axial velocity

erf = error function

E = kinetic energy of clearance flow per blade

F = complex velocity potential

F_b = force on a blade (per unit chord)

g = pitch

G = blade loading parameter; unity for linear loading distribution, see Chapter 5

h = blade thickness

h_t = total enthalpy

H = passage height, b+ τ

J = parameter defined in Eq. (4.14)

k = blade unloading parameter; see Eq. (5.23)

K = function defined in Eq. (4.13)

L = shaft power

$\dot{m}_c$ = leakage flow rate per blade

$\dot{m}$ = through flow

$\dot{M}_c$ = total leakage flow rate

M_1 = inlet relative Mach number

M_c = cross flow Mach number

NB = number of blades

p = static pressure

p_t = total pressure

Q = complex velocity

r = radius

r_c = casing radius

r_h = hub radius

r_m = mean radius

r_t = tip radius

R = radius of blade curvature

Re = Reynolds number

s = distance along camber line or streamwise distance

t = time

t^* = similarity parameter; see Eq. (2.7)

T_{t1} = inlet total temperature

$\overline{u}$ = average streamwise velocity

u' = streamwise velocity perturbation; see Eq. (2.1)

U_0 = upstream velocity in a cross-flow plane

U_t = tip wheel speed

U_m = mid-span wheel speed

v, w = cross-plane velocities in y, z directions

v_c = average tangential velocity of clearance flow

v_w = tangential velocity due to the relative endwall motion

V = velocity of " observer frame"

V_1 = inlet relative velocity

W = turbine work coefficient

x = axial coordinate

y = tangential or cross-flow coordinates

y_c, z_c = coordinates of tip vortex core

y_c^*, z_c^* = non-dimensional coordinates of tip vortex core, $y_c/\tau, z_c/\tau$

y_v, z_v = coordinates of vorticity centroid

y_v^*, z_v^* = non-dimensional coordinates vorticity centroid, $y_v/\tau, z_v/\tau$

Y = abscissa on transformed plane, see Eq. (2.22)

z = spanwise coordinate

z_b = coordinate of centroid of bound vorticity

z_s = $H - z_v$

Z = ordinate on transformed plane

α_1 = absolute inlet flow angle

β = parameter defined in Eq. (2.17)

β_1 = relative inlet flow angle

β_2 = relative exit flow angle

β_m = vector mean flow angle

γ = stagger angle, or specific heat ratio, or vortex sheet strength

Γ = circulation

Γ^* = non-dimensional circulation, see Eq. (2.10)

Γ_b = circulation of bound vortex sheet (blade)

Γ_s = circulation of shed vortex sheet (tip clearance vortex)

δ = boundary layer thickness

δ^* = displacement thickness of a boundary layer

ΔC_p = pressure coefficient ; $\Delta C_p = \Delta p/(\rho V_1^2/2)$

$\overline{\Delta C_p}$ = average pressure coefficient ; $\overline{\Delta C_p} = \overline{\Delta p}/(\rho V_1^2/2)$

ΔE = change in kinetic energy of clearance flow

Δp = pressure difference across blade

$\overline{\Delta p}$ = average pressure difference across blade

Δp_t = total pressure rise of a rotor

ϵ = coordinate along vortex sheet

ε = thickness of shed vortex sheet

η_c = compressor efficiency

η_t = turbine efficiency

θ = camber angle

λ = shaft power coefficient , $L/[\frac{1}{2}\pi(r_c^2 - r_h^2)\rho U_t^3]$

Λ_η = efficiency slope parameter, see Eq. (5.45)

Λ_ψ = loading slope parameter, see Eq. (5.46)

ν = viscosity

ξ = contraction factor, $\xi = \pi/(\pi + 2)$

Ξ = transformed plane

π_t = turbine exit total to inlet total pressure ratio

π_s = compressor stage total pressure ratio

ρ = density

σ = ϕ_2/ϕ_1

τ = clearance

ϕ = flow coefficient, C_x/U_t

ϕ_1 = inlet flow coefficient

ϕ_2 = exit flow coefficient

ϕ_{cr} = critical flow coefficient

Φ = physical plane

φ = velocity potential

ψ = compressor loading coeff. , $\Delta p_t/(\frac{1}{2}\rho U_t^2)$

Ψ = stream function

ω = vorticity

Ω = angular velocity

Subscripts

mean = value at mean radius

p = blade pressure surface

s = blade suction surface

Superscripts

* = non-dimensional characteristic parameter

0 = tip value

Chapter 1

Introduction

1.1 Introduction

There is little need to give a detailed background on the motivation for studying flow in turbomachinery endwall regions. It is well known that: 1) knowledge of the fluid mechanics of the endwall region is critical in developing accurate performance prediction methods (see Koch and Smith, 1976, [27]; Ludwing, 1978, [36]; Wisler, 1985, [60]; Senoo and Ishida, 1986, [48]; Cumpsty, 1989, [10] [1]), and 2) in spite of over forty years of research on the topic, the flow in this region is not very well understood. An additional point is that, in much of the work that has been done, the problem has been cast into one or another simplified models in which essential physical features were suppressed, an example being the attacks on the problem from the standpoint of pitch averaged boundary layer type equation (e.g., Balsa and Mellor, 1975, [3], De Ruyck and Hirsch, 1980, [12]). Approaches of this sort avoided dealing with the complex endwall flow structure by averaging, and thus aiming for a more global description, but there has been little success in developing general predictive procedures along such lines. The approach taken here is inherently different in that three-dimensionality, and the role of the vortical structure associated with the tip clearance flow, are emphasized from the outset.

[1] This reference also gives discussion of previous work on the topic.

There have been many studies of compressor tip clearance flows, but the analysis carried out appear to fall into three main categories. The first is what might be termed leakage models. In these, the clearance flow is regarded as a jet driven by the pressure difference across a blade tip, with the kinetic energy of the jet subsequently lost through mixing (Rains, 1954, [43]; Moore and Tilton, 1988, [39]). Description on this level can give a useful measure of efficiency decrease due to tip clearance flow, but it provides no information on the structure of the passage flow field.

A second main approach makes use of lifting line analysis (Lakshminarayana and Horlock, 1965, [30]; Lakshminarayana, 1970, [29]) to compute the secondary velocity flow field as well as a loss in efficiency stemming from the induced drag of the trailing vortex system. A major drawback, however, is that empirical relations are needed (tip vortex circulation and core size) to close the problem, and these are not universal.

The third category, which has appeared relatively recently, is numerical computation of three-dimensional flow in a blade passage using the Reynolds-averaged Navier-Stokes equations (Pouagare and Delaney, 1986, [42]; Hah, 1986, [19]; Dawes, 1987, [11]; Adamczyk et al, 1989, [2]; Crook, 1989, [9]; Adamczyk et al., 1990, [1]; Storer and Cumpsty, 1990, [53]). The present approach is different from all of the above, but it can be regarded as a strongly complementary adjunct to the computational procedures. In particular, a primary goal is to provide physical insights into the general parameters of interest. In developing the approach, we have focussed on the structure of the vorticity field in the blade passage. Doing this enables one to obtain a useful "skeleton" to aid in inferring the behavior of a complex three-dimensional flow field (Perry and Tan, 1980 [41]). Although, as will be described, the focus on vorticity can lead to a rapid and simple approximate computational procedure, we emphasize that it is the above-mentioned point, the possibility for enhancing physical insight, that is the main factor in our adoption of this approach.

1.2 Literature Review and Discussions on Clearance Flow Models

1.2.1 Background

Tip clearance flows can have a adverse effect on turbomachine performance and account for a large fraction of endwall loss. Stall margin, efficiency, and pressure rise decrease with increasing clearance as illustrated in Figure 1.1 (Ludwing, 1978, [36]; Wisler, 1985, [60]). In general, for one percent increase in clearance-to-span ratio, there is a one to two percent decrease in the efficiency, two to four percent decrease in the pressure rise, and three to six percent decrease in the stall margin.

There have been many experimental studies on clearance flow. However, the focus has often been on the loss associated with the clearance flow, with little detailed data available about the flow itself, so that many fluid mechanic features of the clearance flow are still not clear.

As stated, there has been an abundance of analytical work on turbomachinery tip clearance flows, falling into three main categories, which will be discussed in the following sections.

1.2.2 Leakage Flow Approach

Rains (1954, [43]) presented one of the earliest studies of clearance flow. In his analysis, the clearance flow is decomposed into a through flow and a two dimensional jet in a direction normal to the through flow as shown in Figure 1.2. This decomposition is justified by the fact that pressure gradients across the blade are much larger than those along the blade. As a result, when the leakage flow is transported through the clearance, the velocity along the blade is not appreciably altered compared to the change of velocity normal to the blades.

To estimate the loss in efficiency due to the clearance flow, Rains (1954, [43]) as-

sumed that the flux of kinetic energy associated with the flow normal to the blade was dissipated without recovery, and this assumption has since been used by many other investigators. A simple model was also developed by Rains to account for losses associated with scraping vortices, which stem from the relative motion between endwall boundary layer and blades. Clearance losses were found to vary almost linearly with clearance.

Vavra (1960, [57]) proposed a modified leakage flow model. In this, a linear chordwise blade loading is assumed instead of a uniform one as used by Rains and empirical coefficients are included to correct leakage flow rate as well as viscous effects. However, this does not change the basic parametric form presented by Rains.

A more recent leakage flow model was proposed by Senoo and Ishida (1986, [48]) for predicting the efficiency drop due to clearance flow for axial and centrifugal compressors. The problem is attacked in a different manner than in the previous two references. The drag due to the leakage flow is first shown to be $\dot{m}_c(V_s - V_p)$, where $\dot{m}_c$ is the leakage flow rate, and V_s and V_p are, respectively, the fluid velocity near suction side and pressure side of the blade. The change in efficiency is then calculated from the drag forces. It can be shown (see Senoo and Ishida, 1990, [47]) , however, that the loss in power due to the drag forces is identical to the loss of kinetic energy associated with the clearance flow as assumed by Rains (1954, [43]) and Vavra (1960, [57]), which will be discussed in Chapter 5.

The approaches discussed so far are directed at compressors. There have also been studies of the clearance loss for a turbine (see for example: Booth, 1985, [6], Farokhi, 1987, [16]), and Martinez-Sanchez and Gauthier, 1990, [37]). These studies are also based on the leakage flow approach and hence will not be discussed in detail here. However, it should be pointed out that these studies indicate the decrease in efficiency varies more or less linearly with tip clearance as with compressor.

The leakage flow approaches give reasonable estimates of the efficiency reduction due to clearance. However, no information on the vortical structure of clearance flow

field is available from this approach and, to examine the fluid mechanic features, one has to resort to other approaches.

1.2.3 Lifting Line Approach

Unlike the leakage flow approach, methods using lifting line theory are able to give the clearance loss and a description of the clearance flow field (Betz, 1926; Yokoyama, 1961, [61]; Lakshminarayana and Horlock, 1965, [30]; Lakshminarayana, 1970, [29]).

Two simple lifting line models are illustrated in Figure 1.3, and 1.4. In these, the circulation is assumed constant along the blade span. Due to viscous forces in the clearance region, only part of the circulation, which is obtained from an empirical correlation, is shed off at the blade tip. The locations of the trailing tip vortices are prescribed also. Induced drag due to the trailing vortices are then calculated and related to total pressure losses and hence the efficiency reduction.

One deficiency with the lifting line models is that the locations of shed vortices have to be prescribed in advance. In addition, the use of straight lines for the trailing tip vortices is not really adequate because, as will be seen later, there is generally a change in the slope of the vortex core trajectory near the trailing edge.

The empirical constants, which can vary considerably from geometry to geometry, introduce uncertainties in the predictions as observed by Booth (1985, [6]) , Inoue, Kuroumaru, and Fukuhara (1986, [24]), and Schmidt, Agnew, and Elder (1989, [45]). For example, Schmidt, Agnew, and Elder (1989, [45]) report the empirical constant ".70" used in the loss prediction is not adequate and, based on their experimental results, a constant of ".35" is recommended, which reduces the predicted loss by fifty percent.

A more realistic lifting line model is shown in Figure 1.5 (Lakshminarayana, 1970, [29]), in which the tip clearance vortex is modelled as a Rankine vortex with a finite core rather than a line vortex as in the previous two cases. The core size and circulation of the vortex, however, are again given by empirical correlations and the generality of

these is not clear. For example, the experiments of Sjolander and Amrud (1986, [49]) show that the vortex core size is only half of what predicted by the correlation used in the analysis.

In summary, although the lifting line approach does provide an insight into the passage flow field as well as an estimate of the loss in efficiency due to the clearance, it needs knowledge about the clearance vortex as an input and thus has drawbacks as a predictive tool.

1.2.4 Numerical Computation Approach

A recent approach for studying the clearance flow is the use of numerical computation (Pouagare and Delaney, 1986, [42]; Hah, 1986, [19]; Dawes, 1987, [11]; Adamczyk et al, 1989, [2]; Crook, 1989, [9]; Adamczyk et al., 1990, [1]; Storer and Cumpsty, 1990, [53]). This approach has been shown to be very useful in bringing out important features of the clearance flow and in giving a better understanding of the complex endwall flow. For example, it has been shown that: 1) the clearance flow is mainly inviscid, 2) the relative motion between the endwall and the blade has little effect on compressor clearance flow and 3) the clearance vortex may be the source of a large increase in blockage associated with endwall stall (see Crook, 1989, [9]). These numerical computations are clearly extremely useful but it is time-consuming to study the parametric dependence of the clearance flow field and the clearance loss, i.e. to develop guidelines for a broad range of devices.

1.3 Research Questions

As a summary of the present state of knowledge, therefore, one can say, although methods are now being developed to the clearance flow problems, there are still essential fluid mechanic questions to be answered. From the above discussions, it is clear that, although the clearance flow has been better understood over the past few years, the picture is far from clear and there are still essential fluid mechanic questions remained

to be answered. For example:

1. What parameters characterize the clearance flow?

2. What is the fluid mechanic behavior of the clearance vortex ?

3. How does clearance flow affect overall turbomachine performance (efficiency, pressure rise, and shaft power)?

1.4 Present Approach and Contributions

The goal of this thesis is to develop a clearance flow model which contains the essential features of the phenomenon, to guide interpretation of the experiments and data, to understand parametric trends, and to attack the above research questions.

Our model, which is based on slender body type of thinking, is different from the above-discussed approaches in that: 1) the three-dimensionality and the vortical structure of the clearance flow is emphasized from the outset, and 2) no empirical correlation is needed to close the problem. The basic idea is that the clearance velocity field can be (approximately) decomposed into independent through-flow and cross-flow, since chordwise pressure gradients are much smaller than normal pressure gradients in the clearance region as mentioned earlier. As in the slender body approximation in external aerodynamics, this description implies that three-dimensional , steady, clearance flow can be view as a two-dimensional, unsteady flow.

Using this approach, a similarity scaling for the clearance flow is developed and a generalized description of the tip vortex trajectory is derived. The scaling rule also provides a useful means to explore the parametric dependence of vortex trajectory and strength for a given blade row. Calculations based on the similarity scaling agree well with a wide range of experimental data in regard to flow features such as cross-flow velocity field, static pressure field, and tip clearance vortex trajectory.

In addition, expressions are derived for the decrease in efficiency, loading, and shaft power of a compressor due to clearance. This gives a new means of predicting the drop

in pressure rise and power of a compressor due to the clearance, with no empiricism involved in the description of the clearance flow. Calculations carried out agree well with experimental results. Expressions are also derived for the decrease in efficiency and work for a turbine; these calculations also compare well with several turbine data.

Finally, to justify the assumptions made in the modelling, analyses have been carried out to show: 1) the clearance flows in compressors and fans are mainly inviscid and can often be analyzed on an incompressible flow basis, and 2) in what circumstances the relative endwall motion can have significant effects on the clearance flow.

The major contributions of this thesis can be summarized as follows.

- A new approach for analyzing the clearance flow is presented.
- A similarity scaling for the clearance flow is identified.
- A generalized description of the tip vortex trajectory is proposed
- The parametric dependence of the clearance vortex core trajectory is identified.
- The essential fluid mechanic features of the clearance vortex are brought out.
- Analytical expressions for the loss in efficiency as well as pressure rise and shaft power due to clearance are presented for the first time.

1.5 Organization of the Thesis

The thesis is organized as follows: Chapter 2 presents the clearance flow model and the similarity analysis. Also included are justifications of the inviscid assumption, description of the computational scheme, calculation results, and available experimental data to assess the model adequacy. Chapter 3 shows the clearance flow field inside and downstream of a blade row. Several interesting features of the clearance flow are brought out and physical explanations are given for the behavior. The parametric dependence

of the clearance vortex trajectory are also examined. Justifications of the assumptions made in the modelling are given in Chapter 4. A method for predicting clearance losses and decrease in work as a result of clearance, for both compressors and turbines, is described in Chapter 5, which also gives calculation results and comparison with experimental data. Chapter 6 presents conclusions and suggestions for future research.

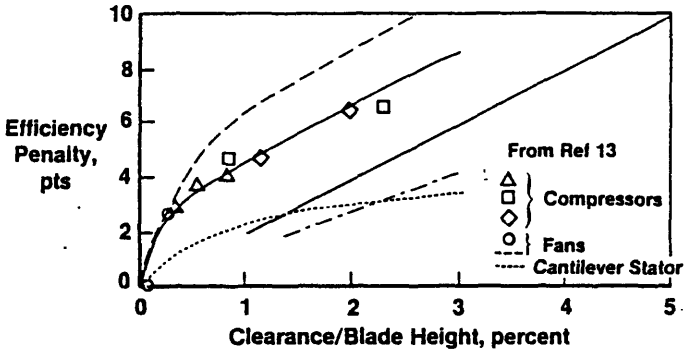

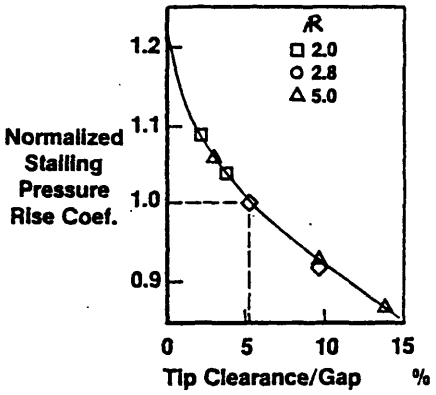

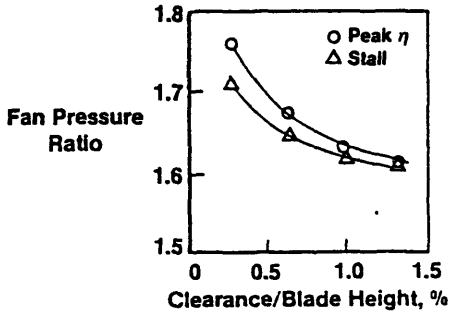

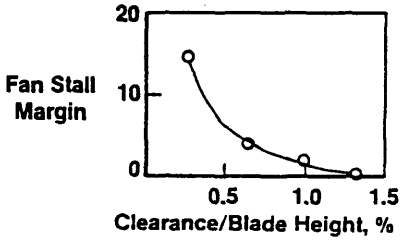

Figure 1.1: Effects of increased clearance on engine performance (Wisler, 1985)

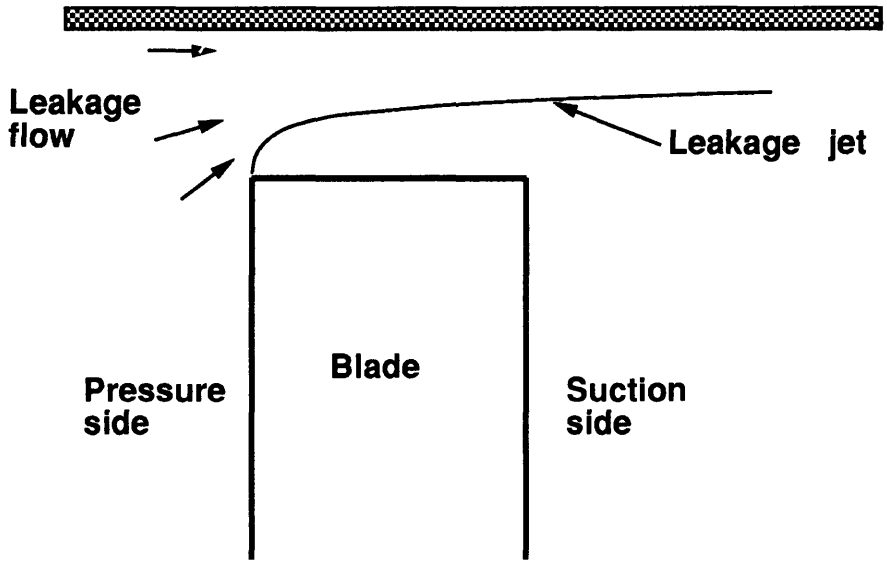

Figure 1.2: Leakage flow model for clearance flow

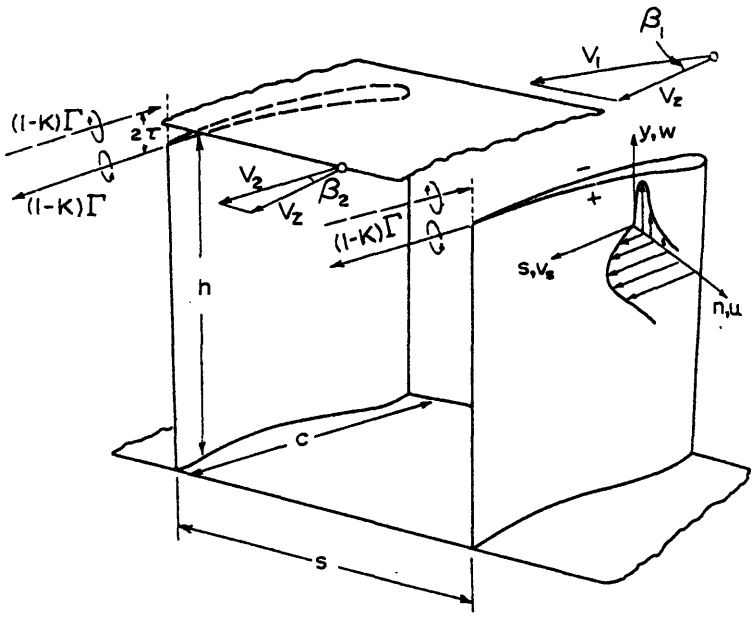

Figure 1.3: Lifting line model A (Lakshminarayana and Horlock, 1965)

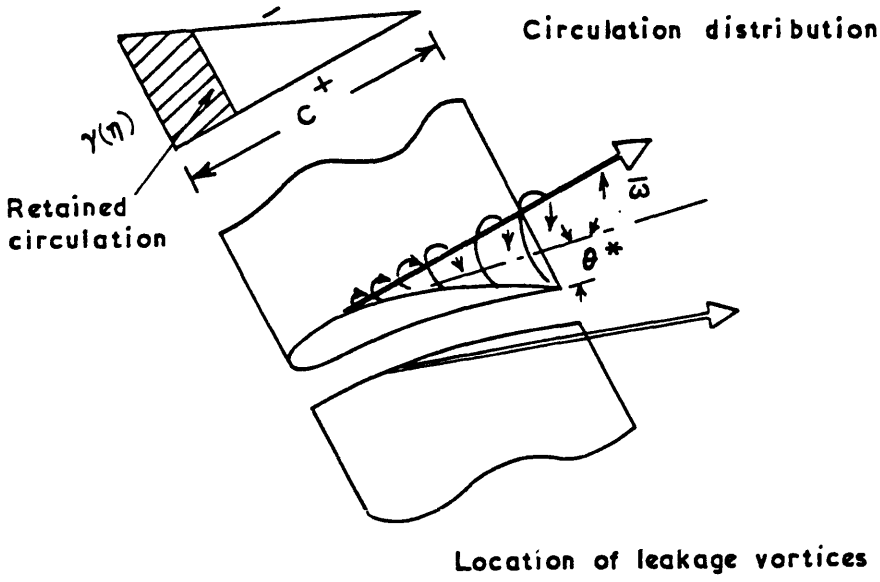

Figure 1.4: Lifting line model B (Lakshminarayana, and Horlock, 1965)

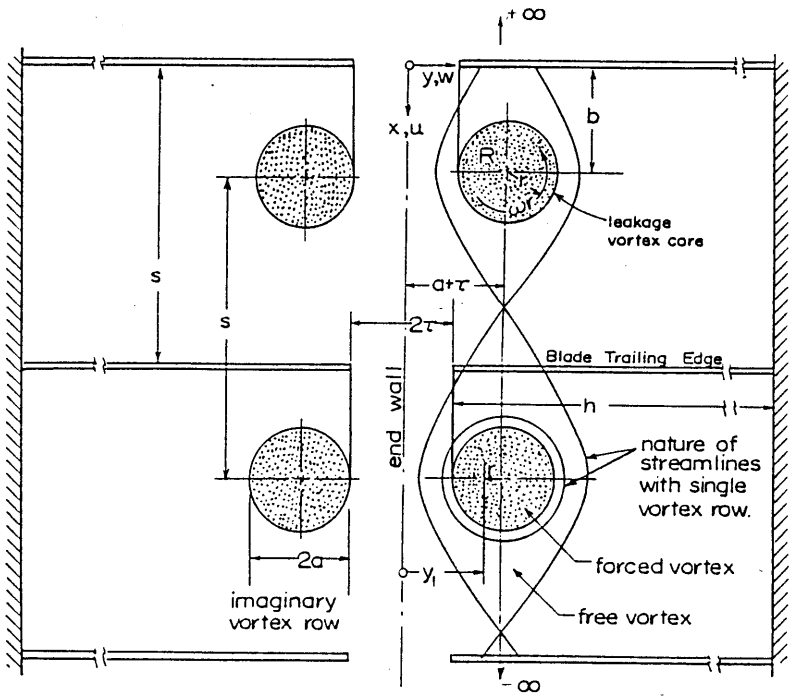

Figure 1.5: Modified lifting line model (Lakshminarayana, 1970)

Chapter 2

Fluid Dynamic Model and Similarity

2.1 Fluid Dynamic Model

The problem examined is the formation of a (tip clearance) vortex due to the flow through the clearance in turbomachinery. Such vortices are clearly seen in experiments (Herzig, Hansen, and Costello, 1953, [20]; Rains, 1954, [43]; Sjolander and Amrud, 1986, [49]; Inoue, Kuroumaru, and Fukuhara, 1986, [24]; Dishart and Moore, 1989, [14]), as well as in recent three-dimensional computations (Pouagare and Delaney, 1986, [42]; Adamczyk et al, 1989, [2]; Crook, 1989, [9]; Adamczyk et al., 1990, [1]). A critical feature in the development of such structures is the *roll-up* process, which is a nonlinear effect; this must be included in any realistic description of the endwall flow.

The flow of interest is three-dimensional and steady. As for slender bodies in external aerodynamics, however, one can model it from the point of view of a two-dimensional, but unsteady, flow. The central idea is that translation along the streamwise direction is analogous to moving in time, i.e. an observer moving with (some average) streamwise velocity is embedded in an unsteady flow field. This implies that the generation of the tip clearance flow, and the roll-up, can thus be treated as an unsteady process in successive cross-flow planes (planes normal to the blade camber). [1]

[1] One condition to do this therefore is the existence of an identifiable appropriate translational velocity for the observer frame. This will be commented on below.

To illustrate the idea in more detail, consider cross-flow planes A, B, C, and D at different chordwise locations a, b, c, and d, respectively, as shown in Figure 2.1.

Location a is at the leading edge and d is at the trailing edge. At station a, the tip clearance flow is initiated so that the flow in cross-flow plane A might be as shown in the lower part of the figure. At subsequent stations through the blade passage, the vortex sheet shed into the clearance will roll up so that other downstream cross-sections might be as illustrated in planes B, C, and D.

The analogy proposed is that the flow pattern in different cross-flow planes is similar to that in a two-dimensional unsteady flow. More specifically, the velocity in the four cross-flow planes of the top part of Figure 2.1 is represented by the unsteady flow at the four different times shown in the lower part of the figure. If this analogy holds, it implies that evolution of the cross-plane flow structure (including tip clearance vortex strength and position) at different streamwise locations is similar to that at different times, when viewed from a moving reference frame. The transformation between time, t, and streamwise location, s, is $t = s/V(s)$ where $V(s)$ is the velocity of the moving frame.

A key argument for adoption of this (slender body type) approach to tip clearance flow is based on the relative length scales in the streamwise and transverse directions. For an inviscid flow, the relevant length scale in the two cross-flow directions will be set by (the size of) the tip clearance, whereas the streamwise length scale is the chord. For high performance turbomachines, the former is much smaller than the latter (generally the former is less than five percent, and sometimes less than one percent of the latter). Because the pressure difference across the blade and along the blade are of the same order of magnitude, the pressure gradients, and acceleration components, in the transverse directions are much larger than those in the streamwise direction.

In addition to the arguments concerning pressure gradients, in order to use a slender body type of approximation we must also be able to identify some (relatively uniform) mean streamwise reference velocity. If so, we can write the streamwise velocity compo-

nents, u, as a passage average value plus a deviation from the average, i.e.

$$u(s,y,z) = \overline{u}(s) + u'(s,y,z) \tag{2.1}$$

where s is measured along the blade camber, y is normal to the camber, z is along the span, and we take $u'/\overline{u} \ll 1$. This strong inequality cannot be strictly true for highly loaded blades if applied everywhere across a blade passage. Its use, however, is appropriate here since the primary interest is in the *local* regions of the flow domain where vorticity is shed and where roll-up occurs. Over such regions, the normalized variation in streamwise velocity, $u'/\overline{u}$, can, in fact, be small. As an example, if we take the mean blade pressure difference Δp equal to $0.5 \cdot \rho V_1^2/2$, and say that the region of interest is twenty five percent pitch, the magnitude of $u'/\overline{u}$ over this region is less than 0.1. Arguments of this type imply, and the subsequent comparison with data will show, that the approximation $u'/\overline{u} \ll 1$ is indeed adequate for the present treatment.

Under the above two conditions, as shown in Appendix A, the (inviscid) equations describing flow in the transverse, or cross flow, plane are decoupled from the equations that describe flow in the streamwise direction. Within this approximation, s can be regarded as the streamwise distance and $V(s)$, the velocity of the moving frame, can be taken as $\overline{u}$. The relation between time and streamwise distance is thus

$$dt = \frac{ds}{\overline{u}} \tag{2.2}$$

The cross-flow plane equations take the form (see Appendix A)

$$\frac{\partial v}{\partial y} + \frac{\partial w}{\partial z} = 0 \tag{2.3}$$

$$\frac{\partial v}{\partial t} + v\frac{\partial v}{\partial y} + w\frac{\partial v}{\partial z} = -\frac{1}{\rho}\frac{\partial p}{\partial y} \tag{2.4}$$

$$\frac{\partial w}{\partial t} + v\frac{\partial w}{\partial y} + w\frac{\partial w}{\partial z} = -\frac{1}{\rho}\frac{\partial p}{\partial z} \tag{2.5}$$

which are the equations describing an inviscid two-dimensional unsteady flow.

In the preceding discussions, the flow has been taken as inviscid. This point has been examined in some detail by other investigators (e.g. Rains, 1954, [43]; Moore and Tilton, 1988, [39]; Storer and Cumpsty, 1990, [53]). These studies show that, while viscous effects do play a role, the dominant features of the flow due to tip clearance are inviscid, and a useful description can be developed on this basis. A more detailed discussion is given in Appendix B.

Three other approximations are also implicit in the analysis. The first is that the effect of adjacent blades on the tip clearance flow is primarily important in setting up the overall pressure difference profile, which drives the flow through the tip clearance, rather than in determining the detailed structure of the tip flow. This implies that the latter can be analyzed as an unsteady flow through a single blade with clearance, rather than through an array of blades, if one uses the appropriate pressure difference. In addition, we represent the blade by its camber only, with thickness neglected. As implied by Moore and Tilton (1988, [39]), the treatment is thus restricted to situations with thin blades (i.e. compressors) where the shear layer (vortex sheet) shed from the pressure surface does not reattach within the tip clearance. Finally, as mentioned in Appendix A, the blade camber is assumed such that the radius of curvature of the tip section camber line is much larger than the chord; this is generally a good approximation for compressors.

2.2 Similarity Analysis

We have so far described the basic framework of the approach (an unsteady two-dimensional analysis of the velocity field on cross-flow planes) and the assumptions. We now examine the consequences of this model. In particular, we show that a similarity solution exists and that this implies a generalized vortex trajectory which is independent of tip clearance. The geometry and nomenclature to be used are given in Figure 2.2, which shows the blade and flow domain at an arbitrary cross-section location, with a schematic of the tip vortex sheet roll-up. The notations used for the vortex trajectory

is indicated in Figure 2.3. Two quantities that will be used in what follows are the *centroid of the shed vorticity*, denoted by (y_v, z_v) and the *center of the tip vortex core*, denoted by (y_c, z_c). This latter is defined as the centroid of the *rolled-up* part of the vortex sheet.

Referring to Figure 2.2, we note that, in almost all practical situations, the blade height (or blade span), b, is much larger than the tip clearance, τ, since $\tau/b \sim O(10^{-2})$. Because of this, the ratio of height/clearance would be expected to affect the local flow over the tip only slightly. If the blade span is not a significant parameter for the local details of the flow in the tip clearance region, however, the only relevant length is the tip clearance. The physical variables that characterize the problem are this tip clearance, τ, pressure difference, Δp , density, ρ, and time, t. Considering a time increment, dt (as expressed in Eq. (2.2)), dimensional analysis shows that the only dimensionless variable that can be formed using the four quantities has the form

$$dt^* = \frac{dt}{\tau}\sqrt{\frac{\Delta p}{\rho}} \tag{2.6}$$

Eq. (2.6) defines a non-dimensional time increment in terms of local values of pressure difference, density, and tip clearance. In the most general situation, these will vary along the chord, but as will be seen later the use of an average loading, denoted as $\overline{\Delta p}$, gives good prediction of the tip vortex core trajectory. If the density and clearance are also taken as constant, Eq. (2.6) can be integrated to give an expression for the non-dimensional time corresponding to a given streamwise location:

$$t^* = \frac{t}{\tau}\sqrt{\frac{\overline{\Delta p}}{\rho}} \tag{2.7}$$

Two tip clearance flow fields will be similar if they correspond to the same t^*. The following non-dimensional quantities will thus all be functions of t^* only [2]:

$$y_c^* \equiv \frac{y_c}{\tau}, \quad z_c^* \equiv \frac{z_c}{\tau} \tag{2.8}$$

[2]It can be shown that z_v^* approaches a constant when $t^* \to \infty$ (see Appendix C).

$$y_v^* \equiv \frac{y_v}{\tau}, \quad z_v^* \equiv \frac{z_v}{\tau} \tag{2.9}$$

$$\Gamma^* \equiv \frac{\Gamma}{\tau\sqrt{\overline{\Delta p}/\rho}} \tag{2.10}$$

$$v^* \equiv \frac{v}{\sqrt{\overline{\Delta p}/\rho}}, \quad w^* \equiv \frac{w}{\sqrt{\overline{\Delta p}/\rho}} \tag{2.11}$$

The distances y_c^* (or z_c^*) are measured between the center of the tip vortex and the camber (or casing), and y_v^* (or z_v^*) is the distance between the centroid of the shed vorticity and the camber (or casing), measured from the mean camber line, in the direction of the local normal, as illustrated in Figures 2.2 and 2.3.

The pressure difference across the blade varies along the span but evaluation of the loading at the mean radius appears to be adequate for good prediction of the tip vortex core trajectory. The non-dimensional time, t^*, can thus be estimated as:

$$t^* = \frac{t}{\tau}\sqrt{(\frac{\overline{\Delta p}}{\rho})_{mean}} \tag{2.12}$$

where

$$t = \int_0^s \frac{ds}{\overline{u}} = \frac{x}{C_x} \tag{2.13}$$

The combined Eqs. (2.12) and (2.13) can be written in terms of flow angles at the mean radius using the expression for ideal pressure rise given in many texts (e.g. Horlock, 1973, [22]):

$$t^* = \frac{c}{\tau}\sqrt{\frac{g(\tan\beta_1 - \tan\beta_2)}{c\tan\beta_m}} \tag{2.14}$$

In Eq. (2.14), g is the blade spacing, c is the chord, β_1 and β_2 are the inlet and outlet flow angles (see Figure 2.3), and β_m refers to the vector mean velocity direction.

2.3 Computational Procedure

2.3.1 Introduction

The functional dependence of Eqs. (2.8) to (2.11) with respect to t^*, as well as any other information needed about the velocity or vorticity fields of the two-dimensional,

unsteady flow, can be computed in a number of ways. That used here is a vortex method. When applicable, these methods have the advantage that, if the location of the vortex sheets are known, the velocities need to be calculated only on the sheets at each time step, rather than in the entire flow. Many such methods are available; a recent review of these is given by Sarpkaya (1989, [44]).

In essence, what is done is to track the vorticity shed (as a vortex sheet) from the tip of the blade. The evolution (in particular the roll-up) of this vortex sheet in time provides, using the relation that has been developed between time and streamwise spatial variable, the three-dimensional structure of the tip leakage vortex. In-depth discussions of vortex methods are given, for example, in the papers by Leonard (1980, [35]) and Sarpkaya (1989, [44]) but several points should be commented on. First, as noted by Sarpkaya (1989, [44]), the fine structure of the computation depends critically on the number of vortices used, the time stepping procedure, and the smoothing techniques applied. More specially, although quantities such as the circulation and the position of the centroid of vorticity (the sum and first moment of the shed vorticity) are essentially invariant to the type of scheme used, the details of the shape of the rolled up vortex sheet are sensitive to the above factors.

To assess the degree to which the results depend on the computational parameters, we have carried out calculations using two different approaches, one involving a conformal transformation of the flow domain (Evans and Bloor, 1977, [15]) and the other an unsteady panel method. In the computations, several different time-stepping schemes, as well as sub-stepping procedure, were examined with time steps (number of vortices) and number of sub-steps varied by factors of ten. The results show that the circulation and vorticity centroid are, as described by the above-mentioned review articles, not sensitive to these variations. For example, there is less than a two percent difference in the computed tip vortex position (y_c) for a factor of ten in time step. In summary, the central point is that the overall features of the vortical flow are of most interest here, and these are not dependent on the details of the computational method.

2.3.2 Conformal Transformation Approach

We now discuss the conformal transformation approach. Point vortices are used to simulate the shed vortex sheet. The flow domain in the physical plane (Φ plane), is mapped into the upper half of the transformed plane (Ξ plane) by a conformal transformation (Evans and Bloor, 1977, [15]) as illustrated in Figures 2.4 and 2.5. The mapping is given by

$$\Phi = \frac{H}{\pi} \tanh^{-1} \sqrt{\frac{\Xi^2 - 1}{\beta^2 - 1}} \tag{2.15}$$

or

$$\Xi = [1 + (\beta^2 - 1) \tanh^2(\frac{\pi \Phi}{2H})]^{1/2} \tag{2.16}$$

In this transformation

$$\beta = \pm \csc \frac{\pi b}{2H} \tag{2.17}$$

correspond to the transformed points at infinity in the physical plane and are thus the locations of a source and sink, respectively, in the transformed plane.

In Fig. 2.4, several locations of interest are indicated, i.e. a_1 to a_6, as well as their coordinates. The corresponding locations in the transformed plane, denoted by uppercase, i.e. A_1 to A_6, are given in Fig. 2.5. In particular, the blade tip, $\Phi = ib$, is mapped to $\Xi = 0$, i.e. the origin of the transformed plane, and either side of the hub of the blade, $\Phi = 0$, is mapped to $\Xi = \pm 1$.

The complex potential for the source and sink combination is

$$F(\Xi) = \frac{HU_0}{\pi} \ln \frac{\Xi + \beta}{\Xi - \beta} \tag{2.18}$$

where U_0 is the uniform flow velocity in the cross flow plane as shown in Fig. 2.4.

Point vortices are introduced into the flow at each time step to simulate the vortex shedding procedure. At a given time, t_N, there are N vortices plus their images in the flow and the complex potential takes the following form:

$$F(\Xi) = \frac{HU_0}{\pi} \ln \frac{\Xi + \beta}{\Xi - \beta} - \frac{i}{2\pi} \sum_{j=1}^{N} \Gamma_j \ln \frac{\Xi - \Xi_j}{\Xi - \overline{\Xi}_j} \tag{2.19}$$

where Ξ_j and Γ_j are, respectively, the location and circulation of the jth vortex and $\overline{\Xi}_j$ is the complex conjugate of Ξ_j.

A vortex is shed at each time step to satisfy the Kutta condition at the blade tip. The location and strength of the shed vortex are determined by the Kutta condition and vorticity flux condition, as discussed below. The vortex is taken to be shed slightly above the tip, at

$$\Phi_{N+1} = i(b + \frac{\varepsilon}{2}) \tag{2.20}$$

with strength Γ_{N+1}. The Kutta condition requires that the origin ($\Xi = 0$) of the transformed plane be a stagnation point. This gives

$$\Gamma_{N+1} = -\frac{Y_{N+1}^2 + Z_{N+1}^2}{Z_{N+1}}(\frac{2U_0 H}{\beta} + \sum_{j=1}^{N} \frac{\Gamma_j Z_j}{Y_j^2 + Z_j^2}) \tag{2.21}$$

where Y_j, Z_j are coordinates of the shed vortices, i.e.

$$\Xi_j = Y_j + i\, Z_j \tag{2.22}$$

The rate at which vorticity is shed into the wake from the tip is given by

$$\frac{\Gamma_{N+1}}{\Delta t} = \frac{1}{2}|Q(\Phi)|^2 \tag{2.23}$$

evaluated at $\Phi = i(b+\varepsilon)$, where Q is complex velocity. This equation, together with Eq. (2.21), determines the value of Γ_{N+1} and the variable ε at each time step. That is, the Kutta condition and the rate of shedding are satisfied simultaneously at each calculation step. The $N+1$ vortices are then convected and, at $(N+2)\ \Delta t$, a new vortex is again introduced into the flow, with its location and strength determined by Eqs. (2.21) and (2.23). The solution is advanced in time following the same procedure so the clearance vortex and its flow field are known at every time step. Once the cross flow is known at some general time t , the three-dimensional, steady, flow is then determined from the correspondence between time t and axial location given by Eq. (2.13).

One point should be commented on regarding the convection velocity of the shed vortices. The complex velocities in the physical and transformed plane are related by

$$Q(\Phi) = Q(\Xi)\, \frac{d\Xi}{d\Phi} \tag{2.24}$$

where Q is the complex velocity. However, this is only true in the flow domain excluding the shed vortices. To determine the convection velocities of the point vortices in the physical plane, Routh's correction must be used (see Appendix D).

2.3.3 Panel Method

Calculations have also been carried out using a panel method approach. As illustrated in Fig. 2.6, the blade is replaced by a series of N (bound) discrete vortices with strength $\Gamma_i, i = 1, N$, located at $a_1, \ldots, a_N$. The circles, denoted by $b_1, \ldots, b_N$, are control points at which the boundary condition of zero normal velocity are to be applied. The wall effect is taken into account by using series of image vortices in the z direction so that the kinematic boundary conditions at the walls are automatically satisfied.

As in the conformal mapping approach, point vortices are introduced into the flow at each time step to simulate the vortex shedding procedure. It is assumed that a vortex with circulation Γ_0 is shed slightly above the blade tip, at $z_0 = b + \varepsilon/2$, where Γ_0 and ε are unknowns to be determined.

There are N+2 unknowns in the problem, i.e. $\Gamma_0, \Gamma_1, \ldots, \Gamma_N$, and ε, and this requires N+2 equations. The boundary condition requires zero normal velocity on the blade so that one has

$$v = 0, \quad at \ \ points \quad b_i, i = 1, N \tag{2.25}$$

The Kutta condition requires

$$\Gamma_0 = (\overline{w}\gamma)_{tip} \ \Delta t \tag{2.26}$$

where $(\overline{w}\gamma)_{tip}$ is the product of the average velocity $[(w_s + w_p)/2]$ and the vorticity at the blade tip and Δt is the time step.

In the actual situation the vorticity is shed continuously into the wake. This implies that the length of the vortex segment which is shed from the tip in time interval Δt will be (approximately) equal to $\overline{w}\Delta t$. If this vortex segment is replaced by a point vortex,

the vortex should be placed at the centroid of the vortex segment, so

$$\varepsilon = (\overline{w})_{tip} \ \Delta t \tag{2.27}$$

Eqs. (2.25), (2.25) and (2.25) provide a set of N+2 equations (N linear and two nonlinear) for the $N+2$ unknowns: $\Gamma_0, \Gamma_1, \ldots, \Gamma_N$, and ε, and these can be solved numerically.

The relationship between pressure difference, bound circulation, and velocity can be found in the following way. First, as shown in Fig. 2.7, the unsteady Bernoulli equation can be applied between the blade hub (station 1) and tip (station 2),

$$\frac{\partial \varphi_1}{\partial t} + \frac{v_1^2 + w_1^2}{2} + \frac{p_1}{\rho} = \frac{\partial \varphi_2}{\partial t} + \frac{v_2^2 + w_2^2}{2} + \frac{p_2}{\rho} \tag{2.28}$$

where φ is the velocity potential. Similarly, applying the Bernoulli equation between station 3 and 4, one has

$$\frac{\partial \varphi_3}{\partial t} + \frac{v_3^2 + w_3^2}{2} + \frac{p_3}{\rho} = \frac{\partial \varphi_4}{\partial t} + \frac{v_4^2 + w_4^2}{2} + \frac{p_4}{\rho} \tag{2.29}$$

From Eqs. (2.28) and (2.29) and knowing that v_1, w_1, v_2, v_3, v_4, and w_4 are all zero, and p_2 is equal to p_3, we have

$$\frac{\partial \varphi_1}{\partial t} - \frac{\partial \varphi_4}{\partial t} + \frac{p_1}{\rho} - \frac{p_4}{\rho} = \frac{\partial \varphi_2}{\partial t} - \frac{\partial \varphi_3}{\partial t} + \frac{w_2^2}{2} - \frac{w_3^2}{2} \tag{2.30}$$

i.e.

$$\frac{\Delta p}{\rho} = \frac{p_1}{\rho} - \frac{p_4}{\rho} = \frac{\partial \varphi_4}{\partial t} - \frac{\partial \varphi_1}{\partial t} + \frac{\partial \varphi_2}{\partial t} - \frac{\partial \varphi_3}{\partial t} + \frac{w_2^2}{2} - \frac{w_3^2}{2} \tag{2.31}$$

The velocity potentials at the hub and tip are related by

$$\varphi_2 = \varphi_1 + \int_1^2 w_p dz \tag{2.32}$$

and

$$\varphi_3 = \varphi_4 + \int_1^2 w_s dz \tag{2.33}$$

where w_p and w_s are the velocity on the pressure and suction surface. From Eqs. (2.32) and (2.33), one has

$$\varphi_1 - \varphi_4 = \varphi_2 - \varphi_3 - \int_1^2 (w_p - w_s) dz \tag{2.34}$$

i.e.

$$\varphi_1 - \varphi_4 = \varphi_2 - \varphi_3 - \Gamma_b \tag{2.35}$$

where Γ_b is the total bound circulation (composed of the vortices Γ_1 to Γ_N). This can be differentiated and put into Eq. (2.31) to give the expression for the pressure difference across the blade

$$\frac{\Delta p}{\rho} \equiv \frac{p_1 - p_4}{\rho} = \frac{\partial \Gamma_b}{\partial t} + \frac{w_2^2}{2} - \frac{w_3^2}{2} \tag{2.36}$$

which can also be written as

$$\frac{\Delta p}{\rho} = \frac{\partial \Gamma_b}{\partial t} + (\gamma \overline{w})_{tip} \tag{2.37}$$

Calculations showed that $\Delta p/\rho U_0^2$ remained almost constant with time t (difference less than four percent), which is to be expected because the flow in the tip region will not have a significant effect on the blade loading far away from the tip. This indicates one can keep U_0 constant to achieve the constant loading condition ($\Delta p/\rho$), discussed in section 2.2, and this approximation is thus adopted in the calculation.

In summary, the bound and shed vortex sheet are represented by point vortices in the panel method calculation. Location and strength of the shed vortex are solved nonlinearly at each time step from the Kutta condition at the blade tip. The vortices are continuously convected away and new shed vorticity is generated at each time step.

Euler forward , modified Euler forward, and Runge- Kutta time marching schemes were used as well as sub-stepping to examined the effects of different schemes on the solutions.

The time step and the number of sub-steppings have been varied by a factor of ten and twenty, respectively, to see their effects on the solutions. The results show that, although the vortex distribution changes, the centroids of the vortices are almost the same for different time marching schemes and time steps used in the calculation. This is can be seen from Fig. 2.8, which gives the vorticity centroid trajectory y_v^* for all the above-mentioned computation schemes. This indicates that although the details of the

vortex sheet may change with different approaches the global features of the sheet (eg. centroid) do not.

2.4 Similarity Results for Flow In The Blade Passage

Computations of coordinates of the centroid of vorticity, y_v, and z_v, are shown in Fig. 2.9. The computations have been carried out assuming constant loading along the blade. While this an oversimplification, computations with a varying Δp show little difference from these results, at least for representative subsonic compressor blade pressure distributions.

A quantity that is more relevant than the centroid of vorticity is the position of the tip vortex, and the non-dimensional tip vortex center position, y_c, is shown in Fig. 2.10. Included in the figure is data from the different tip vortex experiments of Rains (1954, [43]), Smith (1980, [50]), Johnson, (1985, [26]), Inoue and Kuroumaru (1988,[23]), and Takata (1988,[56]). Compressor parameters for these tests are given in Table 2.1. Where velocities were not measured directly in the experiments, the position of the tip vortex is taken as either the center of the low total pressure region (Takata, Smith) [3] or the center of the tip vortex cavitation (Rains). The convection time is calculated based on mean axial velocity.

The experimental data covers a large range of clearances, loadings, and flow coefficients (see Table 2.1). The conditions include moderate loading with large tip clearance (leading to generally low values of t^*) as well as near-stall loadings with small clearance (Smith (1980, [50]) (which lead to large t^*) [4]. The different vortex trajectories, how-

[3]There is some small error involved in doing this, as pointed out by Crook (1989, [9]) and by Lee (1989, [34]). This, however, should be considerably less than the extent of the low total pressure region, and hence (at a given location) small compared to the values of y_c given in the figure.

[4]There are two sets of points plotted for the Smith (1980, [50]) compressor. The open symbols are based solely on conditions at the midspan. This rotor has a very low hub/tip radius ratio (0.4) and a consequent large twist, and it may be expected that midspan conditions do not adequately reflect tip section performance for this configuration. To examine this, we have also considered data based on the actual measurements of the "free stream" tip section pressure difference (at a location 33 tip clearances, i.e. 0.33 chord, from the endwall). These points are plotted as solid symbols in the figure.

Experiments	Flow Coeff. (ϕ)	Clearance/Chord (%), τ/c
Inoue and Kuroumaru	.50	.85
Inoue and Kuroumaru	.50	1.70
Inoue and Kuroumaru	.50	2.55
Inoue and Kuroumaru	.50	4.26
Rains	.45	1.3
Rains	.45	2.6
Rains	.45	5.2
Takata	.62	4.2
Takata	.56	4.2
Takata	.53	4.2
Takata	.50	4.2
Johnson	stator	4.0
Smith	.29	1.0

Table 2.1: Experimental Data

ever, are well described by the single similarity solution curve, in agreement with the dimensional analysis. In addition to providing a relevant dimensionless grouping, the theory thus gives a good absolute prediction of tip vortex location, even when applied at near-stall conditions. It can also be pointed out that the largest percentage deviations from the theory are those for data near leading edges; for these the distance are small and the experimental results, taken from publications, are difficult to read precisely.

An observation from Fig. 2.10 is that the generalized tip vortex trajectory is nearly a straight line, which can be approximately represented by

$$y_c^* = 0.46 t^* \tag{2.38}$$

Taking the pressure difference to be given by its value at the midspan location yields an approximate expression for the tip vortex trajectory as a function of axial position.

$$\frac{y_c}{x} = 0.46 [\sqrt{\frac{g(\tan\beta_1 - \tan\beta_2)}{c \cos\beta_m}}]_{mean} \tag{2.39}$$

If the mean flow parameters are known, one can estimate the tip vortex trajectory well from Eq. (2.39). [5]

[5] We also examined the vortex trajectory and the similarity scaling for the clearance flows based on

Equations (2.38) or (2.39) show that y_c, the (dimensional) locus of the tip vortex trajectory on a constant radius surface, does not depend on clearance. Varying clearance while keeping other parameters the same will not alter the projection of the tip vortex trajectory on this surface although, as will be seen, it will alter the cross-flow pattern [6] (Dean, 1954, [13]; Inoue, Kuroumaru, and Fukuhara, 1986, [24]; and Zhang, 1988, [62]). For example, the experimental result of Inoue, Kuroumaru, and Fukuhara (1986, [24]) is given in Fig. 2.11. In the figure tip clearance flows of a rotor near the trailing edge for various clearances (1mm , 2mm, 3mm, and 5mm) are shown. It is clear that as clearance increases the clearance flow becomes much stronger. However, there is little change in the tangential locations of the vortex cores (y_c) when the clearance is increased by a factor of five.

2.5 Summary

A model for the clearance flow has been formulated, based on a slender body approximation. The (three-dimensional) clearance is considered as a two-dimensional unsteady flow so the clearance flow problem becomes a starting problem in the cross flow plane.

In the model the only length scale in the clearance region is the clearance so there exists a similarity solution for the tip clearance flows, which is based on a normalized time parameter t^* . Based on this similarity, a generalized tip vortex trajectory is proposed and shown to be in good agreement with available experimental data, indicating that the behavior of the clearance flow is dominantly inviscid.

---

leakage flow approach, in which the clearance flow is regarded as a jet (see Appendix E). The analysis shows that there is a similarity scaling for clearance flows and that the similarity parameter is identical to the one given by Eq. (2.7). It also shows that $y_v^*/t^* = \sqrt{2}/4$ (about 0.354), which agree with the value of .365 from the calculation.

[6]This result is obtained based on the above-discussed assumptions. In the actual situation, the clearance does have a slight effect on the locus of the tip vortex trajectory. (Storer, comment on Chen et. al., 1990, [8])

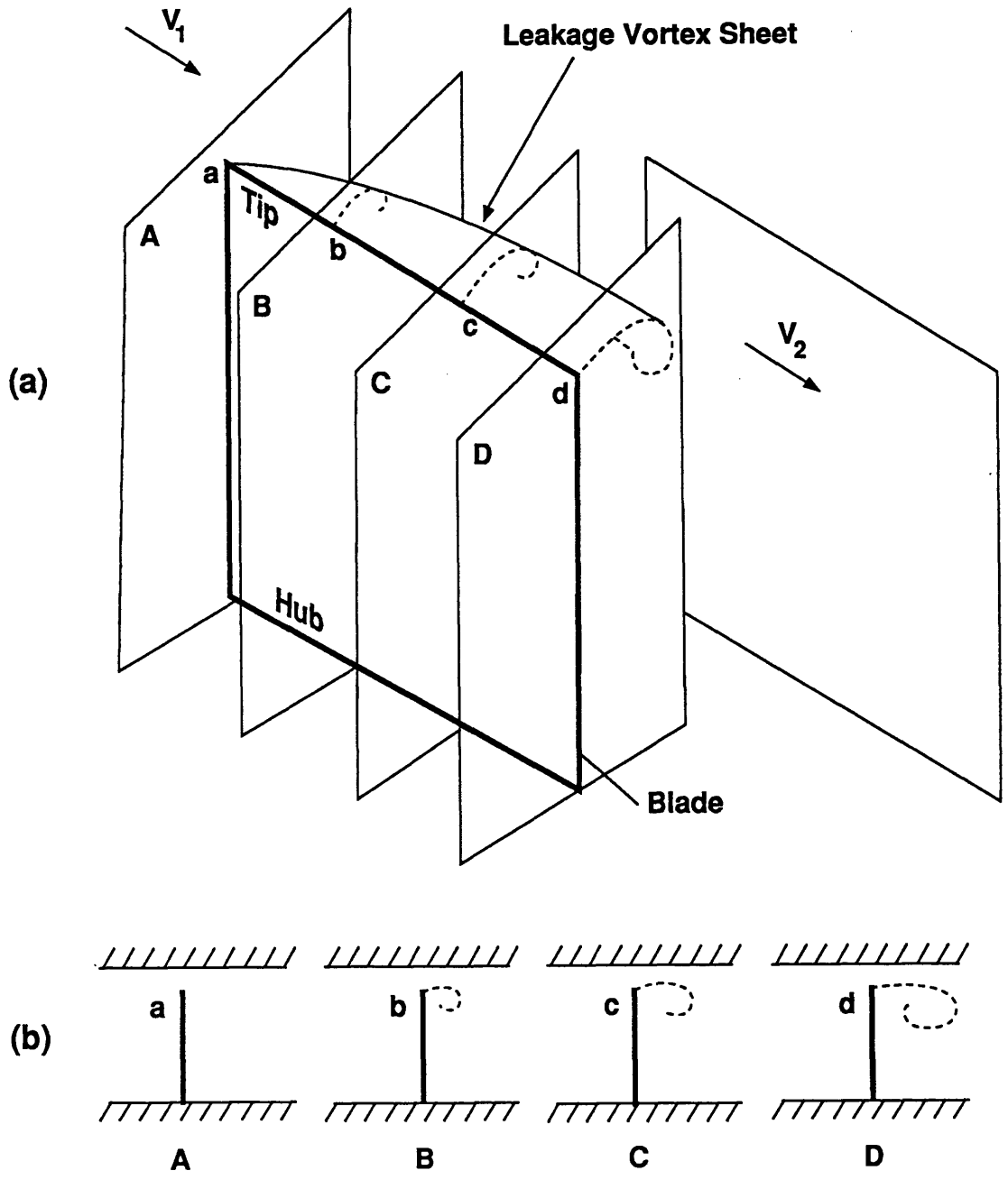

Figure 2.1: Correspondence between three-dimensional steady tip clearance flow and unsteady two-dimensional model flow

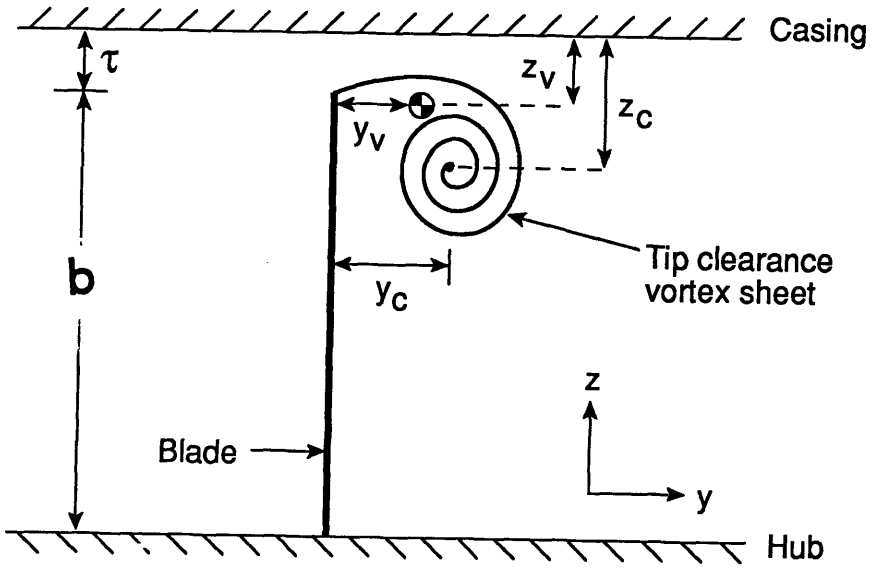

Figure 2.2: Nomenclature and flow domain for tip clearance flow model

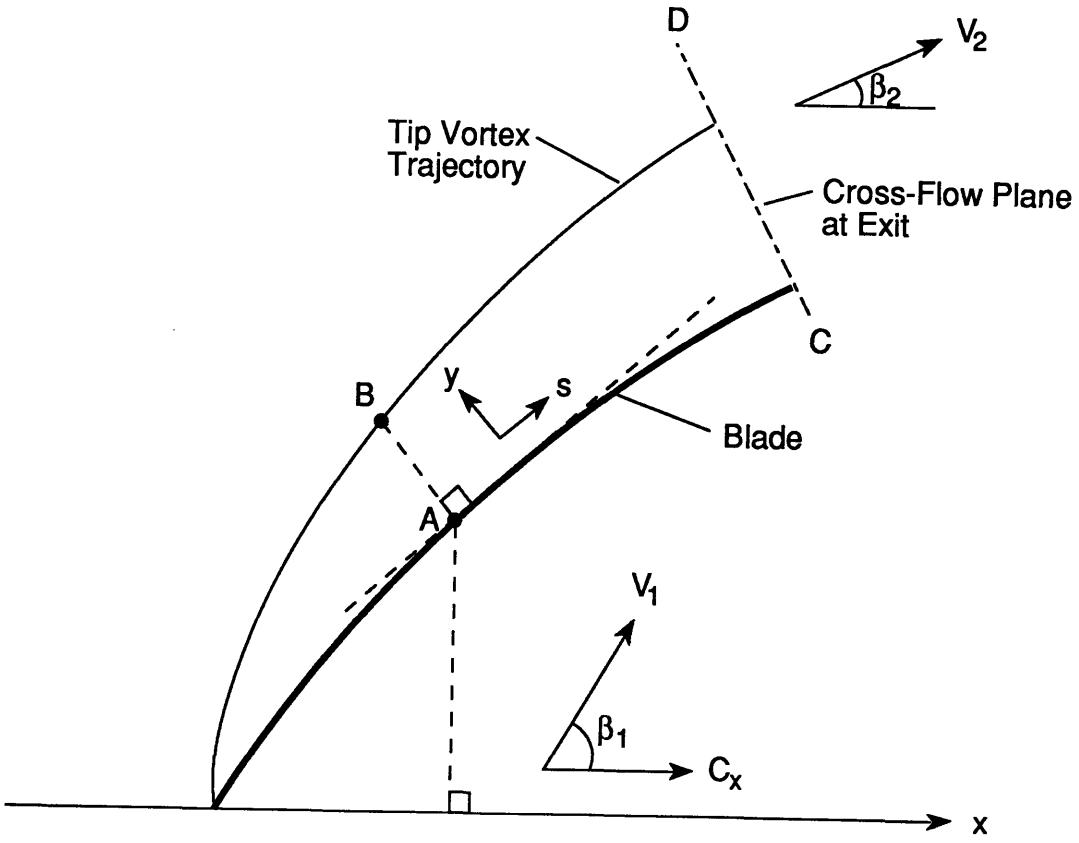

Figure 2.3: Schematic of projection of vortex trajectory on constant radius surface (y_v or y_c)

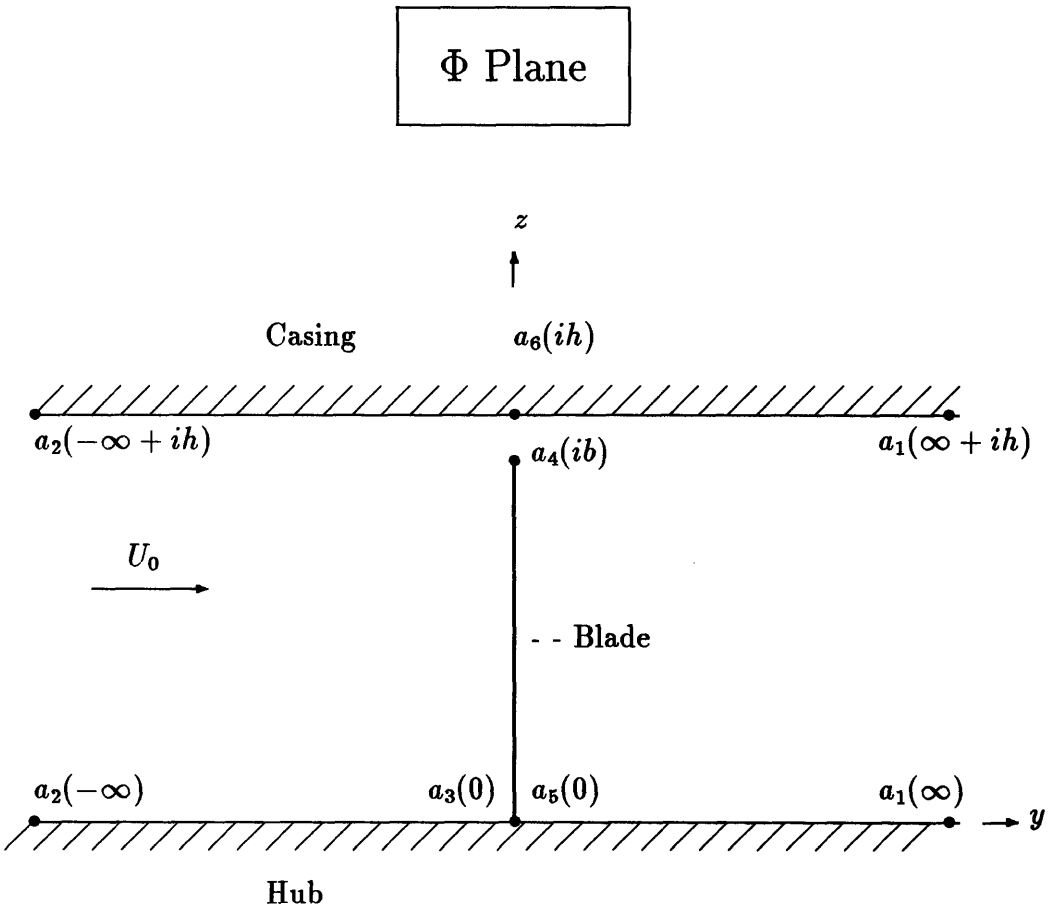

Figure 2.4: Flow domain in physical plane (Φ plane)

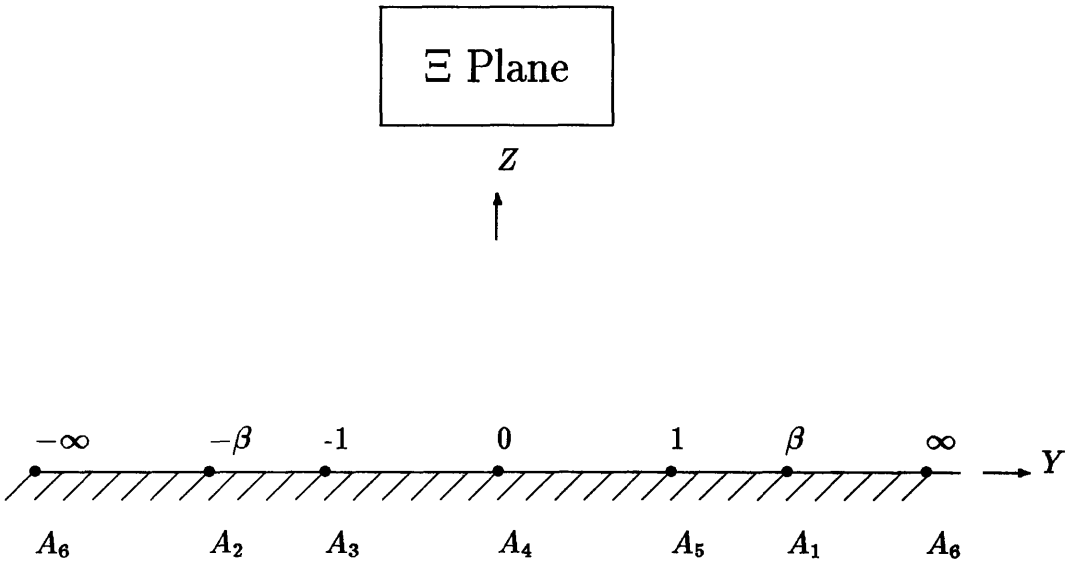

Figure 2.5: Flow domain in transformed plane (Ξ plane)

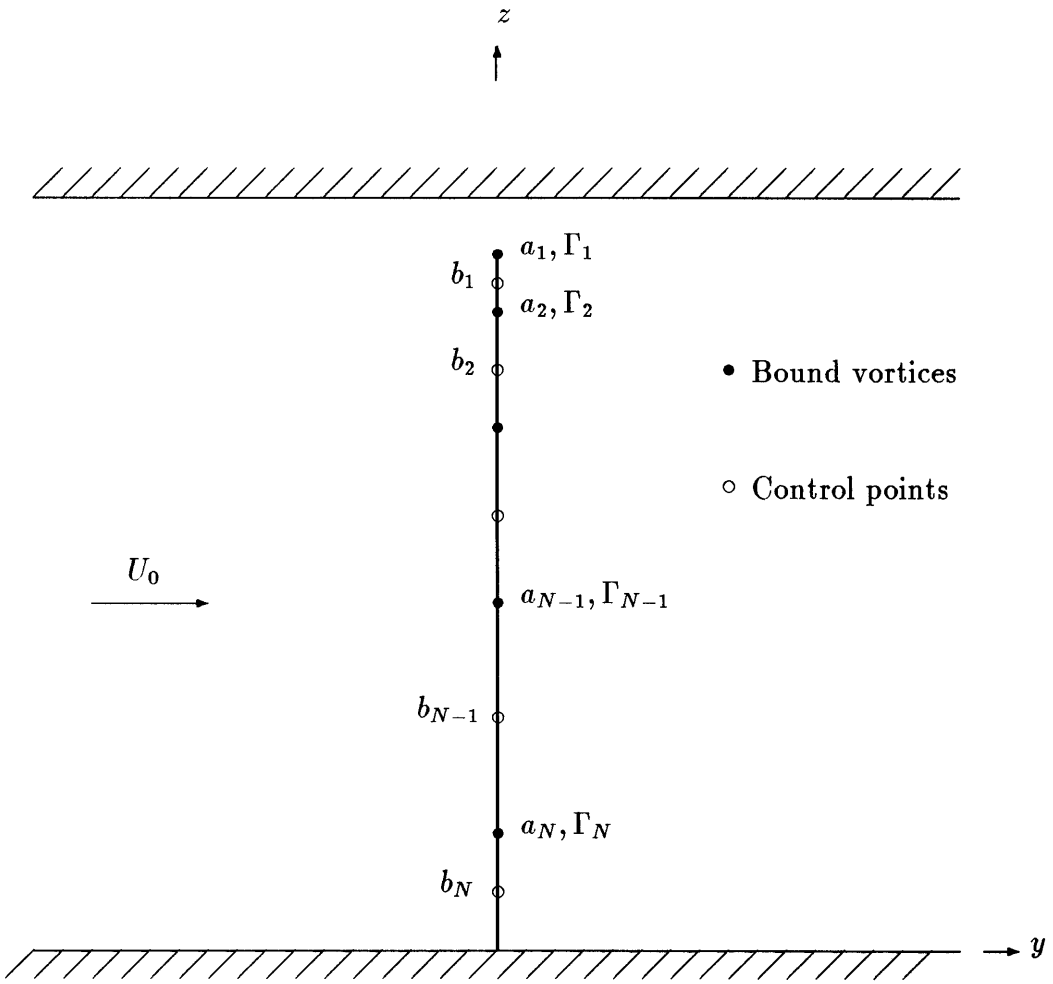

Figure 2.6: Illustration of panel method

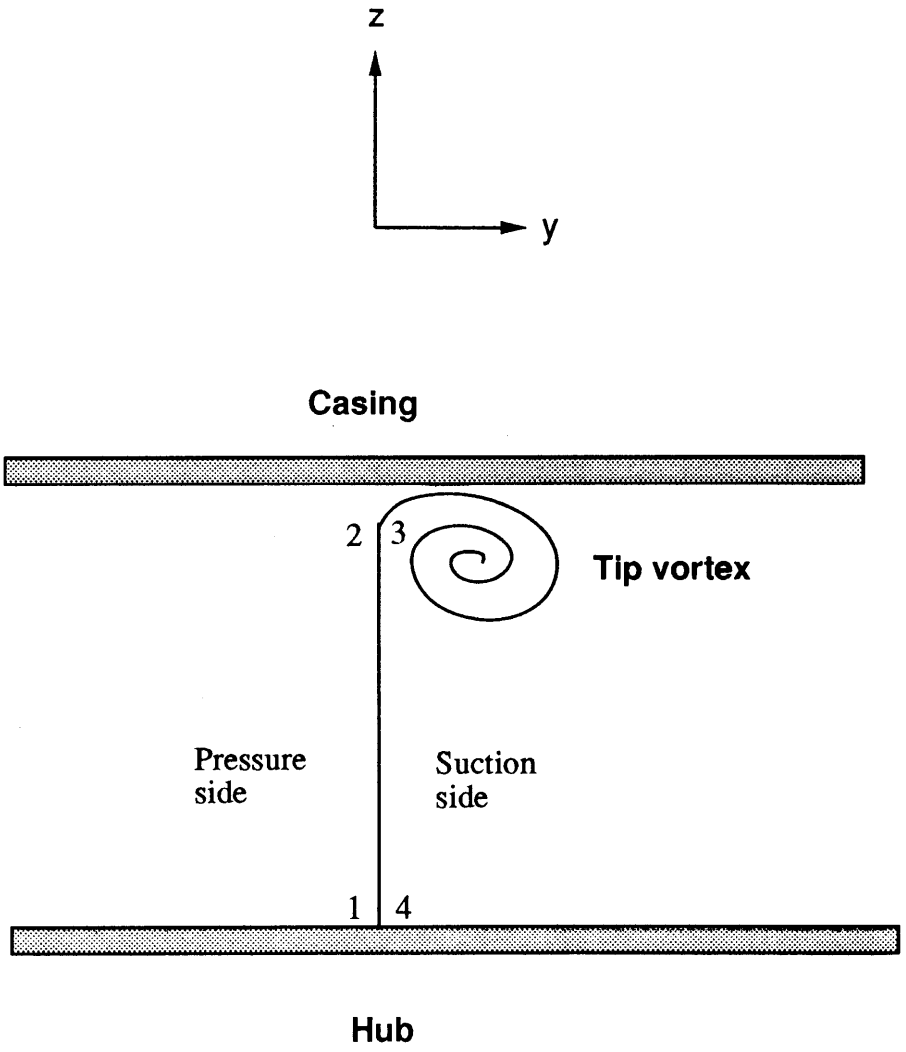

Figure 2.7: Illustration of clearance vortex in a cross flow plane

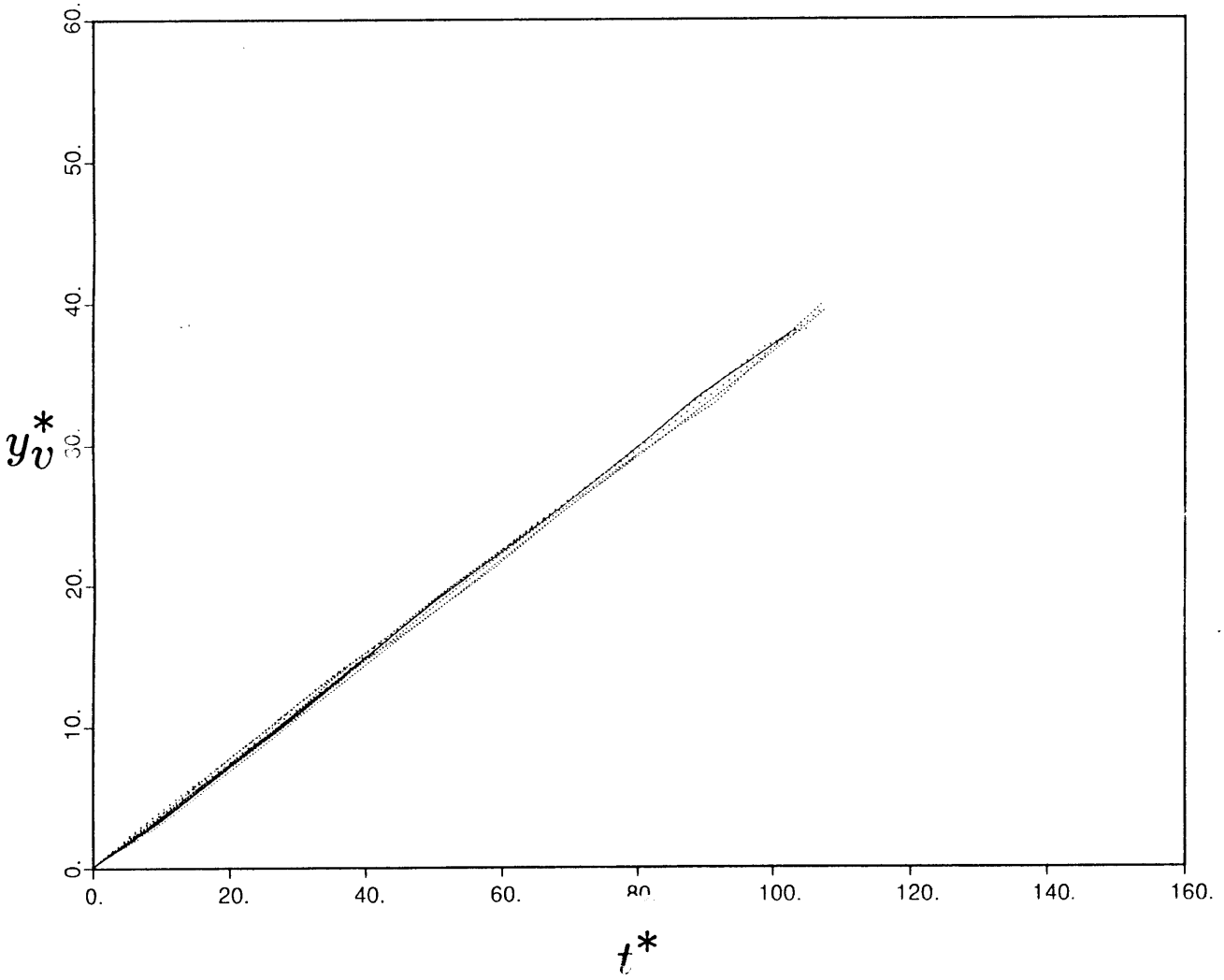

Figure 2.8: Non-dimensional vorticity centroid (y_v^*) for different time marching and subsetpping schemes

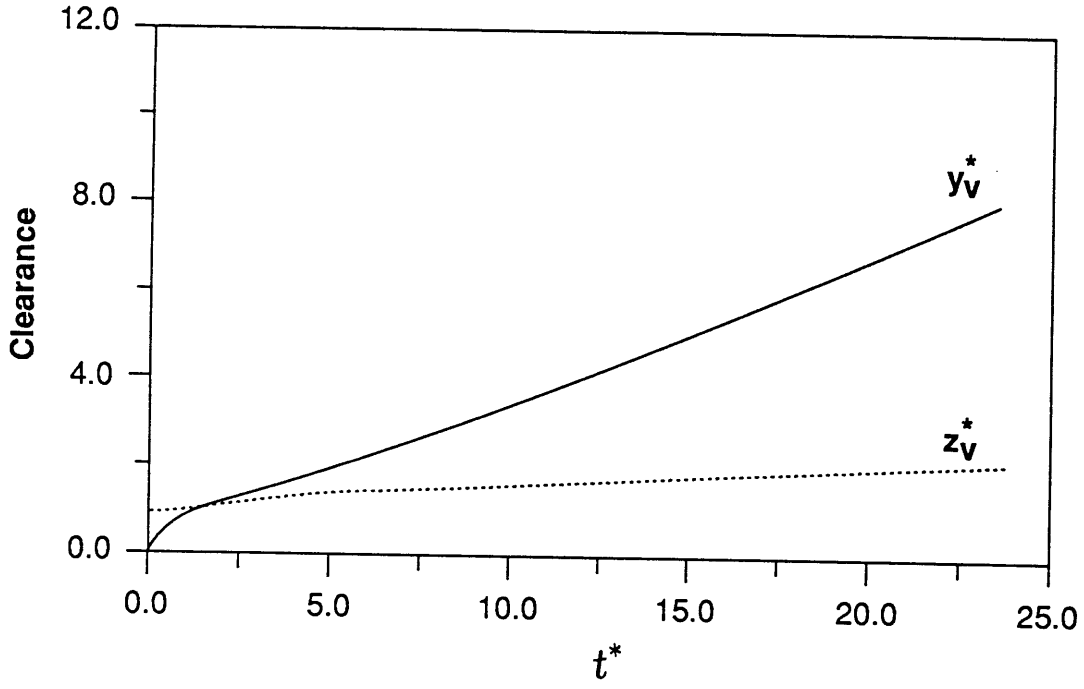

Figure 2.9: Non-dimensional coordinates of vorticity centroid for tip clearance vortex

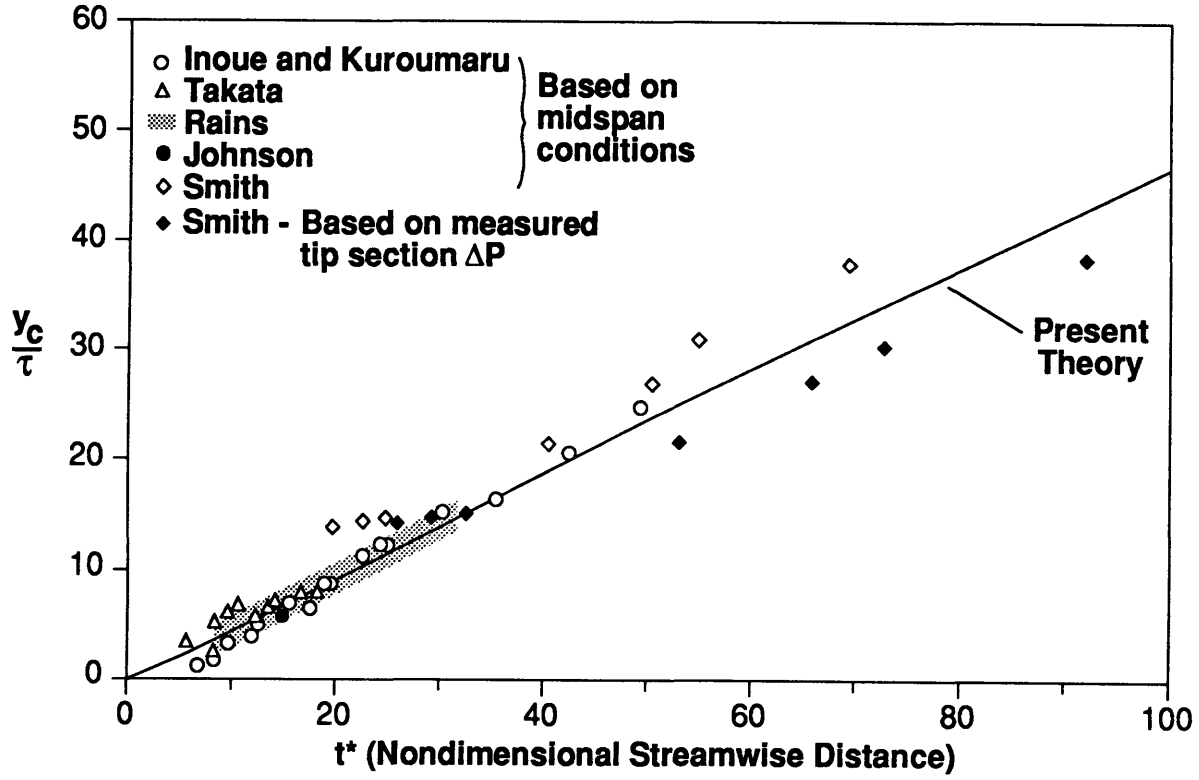

Figure 2.10: Generalized tip clearance vortex core trajectory (projection on constant radius surface)

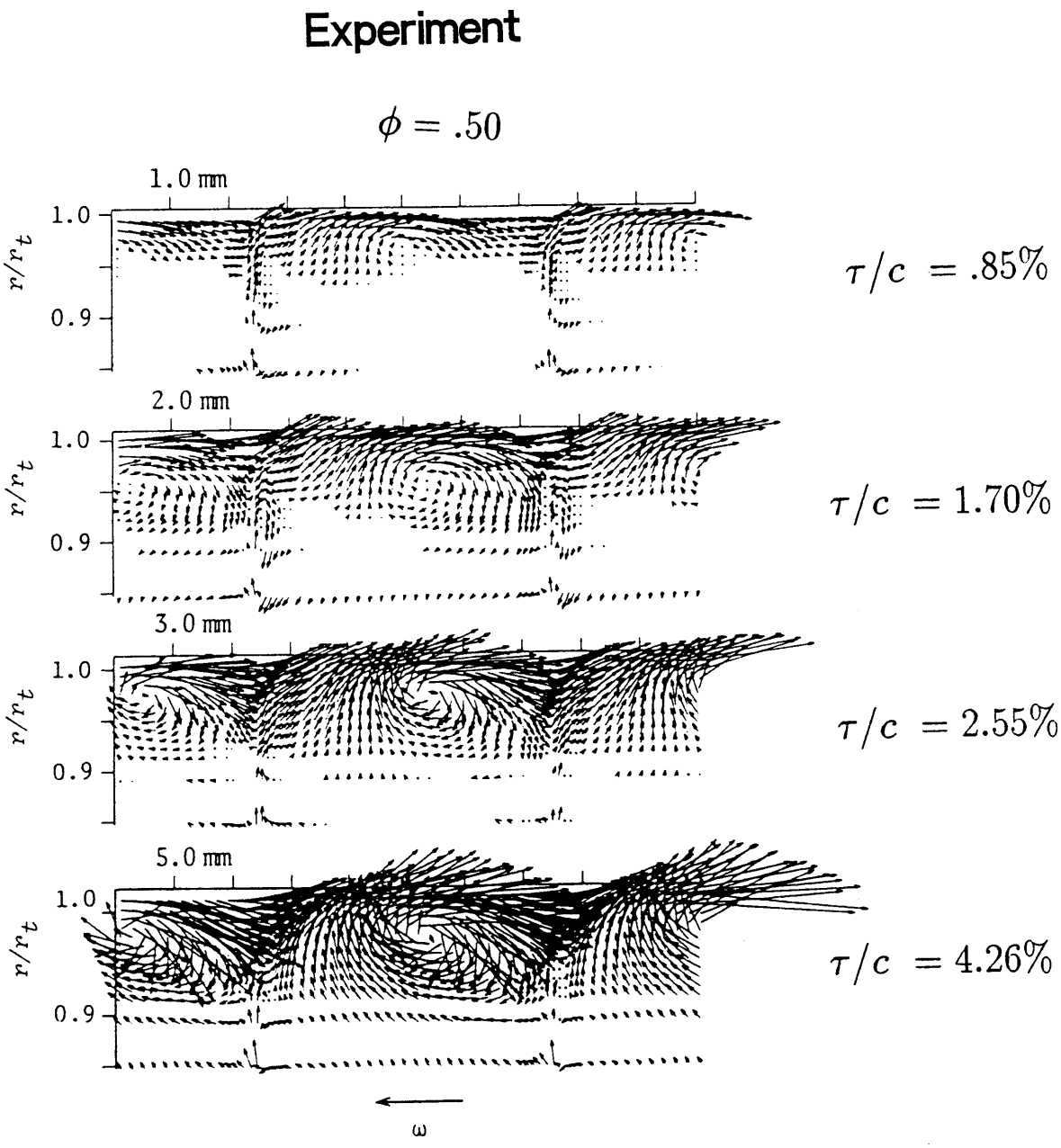

Figure 2.11: Velocity fields for various clearances (Inoue, Kuroumaru, and Fukuhara, 1986)

Chapter 3

Applications of the Model

3.1 Introduction

In this chapter we interrogate the similarity analysis of Chapter 2 in more detail to see how the cross-flow plane velocity field, the vortex trajectory *downstream* of the passage, and the casing wall pressure distribution are affected by overall flow parameters such as tip clearance and blade loading.

3.2 Flow Downstream of the Blade Row

The discussions so far has been of the vorticity and velocity field *in* the blade passage, but the flow *downstream* of the blade row is also of interest. As illustrated in Figures 3.1 and 3.2, this can be calculated by representing the tip vortex as either a single vortex (in line with the assumption made in the blade passage) or as an infinite periodic array of line vortices [1], plus the images needed to satisfy the kinematic boundary conditions at the wall. Formulas for the velocities associated with such array are given, for example, by Lamb (1932, [33]). In line with the approximation made in the passage description, the procedure is to apply such a description everywhere downstream of the cross-flow

[1] To some extent, the arguments made above that relate to only including the vorticity field of a single passage , i.e. of using just an isolated vortex, still apply. However, the influence of the other passages is stronger downstream of the trailing edge than in the passage, since the velocity field decay is dipole-like rather than quadrapole-like.

plane corresponding to the blade trailing edge. The initial conditions for the computations in the downstream region are thus the computed vortex position and strength from the passage tip clearance flow analysis at the trailing edge cross flow plane. As will be seen in the following chapter, calculations showed little difference whether an isolated vortex or a array of vortices was used downstream of the blade row although, as one might expect, the induced velocity for the vortex array was slightly higher than for an isolated vortex.

3.3 Velocity and Vorticity in the Exit Cross-Flow Plane

Inoue, Kuroumaru, and Fukuhara (1986, [24]) have made detailed flow measurements in an axial compressor rotor with various tip clearances and this provides information about the effect of tip clearance on leakage flow. Calculations have been carried out based on the parameters used in the experiment. An example is given in Fig. 3.3, which shows the configuration of the vortex sheet in the cross-flow plane passing through the trailing edge, for a clearance of 2.55 % of chord. Similar behavior is seen at other clearances. The shed vorticity can be regarded as parceled into the tip clearance vortex and an umbilical stretching form the blade tip to the vortex. Although this structure is somewhat similar to that of the flow around a delta wing , there is an important difference because of the presence (and proximity) of the wall and hence of the image vortex system.

Figs. 3.4 and 3.5 presents the cross-flow plane velocity distribution at the cross flow plane passing through trailing edge for four different clearances 0.85, 1.70, 2.55, and 4.26 percent of chord. The velocity vectors shown are normalized with blade tip speed and reference velocity magnitudes are indicated in the figure. The spanwise extent of the influence of the clearance flow is seen to increase as the tip clearance increases.

Fig. 3.6 show the clearance flows for various clearances (0.85, 1.70, 2.55, and 4.26

percent of chord) in an *axial* plane 6.8 % downstream of the trailing edge. These can be quantitatively compared with the experimental measurement of Inoue, Kuroumaru, and Fukuhara (1986, [24]), which are shown in Fig. 3.7. Computed contours of exit flow angle deviation at this axial plane for the different clearances are given in Figs. 3.8 - 3.11 and contours of pitch angles are given in Figs. 3.12 - 3.15. Numbers on the contour plots indicate yaw or pitch angles in degree. Columns in the figures indicate contour intervals. There is substantial underturning (roughly thirty degrees) near the casing wall due to the clearance flow as well as changes in pitch angles of roughly ten degrees. Although the "center of action" shifts with clearance, there is not much change in the magnitudes of these two angles as clearance varies.

Computed and measured of yaw and pitch angle deviations and cross-flow velocity are plotted in Fig. 3.16 for the 2.55 % case. It can be seen that the overall flow structure is well captured by the computation.

It should be emphasized that other authors have shown that a good picture of the cross-flow plane vorticity distribution yield reasonable estimates for the flow field. What is different in the present comparison is that the only information used is midspan inlet and exit flow angles, axial velocity parameter, and camber line. No empirical input is given concerning vortex position and strength.

3.4 Vortex Core Trajectory

We now examine the vortex core trajectory, both in the passage and downstream. As discussed previously, the flow downstream of the blade can be calculated either by representing the tip vortex as a single vortex as in the blade passage, or as a periodic infinite array of line vortices, plus the images needed to satisfy the kinematic boundary condition at the wall. Calculations have been carried out using these two approaches.

Figs. 3.17 - 3.20 show the computed trajectories for different clearances using the data of Inoue, Kuroumaru, and Fukuhara (1986, [24]) and Inoue and Kuroumaru (1988, [23]). Figs. 3.17 and 3.18 are based on a single vortex downstream, whereas, Figs. 3.19

and 3.20 are based on an infinite periodic array of line vortices.

The independence, of the trajectory within the passage, on clearance (as discussed previously) can be seen in the figures, which encompass a factor of five in tip clearance. In addition, in the single vortex approach, the tip vortex moves under the influence of the induced velocity by its image only. With the vortex array, the induced velocity from other vortices are in the direction of the motion and the array will move faster than the single vortex; this can be seen from comparing , for example, Figs. 3.17 and 3.19. Although the vortex array method yields better agreement with the data than the single vortex representation, the difference is small.

An evident feature of the trajectories is the change in slope at the exit cross-flow plane. This can be explained with reference to the image system of the tip clearance vortex, drawn schematically in Fig.3.21. The left-hand side of the figure shows a vortex (a) near a blade, with the three images needed to satisfy the relevant kinematic constraints (neglecting the non-zero velocity in the clearance region). On the right, the vortex is shown in the region downstream of the blade, where there is only one image vortex (b). The horizontal velocity of vortex a due to b alone is greater than that due to b and c (d induces no horizontal velocity), so that the cross-flow plane velocity is larger downstream of the blade. For constant axial velocity, the slope of the trajectory will thus be larger in the downstream region. (There is also an effect due to the vorticity in the umbilical sheet between blade tip and vortex, but this is small compared to that associated with the image system.)

In the actual situation, there will not be a slope discontinuity since the influence of the blade decays in a finite distance, rather than abruptly as in the model. However, the change in the slope of the vortex trajectory can still be rather sharp, as seen in Fig. 3.22, which is a photograph of tip vortex cavitation in an axial flow pump run in water (Rains, 1954, [43]). If the low pressure in the cavitation region is taken to correspond to the vortex core: (1) comparison can be made with the theory (which is also plotted in the figure) and the two agree well; and (2) the change in slope near the passage exit can

be noted. The change in slope has also been shown in recent numerical computational results of Storer (1990, [52]).

We can also examine the radial motion of the tip vortex as in Fig. 3.23. The calculations show that the tip vortex center initially moves away from the wall as it travels from the leading edge the trailing edge, but downstream of the trailing edge, the center of the vortex remains at a nearly constant radial locations. This can be understood if we note that the centroid of the vorticity and the center of the vortex are not very different and, within the description given by the model, the former will remain at a constant radial location in the downstream region. This behavior can be derived directly from the two statements of conservation of circulation and of impulse; the derivation is given in Appendix F. The data is somewhat sparse but it appears to bear out the idea of constant radial position.

3.5 Effect of Non-Constant Pressure Difference

To examine the influence of the assumption of constant pressure difference across the blade on the result, calculations have been carried out using a representative compressor pressure difference distribution (Cumpsty, 1989, [10]), shown in Fig. 3.24. The calculated tip vortex center using this pressure distribution is given in Fig. 3.25, where it is compared with the trajectory computed assuming a uniform pressure difference, with the mean pressure coefficient the same in the two cases. It is seen that the detailed blade pressure distribution has little effect on the evolution of the tip vortex. This implies that the influence of blade loading on the trajectory is not a local effect but is rather determined by the global blade row parameters, at least to the approximation made here.

3.6 Endwall Static Pressure Field

Another quantity given by the theory is the variation in endwall pressure, which was calculated from unsteady Euler equation. The two-dimensional unsteady model

includes no description of the variation in pressure level along the blade, because it deals only with the pressure difference. We therefore adopt the simplest hypothesis, namely that pitch averaged static pressure rises linearly from leading edge to trailing edge. The wall static pressure described is thus the predicted static pressure from the unsteady analysis, referenced to this linear background increase. The computed endwall static pressure is compared to the measurements in Fig. 3.26, which shows data from Inoue and Kuroumaru (1988,[23]) for three different tip clearances. Two trends are seen in the results. First, the magnitude of the trough in static pressure increases as the clearance decreases, because the tip vortex is closer to the endwall. Second, the location of the minimum static pressure tends to move downstream with increasing clearance. These trends appear in both data and the analysis, and can also be seen from the experimental result of Dean (1954, [13]).

3.7 Effect of Compressor Operating Point on Vortex Position

Takata (1988, [56]) has examined the effect of operating point on vortex position by measuring the trajectory of the low total pressure region in the rotor tip endwall flow for different mass flows, from design point to stall. Calculations and data from this configuration are shown in Figs. 3.27, 3.28, and 3.29 where the computed core trajectory and the regions of lowest total pressure are indicated. As might be expected, the tip vortex moves further from the suction surface as mass flow decreases because the convection time and the shed vortex sheet strength both increase. The experimental results here also show the change in slope of the tip vortex trajectory near the trailing edge.

3.8 Applications to High Speed Machines

The analysis was formulated neglecting the effects of compressibility, and comparison thus far has been with low speed compressor data. As is discussed in Appendix G,

Cases	% Design Speed	Pressure Ratio
1	90	1.32
2	90	1.52
3	95	1.60
4	100	1.37
5	100	1.51

Table 3.1: High speed data

however, the compressibility effects in the clearance flow do not appear to be important at least for a compressor. If so, the analysis can be applied to describe the behavior of high speed machines. There are considerably fewer published endwall flow field measurements for these devises, and we have found only one data set with enough information so that comparison can be made. This is a transonic fan whose performance was reported by Ware, Kobayashi, and Jachson (1973, [58]). The design speed was 489 m/s and the design pressure ratio was 1.5. Tip vortex trajectories were located using holography. (In contrast to the low speed experiments, the trajectories could not be directly inferred for the shapes of the isobars on the casing). Table 3.1 shows the flow parameters for the available data.

In Fig. 3.30 the experimental tip vortex trajectories are plotted on the similarity curve described in connection with Fig. 2.10. While the agreement may be surprising at first, examination of the data in the report indicates that pressure differences across the blades are such that the Mach numbers associated with the cross-flow plane velocities are subsonic. Even for situations in which the relative Mach numbers are larger than unity, therefore the basic ideas set forth concerning tip clearance vortex formation and evolution still can be applied. (This is analogous to a highly swept delta wing where the through flow can be supersonic, but the cross flow remains incompressible.)

3.9 Summary and Conclusions

Clearance flow in the blade passage as well as downstream of the blade trailing edge has been investigated in this chapter. A parametric study has been carried out to examine the effect of flow parameters such as tip clearance and operating point on the velocity field, flow angle deviations, casing pressure distribution, and the vortex core trajectory inside and downstream of blade passage. The effect of blade loading distribution on the vortex core trajectory has also been examined.

The calculations carried out agree well with experimental results and several interesting features of a clearance vortex have been brought out. First, there is a change in the slope of the vortex center trajectory near the trailing edge due to the change of kinematic boundary condition there. Second, as a result of conservation of circulation and impulse, the tip vortex center stays at a constant radial location downstream of the blade trailing edge. In addition, the tip vortex alters the pressure distribution on the blade near the endwall region, especially that on the suction surface. As tip clearance increases, the region of minimum pressure moves downstream and the magnitude of the minimum pressure decreases. Finally, as one may expect, the tip vortex core moves further away from the suction surface as mass flow decreases.

The analysis has also been applied to describe the vortex trajectory in a high speed machine. The prediction agrees well with the experimental data, indicating the compressibility effect in the clearance flow is not important. In addition, an expression for the clearance flow Mach number is derived and this quantity is shown to be significantly less than unity from many practical situations in fan and compressors.

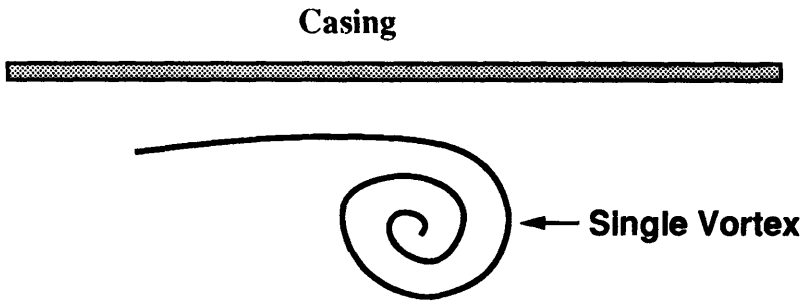

Figure 3.1: Schematic of tip vortex downstream (Single tip vortex)

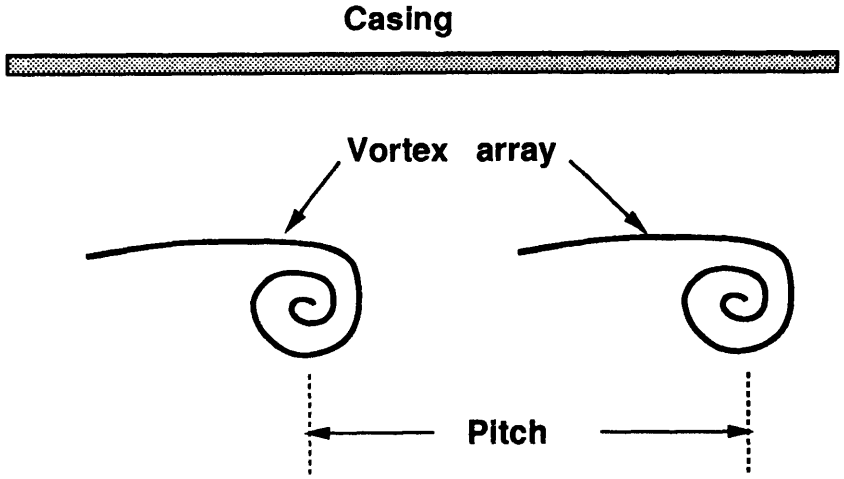

Figure 3.2: Schematic of tip vortex downstream (Vortex array)

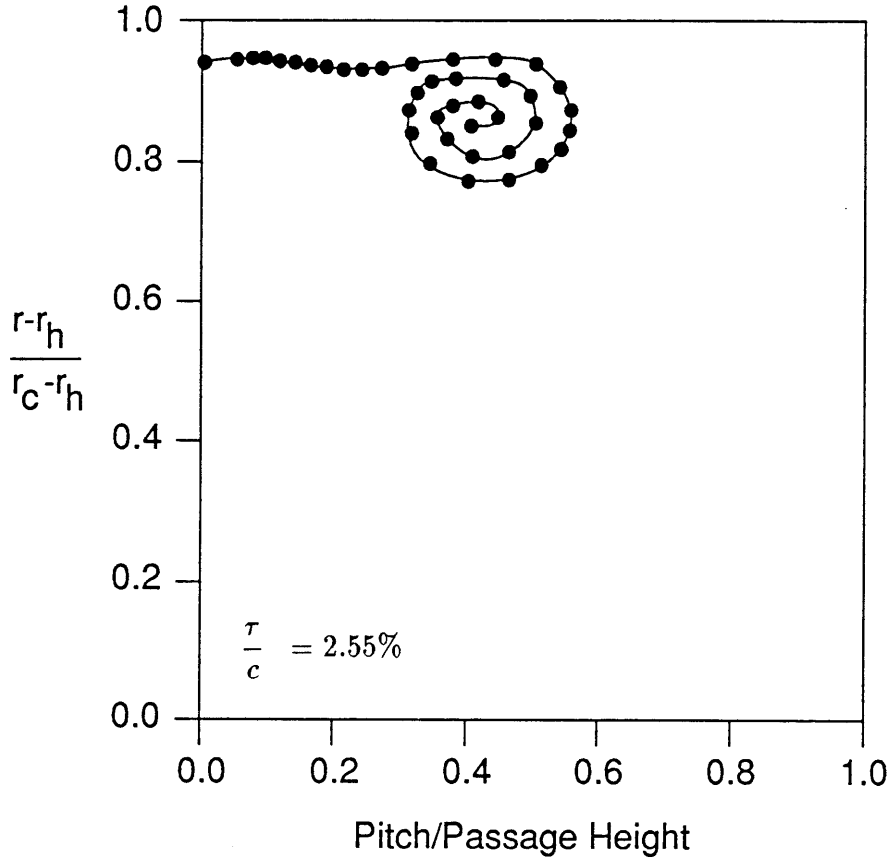

Figure 3.3: Computed vorticity distribution at passage exit cross-plane; parameters based on data of Inoue, Kuroumaru, and Fukuhara, 1986 ($\phi = 0.5$, $\tau/c = 2.55\%$)

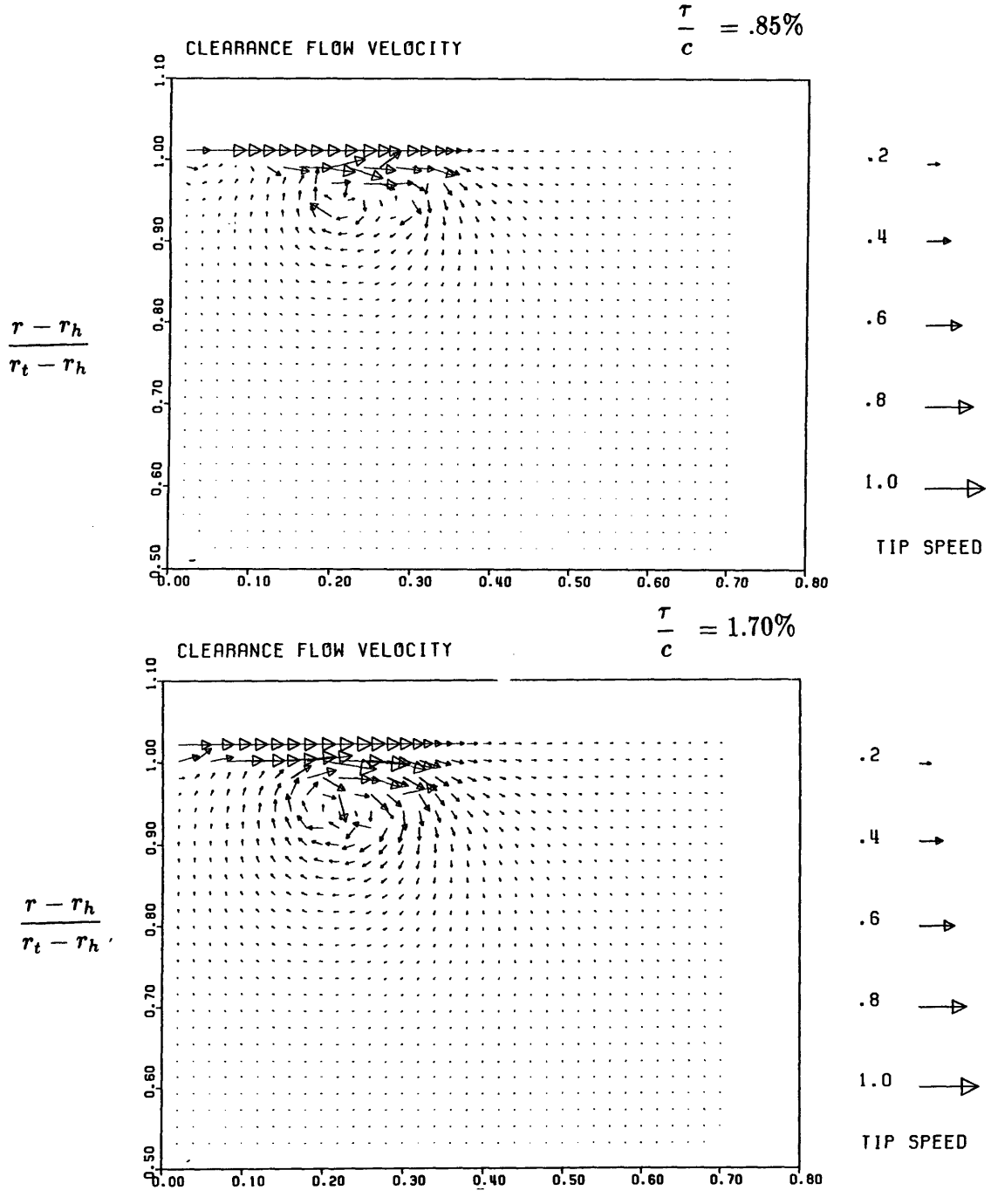

Figure 3.4: Cross-flow plane velocity at passage exit for two different tip clearances; parameters based on data of Inoue, Kuroumaru, and Fukuhara, 1986 ($\phi = 0.5$, $\tau/c =$ 0.85% and 1.70%)

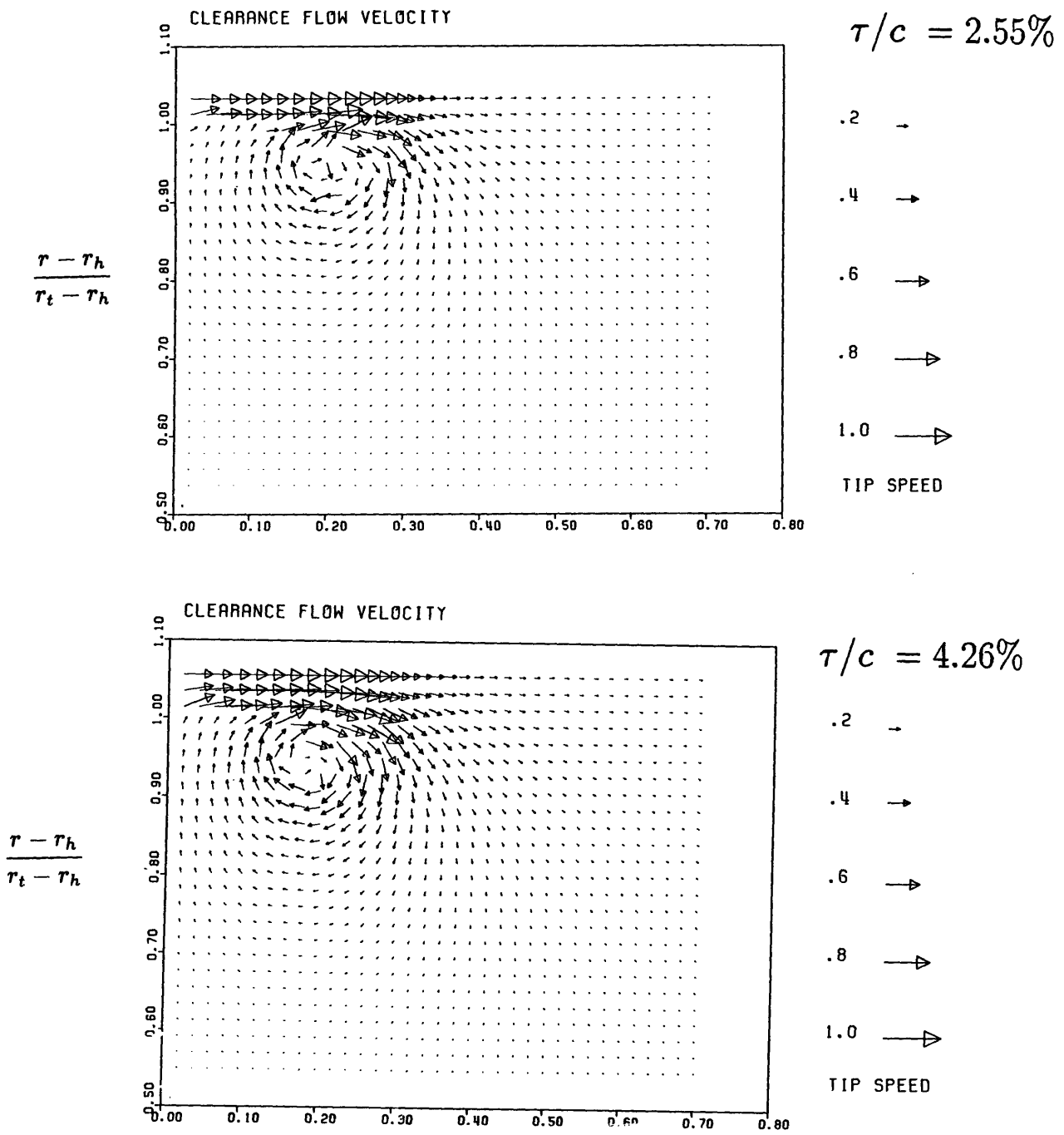

Figure 3.5: Cross-flow plane velocity at passage exit for two different tip clearances; parameters based on data of Inoue, Kuroumaru, and Fukuhara, 1986 ($\phi = 0.5$, $\tau/c =$ 2.55% and 4.26%)

Calculation

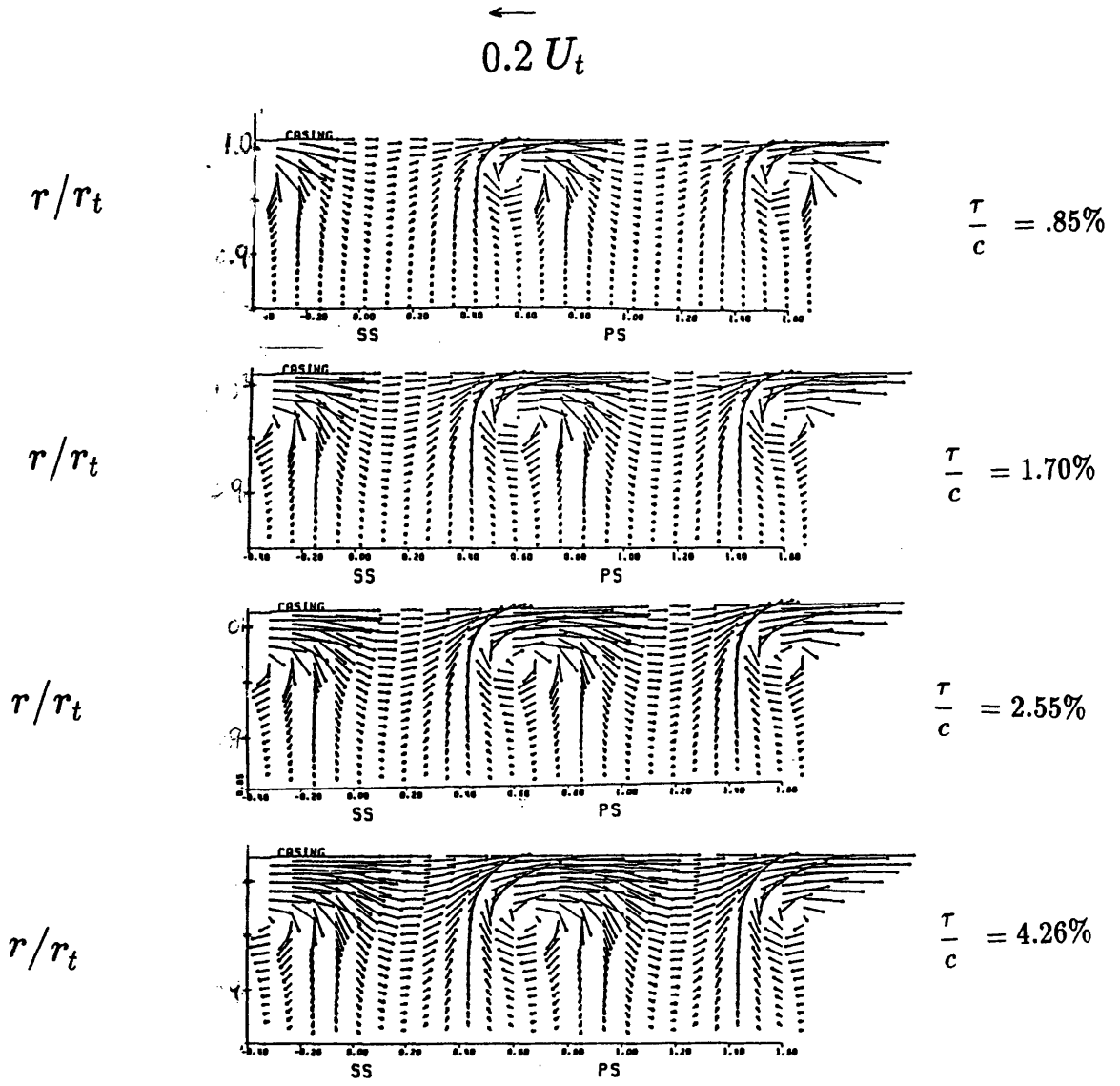

Figure 3.6: Computed clearance flow downstream of a rotor trailing edge; parameters based on data of Inoue, Kuroumaru, and Fukuhara, 1986 ($\phi = 0.5, r_h/r_t = 0.6$)

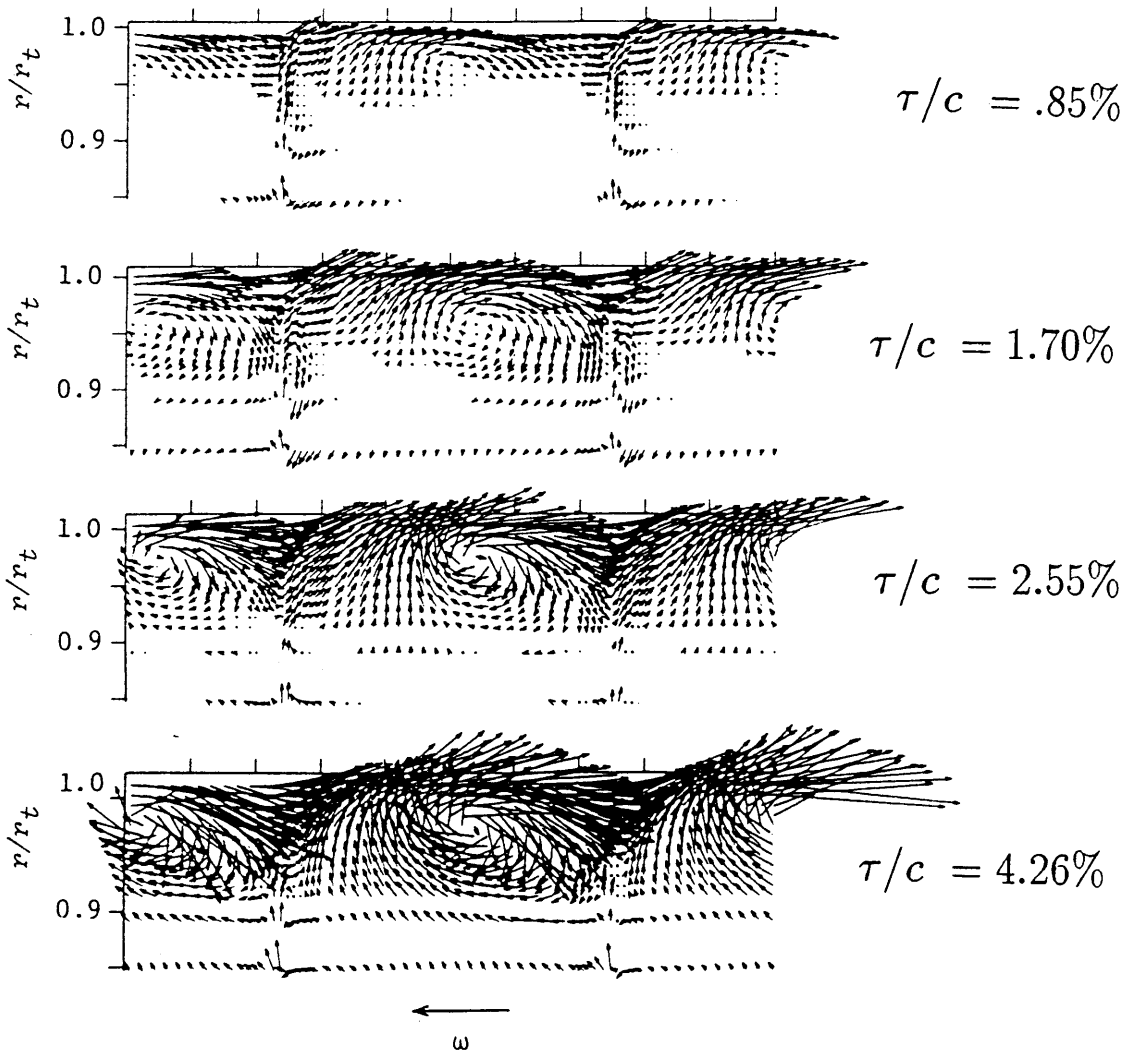

Figure 3.7: Clearance flow near a rotor trailing edge (Inoue, Kuroumaru, and Fukuhara, 1986)

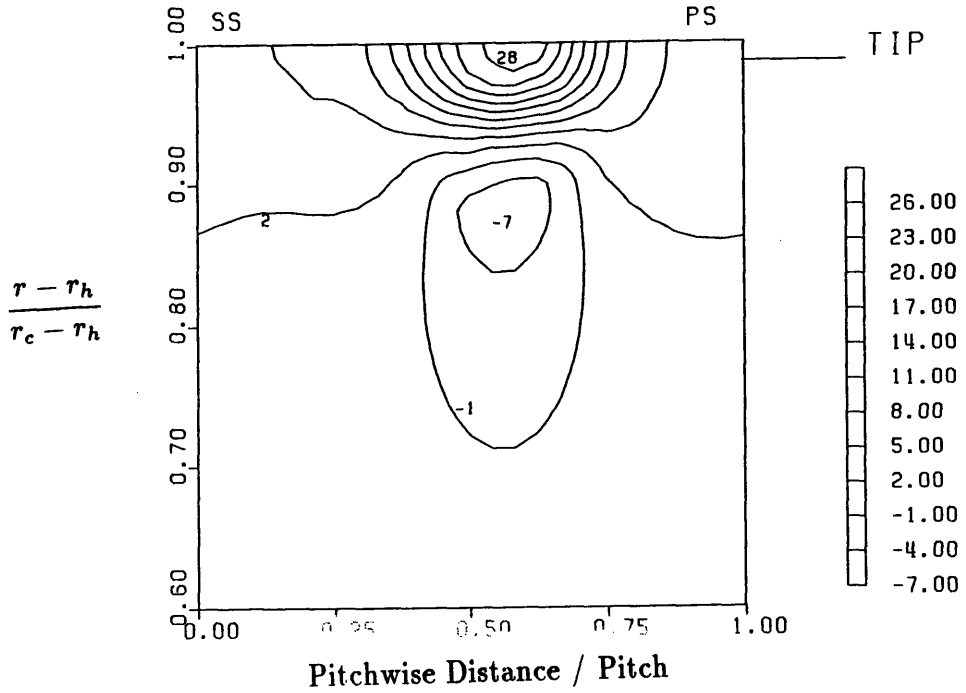

Figure 3.8: Computed exit flow angle deviation due to clearance flow ; parameters based on data of Inoue, Kuroumaru, and Fukuhara, 1986 ($\phi = 0.5$, $\tau/c = 0.85\%$)

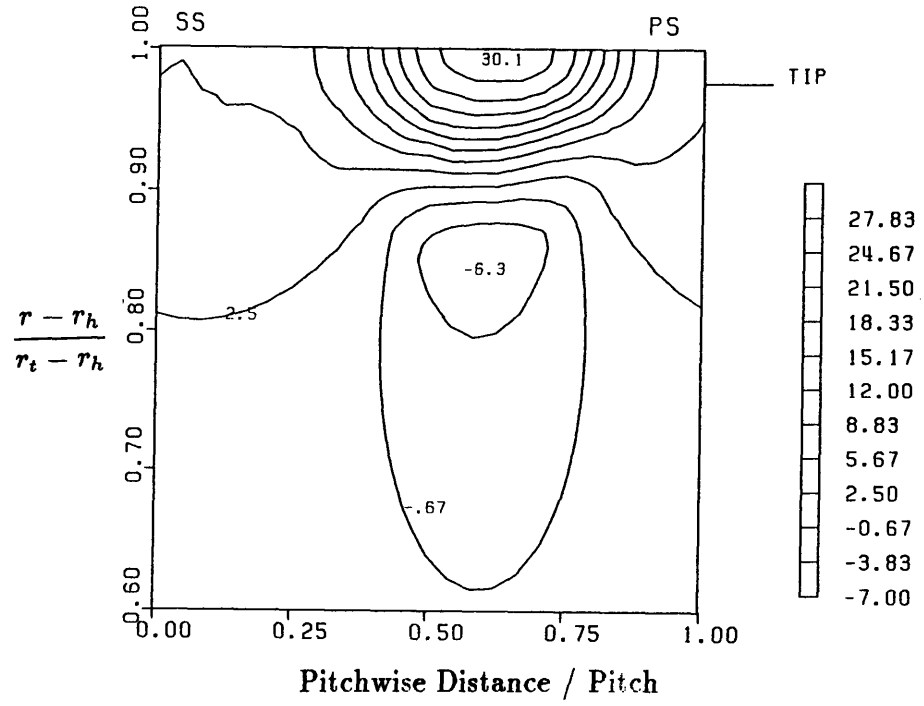

Figure 3.9: Computed exit flow angle deviation due to clearance flow; parameters based on data of Inoue, Kuroumaru, and Fukuhara, 1986 ($\phi = 0.5$, $\tau/c = 1.70\%$)

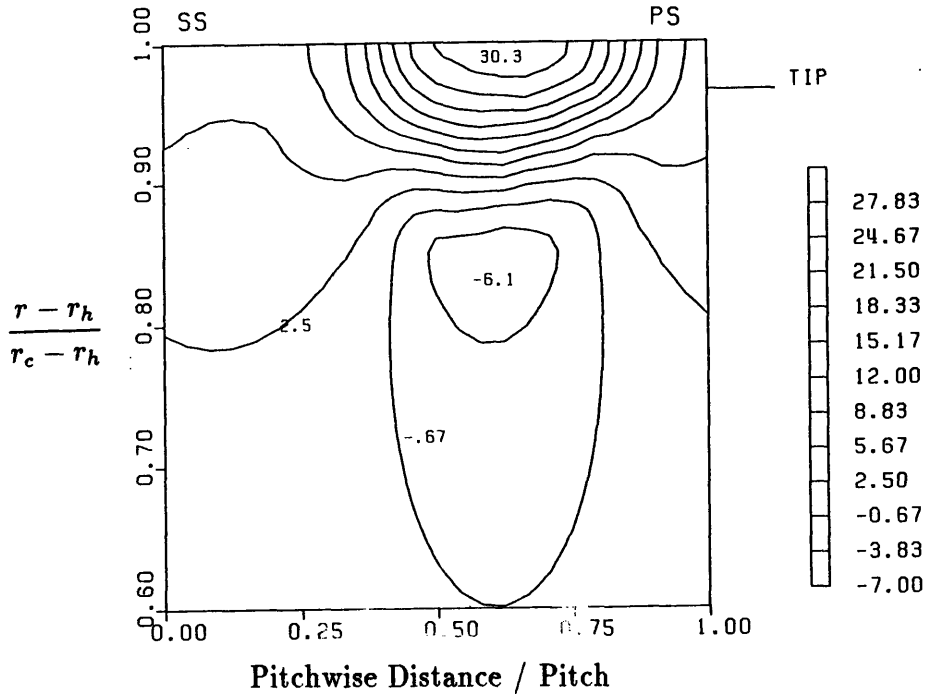

Figure 3.10: Computed exit flow angle deviation due to clearance flow; parameters based on data of Inoue, Kuroumaru, and Fukuhara, 1986 ($\phi = 0.5$, $\tau/c = 2.55\%$)

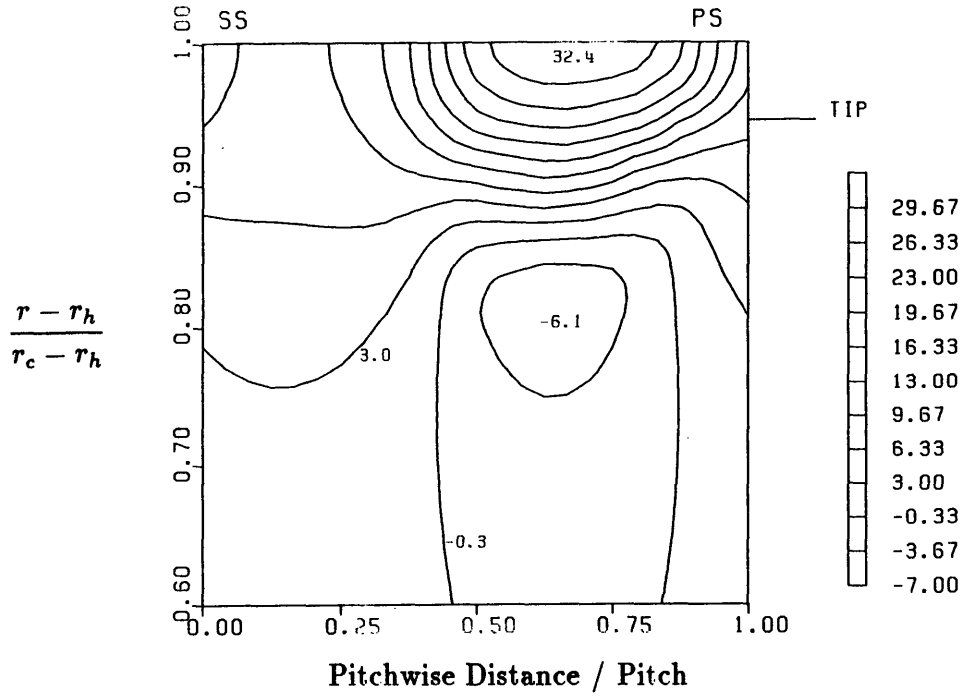

Figure 3.11: Computed exit flow angle deviation due to clearance flow; parameters based on data of Inoue, Kuroumaru, and Fukuhara, 1986 ($\phi = 0.5$, $\tau/c = 4.26\%$)

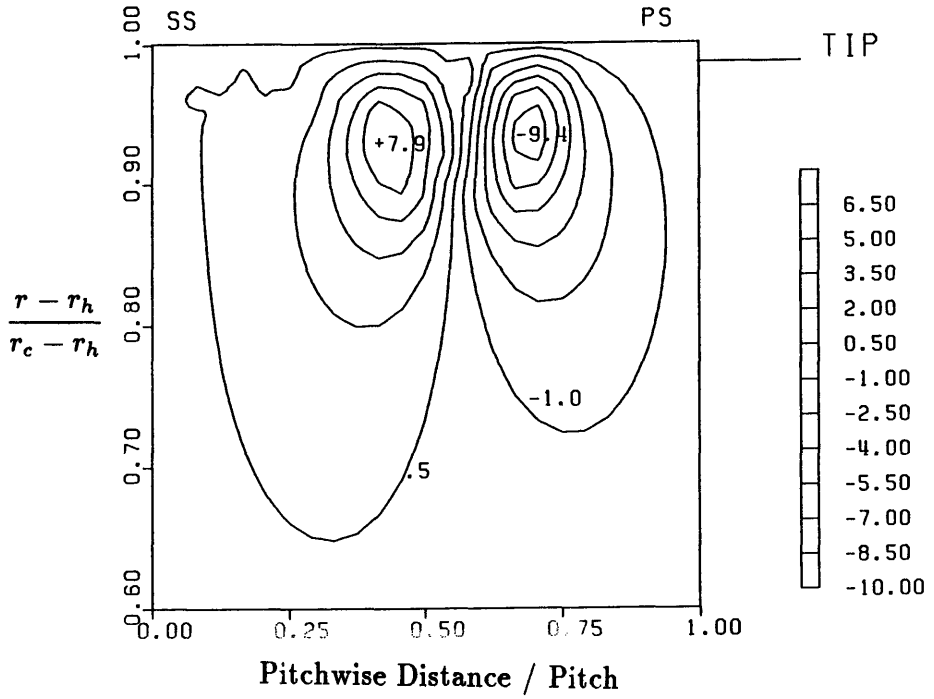

Figure 3.12: Computed exit pitch angles due to clearance flow; parameters based on data of Inoue, Kuroumaru, and Fukuhara, 1986 ($\phi = 0.5$, $\tau/c = 0.85\%$)

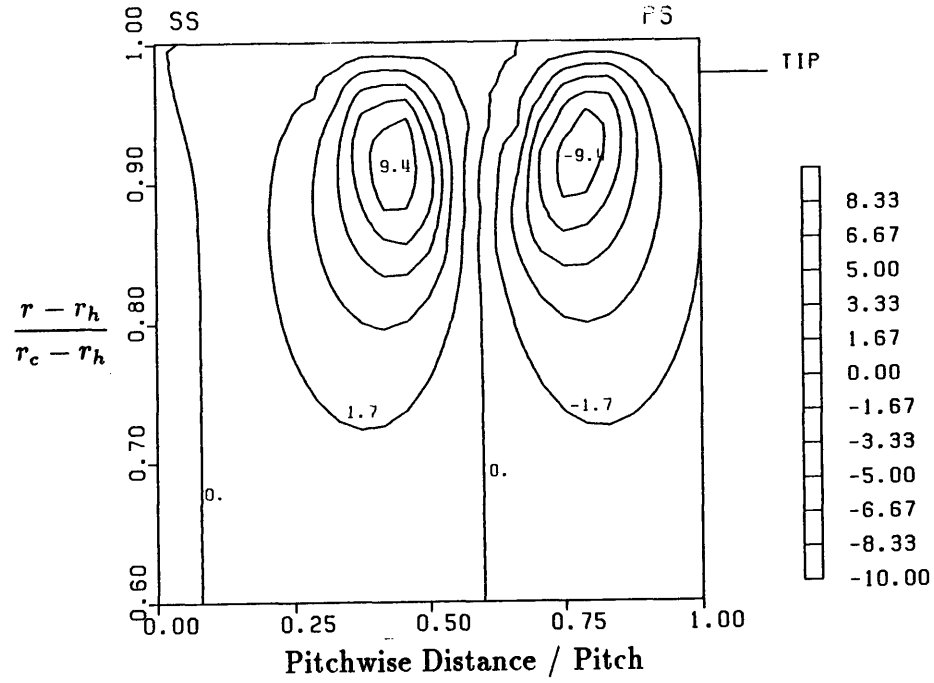

Figure 3.13: Computed exit pitch angles due to clearance flow; parameters based on data of Inoue, Kuroumaru, and Fukuhara, 1986 ($\phi = 0.5$, $\tau/c = 1.70\%$)

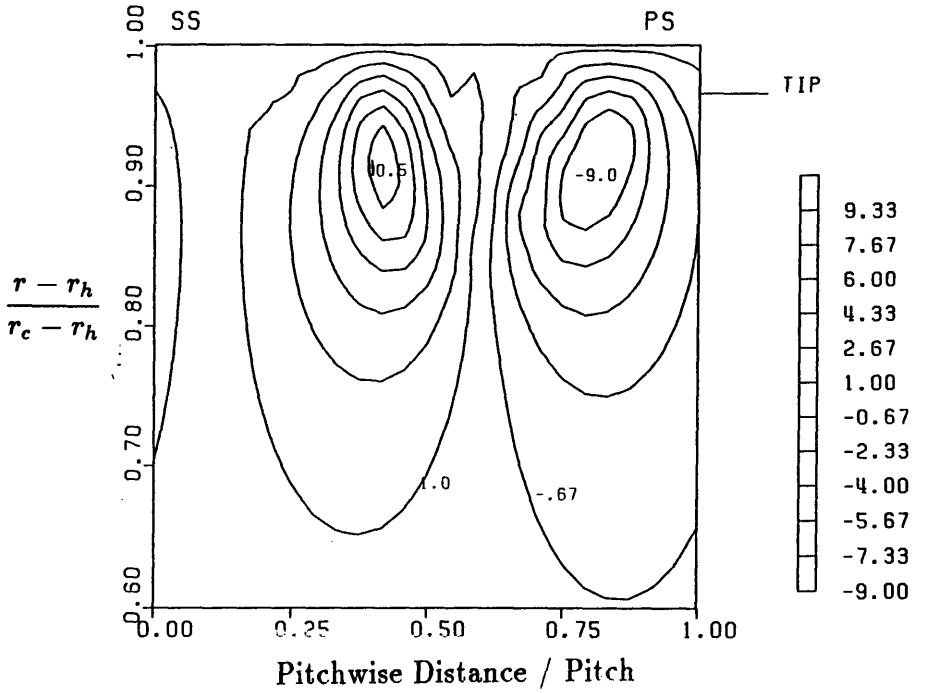

Figure 3.14: Computed exit pitch angles due to clearance flow; parameters based on data of Inoue, Kuroumaru, and Fukuhara, 1986 ($\phi = 0.5$, $\tau/c = 2.55\%$)

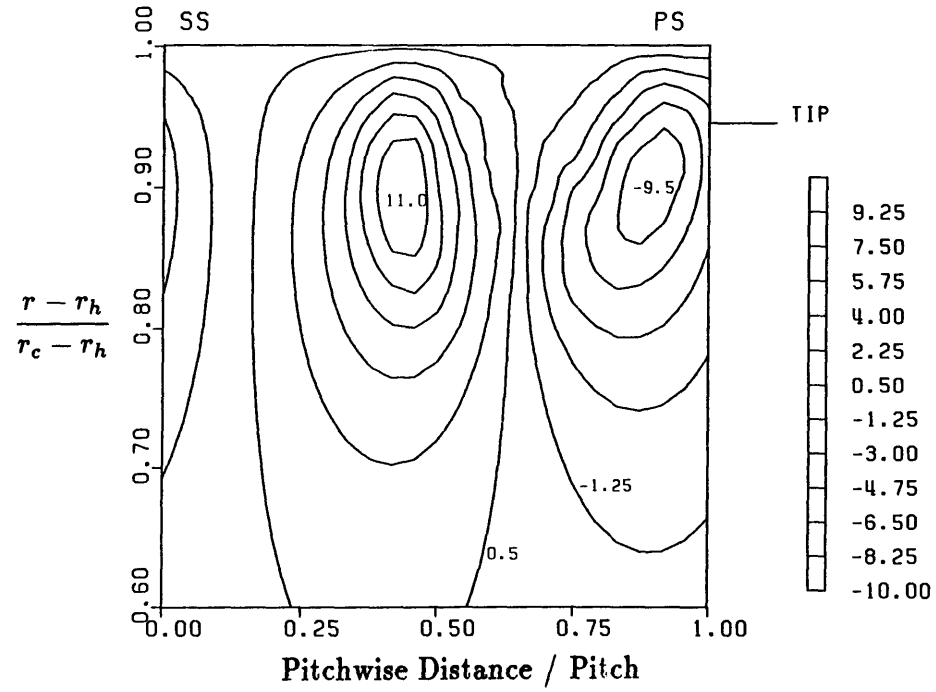

Figure 3.15: Computed exit pitch angles due to clearance flow; parameters based on data of Inoue, Kuroumaru, and Fukuhara, 1986 ($\phi = 0.5$, $\tau/c = 4.26\%$)

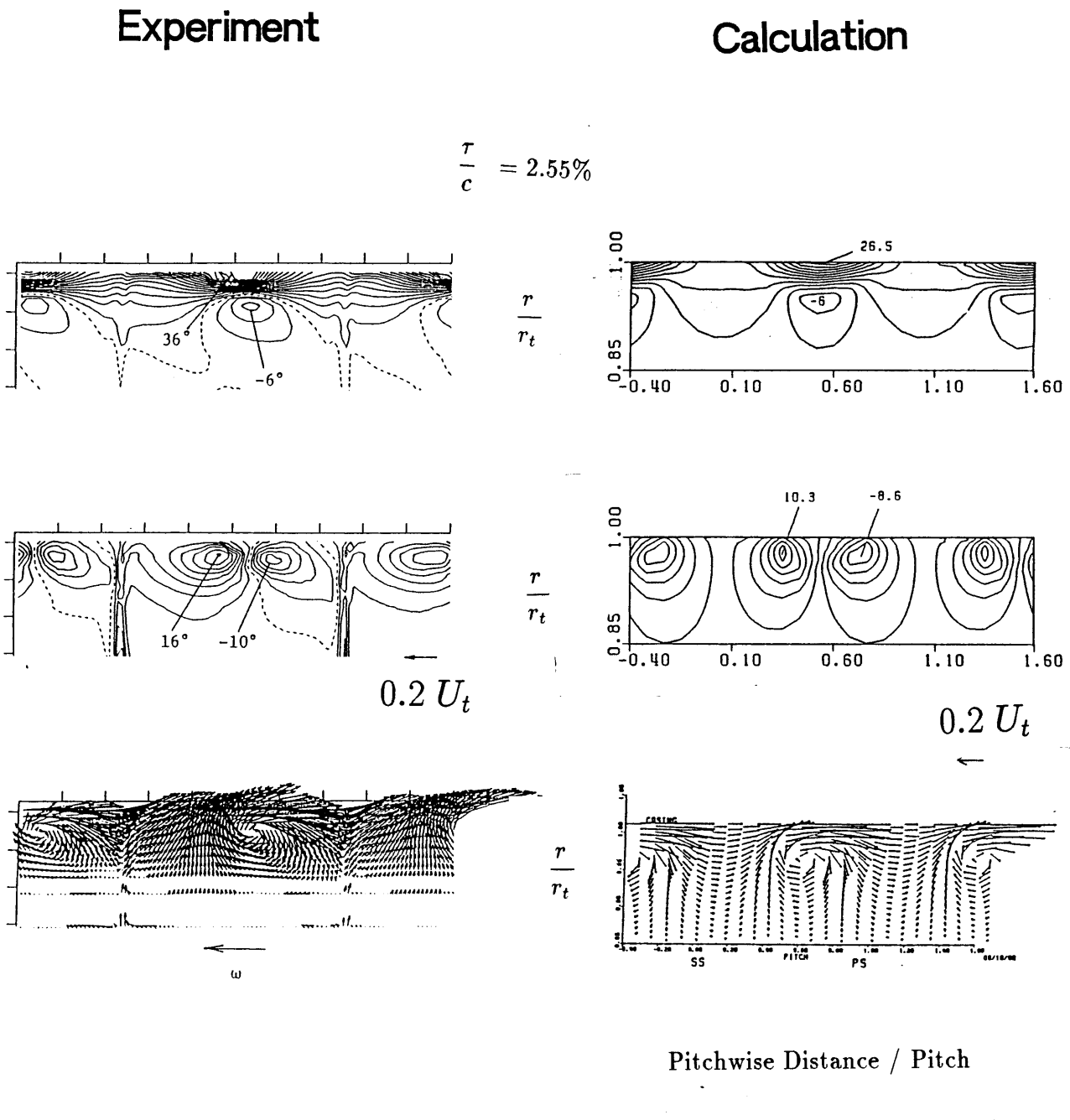

Figure 3.16: Computed and measured exit yaw angle, pitch angle, and velocity deviations from axisymmetric mean; $\phi = 0.5$, $\tau/c = 2.55\%$ (Inoue, Kuroumaru, and Fukuhara, 1986)

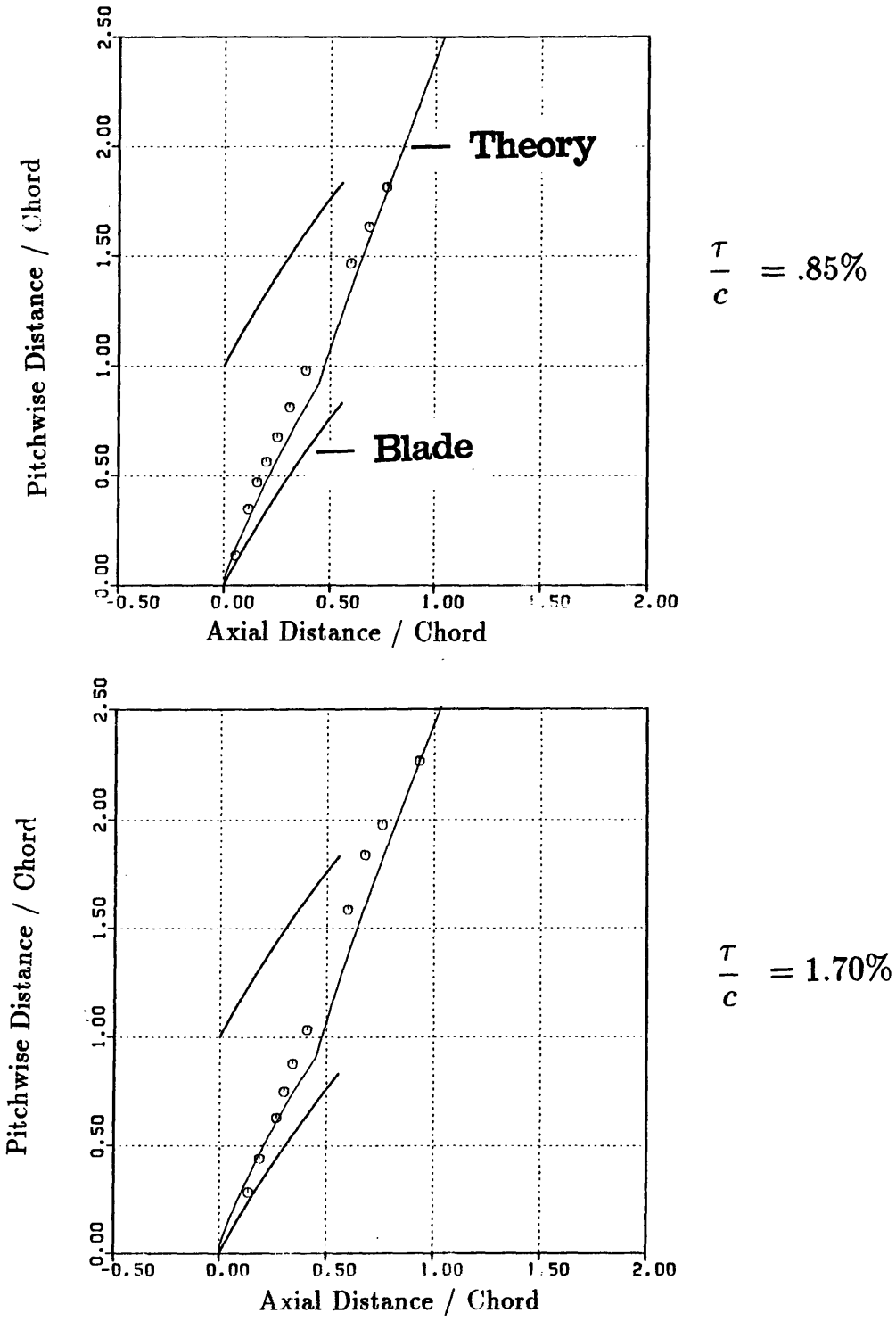

Figure 3.17: Circumferential position of clearance vortex center (y_c), data from Inoue, Kuroumaru, and Fukuhara (1986) and Inoue and Kuroumaru (1988) ; $\phi = 0.5$, $\tau/c =$ 0.85% and 1.70 % (Single vortex approach)

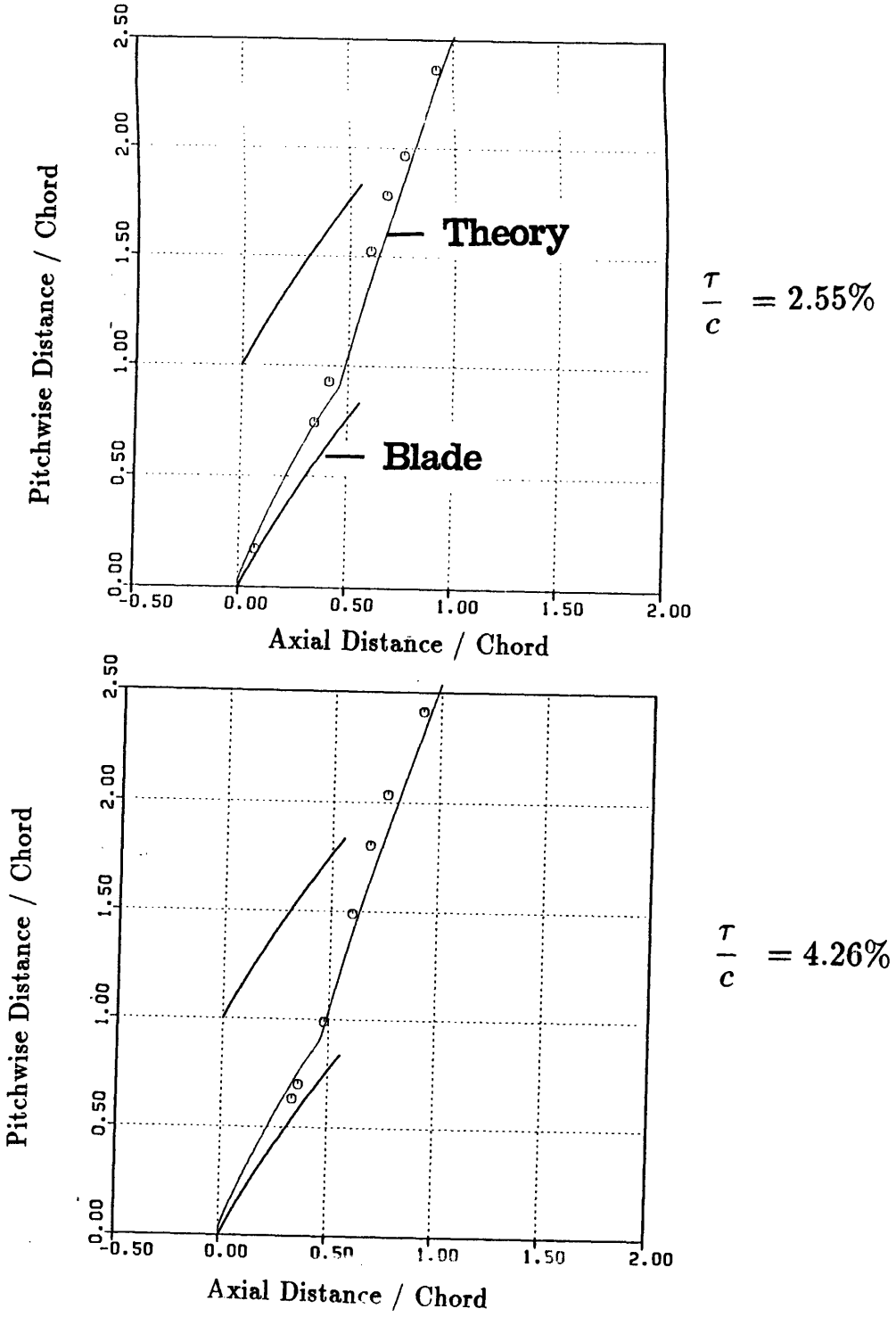

Figure 3.18: Circumferential position of clearance vortex center (y_c), data from Inoue, Kuroumaru, and Fukuhara (1986) and Inoue and Kuroumaru (1988) ; $\phi = 0.5$, $\tau/c =$ 2.55% and 4.26 % (Single vortex approach)

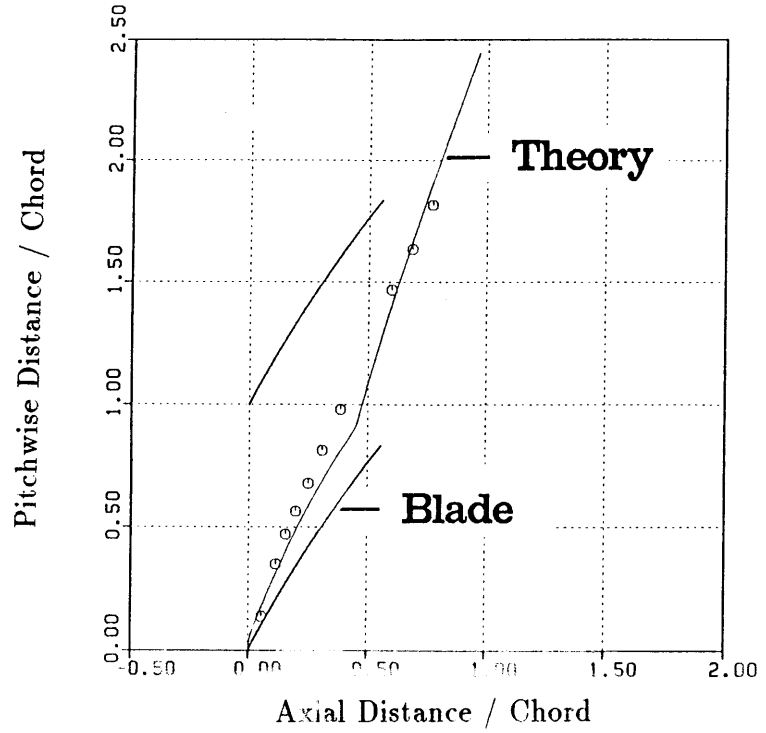

$\frac{\tau}{c} = .85\%$

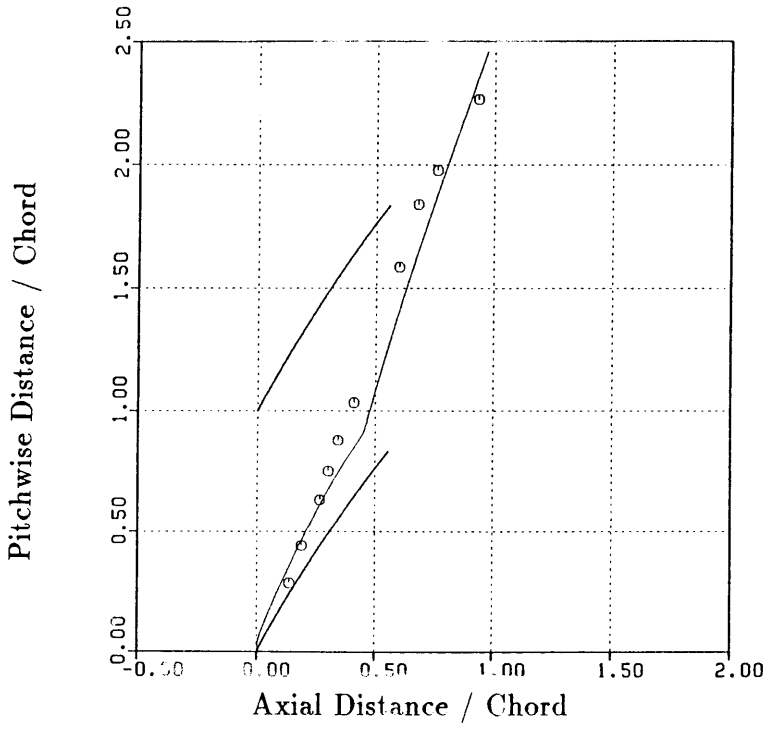

$\frac{\tau}{c} = 1.70\%$

Figure 3.19: Circumferential position of clearance vortex center (y_c), data from Inoue, Kuroumaru, and Fukuhara (1986) and Inoue and Kuroumaru (1988); $\phi = 0.5$, $\tau/c =$ .85% and 1.70 % (Vortex array approach)

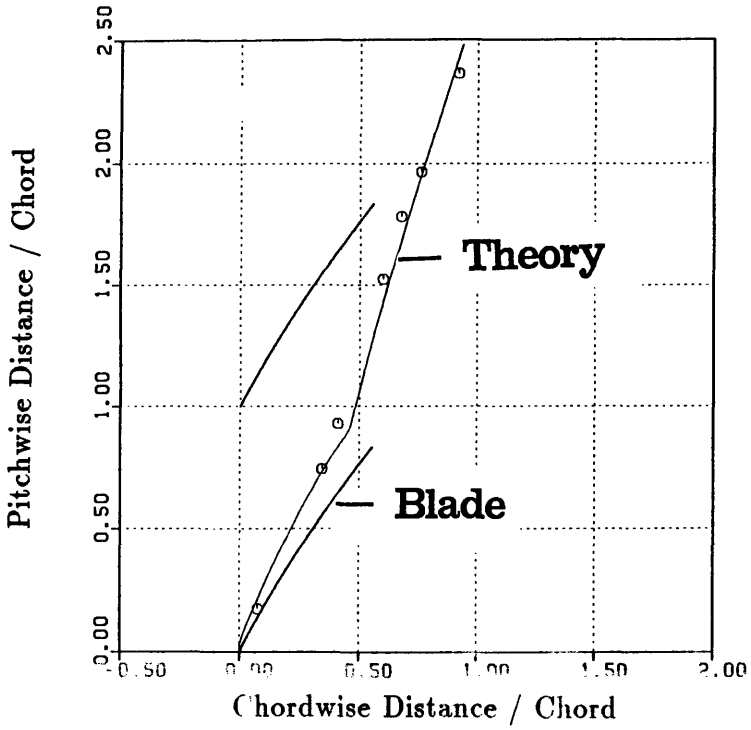

$\frac{\tau}{c} = 2.55\%$

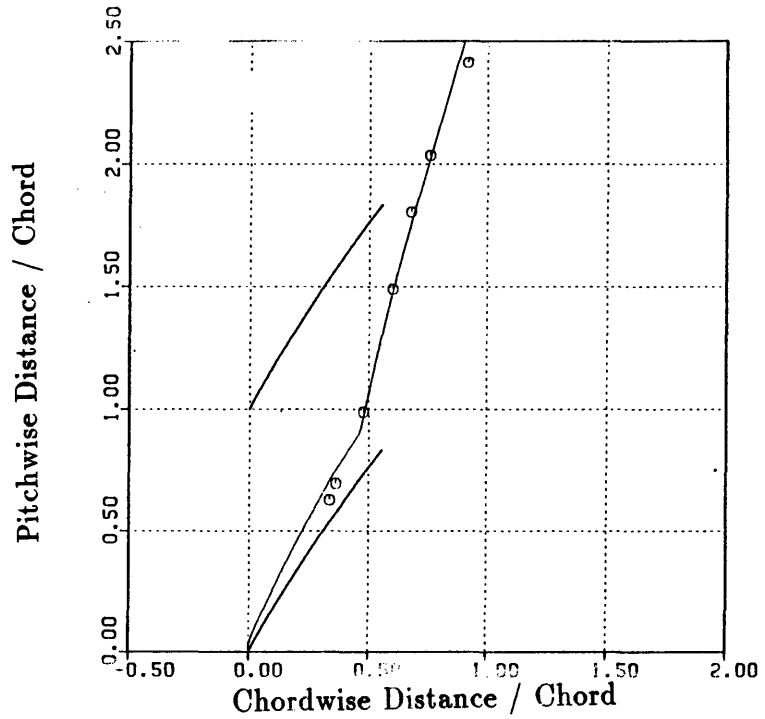

$\frac{\tau}{c} = 4.26\%$

Figure 3.20: Circumferential position of clearance vortex center (y_c), data from Inoue, Kuroumaru, and Fukuhara (1986) and Inoue and Kuroumaru (1988); $\phi = 0.5$, $\tau/c = 2.55\%$ and 4.26 % (Vortex array approach)

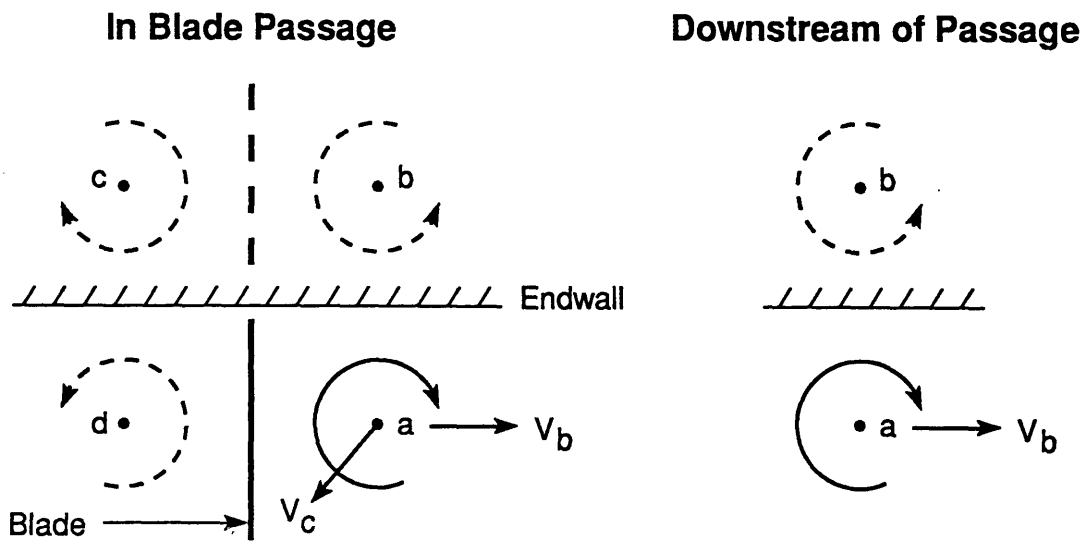

Figure 3.21: Vortex and image system in passage and downstream

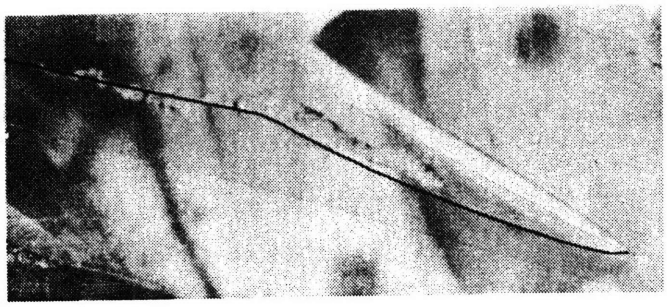

$(a)\tau/c = 2.6\%,\ \phi = .45$

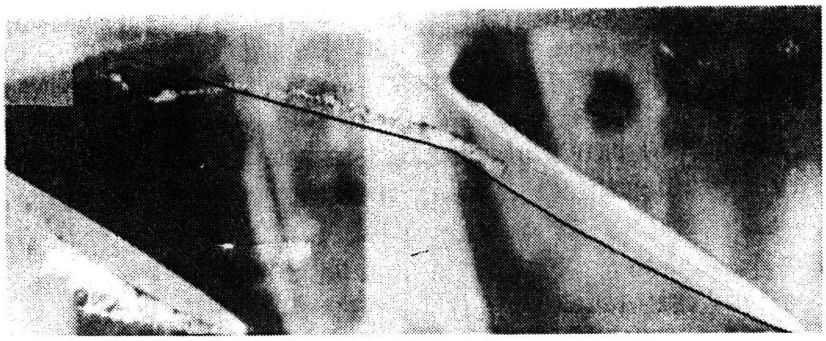

$(b)\tau/c = 5.2\%,\ \phi = .45$

Figure 3.22: Vortex trajectory shown by cavitation (data of Rains, 1954); solid line shows calculations based on present theory, (a) $\tau/c = 2.6\%$, (b) $\tau/c = 5.2\%$

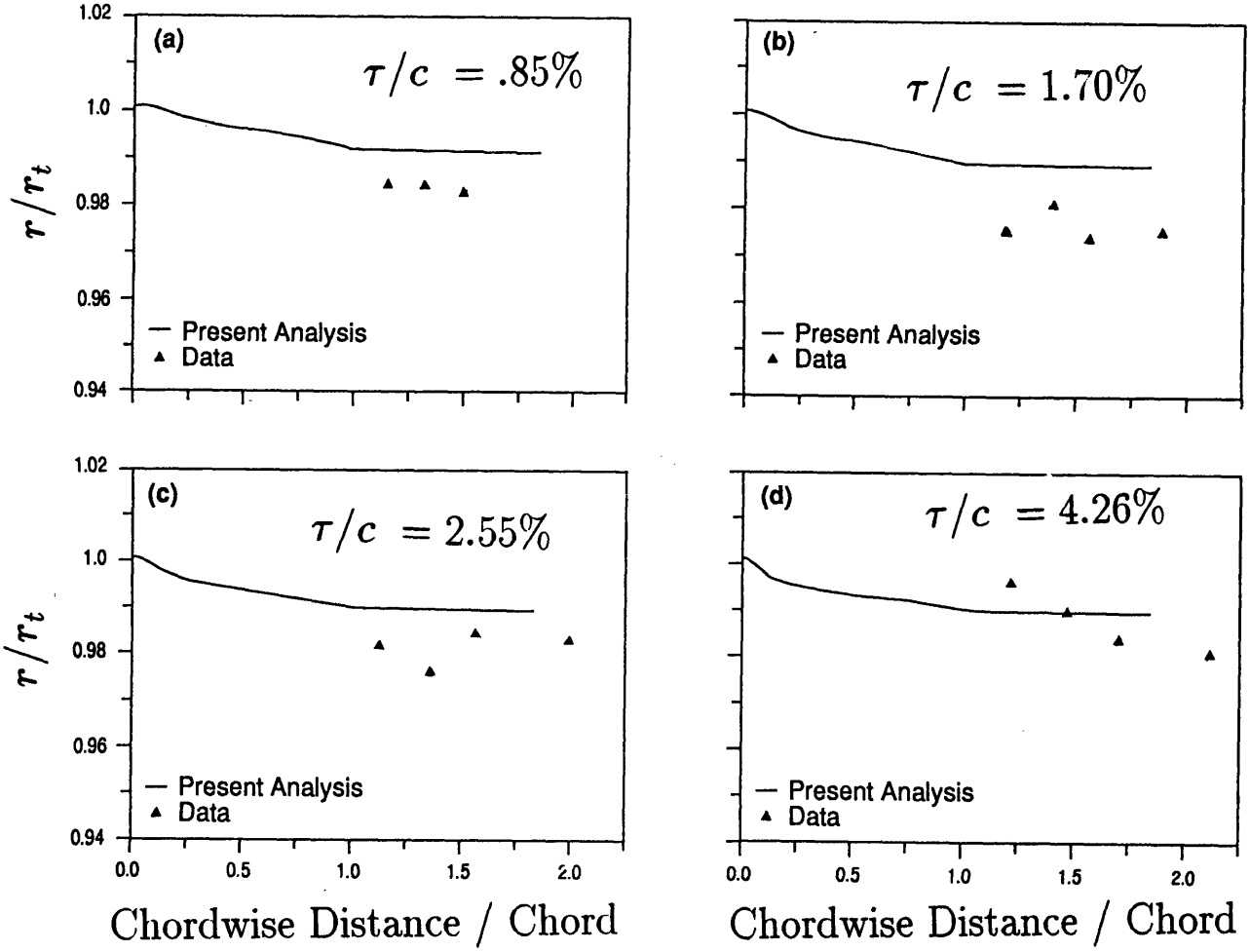

Figure 3.23: Radial motion of tip clearance vortex, data from Inoue, Kuroumaru, and Fukuhara (1986); $\phi = 0.5$

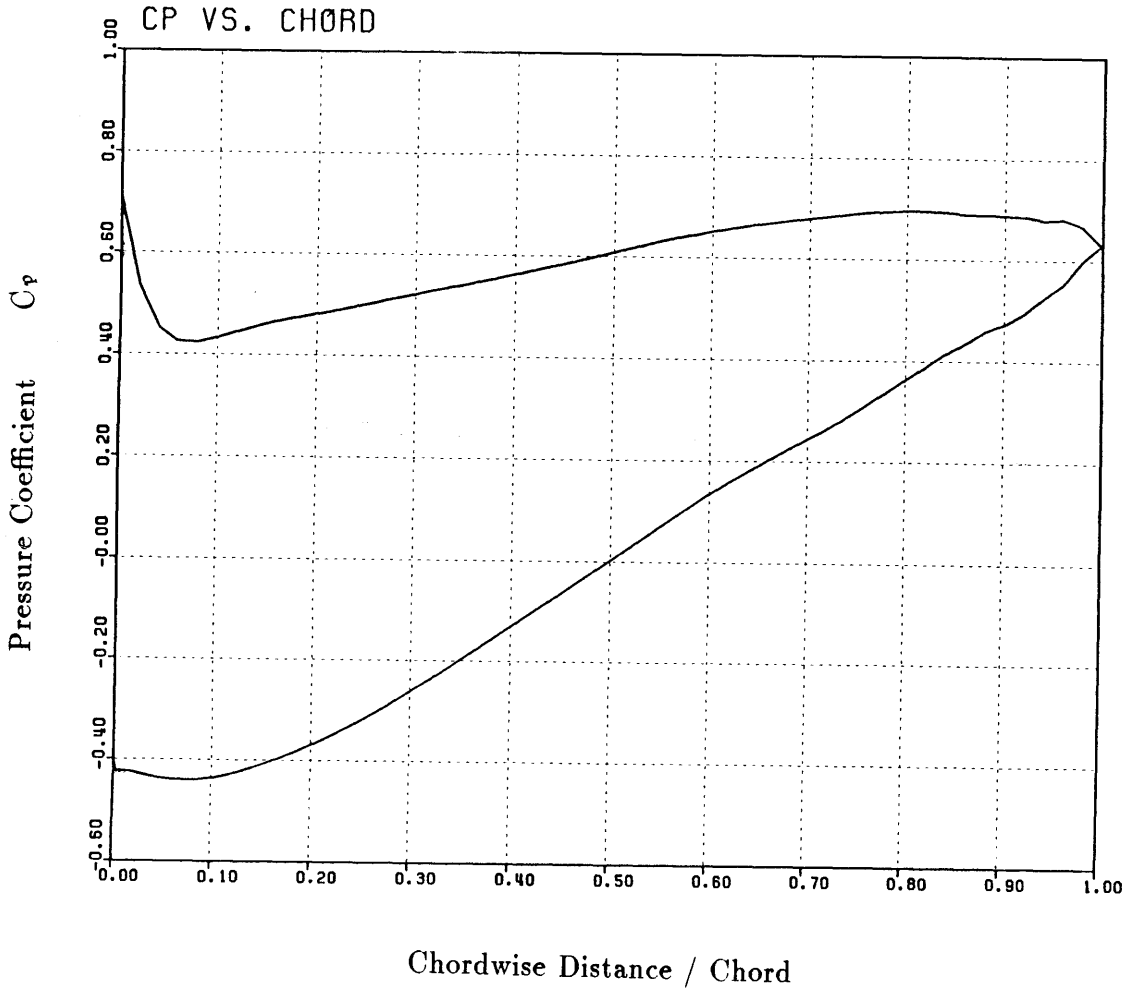

Figure 3.24: Representative pressure distribution on compressor blade (Cumpsty, 1990)

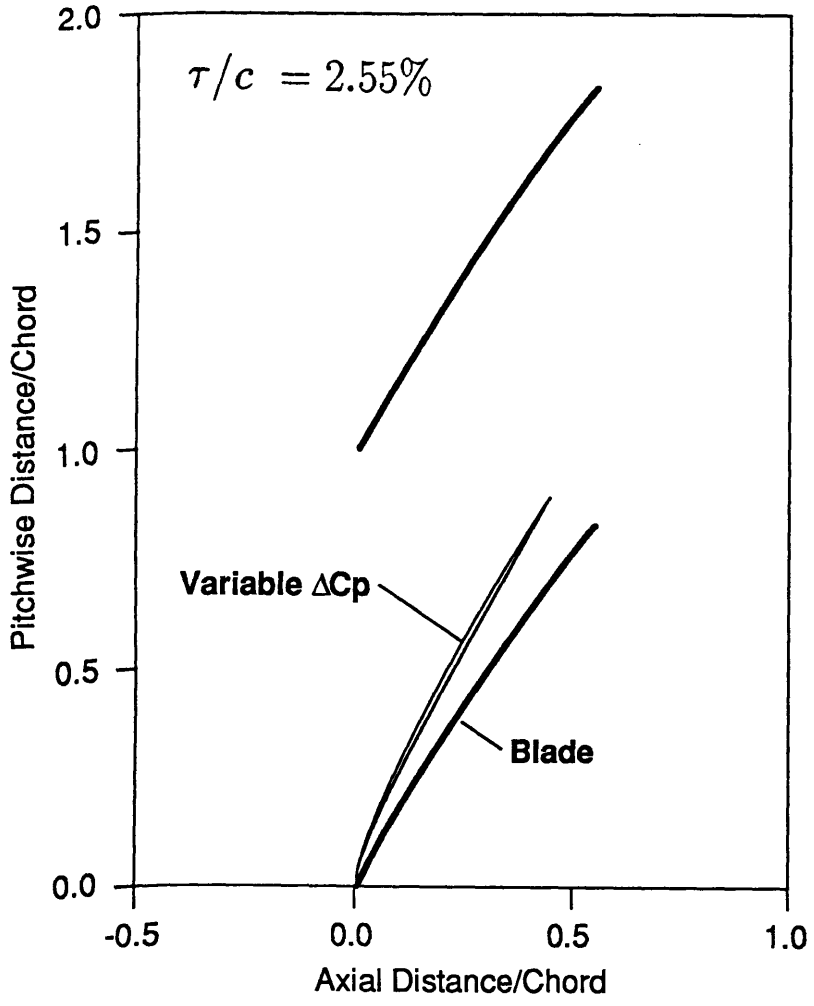

Figure 3.25: Vortex trajectory computed based on constant blade pressure difference and on generic pressure distribution

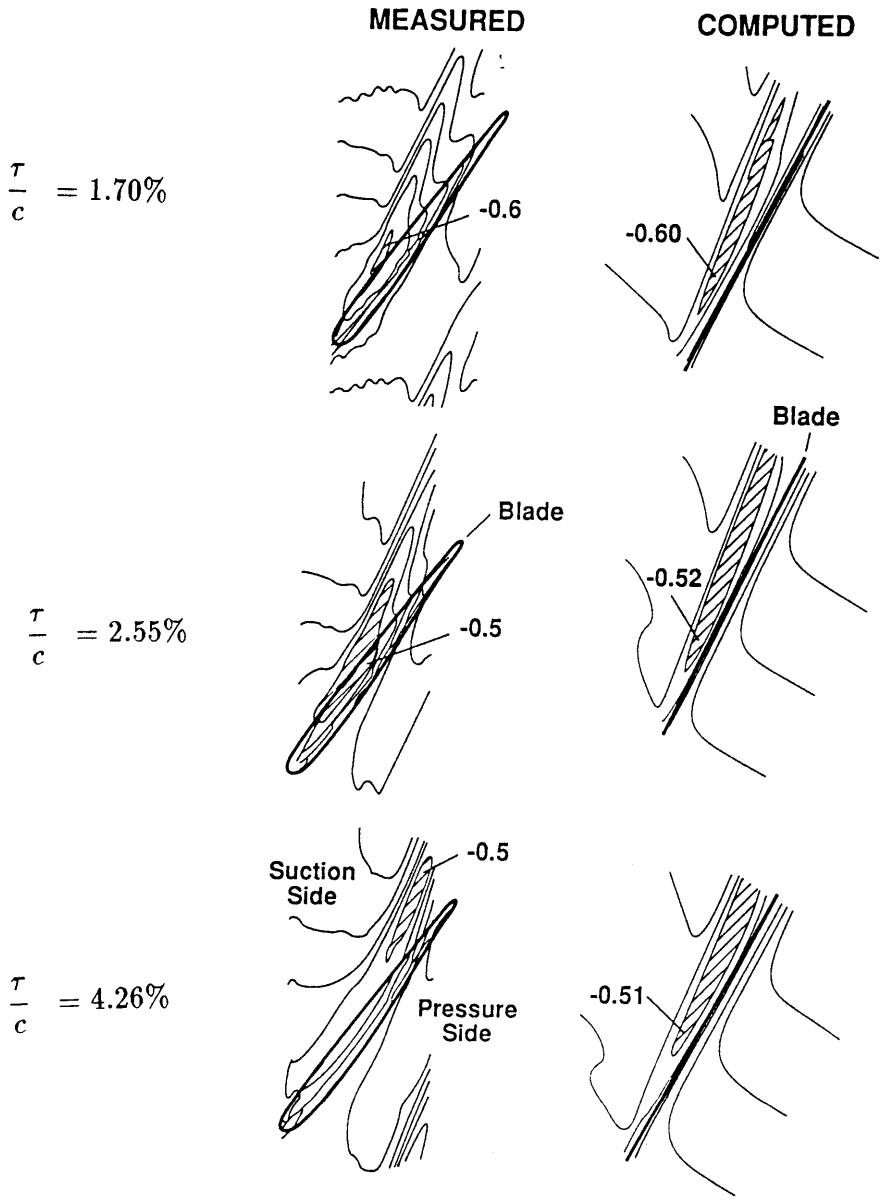

Figure 3.26: Computed and measured endwall static pressure distribution (data of Inoue and Kuroumaru, 1988)

$\phi = .62,,\ \tau/c = 4.26\%$

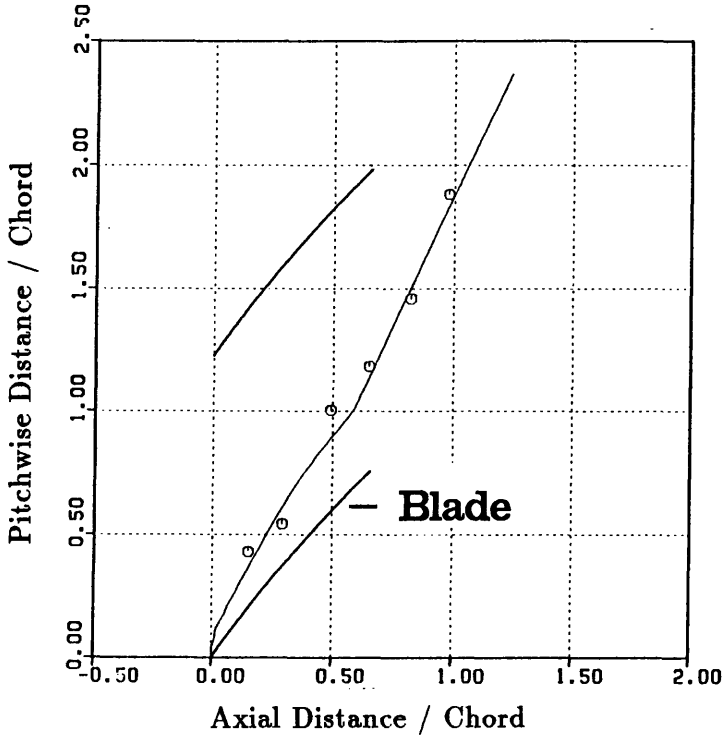

Figure 3.27: Effect of operating point on clearance vortex trajectory ; $\phi = .62$, $\tau/c = 4.26\%$ (data of Takata, 1988)

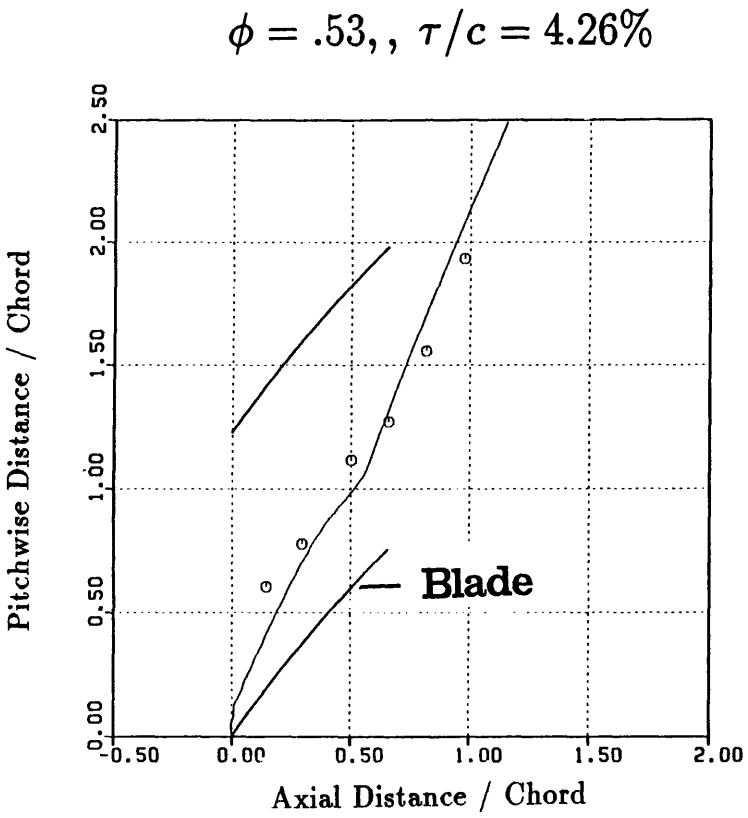

Figure 3.28: Effect of operating point on clearance vortex trajectory ; $\phi = .53$, $\tau/c = 4.26\%$ (data of Takata, 1988)

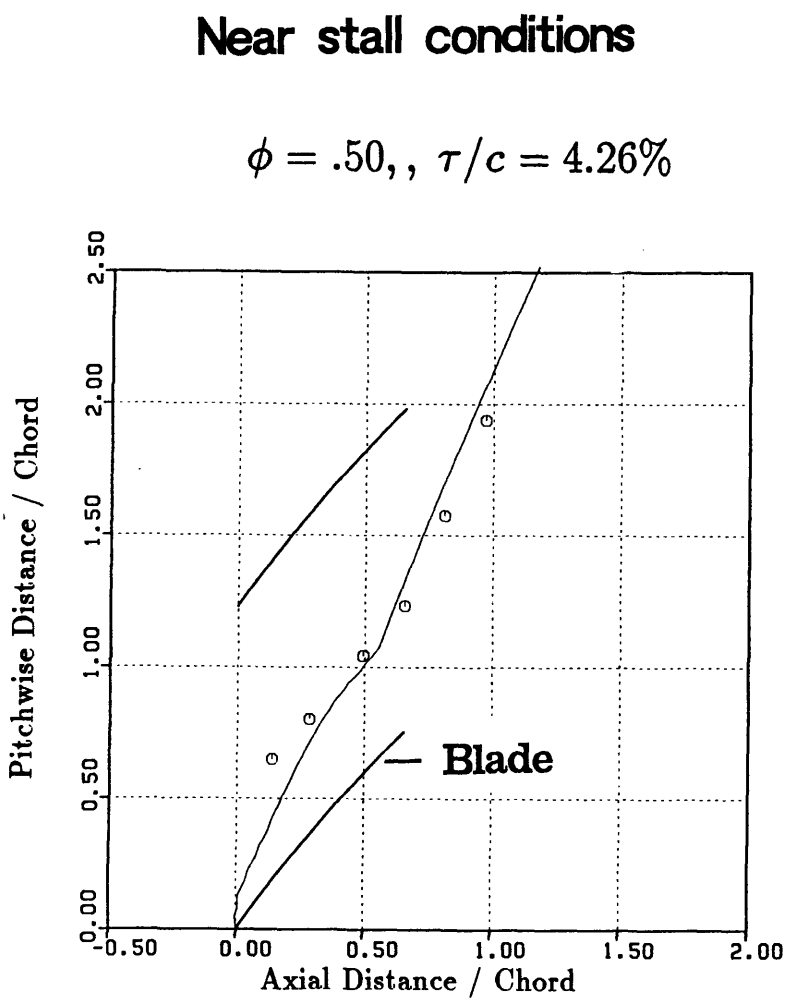

Figure 3.29: Effect of operating point on clearance vortex trajectory ; $\phi = .50$, $\tau/c = 4.26\%$ (data of Takata, 1988)

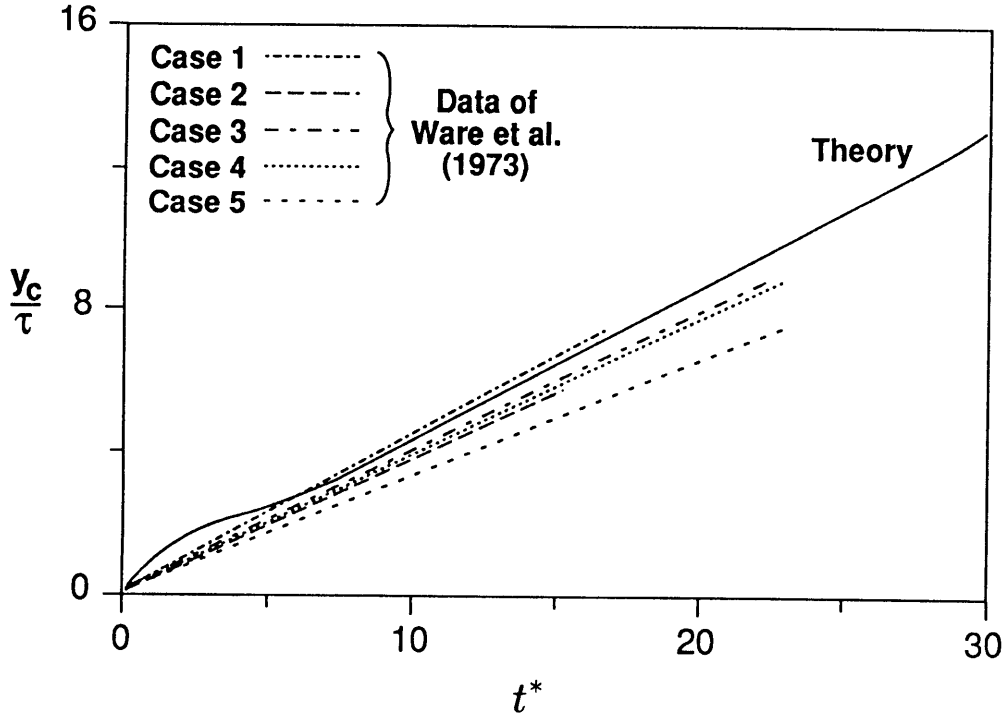

Figure 3.30: Generalized tip clearance vortex core trajectory for a transonic fan

Chapter 4

Examination of the Assumptions in the Flow Model

4.1 Effects of Classical Secondary Flow

The analysis presented neglects any effects due to what can be termed "classical secondary flow", i.e. the cross-flow plane velocities associated with streamwise vorticity due to inlet boundary layers. The implication is thus that the velocity field associated with the tip clearance vortex dominates that due to classical secondary flow, and it is appropriate to examine this assumption.

To do this, we have computed the secondary flow for the configuration of Inoue and Kuroumaru (1988, [23]), using the measured inlet boundary layer profiles. The computation procedure is straightforward and is given in Appendix H. The inlet boundary layer is the same for all the different clearances, so that one figure represents all four cases. The cross-flow velocity field at exit is plotted in Fig. 4.1 to the same scale as Fig. 3.4 and 3.5. Comparing the figures, the velocities associated with the clearance vortex are much larger than those due to secondary flow. For example, the kinetic energy associated with the secondary flow is only three percent of that associated with the clearance flow for $\tau/c = 2.55$ %. The clearance flow velocities dominate in this region and hence the clearance loss is expected to be much higher than the loss associated with

the secondary flow. Similar conclusions have been made by Lakshminarayana, Sitaram, and Zhang (1985, [32]) on a compressor rotor in which they found losses due to the secondary flow and annulus-wall boundary layer were small compared to the tip leakage loss.

Based on the data we have examined so far, this is generally true for rotor tip clearance flow, which is the situation of greatest practical interest. When secondary flows do become comparable with the clearance flows, as in many cascade experiments, the predicted tip vortex core trajectories would need to be modified to include the secondary flow effects.

The influence of secondary flow on the clearance vortex location can be seen from the experimental results of Lakshminarayana and Horlock (1965, [30]). In the experiment, a cascade with slotted blades was used to examine the effect of incoming velocity profile on the clearance flow. The vorticity contours downstream for an uniform upstream flow and a boundary layer type of inflow are given in Figs. 4.2 and 4.3, respectively. Two points are noted from the figures. First, for the uniform inflow case, the vortex cores are located at roughly the same distance from the suction surface for a six fold variation in clearance. This reconfirms the conclusion of the similarity analysis, vortex pitchwise location does not depend on the size of tip clearance, is a good approximation for the actual flow. Second, with inlet boundary layer, the vortex cores are located at different pitchwise locations and closer to the suction surface as a result of secondary flow effects.

There have been many experimental studies on clearance flow in cascades. However, most of the studies are on turbines. They also provide little information on clearance vortex trajectory in blade passage. A study on compressor cascade which provides all the data needed for the vortex calculation and the measurements of vortex core has been carried out by Dean (1954, [13]). Fig. 4.4 shows the calculated velocity field of the clearance flow and the secondary flow associated with endwall boundary layer. The magnitudes of the cross flow velocities are comparable so that secondary flow effects need to be included to predict the clearance vortex trajectory.

The secondary flow effects were taken into account by calculating the secondary flow velocity at the vortex core in the trailing edge cross-flow plane. This velocity is then linearly interpolated from leading edge to trailing edge and added to the clearance velocity at the vortex core. The calculated tip vortex trajectory including the secondary flow effects is plotted in Fig. 4.5. Also shown in the figure is the vortex trajectory without correction for the secondary flow effects as well as measurement of Dean (1954, [13]). The corrected tip vortex trajectory is located closer to the suction surface and gives better agreement with the experimental data. This shows that secondary flow needs to be included to predict the vortex trajectory when it is comparable to clearance flow.

4.2 Effect of Radial Non-Uniformities

The data shown have been for situations in which the incoming boundary layers were relatively thin (except for the cascade results). More specifically, the axial velocity profile has been such that the tip clearance vortex could be considered to be embedded in a stream with velocity equal to the free stream evaluated at the midspan. There are many situations in which this is not a valid approximation because the axial velocity decreases substantially from the midspan station to the location of the vortex center.

It this occurs, the present analysis will be based on a convection time that is too short and will give a value for distance of the vortex from the blade which is too small. To examine this, calculation has been carried out based on the data from the experiment of Lakshminarayana and Murthy (1988, [31]), in which detailed measurement of the flow field in the tip region of a compressor rotor was carried out. It is found that, if one makes a crude correction for this effect by using the measured *inlet* axial velocity at the blade tip, the trajectory is well predicted (Fig. 4.6). In terms of the overall fluid mechanics, the basic analytical framework is still valid, however one must account for the mean flow non-uniformity.

4.3 Effects of Relative Wall Motion

4.3.1 Background

There is conflicting evidence in the literature regarding the influence of relative wall motion, i.e. the motion between the endwall and blade tip, on the clearance flow. A spinning disc experiment by Mayle and Metzger (1982, [38]) has indicated that there is no measurable effect of the moving wall on the blade tip heat transfer coefficients for a turbine, with speed ranging from 10 % to 100 % of the mean leakage flow velocity. They also carried out a simple analysis which showed the effect of wall motion on the heat transfer coefficients is small.

Morphis and Bindon (1988, [40]) examined the effect of wall motion on the blade tip pressure distribution on an annular turbine cascade with a rotating casing. They conclude that "the effect of relative motion did not have a significant effect on the blade gap pressure distribution." For a compressor, the numerical results of Crook (1989, [9]) also show that wall motion has a negligible effect on the endwall flow.

On the other hand, flow visualization by Herzig, Hansen, and Costello (1953, [20]) suggests that, for a turbine cascade, the clearance flow decreases considerably when the wall is moved at moderate speed and there is no clearance flow when the wall is moved at high speed. Dean (1954, [13]) also noted the vortex core was moved away from the suction surface of a compressor rig as the wall speed increases.

Graham (1985, [17]) carried out an experiment on a water turbine cascade, which showed clearance flow was reduced and then stopped when wall speed was increased.

In summary, while some studies suggest that the influence of relative wall motion on clearance flow can be neglected, a significant change in the behavior of clearance flow due to wall motion has also been observed. It is thus of interest to assess when wall motion can have a large effect on the clearance flow. Such an analysis is described in the following section.

4.3.2 Approximate Analysis of the Effect of Wall Motion

We have carried out a simple analysis attempting to clarify the role of wall motion. First we examine the effects of relative wall motion in a compressor. The fluid on the wall is moving with tip speed U_t relative to the blade. This fluid motion can be treated as the smoothing-out of a shear layer in a semi-infinite region with velocity U_t on the wall as shown in Fig. 4.7. The transformation between time t and axial location x is the same as discussed in Chapter 2. The induced velocity in the clearance region is then

$$\frac{v_w}{U_t} = 1 - erf(\frac{\tau}{\sqrt{4\nu t}}) \tag{4.1}$$

where v_w is the velocity with wall motion, U_t is the relative rotational speed at tip, erf is the error function, and ν is the viscosity. Let the convection time be t_w, Eq. (4.1) is written

$$\frac{v_w}{U_t} = 1 - erf(\frac{\tau}{\sqrt{4\nu t_w}}) \tag{4.2}$$

The clearance flow velocity can be written

$$\frac{v_c}{U_t} = \frac{\phi}{\cos\beta_1}\sqrt{\frac{\Delta C_p}{2}} \tag{4.3}$$

so that the ratio of v_w to the clearance velocity v_c is

$$\frac{v_w}{v_c} = \frac{\cos\beta_1}{\phi}\sqrt{\frac{2}{\Delta C_p}}\ [1 - erf(\frac{\tau}{\sqrt{4\nu t_w}})] \tag{4.4}$$

Eq. (4.4) can be simplified if the convection time t_w is based on an average axial velocity instead of the axial velocity in the endwall region. Under this approximation, t_w is given by [1] , i.e.

$$t_w = \frac{c\ \cos\gamma}{C_x} \tag{4.5}$$

and

$$\nu\ t_w = \nu\frac{c\ \cos\gamma}{C_x} = \frac{\nu}{cV_1}\ \frac{V_1}{C_x}\ c^2\ \cos\gamma \tag{4.6}$$

[1]The wall effects have been examined in some cascade experiments by rotating the endwall. In these cases the convection time should be based on axial length of the rotating wall instead of the axial chord, $c\ \cos\gamma$.

Note $C_x/V_1 \simeq \cos\gamma$ so that the above equation can be written

$$\frac{\nu\, t_w}{\tau^2} = \frac{1}{Re}\frac{c^2}{\tau^2} \tag{4.7}$$

This can be put into Eq.(4.4) to give,

$$\frac{v_w}{v_c} = \frac{\cos\beta_1}{\phi}\sqrt{\frac{2}{\Delta C_p}}[1 - erf(\frac{\tau}{2c}\sqrt{Re}\ )] \tag{4.8}$$

This shows that relative wall motion can have a significant effect on clearance flow for a machine with small clearance and Reynolds number, and large flow coefficient.

We now examine the condition under which v_w is an order of magnitude less than v_c, i.e. $v_w/v_c \sim O(10^{-1})$, so that the effects of relative wall motion on the clearance flow can be neglected. First we note that in a turbomachine $v_c/U_t \sim O(1)$, which means

$$\frac{\cos\beta_1}{\phi}\sqrt{\frac{2}{\Delta C_p}} \sim O(1)$$

Therefore, for $v_w/v_c \leq O(10^{-1})$, it is necessary that

$$1 - erf(\frac{\tau}{2c}\sqrt{Re}\ ) \leq 0.1 \tag{4.9}$$

This is satisfied if

$$\frac{\tau}{c}\sqrt{Re} \geq 2.3 \tag{4.10}$$

The order of magnitude analysis indicated that the wall effect will not be important when $\frac{\tau}{c}\sqrt{Re} \geq 2.3$. [2]

The analysis discussed so far is directed at compressors. For a turbine, the flow due to wall motion is regarded as a smoothing-out of a viscous layer between two parallel walls: one moving with tip velocity U_t with the other held stationary (see Fig. 4.8) since the thickness of a turbine blade is much larger than the clearance,

The velocity at the center of the gap , i.e. half clearance height from the endwall, is

$$\frac{v_w}{U_t} = \frac{1}{2}[1 - \frac{4}{\pi}\sum_{n=1}^{\infty}\frac{1}{n}\sin\frac{n\pi}{2}\exp(-n^2\pi^2\nu\, t_w/\tau^2)] \tag{4.11}$$

[2]The analysis assumes the flow induced by the wall motion is laminar. If the flow is turbulent, the results still apply except a turbulent viscosity has to be used instead of ν.

Experiments	$\tau/c(\%)$	$v_w/v_c(\%)$	$\frac{\tau}{c}\sqrt{Re}$	Comments
Inoue and Kuroumaru	.85	1.2	4.1	Compressor rotor
Inoue and Kuroumaru	1.70	0.0	8.3	Compressor rotor
Inoue and Kuroumaru	2.55	0.0	12.4	Compressor rotor
Inoue and Kuroumaru	4.26	0.0	20.7	Compressor rotor
Morphis and Bindon	1.0	19.0	3.9	Turbine cascade
Morphis and Bindon	2.0	0.7	7.9	Turbine cascade
Morphis and Bindon	4.0	0.0	15.5	Turbine cascade
Herzig et al	.94	-	1.5	Cascade
Graham	0.55	-	1.7	Turbine cascade
Graham	1.15	-	3.6	Turbine cascade
Graham	2.31	-	7.3	Turbine cascade

Table 4.1: Effects of relative wall motion

Substituting in v_c from Eq.(4.3) and νt_w from Eq.(4.7), one has

$$\frac{v_w}{v_c} = \frac{\cos\beta_1}{\phi}\sqrt{\frac{2}{\Delta C_p}}K(e) \tag{4.12}$$

where

$$K(J) \equiv \frac{1}{2}[1 - \frac{4}{\pi}\sum_{n=1}^{\infty}\frac{1}{n}\sin\frac{n\pi}{2}\exp(-n^2 J)] \tag{4.13}$$

and

$$J \equiv \pi^2 \frac{1}{Re}\frac{c^2}{\tau^2} \tag{4.14}$$

The function $K(J)$ is given in Fig. 4.9. As in the compressor case, further simplification of the results has been done to show that the wall effects will not be important if

$$\frac{\tau}{c}\sqrt{Re} \geq 4.7 \tag{4.15}$$

Calculations have been carried out for several experiments: 1) Inoue, Kuroumaru, and Fukuhara (1986, [24]), 2) Morphis and Bindon (1988, [40]), 3) Herzig, Hansen, and Costello (1953, [20]), and 4) Graham (1985, [17]), and the results are given in Table 4.1.

For the compressor experiment of Inoue, Kuroumaru, and Fukuhara (1986, [24]) the results indicate that the wall effect is negligible. For the turbine experiment of Morphis

and Bindon (1988, [40]) the calculations suggest that the effect of wall motion on the clearance flow is negligible, which agrees with the experimental observations.

On the other hand, the results indicate that the flow due to wall motion is comparable to the clearance flow in the cascade experiment of Herzig, Hansen, and Costello (1953, [20]) and turbine experiment of Graham (1985, [17]). The behavior of clearance flow will therefore be modified by the wall motion for these two configurations, which has also be observed from the experiments.

In summary, a simple approach has been described for assessing the significance of relative wall motion on clearance flow in a turbomachine. Agreement between the trends seen in calculation and experiment suggests that the simple analysis appears to be useful in assessing the wall effect and provides a guideline on the adequacy of the flow model as far as the wall motion is concerned.

4.4 Summary and Conclusions

This chapter presents several results:

- The secondary flow in a compressor rotor is in general small compared to the clearance flow.
- For a cascade, the secondary flow may be important. If so, analysis of vortex trajectory must take this into account.
- The local (tip) axial velocity should be used in calculating the convection time of a tip vortex if there is a strong radial variation in axial velocity profile.
- A method is presented for studying the importance of wall motion on clearance flow in a compressor as well as a turbine. It is concluded that, depending on geometry, the wall motion can induce secondary flow comparable to the clearance flow.

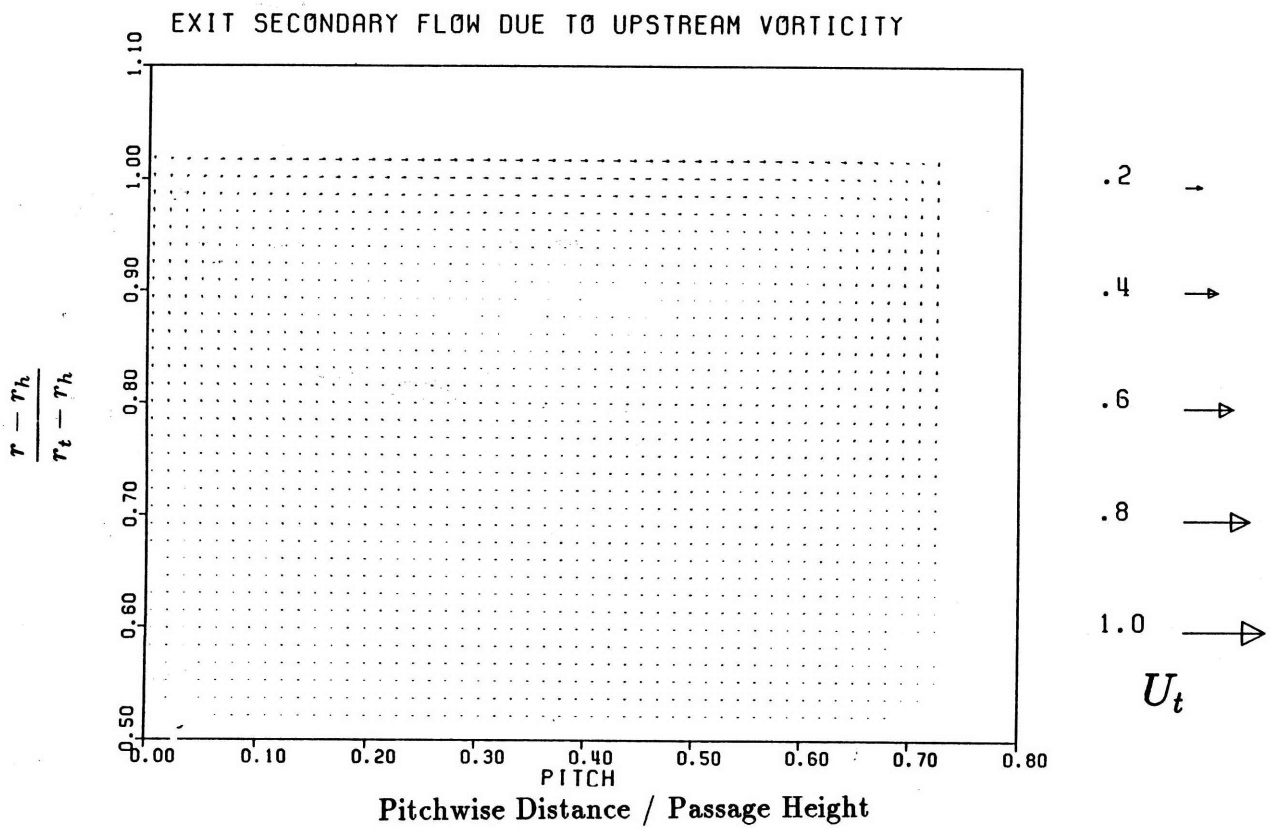

Figure 4.1: "Classical" secondary flow due to inlet boundary layer (Inlet boundary layer profile)

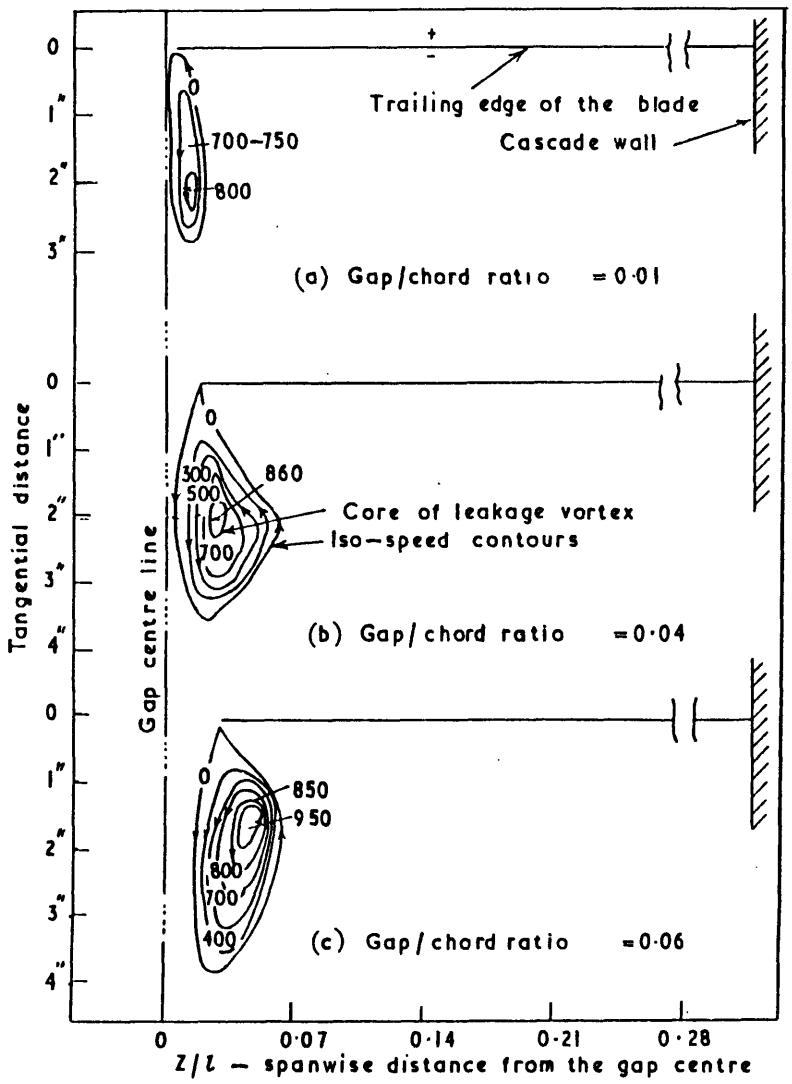

Figure 4.2: Vorticity contours, data of Lakshminarayana and Horlock (1965) (Uniform inflow)

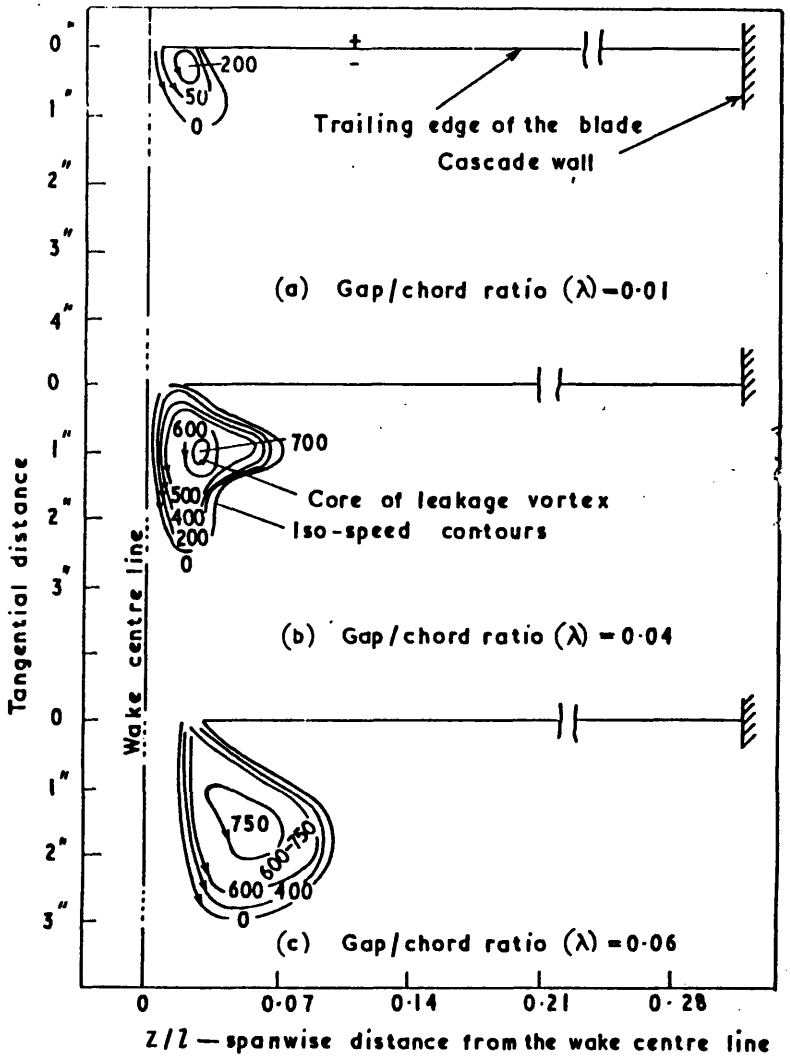

Figure 4.3: Vorticity contours, data of Lakshminarayana and Horlock (1965) (Boundary layer type of inflow)

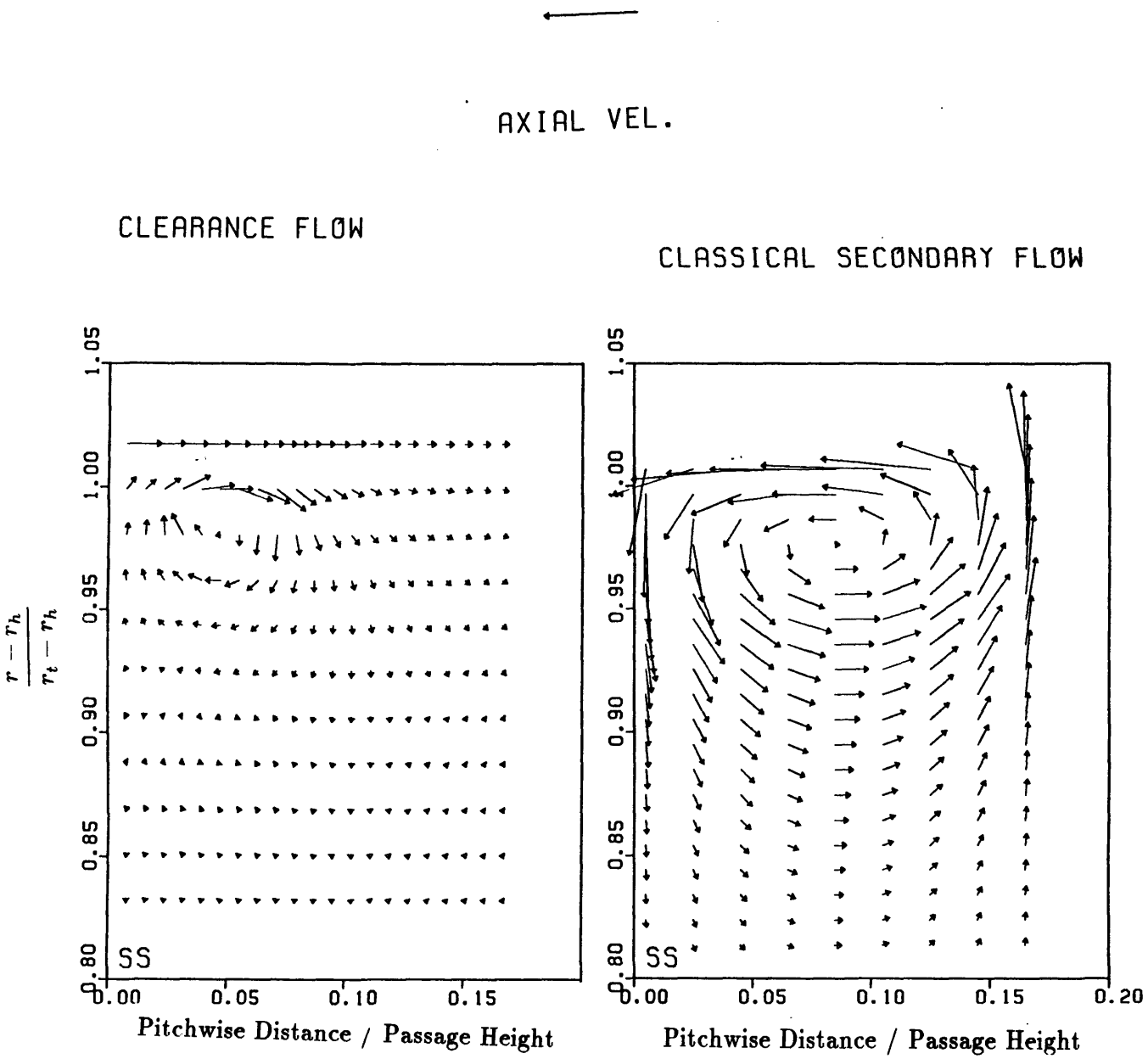

Figure 4.4: Computed clearance and secondary flow velocities; parameters based on data of Dean (1954)

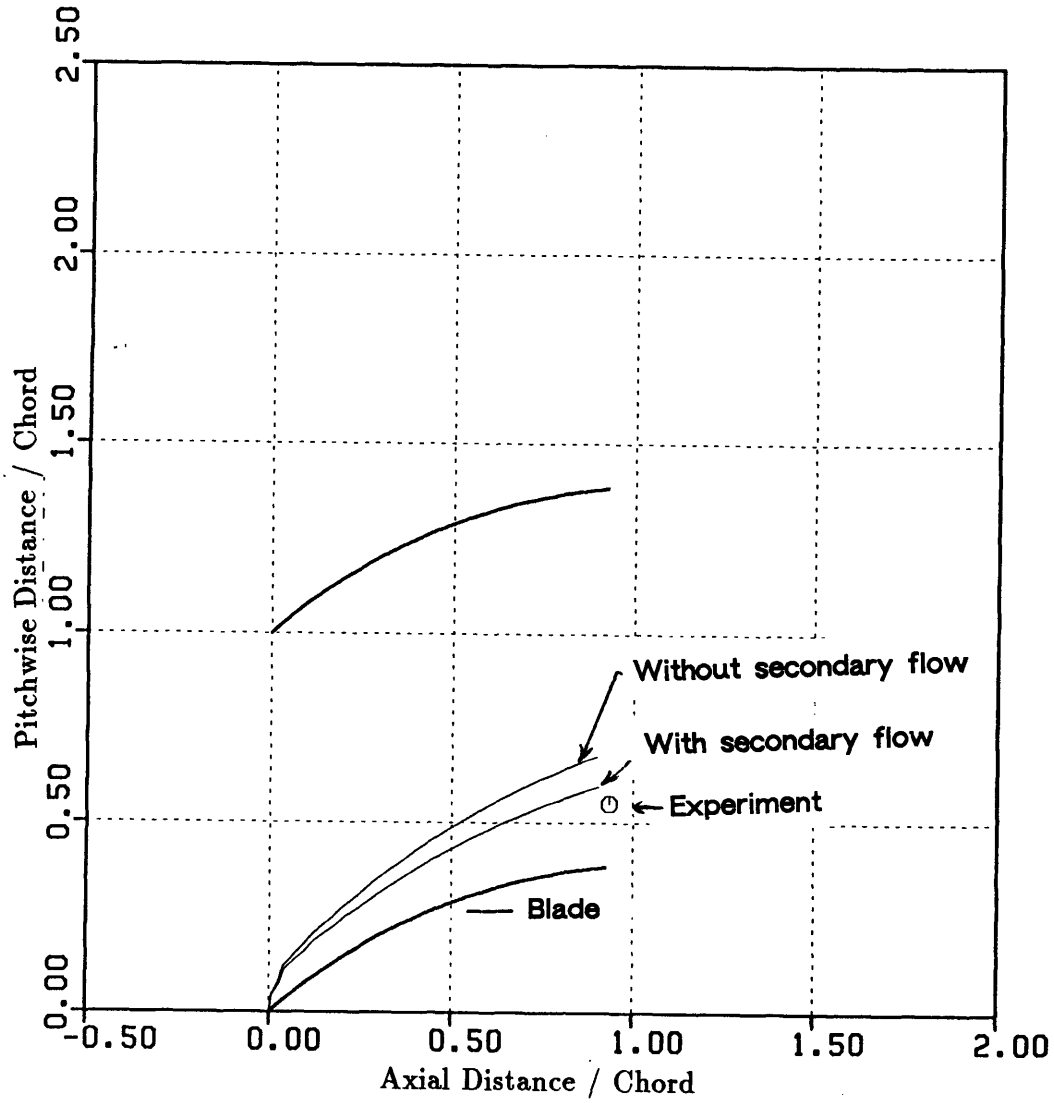

Figure 4.5: The effect of classical secondary flow on vortex core trajectory, data of Dean (1954)

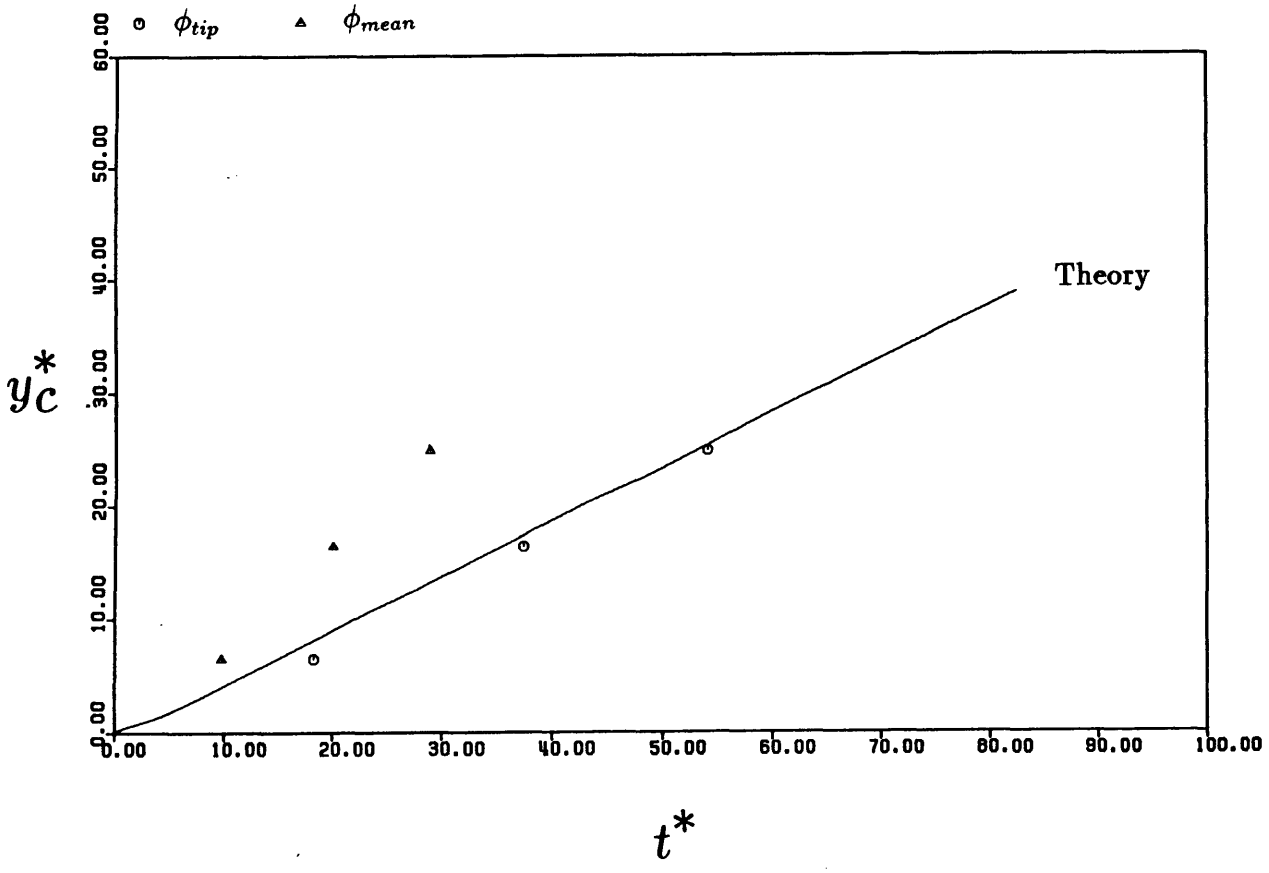

Figure 4.6: Effect of radial non-uniformity on tip vortex trajectory, data from Lakshminarayana and Murthy (1988)

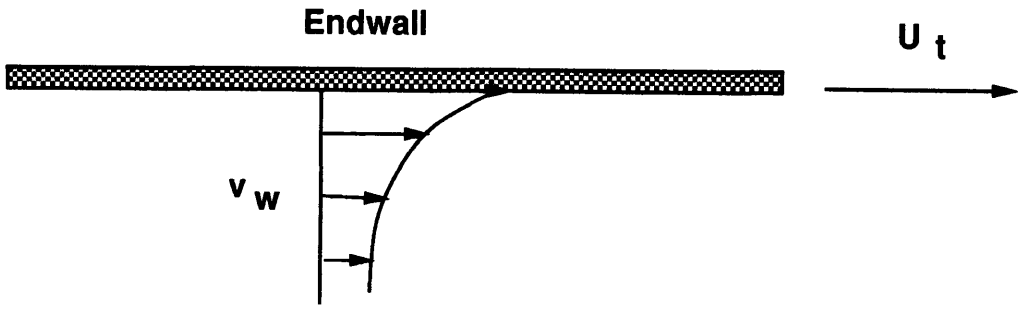

Figure 4.7: Schematic of smoothing-out of a shear layer in a semi-infinite region

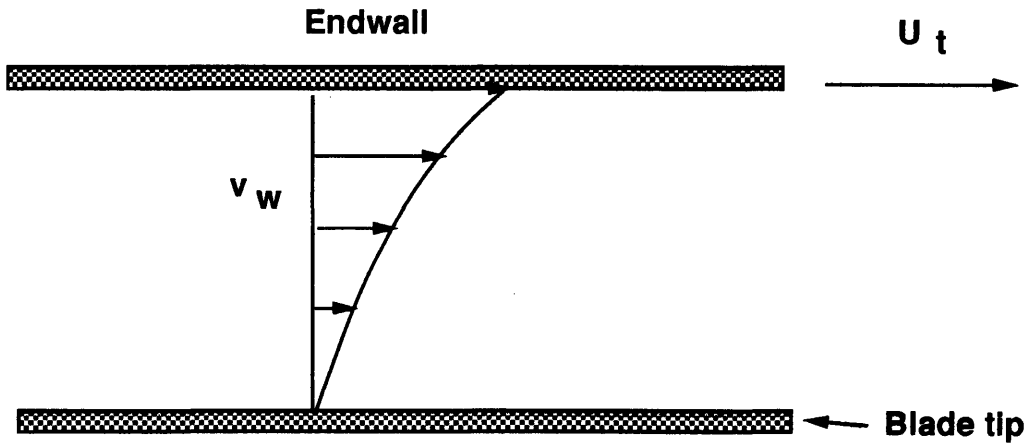

Figure 4.8: Schematic of smoothing-out of a shear layer between two flat plates

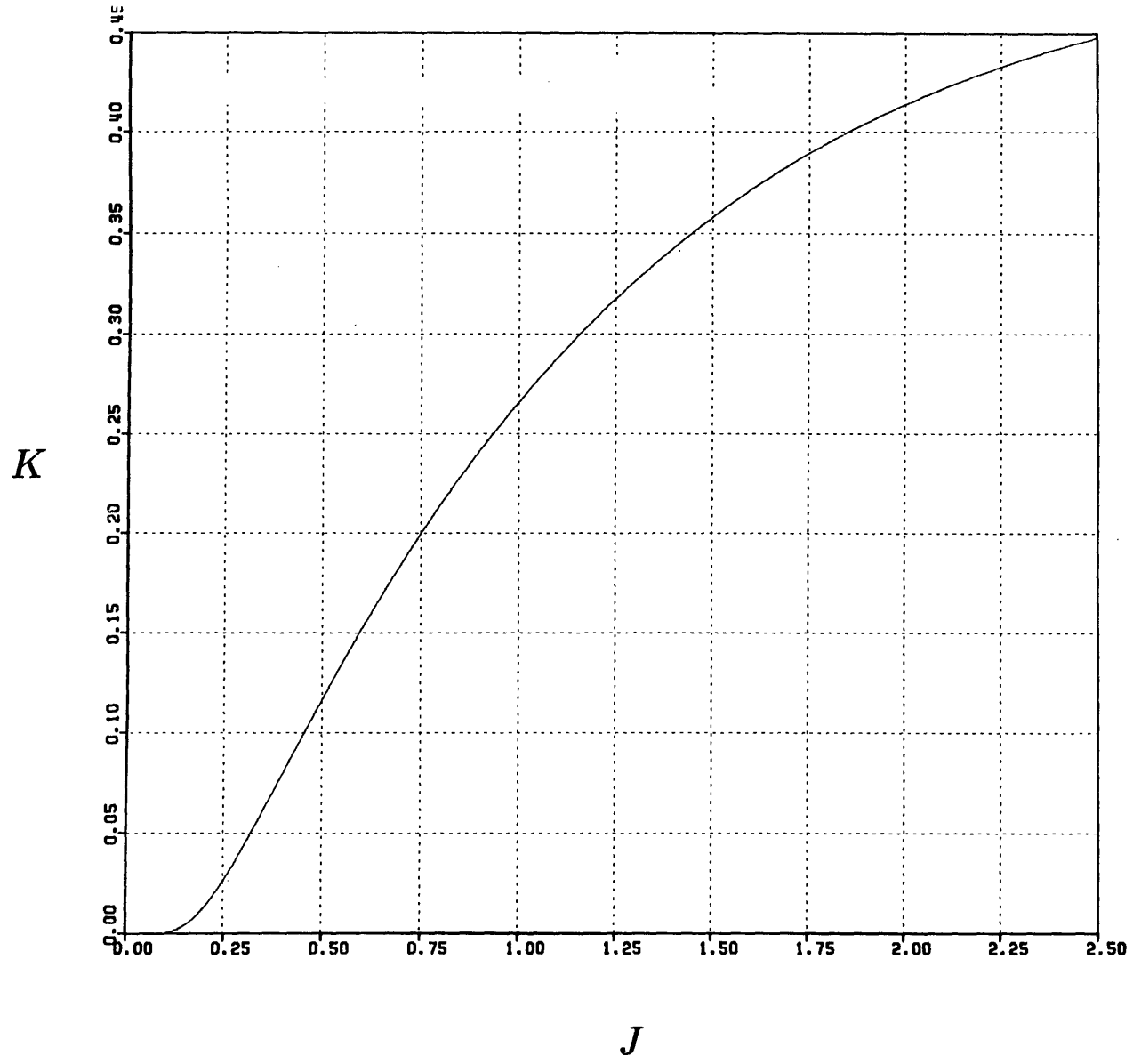

Figure 4.9: Function K vs. J

Chapter 5

Tip Clearance Losses

5.1 Introduction

Despite considerable work has been carried out on the topic of clearance losses, the origin and parametric dependence of the loss are still not well understood. Although many studies indicate that clearance loss varies linearly (or nearly linearly) with the clearance, the mechanism postulated for the losses is different and different parametric dependence of the losses thus also exist in the literature. For example the dependence on blade pressure difference has been variously given as $(\Delta p)^{3/2}$ (leakage flow approach), $(\Delta p)^2$ (lifting line approach), or $(\Delta p)^{1/2}$ (area ratio approach) [1].

The need to use empirical constants or correlations, which vary considerably from geometry to geometry also, limits the usefulness of present approaches. Finally, existing approaches emphasize the prediction of efficiency reduction due to clearance and little attempt has been made to study how the clearance affects other performance parameters such as shaft power.

The objectives of this chapter are then as follows:

- Presentation of a model for clearance losses and change in shaft power with clearance, based on the ideas of Chapter 3.
- Identification of parametric trends of clearance loss.

[1]The area approach relates clearance loss to leakage flow area. It is assumed that the clearance loss is proportional to the leakage flow and the proportionality constant is obtained from empirical data (Stodola, 1924, Traupel 1958, and Bammert et al., 1968)(refer to Farokhi, 1987, [16]).

- Examination of means to minimize clearance loss.

5.2 Compressor Tip Clearance Loss

5.2.1 Introduction

Based on the flow model, a method attempting to give a quantitative measure of compressor tip clearance loss is described here. As in the leakage flow approach, we assume that this kinetic energy is eventually lost without any recovery. From this consideration, an expression for the clearance loss is derived.

The change in shaft power due to clearance is then derived from the flow model. This combined with the clearance loss enables one to find the expressions for the decrease in efficiency as well as total pressure rise due to clearance for a compressor. This is the first time that a method attempting to predict the change in compressor performance other than the efficiency due to clearance has been presented.

5.2.2 Effects of Clearance on Compressor Performance

We define a non-dimensional total pressure rise coefficient, denoted by ψ, and a shaft power coefficient, denoted by λ, as follows:

$$\psi = \frac{p_{t2} - p_{t1}}{\rho U_t^2/2} \tag{5.1}$$

$$\lambda = \frac{L}{\rho U_t^3 \pi (r_c^2 - r_h^2)/2} \tag{5.2}$$

where p_{t1} and p_{t2} are, respectively, the total pressure at the inlet and exit of a compressor rotor, and L is the shaft power to the rotor. For incompressible flow, the total to total efficiency of the compressor rotor, denoted by η_c, is

$$\eta_c = \frac{\phi\,\psi}{\lambda} \tag{5.3}$$

For small changes in ψ and λ, the variation of efficiency with clearance under

constant mass flow can be written as

$$\frac{\Delta\eta_c}{\eta_c} = \frac{\Delta\psi}{\psi} - \frac{\Delta\lambda}{\lambda} \tag{5.4}$$

where $\Delta\eta_c/\eta_c, \Delta\psi/\psi$, and $\Delta\lambda/\lambda$ are the change in efficiency, total pressure, and shaft power coefficient, respectively, due to the change in tip clearance, $\Delta\tau/\tau$. The total pressure coefficient variation, $\Delta\psi$, consists of two parts: one from the change in tip clearance loss (non-isentropic part); the other from the change in shaft power (isentropic part) with clearance. One can therefore write

$$\frac{\Delta\psi}{\psi} = \frac{\Delta\psi_1}{\psi} + \frac{\Delta\psi_2}{\psi} \tag{5.5}$$

where $\Delta\psi_1$ and $\Delta\psi_2$ are, respectively, variations of total pressure coefficient from the change in clearance loss and shaft power as a result of clearance variation. Assuming losses other than the clearance loss remain constant as the clearance varies, we have, from the conservation of energy, the change in power ($\Delta\lambda$) is equal to the change in work done on the fluid ($\phi\ \Delta\psi_2$), i.e.

$$\Delta\lambda = \phi\ \ \Delta\psi_2 \tag{5.6}$$

Substituting Eqs. (5.5), (5.6), into Eq. (5.4), gives

$$\frac{\Delta\eta_c}{\eta_c} = \frac{\Delta\psi_1}{\psi} + (1-\eta_c)\frac{\Delta\psi_2}{\psi} \tag{5.7}$$

The expressions for the change in the total pressure rise, $\Delta\psi_1$ and $\Delta\psi_2$, will be derived in the next two sections.

5.2.3 Clearance Loss

To examine the loss in energy due to the clearance, we consider the clearance flow in the cross flow plane as shown in Fig. 5.1. Because of flow unsteadiness, there is a total pressure (and static pressure) change upstream to downstream. As described earlier, the kinetic energy of clearance flow associated with the velocity components normal to

the main stream, i.e. the kinetic energy associated with the cross flow, is taken to be lost through mixing. The flux of mechanical energy in the cross flow per blade, denoted by E, is

$$E = \int_{LE}^{TE} \frac{(p_{ta} - p_{tb})}{\rho} \dot{m}_c \, ds \tag{5.8}$$

where $\dot{m}_c$ is the leakage mass flow, and s is the streamwise coordinate. Because the cross flow is uniform upstream and downstream, i.e. $v_a = v_b$, as shown in the figure, the total pressure difference is equal to the static pressure difference, i.e.

$$p_{ta} - p_{tb} = p_a - p_b = \Delta p \tag{5.9}$$

We define v_c is the tangential velocity of the cross flow in the clearance region averaged over clearance such that leakage mass flow is given by

$$\dot{m}_c = \rho \, v_c \, \tau \tag{5.10}$$

The vortex calculation (both conformal mapping and panel method) gives [2]

$$\frac{\Delta p}{\rho \, v_c^2} \simeq 1.0 \tag{5.11}$$

From Eqs. (5.8) to (5.11), it can be shown

$$E = \frac{1}{2\sqrt{2}} \frac{\rho C_x^3 \, \tau}{\cos^3 \beta_1} \int_{LE}^{TE} \Delta C_p^{3/2} \, ds \tag{5.12}$$

The variation in the clearance loss E with clearance is then

$$\Delta E = \frac{1}{2\sqrt{2}} \frac{\rho C_x^3 \, \Delta\tau}{\cos^3 \beta_1} \int_{LE}^{TE} \Delta C_p^{3/2} \, ds \tag{5.13}$$

Note $\Delta\psi_1$, discussed in the preceding section, is given by

$$\Delta\psi_1 = - \frac{NB \; \Delta E}{\dot{m} U_t^2/2} \tag{5.14}$$

where NB is number of blades and $\dot{m}$ is the mass flow rate of the rotor. In general, the blade loading varies along the chord so that $\Delta C_p = \Delta C_p(s)$. If $\Delta C_p(s)$ is prescribed,

[2]The vortex calculation gives the value of $\Delta p/\rho v_c^2$ between 1.00 and 1.04 for the different computation schemes discussed in Chapter 2. We used $\Delta p/\rho v_c^2 = 1.0$ in the loss calculation.

$\Delta\psi_1$ can be calculated from Eqs. (5.13) and (5.14). The form of $\Delta\psi_1/\psi$ is

$$\frac{\Delta\psi_1}{\psi} = -\frac{4G}{5}\frac{\phi^2}{\psi\cos^3\beta_1}\frac{c^0}{g}\overline{\Delta C_p}^{3/2}\left(\frac{\Delta\tau}{H}\right) \tag{5.15}$$

where G is a constant which depends on the loading distribution. For example, it equals unity for a linear loading distribution and $5/(4\sqrt{2})$ for a constant loading distribution. $\overline{\Delta C_p}$ is the averaged blade loading at mid span and once it is given, $\Delta\psi_1/\psi$ can then be computed from Eq. (5.15). If information about $\overline{\Delta C_p}$ is not available, an ideal loading coefficient can be used:

$$\overline{\Delta C_p} = 2\frac{g}{c}\frac{\cos^2\beta_1}{\cos\beta_m}(\tan\beta_1 - \tan\beta_2) \tag{5.16}$$

Using Eq. (5.16) into Eq. (5.15) gives

$$\frac{\Delta\psi_1}{\psi} = -\frac{8\sqrt{2}}{5}\frac{G\,\phi^2}{\psi}\left(\frac{c^0}{c}\right)\sqrt{\frac{g}{c}}\left(\frac{\tan\beta_1 - \tan\beta_2}{\cos\beta_m}\right)^{3/2}\left(\frac{\Delta\tau}{H}\right) \tag{5.17}$$

as an estimate for $\Delta\psi_1/\psi$. For the same total blade loading, $\Delta\psi_1/\psi$ for a compressor with constant chordwise blade loading distribution is about 12 % lower than for a triangular one. This implies that, as far as clearance loss is concerned, the chordwise blade loading distribution should be tailored such that it is as uniform as possible.

The loss of kinetic energy associated with the cross flow can be viewed as a mixing loss, which is explained as follows. Consider a cross flow (with velocity v_c), which leaves the clearance region and enters the blade passage. The cross flow thus undergoes a sudden expansion because the height of the cross flow passage changes from the clearance τ to the passage height H. The total pressure loss due to this expansion can be found to be (see Batchelor (1967, [4])) $(1-\frac{\tau}{H})^2\ \frac{\rho v_c^2}{2}$, which is approximately equal to $\frac{\rho v_c^2}{2}$, and the loss due to the mixing is thus $\dot{m}_c\ \frac{\rho v_c^2}{2}$, where $\dot{m}_c$ is the clearance mass flow. The mixing loss is therefore identical to the loss of the cross flow kinetic energy. [3]

[3]There is also a mixing loss due to the difference in streamwise velocity in the clearance flow (V_p) and main flow (V_s) on the suction side, where V_p and V_s are the free stream velocities at the pressure side and suction side. However, it is small compared to the mixing loss in the cross flow. An indicator of the magnitude of the loss of mixing out two streams is $\Delta V/\overline{V}$, where ΔV is the velocity difference and $\overline{V}$ is the mean velocity of the two streams. If we take the mean blade pressure difference Δp equal to $0.5\cdot\rho V_1^2/2$, $\Delta V/\overline{V}$ is 0.25 for the streamwise mixing; whereas $\Delta V/\overline{V}$ is two for the cross-flow mixing. The former mixing loss is small compared to the latter and can then be neglected.

It should be pointed out that the above-discussed loss is based on a kinetic energy consideration, i.e. the kinetic energy associated with the cross-flow is lost. The same loss can also be obtained from a momentum consideration (see Senoo and Ishida, 1986, [48]), which is discussed as follows. As clearance increases, there is a decrease in axial momentum of the fluid and therefore a decrease in power due to flow leakage. Based on this consideration, the decrease in efficiency with increasing clearance can be calculated. The change in power can be shown equal to the kinetic energy associated with the cross flow. A more detailed discussion in given in Appendix J (also see Senoo, 1990, [47] for more details). In fact, one can show that the parametric dependence of the clearance loss given by Eq. (5.15) is identical to that in Senoo (1986, [48]). The only difference is that we use mid-span loading as the driving force of clearance flow and, therefore, have different constants in the results.

5.2.4 Effect of Tip Clearance on Shaft Power

Consider the clearance flow on a cross flow plane. The blade is unloaded near the tip as shown in Fig. 5.2. The force per unit chord length is given by

$$F_b = \int_0^b (p_p - p_s)\, dz \tag{5.18}$$

where p_p and p_s are, respectively, the pressure on the pressure and suction surfaces. It is useful to define an effective span, denoted by b_{eff}, and an unloading parameter, denoted by b_{un}, as follows:

$$b_{eff} = \frac{F_b}{\Delta p} \tag{5.19}$$

$$b_{un} = b - b_{eff} \tag{5.20}$$

where Δp is the mid-span blade loading. The shaft power can be written [4]

$$L = \Omega \ \Delta p \ b_{eff}(r_h + \frac{b_{eff}}{2}) \tag{5.21}$$

The change in shaft power with τ is thus given by [5]

$$\frac{\Delta L}{\Omega \overline{\Delta p}} = \frac{\partial b_{eff}}{\partial \tau} \Delta\tau \ (r_h + \frac{b_{eff}}{2}) + b_{eff} \frac{1}{2} (\frac{\partial b_{eff}}{\partial \tau}\Delta\tau) + H.O.T. \tag{5.22}$$

Note that, because τ/b is of order 10^{-2}, the only length scale in the cross flow plane can be assumed to be clearance. The unloading parameter, b_{un}, will scale linearly with τ so that one can write

$$b_{un} = k\tau \tag{5.23}$$

where k is an universal constant found to be 0.31 based on the spanwise loading distribution from the vortex calculation. The change of effective span with clearance is

$$\frac{\partial b_{eff}}{\partial \tau} = -(1 + k) \tag{5.24}$$

$\Delta\psi_2$ can be calculated as follows. Note that from Eq. (5.3) and (5.6)

$$\frac{\Delta\psi_2}{\psi} = \frac{\Delta\lambda}{\eta_c\lambda} = \frac{\Delta L}{\eta_c L} \tag{5.25}$$

This combined with Eqs. (5.21) , (5.22), and (5.24) gives, after some algebra,

$$\frac{\Delta\psi_2}{\psi} = -(\frac{1+k}{\eta_c}) (\frac{r_t}{r_m}) (\frac{\Delta\tau}{b}) + O(\frac{\Delta\tau}{b})^2 + \cdots \tag{5.26}$$

Substituting Eqs. (5.15) and (5.26) into Eqs. (5.7) and (5.5), the decrease in efficiency, total pressure rise, and shaft power due to clearance variation, which is done at constant flow coefficient, are found to be

[4] It is implied in the analysis that the blade loading is uniform from hub to tip as in a cascade. In a compressor rotor, however, the blade loading will in general vary along the span. We have looked at the effect of the spanwise loading distribution on the shaft power. We took a linear spanwise loading distribution with the same midspan loading (and thus the same total force) as the one with the uniform loading. The calculations carried out showed that the difference in the shaft power is only 8.3/3.7 % if hub-to-tip ratio is 0.6/.8 .

[5] As the clearance varies the streamlines will shift along the span. However, it can be shown that (see Appendix I) the change in the flow coefficient away from the gap is negligible and the midspan flow coefficient can be treated as independent of clearance

$$-\frac{\Delta\eta_c}{\eta_c} = \frac{4}{5}\frac{G\,\phi^2}{\psi\,\cos^3\beta_1}\,\frac{c^0}{g}\,\overline{\Delta C_p}^{3/2}\,(\frac{\Delta\tau}{H}) + (\frac{1-\eta_c}{\eta_c})\,(1+k)\,(\frac{r_t}{r_m})\,(\frac{\Delta\tau}{b}) \qquad (5.27)$$

$$-\frac{\Delta\psi}{\psi} = \frac{4}{5}\frac{G\,\phi^2}{\psi\,\cos^3\beta_1}\,\frac{c^0}{g}\,\overline{\Delta C_p}^{3/2}\,(\frac{\Delta\tau}{H}) + (\frac{1+k}{\eta_c})\,(\frac{r_t}{r_m})\,(\frac{\Delta\tau}{b}) \qquad (5.28)$$

and

$$-\frac{\Delta\lambda}{\lambda} = (1+k)\,(\frac{r_t}{r_m})\,(\frac{\Delta\tau}{b}) \qquad (5.29)$$

These are the desired results. If $\overline{\Delta C_p}$ is not available, the ideal loading coefficient given in Eq. (5.16) can be used and Eqs. (5.27) and (5.28) becomes

$$-\frac{\Delta\eta_c}{\eta_c} = \frac{8\sqrt{2}}{5}\,\frac{G\,\phi^2}{\psi}\,(\frac{c^0}{c})\,\sqrt{\frac{g}{c}}\,(\frac{\tan\beta_1-\tan\beta_2}{\cos\beta_m})^{3/2}\,(\frac{\Delta\tau}{H}) + (\frac{1-\eta_c}{\eta_c})\,(1+k)\,(\frac{r_t}{r_m})\,(\frac{\Delta\tau}{b}) \qquad (5.30)$$

and

$$-\frac{\Delta\psi}{\psi} = \frac{8\sqrt{2}}{5}\,\frac{G\,\phi^2}{\psi}\,(\frac{c^0}{c})\,\sqrt{\frac{g}{c}}\,(\frac{\tan\beta_1-\tan\beta_2}{\cos\beta_m})^{3/2}\,(\frac{\Delta\tau}{H}) + (\frac{1+k}{\eta_c})\,(\frac{r_t}{r_m})\,(\frac{\Delta\tau}{b}) \qquad (5.31)$$

The results show several interesting points. First, the decrease in efficiency, total pressure rise, and shaft power vary essentially linearly with clearance as shown in Eqs. (5.27) , (5.28) and (5.29). In addition, recall that the first and second terms on the right hand side of Eqs. (5.30) and (5.31) come , respectively, from the change in the clearance loss and shaft power. Eq. (5.30) shows that the change in efficiency comes mainly from the change in the clearance loss because $\eta_c \sim O(1)$ and the second term on the right hand side of the equation is much less than the first term. The power reduction leads to a substantial reduction of the pressure rise because the two terms on the r.h.s. of Eq. (5.31) are of the same order of magnitude. As a result, the pressure rise variation , $\Delta\psi/\psi$, will be roughly twice as large as the efficiency variation, $\Delta\eta_c/\eta_c$. Finally the change in efficiency and loading will be less for a compressor with a uniform blade loading than the one with a linear loading.

It should be emphasized that the the results are obtained at constant flow coefficient. Moreover, it is assumed that the losses other than the clearance loss remain constant

as the clearance varies. This implies the results are to be applied at near design point conditions. One then should be cautious if the results are applied away from the design point where small change in the incidence angle due to the clearance variation may result in a significant change in the losses. The blockage may also increase considerably with clearance away from design point. The results shown in Eqs. (5.30) and (5.31) can easily be extended to multistage compressors and will not be elaborated here.

5.2.5 Parametric Study of Clearance Loss

We now examine the parametric dependence of clearance loss. First an ideal total pressure rise across a rotor, denoted by Δp_t, is written

$$\frac{\Delta p_t}{\rho} = U_m C_x(\tan\beta_1 - \tan\beta_2) \tag{5.32}$$

where U_m is the mid span wheel speed, and the pressure rise coefficient ψ can be written as

$$\psi = 2\phi\frac{r_m}{r_t}(\tan\beta_1 - \tan\beta_2) \tag{5.33}$$

This combined with Eqs. (5.15) and (5.16) gives

$$\frac{\Delta\psi_1}{\psi} \sim \frac{\Delta\eta_c}{\eta_c} \sim -\sqrt{\phi\,\psi}\,(\frac{1}{\cos\beta_m})^{3/2}\sqrt{\frac{g}{c}}\,(\frac{r_t}{r_m})^{3/2}\ \frac{\Delta\tau}{H} \tag{5.34}$$

This indicates that, for constant clearance-to-span ratio, a compressor with high hub-to-tip ratio will have smaller loss in efficiency and pressure rise from flow leakage. It also indicates that high solidity decreases the clearance loss. This may appear unreasonable because high solidity means more blades and hence more opportunities for flow leakage. However, it can be shown that the kinetic energy of a clearance flow decreases as blade pitch becomes smaller.

Considering the total leakage flow, $\dot{M}_c$, and the associated total kinetic energy, E_{total}, one has from Eq. (5.10)

$$\dot{M}_c \sim NB\ v_c$$

and

$$E_{total} \sim NB \ v_c^3$$

,where NB is number of blades. Note that

$$NB \sim \frac{1}{g}$$

and from Eq. (5.16), for constant inlet and exit flow angles,

$$v_c \sim \sqrt{\Delta p} \sim \sqrt{g/c}$$

one has

$$\dot{M}_c \sim \frac{1}{\sqrt{g}} \tag{5.35}$$

and

$$E_{total} \sim \sqrt{g} \tag{5.36}$$

The analysis shows, although there is more flow leakage for a blade row with smaller pitch, the associated kinetic energy loss is less. It should be pointed out that the analysis assumed constant chord and flow angles as blade pitch varies.

5.2.6 Effects of Operating Point on Clearance Loss

Given geometric parameters such as τ, g/c, and r_m/r_t, clearance loss will vary with operating point. The flow coefficient, ϕ_{cr}, where minimum clearance loss takes place is investigated here. The minimum clearance loss occurs when

$$\frac{d(\Delta\eta_c/\eta_c)}{d\phi} = 0 \tag{5.37}$$

Differentiating Eq. (5.34) with respect to ϕ shows that the minimum clearance loss [6]

$$\frac{1}{\phi} + \frac{1}{\psi}\frac{d\psi}{d\phi} + 3 \ \tan\beta_m \frac{d\beta_m}{d\phi} = 0 \tag{5.38}$$

[6] One can show that this is the condition for minimum clearance loss in a compressor by taking the second derivative of Eq. (5.34) with respect to ϕ.

Note that

$$\tan\beta_m = \frac{1}{2}(\tan\beta_1 + \tan\beta_2) \tag{5.39}$$

Assuming constant exit flow angle, it can be shown that

$$\frac{d\beta_m}{d\beta_1} = \frac{1}{2}\frac{\cos^2\beta_m}{\cos^2\beta_1} \tag{5.40}$$

Also from mid-span velocity diagram at the inlet as sketched in Fig. 5.3 one has

$$\tan\beta_1 + \tan\alpha_1 = \frac{1}{\phi}(\frac{r_m}{r_t}) \tag{5.41}$$

where α_1 is the inlet absolute flow angle. Eq. (5.41) can be differentiated w.r.t. ϕ to give

$$\frac{d\beta_1}{d\phi} = -\frac{\cos^2\beta_1}{\phi^2}(\frac{r_m}{r_t}) \tag{5.42}$$

Putting this into Eq. (5.40) gives

$$\frac{d\beta_m}{d\phi} = -\frac{1}{2}\frac{\cos^2\beta_m}{\phi^2}(\frac{r_m}{r_t}) \tag{5.43}$$

From Eqs. (5.38) and (5.43), the flow coefficient ϕ_{cr} for the minimum clearance loss is given by the solution of

$$\frac{1}{\phi_{cr}} + \frac{1}{\psi}(\frac{d\psi}{d\phi})|_{cr} - \frac{3}{4}(\frac{r_m}{r_t})\frac{\sin 2\beta_m}{\phi_{cr}^2} = 0 \tag{5.44}$$

According to the analysis clearance loss will be smaller if design flow coefficients is close to ϕ_{cr}. The optimum occurs when the two coefficients are identical.

5.2.7 Effects of Chordwise Loading Distribution on Clearance Loss

As mentioned earlier, a blade row with a uniform (chordwise) blade loading distribution will have smaller clearance loss than that with a linear one. We now examine this a bit further.

Experiments	ϕ	r_h/r_t	Comments
1. Inoue et al.	.50	.60	Isolated rotor
2. Wisler	.41	.85	Four-stage compressor
3. Jefferson and Turner	.86	.82	Eight-stage compressor
4. Spencer	.25	.55	Pump

Table 5.1: Compressor experiments on effects of clearance on performance

The objective is to obtain a chordwise blade loading distribution that would have a minimum clearance loss but under the constraint that total blade force remains constant. The relevant mathematical problem is then to minimize the integral $\int \Delta p^{3/2} ds$ under the constraint that $\int \Delta p(s) ds$ = constant. It can easily be shown from the calculus of variations that a uniform loading distribution will have the minimum clearance loss. Therefore the chordwise loading distribution in a turbomachine should be kept as uniform as possible to alleviate the clearance loss.

5.2.8 Calculation Results and Discussions

We have derived the expressions for the change in compressor efficiency, total pressure rise, and shaft power with clearance. Calculations have been carried out based on the parameters at design flow coefficient in the experiment of Inoue et al. (1986,[24]), Wisler (1984, [59]), Jefferson and Turner (1958, [25]), and Spencer (1956, [51]) (see Table 5.1), and the results are discussed below.

First, detailed measurements for the clearance flow in an isolated rotor has been carried out by Inoue et al. (1986,[24]). In the experiment the tip clearance was varied from 0.5 mm to 5.0 mm by moving the casing. The performance of the rotor was measured at five different clearances, i.e., 0.5 mm, 1.0 mm, 2.0 mm, 3.0 mm, and 5.0 mm.

In the calculation the baseline was taken to be the minimum clearance case (0.5 mm) at the design point, $\phi = 0.50$. The loss in performance with clearance were then calculated from Eqs. (5.30) and (5.31) with $G = 1$. The computed reduction of efficiency and loading coefficient with increasing clearance are plotted in Fig. 5.4 , which also shows the experimental data.

Both the theory and the experiment indicate a linear relationship between the loss and the clearance. The degradation of performance with clearance is substantial. One percent increase in τ/H causes the efficiency to drop by about 1.3 % and the total pressure rise by about 3 %. As point out earlier, the large decrease in total pressure rise comes from the combination of an increase in the clearance loss and a decrease in the shaft power.

Since the change of efficiency and loading vary almost linearly with clearance, it is useful to define two slope parameters as follows:

$$\Lambda_{\eta_c} = \frac{\Delta\eta_c/\eta_c}{\Delta\tau/H} \tag{5.45}$$

and

$$\Lambda_{\psi} = \frac{\Delta\psi/\psi}{\Delta\tau/H} \tag{5.46}$$

To calculate the slope parameters, the results from experiments and calculations have been least-square fitted by straight lines, whose slopes are thus the slope parameters. The results from the theory and the experiment of Inoue et al. (1986,[24]) are given in Table 5.2.

The theory has also been compared to other loss prediction correlations. As typical of the above-discussed three different approaches, , we have compared our results with the loss correlations of: 1) Rains (leakage flow approach), 2) Lakshminarayana (lifting line approach), and 3) Robinson (area ratio approach). Computed efficiency variations from the three correlations are shown in Fig. 5.5 as well as the present theory and the

Experiments	ϕ	Experiment		Theory	
		Λ_η	Λ_ψ	Λ_η	Λ_ψ
1. Inoue et al.	.50	1.32	2.86	1.34	3.10
2. Wisler	.41	1.04	2.20	.98	2.45
3. Jefferson and Turner	.86	3.10	4.90	2.63	4.07
4. Spencer	.25	4.10	10.77	3.98	5.68

Table 5.2: Experimental and computed slope parameters

experimental data. The present theory and the Rains' correlation, which is similar to the present theory, show good agreements with the data.

The second case examined is a four stage compressor experiment of Wisler (1984, [59]) as indicated in Table 5.1. The compressor were tested at two values of clearances to study the effect of clearance on the compressor overall performance.

The calculated decrease in efficiency and stage loading with clearance as well as the measurements are shown in Fig. 5.6 and the slope parameters are given in Table 5.2. Again the baseline case was the smaller clearance at the design point. As in the previous case there is a considerable performance penalty from flow leakage and the total pressure rise variation is about twice as large as the efficiency variation.

The theory was also compared with the experimental results of an eight-stage compressor, known as "Alice" (see Jefferson and Turner, 1958, [25]), as well as an axial-flow propeller pump (Spencer, 1956, [51]); both at design conditions. Design flow coefficient and hub-to-tip ratio of these two machines are given in Table 5.1 [7]. Fig. 5.7 shows the computed and measured efficiency and pressure rise variation plotted against clearance variation ($\Delta\tau/H$) for the Alice compressor. The influence of clearance on efficiency and head coefficient in the axial pump are shown in Figs. 5.8 and 5.9. The slope parameters of these two machines are given in Table 5.2. As in the previous two cases, there is severe effect of clearance on the overall performance and the change in total pressure rise is larger than the change in efficiency.

[7]The flow coefficient of Spencer pump, shown in Table 5.1, is the inlet and exit averaged flow coefficient, because there is a considerable change in axial velocity due to a change in hub radius.

The ratio of actual to predicted difference in efficiency and pressure rise versus clearance for the four compressor cases are shown in Figure 5.10 and 5.11. The theory agrees well with the experimental data for the two modern compressors (Inoue et al. (1986,[24]) and Wilser (1984, [59])). There appears to be loss sources other than the clearance loss in the Spencer pump because the agreement is poor. However, no enough information is available from the experiment to assess the causes.

5.3 Turbine Tip Clearance Loss

5.3.1 Introduction

The reduction of efficiency and specific work of a turbine with increasing clearance are investigated here. The analysis is similar to that for a compressor except the compressibility effect in the through flow has to be included in calculating the blade loading because main flow is often subsonic or transonic. Moreover, because blade thickness in a turbine is generally larger than clearance, the clearance flow may reattach at blade tip. The effects of the flow reattachment on leakage mass flow and losses are also examined. Calculation has been carried out at constant inlet to exit total pressure ratio since most of the experimental data is obtained in this manner. The comparisons with experiments are given and discussed.

5.3.2 Variation of Efficiency with Clearance

The efficiency of a turbine is defined as

$$\eta_t = \frac{L}{\dot{m} h_{t1} [1 - \pi_t^{(\gamma-1)/\gamma}]} \tag{5.47}$$

,where L is the shaft power, $\dot{m}$ is the mass flow, h_{t1} is the total enthalpy at turbine inlet, π_t is the exit to inlet total pressure ratio, and γ is the specific heat ratio. Following the same analysis as for a compressor, the variation of efficiency with clearance for a turbine under constant π_t can be obtained. The derivation is given in Appendix K and

only the result is shown here

$$\frac{\Delta\eta_t}{\eta_t} = \frac{\Delta W}{W} = -\frac{8\sqrt{2}}{5}\frac{AG}{B}\zeta\,\phi^2\,(\frac{c^0}{c})\sqrt{\frac{s}{c}}\,(\frac{\Delta\tau}{H}) \tag{5.48}$$

where

$$A = \sqrt{\frac{1+\sigma}{2}}\{(\tan\beta_1 - \sigma\tan\beta_2)^2 + [1-\chi-\sigma+\frac{\gamma-1}{2\gamma\sigma}(sec^2\beta_1 - \sigma^2 sec^2\beta_2)]^2\}^{3/4}$$

$$B = \frac{2W}{U_t^2} = \frac{1800}{\pi^2 r_t^2}\,\frac{W/\vartheta_{cr}}{(N/\sqrt{\vartheta_{cr}})}$$

$$\zeta = \frac{\theta^0/2}{\sin(\theta^0/2)}$$

$$\sigma = \phi_2/\phi_1$$

$$\chi = \frac{1-1/\sigma}{\gamma M_1^2\cos^2\beta_1}$$

and θ^0 is the tip camber angle, W is the specific work, ϕ_1 and ϕ_2 are the flow coefficients at the inlet and exit, respectively, M_1 is the inlet relative Mach number ,N is the rotational speed, rpm, and ϑ_{cr} is the squared ratio of critical velocity at turbine inlet to critical velocity at U.S. standard sea-level temperature.

Two things should be pointed out here. First is that the exit flow angle, β_2, is defined positive for a compressor and negative for a turbine. Second is that in a turbine the main flow is often subsonic or transonic so that compressibility has been taken into account in deriving the blade loading. It can be shown that the parameter A reduces to the incompressible form as $M_1 \to 0$, i.e.

$$A = (\frac{\tan\beta_1 - \tan\beta_2}{\cos\beta_m})^{3/2}$$

It was assumed that the clearance flow is not re-attached at the blade tip. This is believed to be true for most of the compressors because of relatively thin blades. However, turbine blades normally have thickness larger than the clearance and the clearance flow can reattach at the blade tip as discussed by Moore and Tilton (1988, [39]). The reattachment of a clearance flow inside the gap can result in a larger clearance loss, as discussed in Appendix L.

	Experiments	No. of stages	r_h/r_t	$1/\ \pi_t$	No. of τ's tested	Λ_η	
						Exp	Cal*
1	Kofskey and Nusbaum (1968)	2	.75	1.23	2	3.78	1.34
2	Haas and Kofskey (1979)	1	.84	2.77	Many	1.94	1.75
3	Szanca et al. (1974)	1	.85	1.80	3	1.57	1.43
4	Holeski and Futral (1969)	1	.60	1.48	4	2.94	1.84

Table 5.3: Tip clearance losses in Turbines (Experiments and Calculations)

5.3.3 Calculation Results and Discussions

Calculation has been carried out based on the parameters of four different turbines: 1) Kofskey and Nusbaum (1968, [28]), 2) Haas and Kofskey (1979, [18]), 3) Szanca et al. (1974, [55]), and 4) Holeski and Futral (1969, [21]). The baseline case was again the smallest clearance. The calculation results are given in Table 5.3 as well as in Figs. 5.12 to 5.15. Also shown is the experimental data for comparisons.

As can be seen from the figures, there appears to be a linear variation in the efficiency with clearance, similar to a compressor. The theory compares well with the measurements of Haas and Kofskey (1979, [18]), and Szanca et al. (1974, [55]). However, comparison is not as good for the experiment of of Kofskey and Nusbaum (1968, [28]), and Holeski and Futral (1969, [21]). One may suspect this is due to the viscous effect because turbine pressure ratio is much higher in the former two experiments (1.80 and 2.77) than in the latter two (1.23 and 1.48). In order to examined this effect as well as the effect due to wall motion, we have applied Eqs. (B.6) and (4.12) to the turbine experiments and the results are tabulated in Table 5.4. Note that, in the experiment of Haas and Kofskey (1979, [18]), there are more than ten clearances examined, from

about two to five percent of passage height. For simplicity and without changing the results, we have only chosen four representative clearances, i.e. τ/H = 2 %, 3 %, 4 %, and 5 %.

The result show that, for the experiment of Kofskey and Nusbaum (1968, [28]), the velocities due to the relative wall motion are comparable to the clearance flow velocities because of very low Reynolds number (about 8900). The wall motion can thus play a role in the endwall flow. This is regarded as one possible reason that the theory compares poorly with the experiment.

For the experiment of Holeski and Futral (1969, [21]), the calculation results indicate that the effects of viscosity and relative wall motion are not significant and therefore the error in the efficiency prediction is not due to these effects. However, we note this turbine rotor has a relative low hub-to-tip radius ratio (0.6) and a consequent large twist. Therefore, the midspan conditions may not reflect the tip section performance. In particular, the inlet flow angle varies from positive 57.6 degrees at hub, to negative 2 degrees at mid-span, and to negative 55.4 degrees at tip, a total 113 degrees change in the inlet flow angle. The use of mid-span conditions to calculate the clearance loss is thus not appropriate here. We have calculated the efficiency loss using tip conditions and the result, as shown in Fig. 5.15, gives a better comparison with the data.

We also note that, for the experiments of Haas and Kofskey (1979, [18]), and Szanca et al. (1974,[55]), viscous effects and relative wall motion are found to be insignificant from the analysis. Also the hub-to-tip radius ratios are relatively high (0.84 and 0.85). All of these appear to contribute to the good comparisons.

Also shown in the table is the cross flow Mach number, M_c, calculated from Eq. (G.8). The results indicate that the compressibility effect on the clearance flow is not significant for the cases examined.

As a summary, we plotted the ratio of actual to predicted difference in turbine efficiency versus clearance for the four experiments and the results are given in Figure 5.16. The theory compares well with the data covering a large range of stage pressure

Experiments	τ/H (%)	δ^*/τ (%)	v_w/v_c (%)	M_c	r_h/r_t
Kofskey and Nusbaum	1.06	20.7	87.4	.17	.75
Kofskey and Nusbaum	2.47	8.9	51.4	.17	.75
Haas and Kofskey	2.0	14.0	19.5	.38	.84
Haas and Kofskey	3.0	9.3	3.6	.38	.84
Haas and Kofskey	4.0	7.0	0.4	.38	.84
Haas and Kofskey	5.0	5.6	0.0	.38	.84
Szanca et al.	2.3	7.7	1.2	.38	.85
Szanca et al.	3.3	5.3	0.0	.38	.85
Szanca et al.	6.7	2.6	0.0	.38	.85
Holeski and Futral	1.2	9.7	53.1	.31	.6
Holeski and Futral	3.1	3.8	0.9	.31	.6
Holeski and Futral	5.0	2.3	0.0	.31	.6
Holeski and Futral	8.0	1.5	0.0	.31	.6

Table 5.4: Effects of viscosity and wall motion in various experiments

ratio, hub-to-tip radius ratios, and clearances, and thus provides a useful means to assess the clearance losses in both compressors and turbines.

5.4 Summary and Conclusions

Based on the flow model and the assumption that the kinetic energy associated with the clearance flow is lost through mixing, analytical expressions have been derived for the decrease in efficiency, total pressure rise, and shaft power due to clearance for a compressor. Calculations have been carried out based on the parameters in four different compressor experiments. The results also show that the loss increases almost linearly with clearance and the fractional change in compressor total pressure rise is about twice as large the efficiency variation.

Analysis has also been carried out to show that the clearance loss will be smaller if the chordwise blade loading is kept as uniform as possible. An expression is also derived for the flow coefficient at which clearance losses will be minimum for a given machine.

Expressions for the reduction of efficiency and specific work of a turbine due to

clearance have also been derived. Calculations carried out agrees with experimental results. Because of relative thick blades, the clearance flow in a turbine can reattach at the blade tip and a simple analysis has been carried out to show that leakage flow and clearance losses will be higher if the flow reattachment occurs.

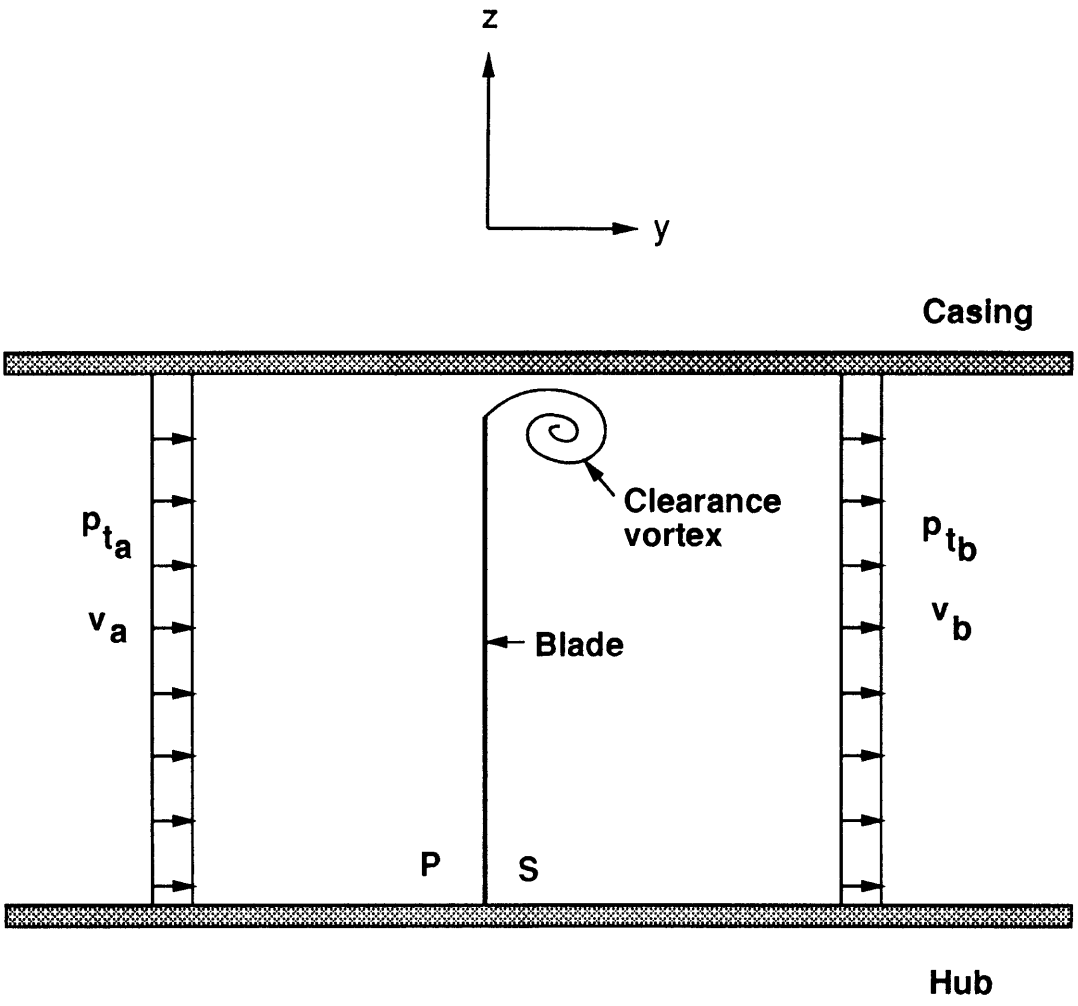

Figure 5.1: Clearance flow on a cross flow plane

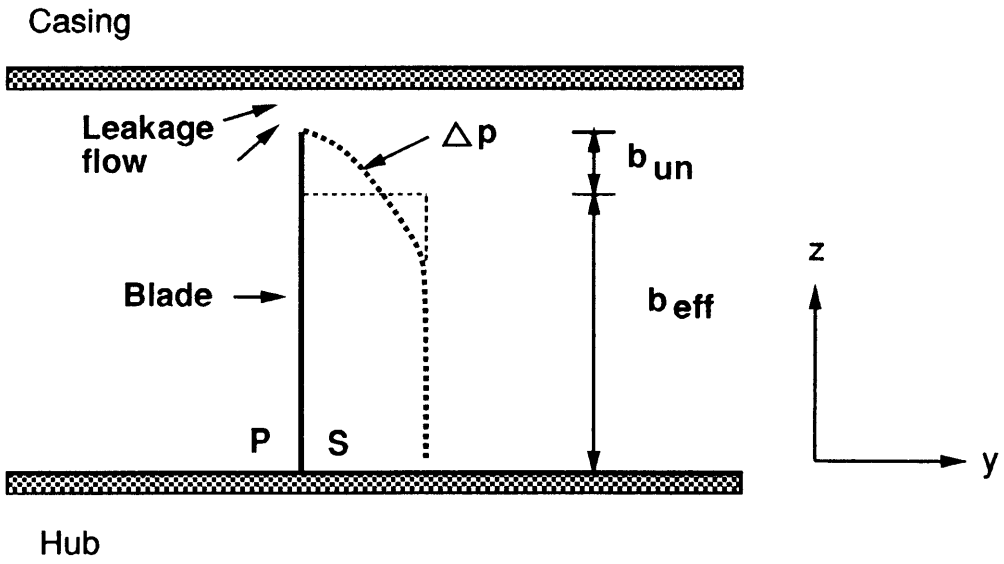

Figure 5.2: Schematic of blade tip unloading

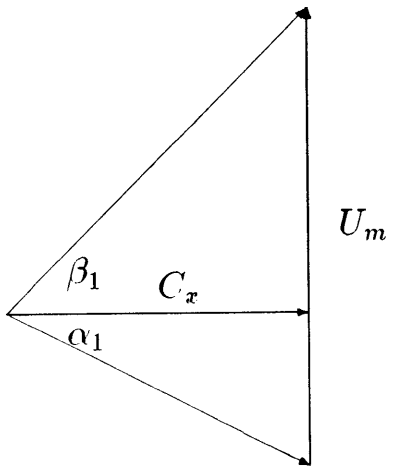

Figure 5.3: Mid-span velocity diagram at a rotor inlet

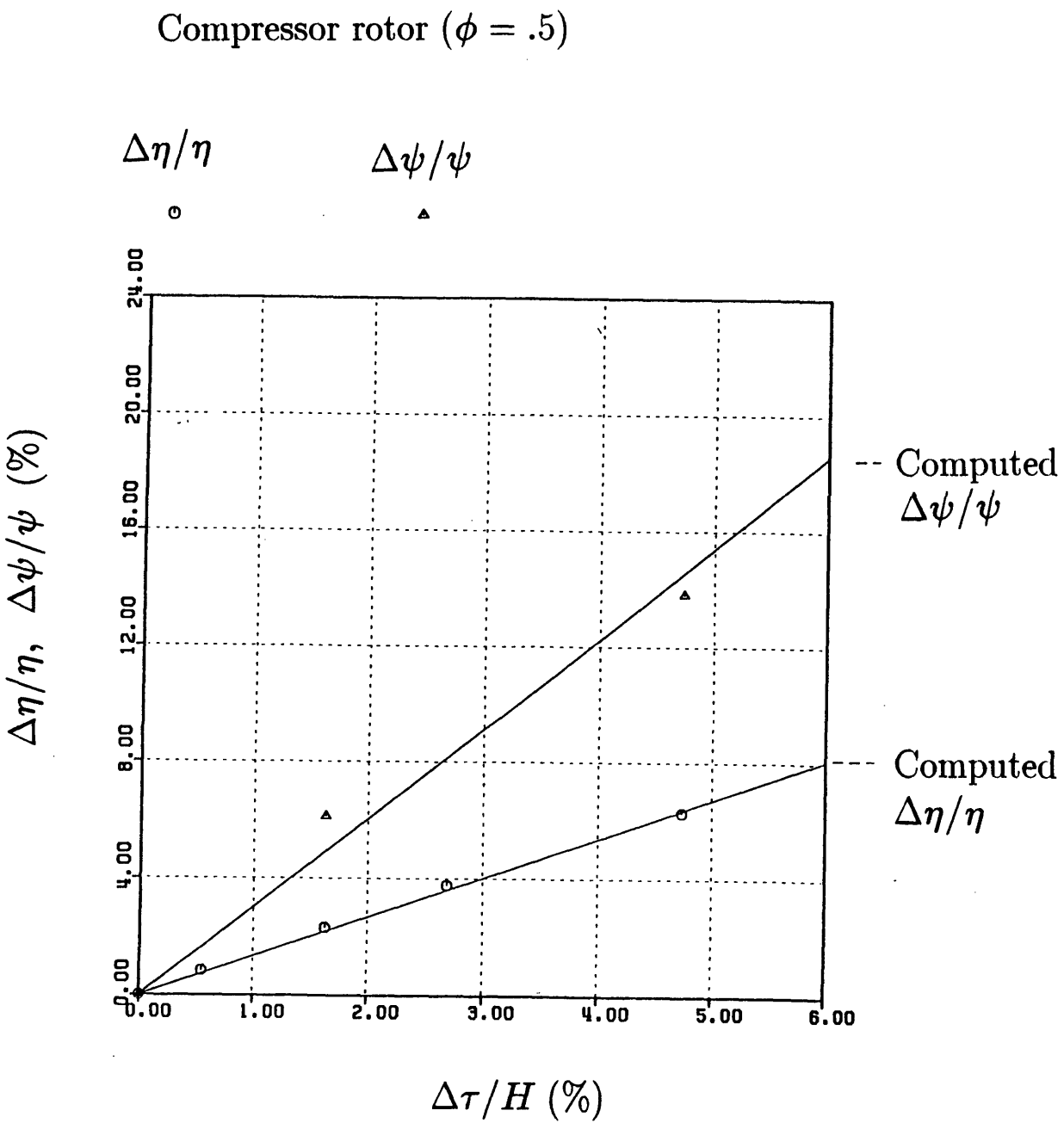

Figure 5.4: Effects of clearance on rotor efficiency and total pressure rise (Solid lines - Calculation; Symbols - Experiment (Inoue et al., 1985))

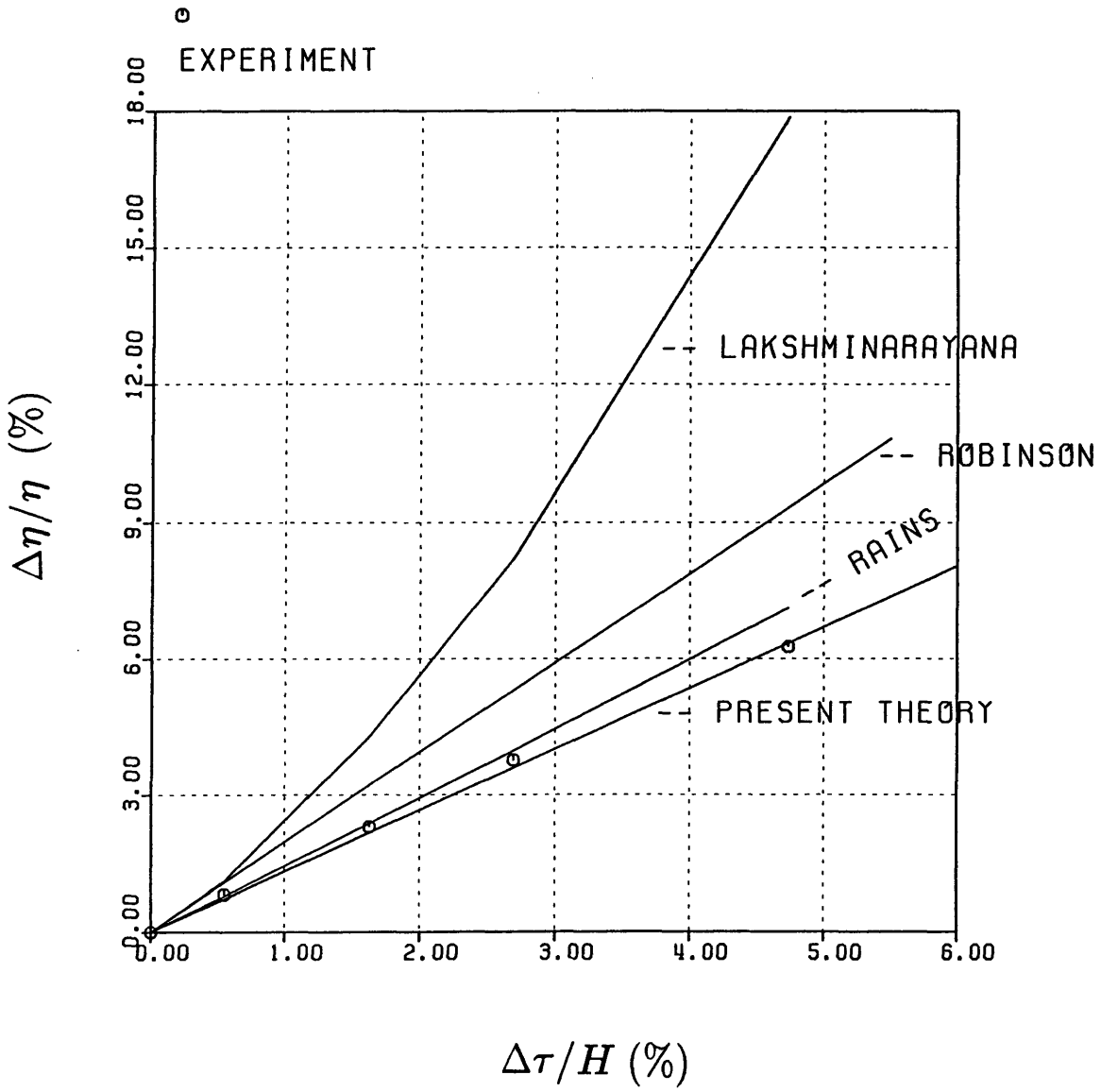

Figure 5.5: Variation of efficiency with clearance for different correlations. (Solid lines - Predictions; Symbols - Experiment (Inoue et al., 1985))

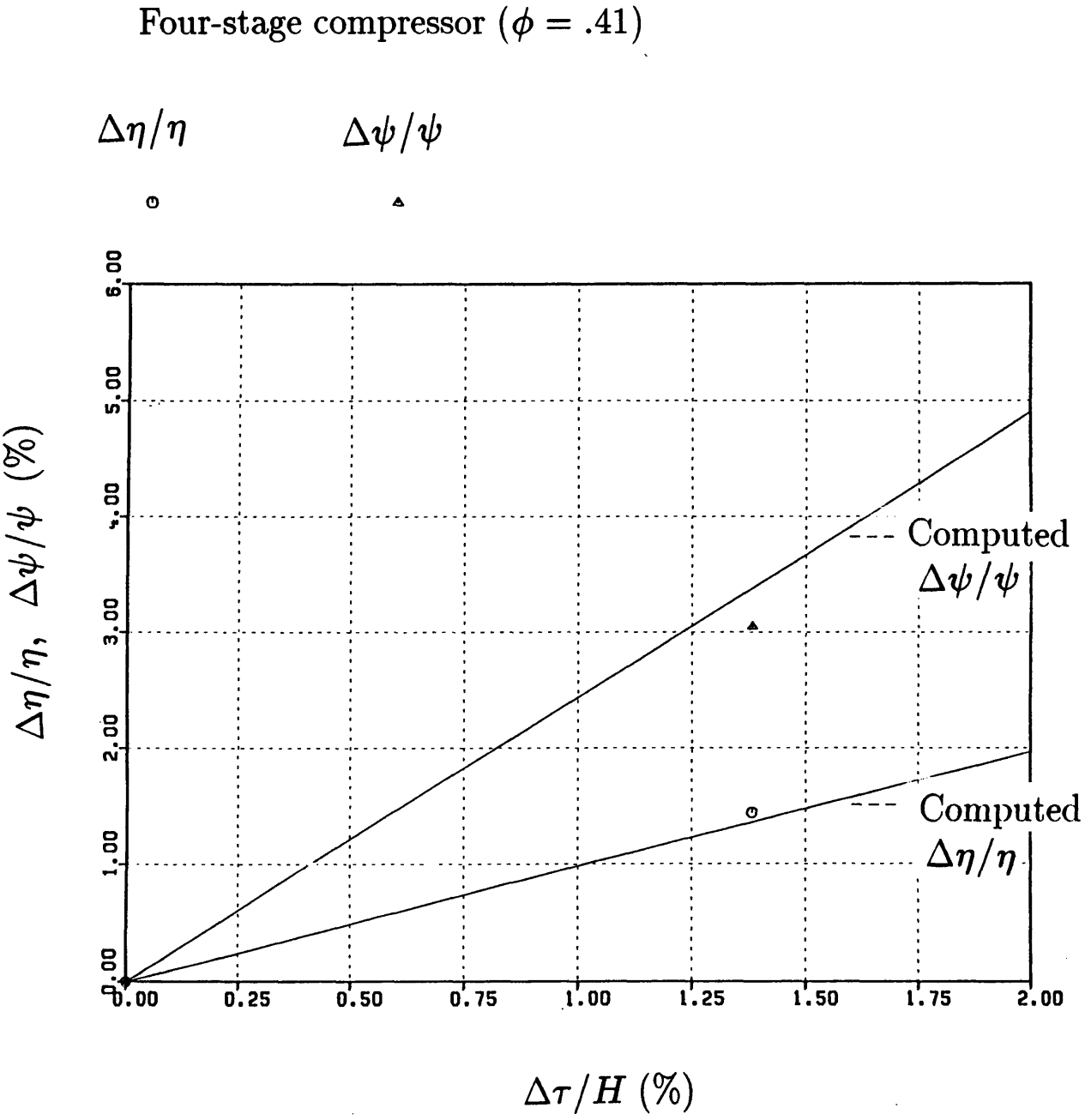

Figure 5.6: Effects of clearance on compressor efficiency and total pressure rise (Solid lines - Calculation; Symbols - Experiment (Wisler, 1984))

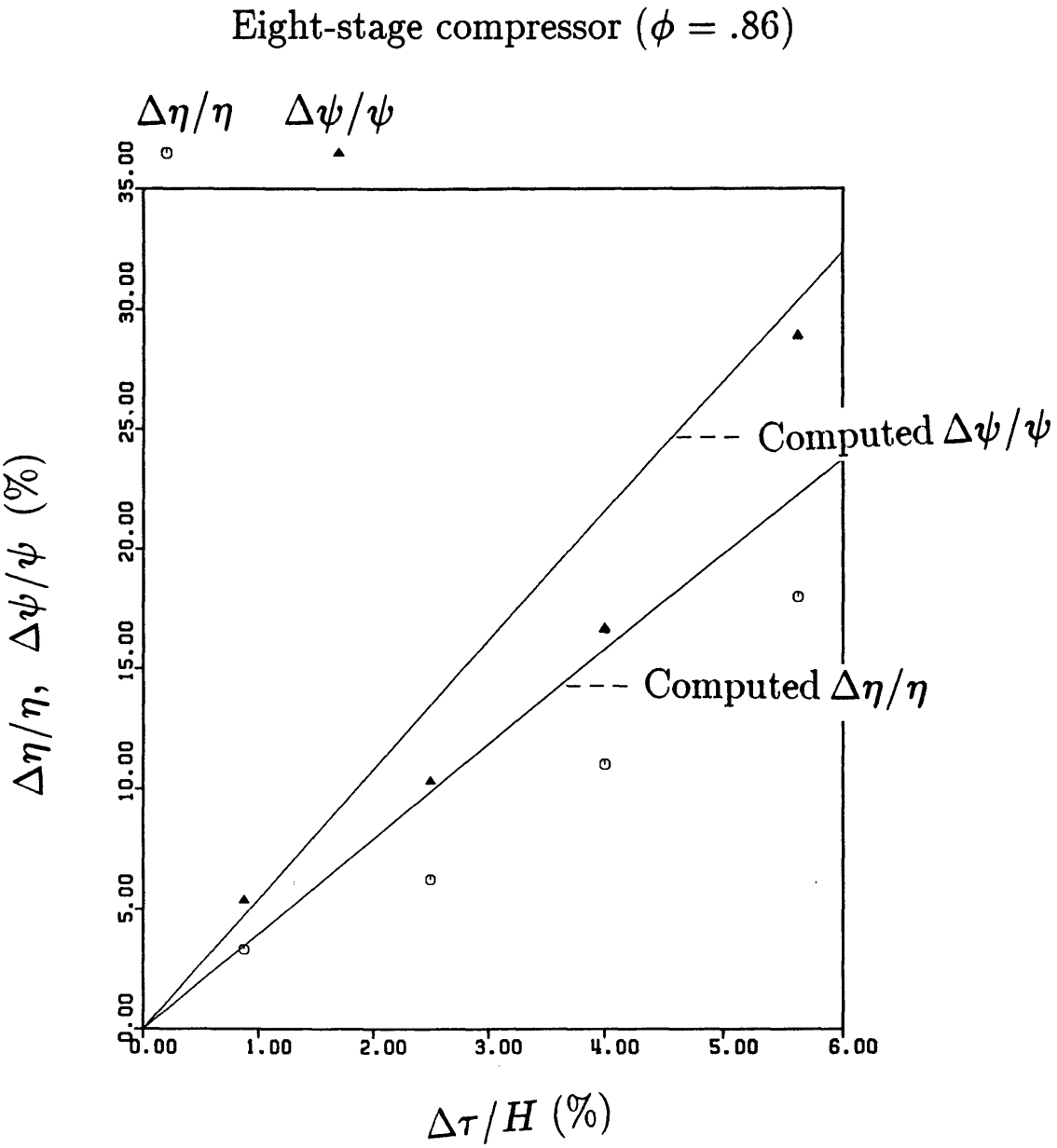

Figure 5.7: Effects of increased clearance on compressor efficiency and pressure rise (Solid lines- Calculations; Symbols - Experiment (Jefferson and Turner, 1958))

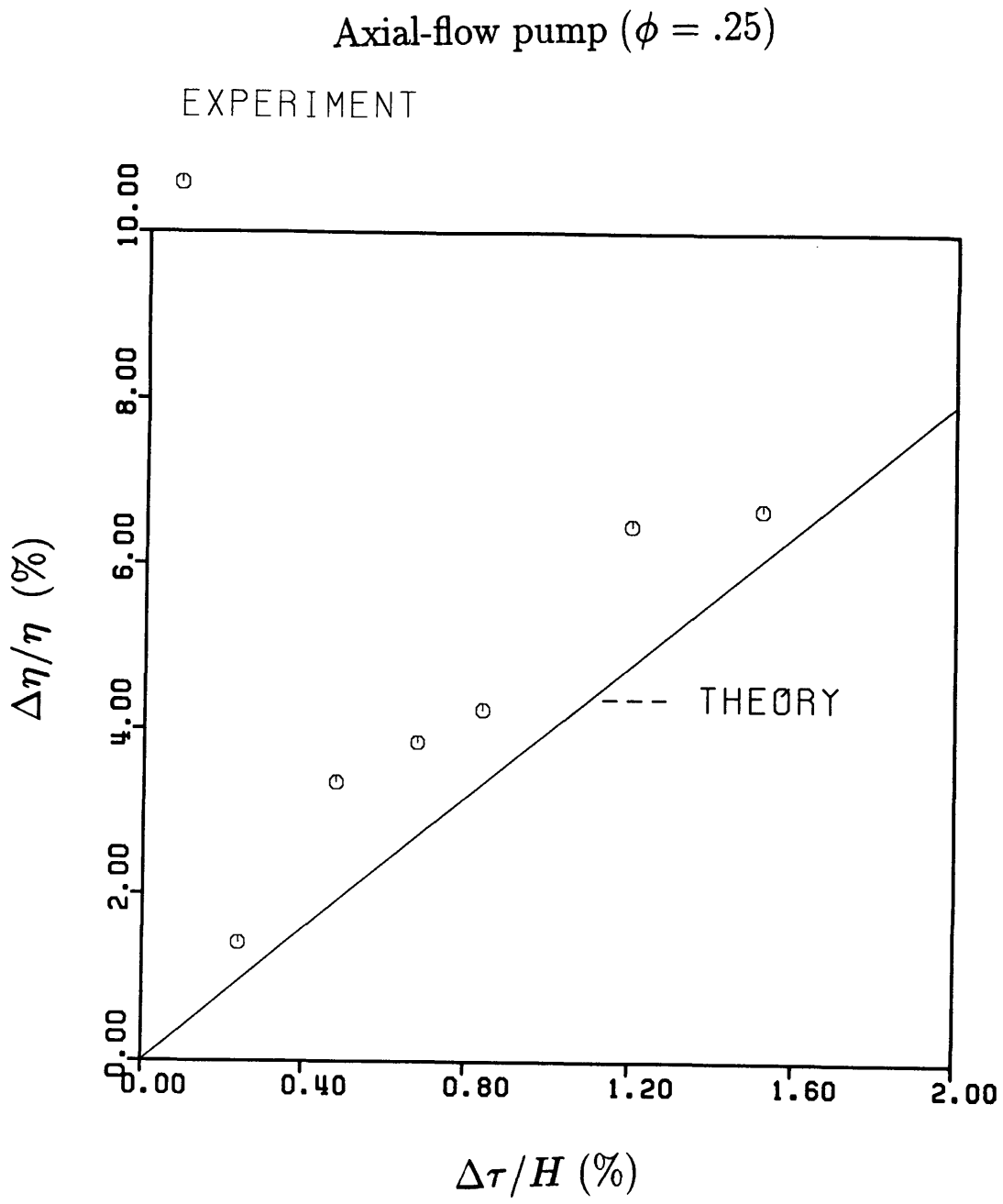

Figure 5.8: Effects of clearance on pump efficiency (Solid line - Calculation; Symbols - Experiment (Spencer, 1956))

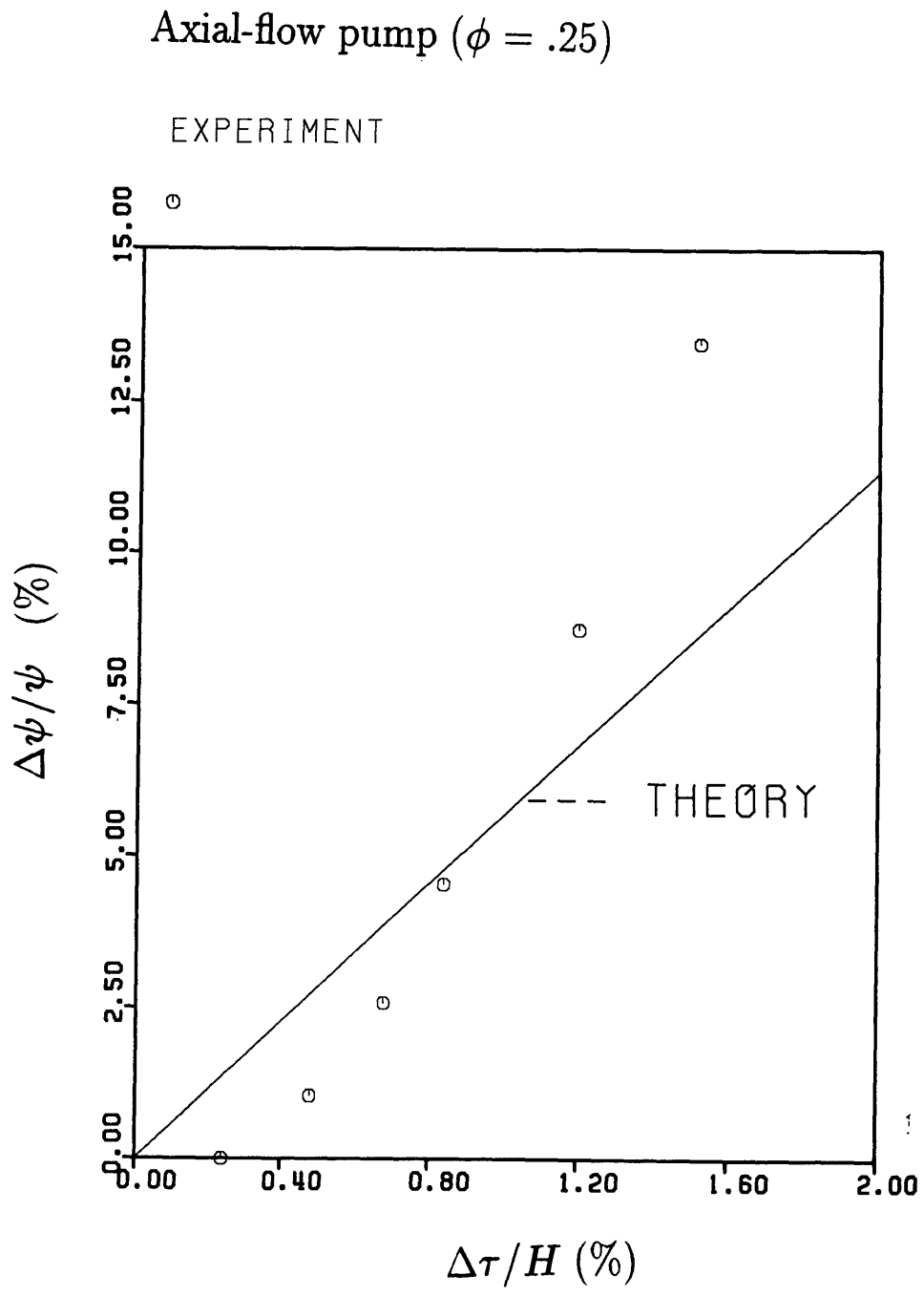

Figure 5.9: Effects of clearance on pump head rise coefficient (Solid line - Calculation; Symbols - Experiment (Spencer, 1956))

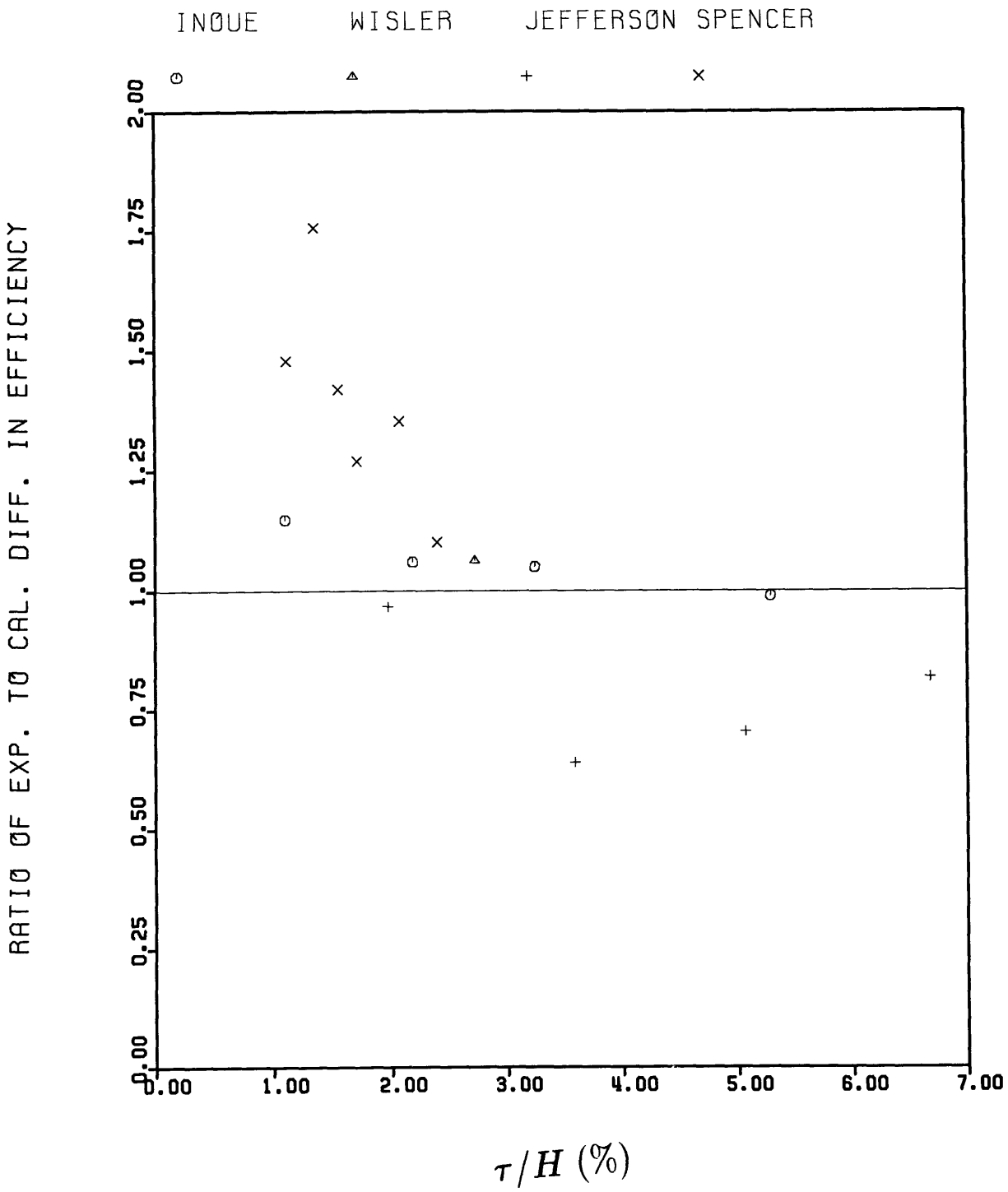

Figure 5.10: The ratio of actual to predicted difference in compressor efficiency versus clearance

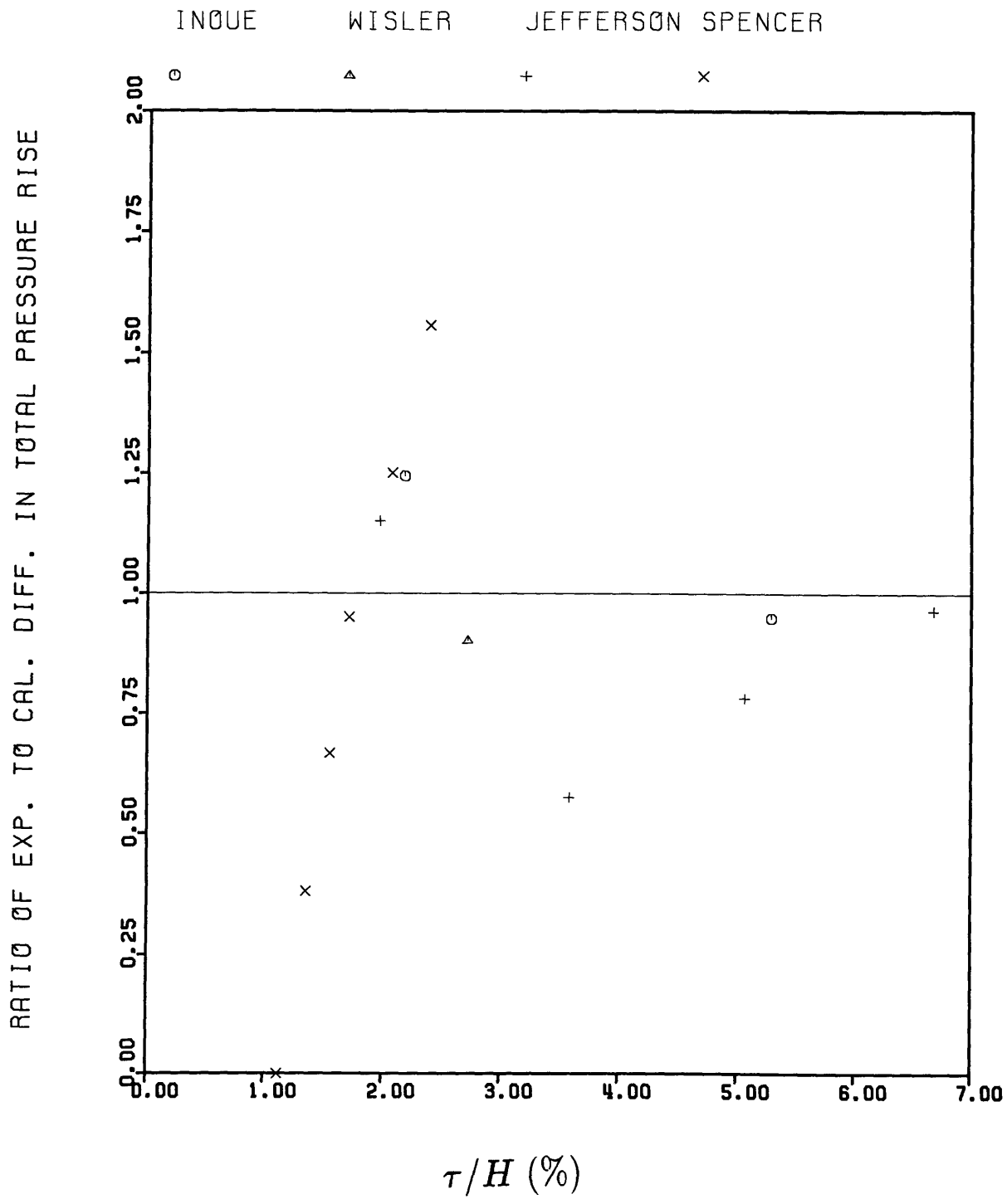

Figure 5.11: The ratio of actual to predicted difference in compressor pressure rise versus clearance

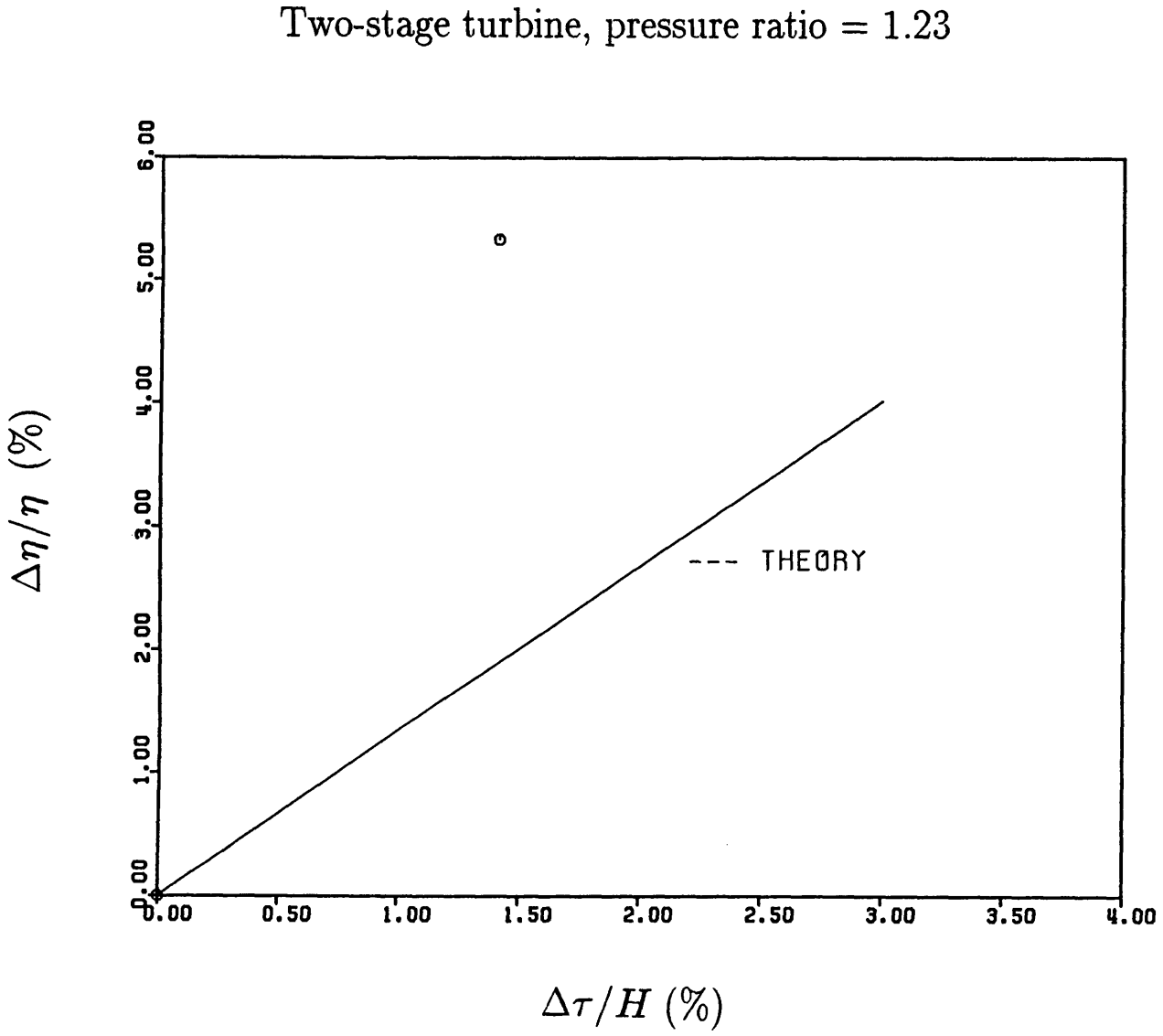

Figure 5.12: Effects of increased clearance on turbine efficiency (Solid line - Calculation; Symbol - Experiment (Kofskey and Nusbaum, 1968))

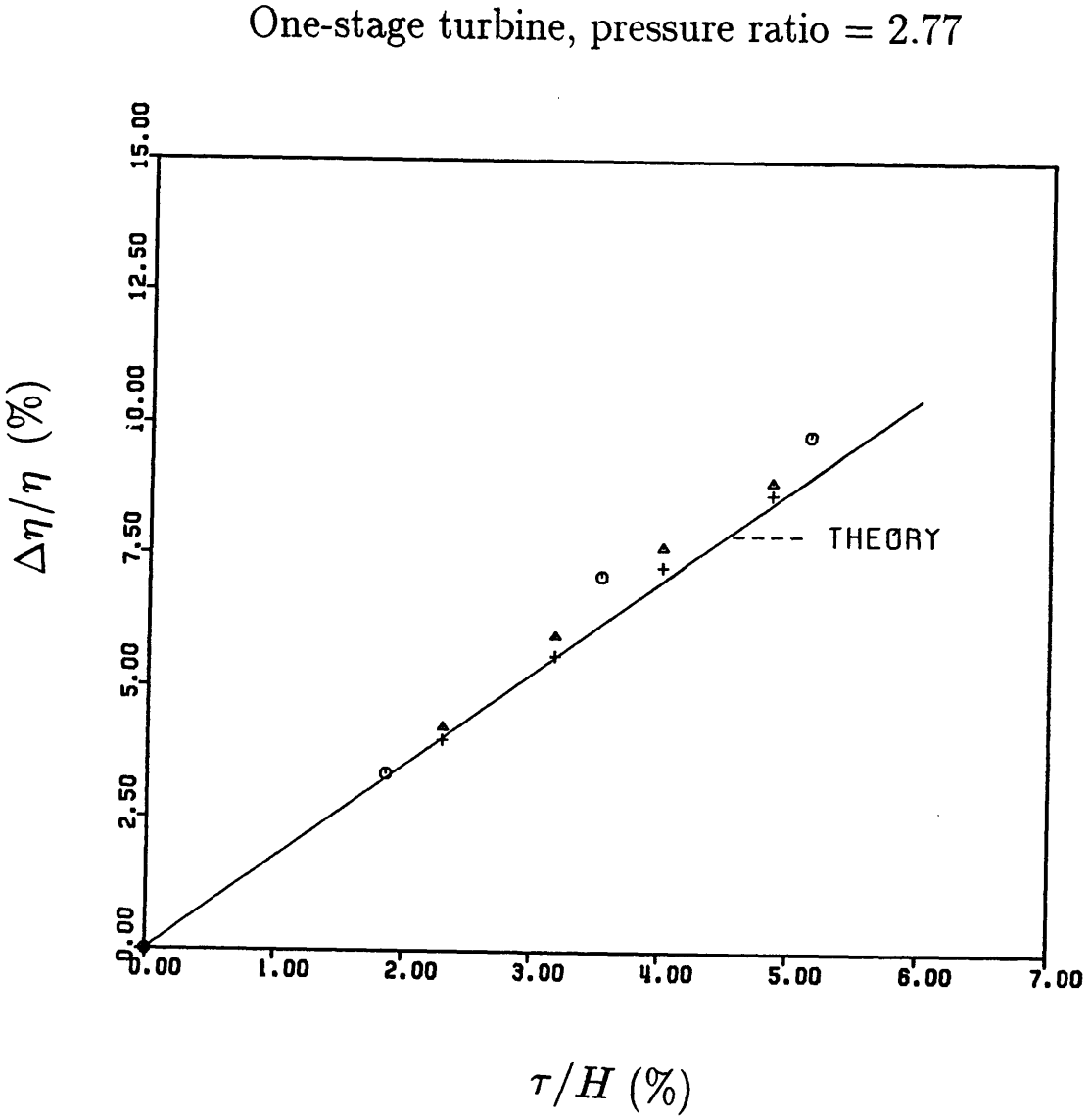

Figure 5.13: Effects of increased clearance on turbine efficiency (Solid line - Calculation; Symbols - Experiment (Haas and Kofskey, 1979))

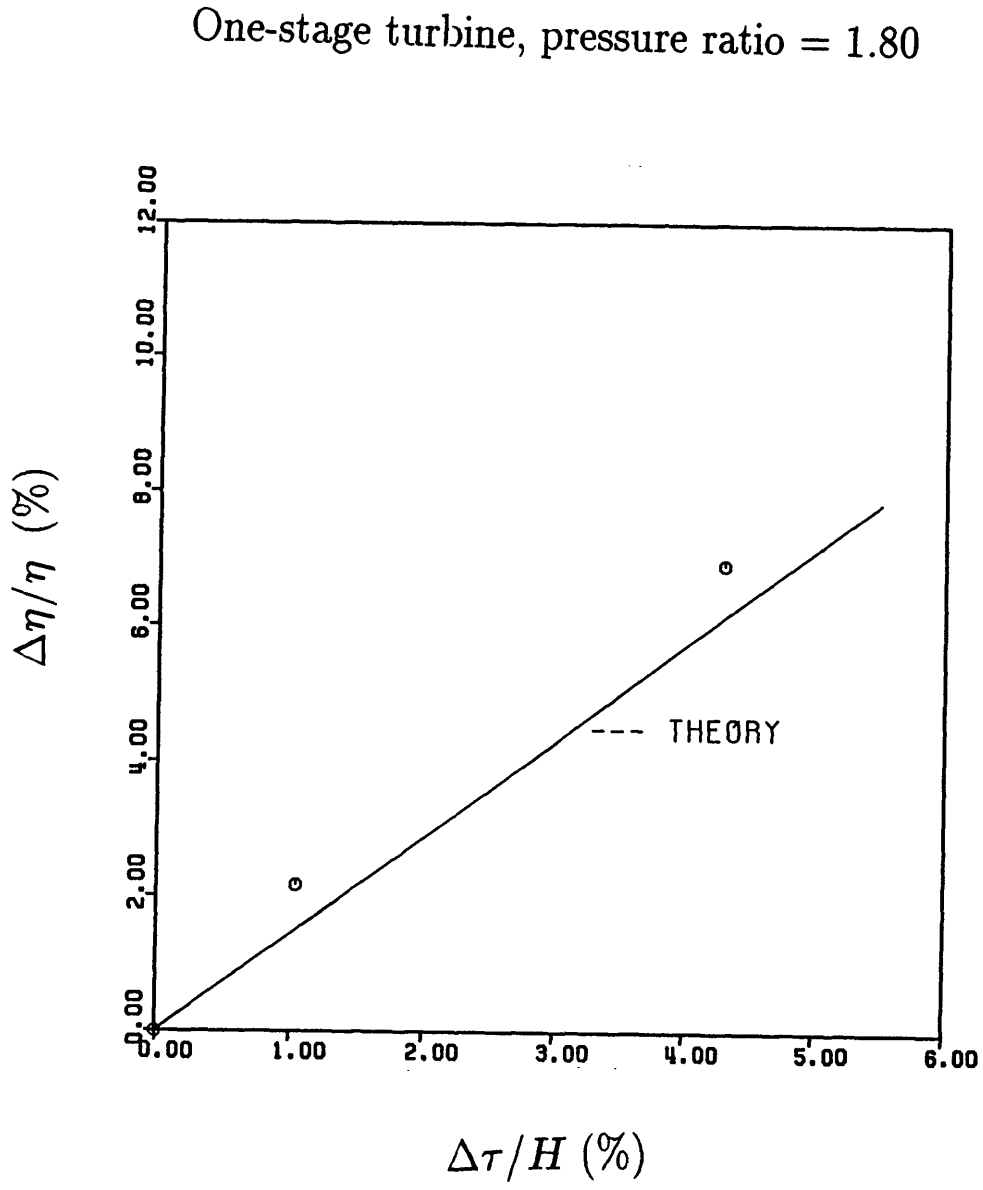

Figure 5.14: Effects of increased clearance on turbine efficiency (Solid line - Calculation; Symbols - Experiment (Szanca et al., 1974))

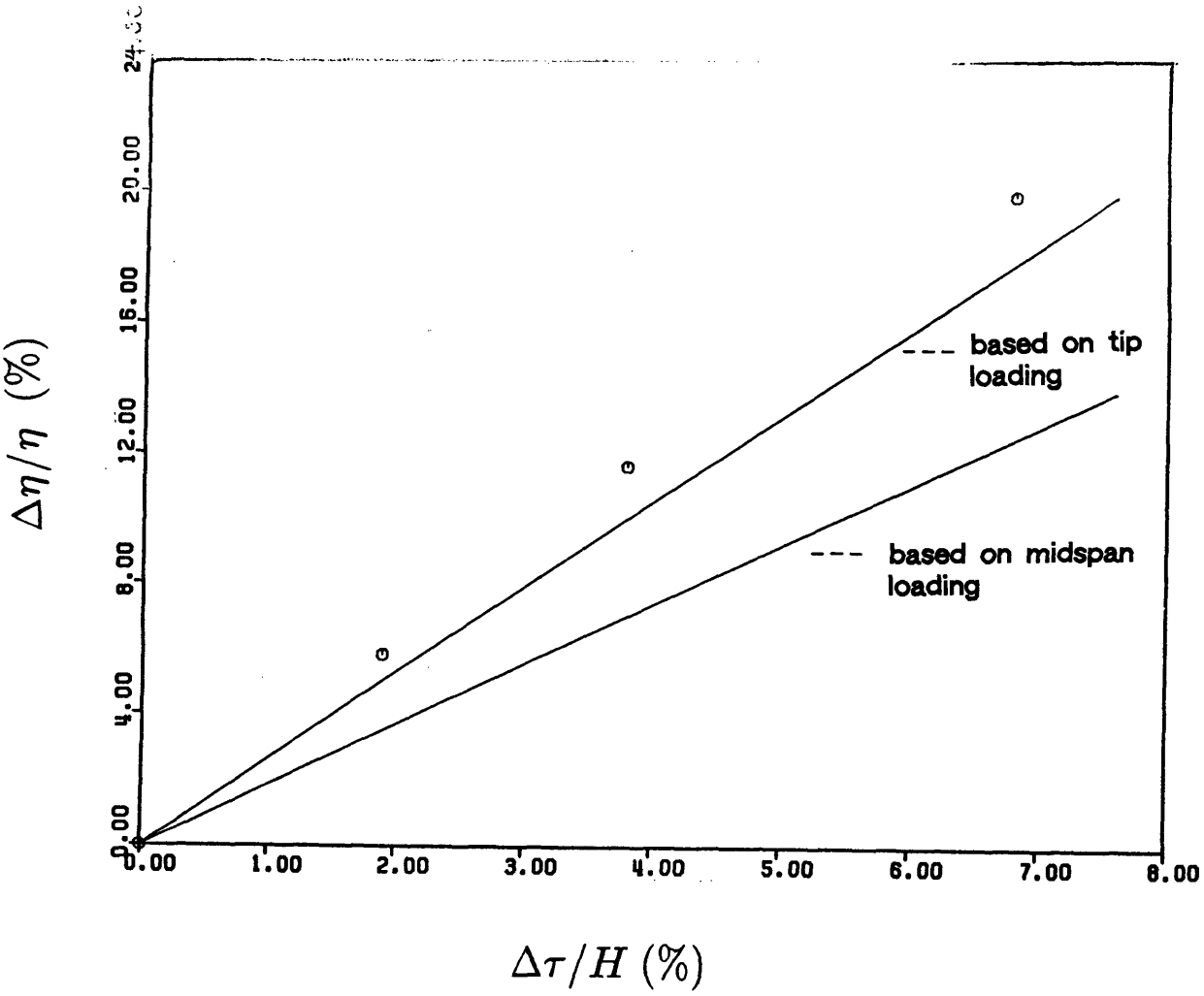

Figure 5.15: Effects of increased clearance on turbine efficiency (Solid line - Calculations; Symbols - Experiment (Holeski and Futral, 1968))

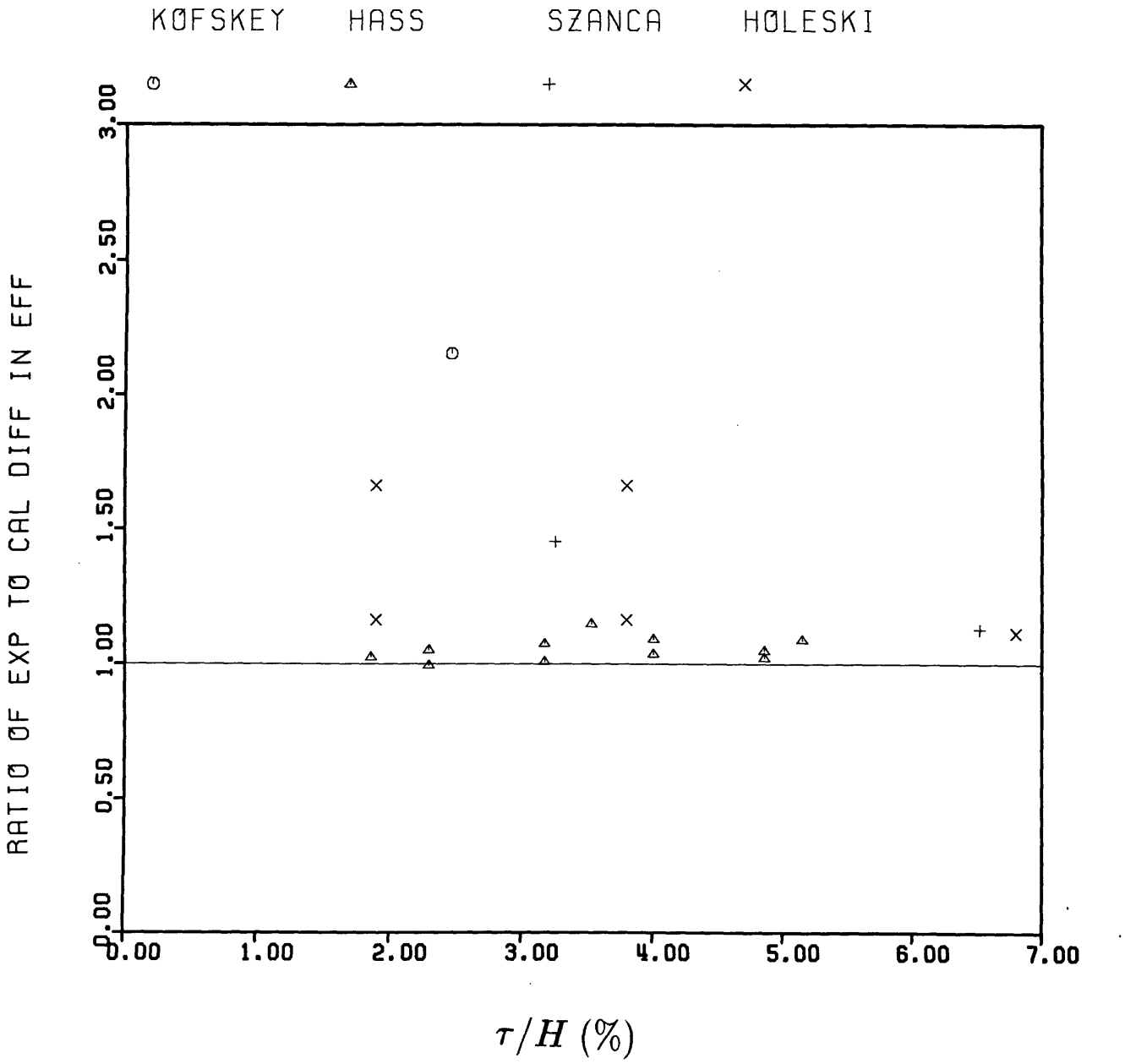

Figure 5.16: The ratio of actual to predicted difference in turbine efficiency versus clearance

Chapter 6

Summary and Conclusions

A new approach, based on an inviscid slender body approximation, has been presented for analyzing turbomachinery tip clearance flows. In developing the approach, focus has been on the mechanism and structure of the vorticity field in the blade passage. This enables one to obtain a simple but useful description of the clearance flow field. The analysis requires only mean blade flow angles and camber line as inputs, and the calculations agree with a wide range of experimental data in regard to essential flow features as well as overall performance.

The conclusions of this thesis are given below. They can be divided into three areas: 1) flow features, 2) tip clearance loss in a turbomachine, and 3) additional results. Recommendations are also made for future work in the area of turbomachinery tip clearance flow.

6.1 Flow Features

- There exists a similarity parameter, t^*, defined as $\frac{t}{\tau}\sqrt{\frac{\overline{\Delta p}}{\rho}}$, for clearance flows. Two clearance flows will be similar if they correspond to the same t^*.
- Following from this similarity, there is a generalized trajectory for the tip clearance vortex, which can be applied to any compressor blading.

- For a given machine the (x, θ) trajectory of the tip vortex core in the blade passage is, to a good approximation, independent of the magnitude of the tip clearance.
- For large t^*, the center of the tip clearance vortex approaches a constant radial location.
- The clearance flow is driven by the blade pressure difference away form the clearance region.
- The endwall static pressure distribution is modified by presence of the tip clearance vortex and the minimum pressure decreases with increase in tip clearance.
- A change in the direction of the vortex trajectory occurs at the blade row trailing edge.
- The centroid of vorticity in the vortex sheet shed from the blade tip remains at a constant radial position downstream of the trailing.

Physical explanations are given for these flow features. Calculations carried out based on the similarity analysis agree very well with experimental results.

6.2 Tip Clearance Losses in a Turbomachine

The present flow model enables one to compute the blade tip unloading and the kinetic energy in the crossflow without any empiricism. If the assumption is made that the crossflow kinetic energy cannot be recoverable as useful work, then analytical expressions for the decrease in overall performance (efficiency, pressure rise, and work) due to clearance can be obtained. This is the first time that a predictive method for calculating the change in compressor performance other than the efficiency due to clearance has been presented. Major conclusions from the investigation on the clearance losses are

- Clearance losses (efficiency and pressure rise) vary almost linearly with clearance.
- Decrease in compressor total pressure rise due to clearance is larger than (roughly twice) the decrease in efficiency.
- Computed results using the present prediction scheme agree with available experimental data. This implies that crossflow kinetic energy associated with the tip clearance vortex gives a good measure of clearance losses.

6.3 Additional Results

The thesis also presents the following results:

- A simple analysis is presented to assess whether the clearance flow is inviscid. The result indicates that the clearance flow can be viewed as inviscid for most of the turbomachinery applications.
- The secondary flow in compressor rotors is in general small compared to the clearance flow.
- The cross-flow due to clearance in a compressor may be treated as incompressible even if the relative Mach number is transonic.

6.4 Recommendations

This study shows that emphasis on vortical structures associated with clearance is well worthwhile in that such an approach gives considerable physical insight into the overall flow features. The resulting model also appears to be useful in predicting losses due to clearance. This suggests that the focus on vortical structures in clearance flows is a fruitful line of endeavor. Because the clearance flow has a significant influence on compressor performance and stall margin, the role it plays on: 1) limiting compressor pressure rise capability, and 2) setting stall inception, should further be investigated, with emphasis on the vortical structures.

We believe that the area increase of the clearance vortex as it passes through the blade passage may be the source of the blockage that limits the pressure rise of a compressor. A preliminary study on this has been carried out (discussed in Appendix M), using the simple model of a Rankine vortex in a diffuser. Calculations showed that the pressure rise characteristic of the diffuser could peak over as a function of diffuser area due to the rapid increase of the vortex area. This may indicate that the clearance vortical structures play a key role in the compressor pressure rise capability. It would be very useful to carry out an experiment based on the simple model; an experiment to examine vortex/main stream pressure gradient interaction. This would help one to understand parametric trends and flow features in a compressor since major elements in the diffuser are also present in a compressor.

Numerical computations have been shown to be useful in bringing out important features of the clearance flow (e.g. Crook, 1989, [9]; Adamczyk et al, 1989, [2]; Adamczyk et al., 1990, [1]; Storer and Cumpsty, 1990, [53]). Another avenue of research that should be pursued is using this approach to examine how the vortical structures grow in size as compressor loading increases and its influence on the compressor presure rise. This could be done by using a Navier-Stokes solver to analyze the flow in a compressor operating along a speed line from design point to peak pressure rise point. Such an approach would shed some light on the source of blockage that limits the pressure rise. Recent computations of Adamczyk imply that it is the area increase of the clearance vortex as it passes though the blade row, not the endwall boundary layer, that is the source of the blockage with stall.

Finally, we note that the current status of computer hardware and numerical schemes for turbomachinery flow does not allow one to predict detailed flow features associated with stall onset and compressor operation in rotating stall. For instance, rotating stall often occurs on a length scale much larger than a blade pitch while current calculations are confined to flow in a single blade passage. It would thus also be desirable to develop a means for predicting the stability of the steady, three-dimensional flow (based on

numerical computation results) at compressor operating point near the peak pressure rise to address fluid dynamical issues associated with the stall inception. One could then examine the stability of the clearance vortex at the stall inception to gain an insight into links between the compressor stall and (clearance) vortex breakdown.

Appendix A

The Equations of Motion for Clearance Flows

For inviscid, three-dimensional, steady, incompressible flows, the equations of mass and momentum conservations in curvilinear coordinates are given, respectively, by

$$\frac{R}{R+y}\frac{\partial u}{\partial s}+\frac{\partial v}{\partial y}+\frac{v}{R+y}+\frac{\partial w}{\partial z}=0$$

$$\frac{R}{R+y}u\frac{\partial u}{\partial s}+v\frac{\partial u}{\partial y}+w\frac{\partial u}{\partial z}+\frac{uv}{R+y}=-\frac{R}{R+y}\frac{1}{\rho}\frac{\partial p}{\partial s}$$

$$\frac{R}{R+y}u\frac{\partial v}{\partial s}+v\frac{\partial v}{\partial y}+w\frac{\partial v}{\partial z}-\frac{u^2}{R+y}=-\frac{1}{\rho}\frac{\partial p}{\partial y}$$

$$\frac{R}{R+y}u\frac{\partial w}{\partial s}+v\frac{\partial w}{\partial y}+w\frac{\partial w}{\partial z}=-\frac{1}{\rho}\frac{\partial p}{\partial z}$$

where s is measured along th camber, y is measured normal to th camber, and z is measure along the span. R(s) is the radius of curvature of a blade camber line.

The streamwise component of velocity u can be written as

$$u(s,y,z)=\overline{u}(s)+u'(s,y,z),$$

where $\overline{u}(s)$ is the through flow velocity. As discussed in chapter two, we assumed that

$$\frac{u'(s,y,z)}{\overline{u}(s)}\ll 1$$

the governing equations then become

$$\frac{R}{R+y}\frac{d\overline{u}}{ds}+\frac{\partial v}{\partial y}+\frac{v}{R+y}+\frac{\partial w}{\partial z}=0$$

$$\frac{R}{R+y}\overline{u}\frac{d\overline{u}}{ds}+v\frac{\partial u'}{\partial y}+w\frac{\partial u'}{\partial z}+\frac{\overline{u}v}{R+y}=-\frac{R}{R+y}\frac{1}{\rho}\frac{\partial p}{\partial s}$$

$$\frac{R}{R+y}\overline{u}\frac{\partial v}{\partial s}+v\frac{\partial v}{\partial y}+w\frac{\partial v}{\partial z}-\frac{\overline{u}^2}{R+y}=-\frac{1}{\rho}\frac{\partial p}{\partial y}$$

$$\frac{R}{R+y}\overline{u}\frac{\partial w}{\partial s}+v\frac{\partial w}{\partial y}+w\frac{\partial w}{\partial z}=-\frac{1}{\rho}\frac{\partial p}{\partial z}$$

For the clearance flow, the characteristic length in the s direction is the chord length c. We take that in the y and z directions at some multiple of the clearance, τ. In compressor and fan applications, τ/c is of the order 10^{-2}, and the chord is generally much less than the radius of curvature $R(s)$. The dominant terms in the equations of motion are thus

$$\frac{\partial v}{\partial y}+\frac{\partial w}{\partial z}=0 \tag{A.1}$$

$$\frac{\partial v}{\partial t}+v\frac{\partial v}{\partial y}+w\frac{\partial v}{\partial z}=-\frac{1}{\rho}\frac{\partial p}{\partial y} \tag{A.2}$$

$$\frac{\partial w}{\partial t}+v\frac{\partial w}{\partial y}+w\frac{\partial w}{\partial z}=-\frac{1}{\rho}\frac{\partial p}{\partial z} \tag{A.3}$$

$$\overline{u}\frac{d\overline{u}}{ds}=-\frac{1}{\rho}\frac{\partial p}{\partial s} \tag{A.4}$$

where we have made the substitution $ds=\overline{u}dt$. Equations (A.1), (A.2), and (A.3) are the governing equations of a two-dimensional unsteady (cross) flow, and Eq. (A.4) is the equation for the through flow. The clearance flow can then be decoupled into cross-flow and through flow.

Appendix B

Inviscid Nature of Clearance Flows

B.1 Previous Studies and Background

Clearance flow has been examined by many investigators and the results have indicated that the clearance flow may be regarded as primarily inviscid, inside and outside the gap except for very tight clearance. Rains (1954, [43]), based on his experimental results, suggested a simple correlation to predict the importance of viscous forces in the clearance flow and concludes that "the frictional resistance to flow through the tip clearance was found to be small for the dimensions that are ordinarily mechanically feasible."

Booth, Dodge , and Hepworth (1982, [7]) calculated the leakage mass flow in a turbine using a slow-flow approximation that is similar to thin-film lubrication theory. The predicted leakage flow was approximately half of the turbine through flow for one percent clearance-to-chord ratio, which is not realistic. The leakage flow was then assumed inviscid and calculations showed that the leakage flow was approximately two percent of the through flow. Therefore, they concluded that the leakage flow could be regarded as inviscid. To examine this further, experiments were conducted on a series of three water flow rigs and the results supported the conclusion.

The results of Sjolander and Amrud (1986, [49]), and Moore and Tilton (1988, [39]) on turbine cascades, and Storer and Cumpsty (1990, [53]) on a compressor cascade have

also supported the inviscid nature of the clearance flow.

We have assessed the inviscid nature of the clearance using a simple analysis based on the relative length scales of clearance and boundary layer thickness; this is described in the following section.

B.2 Simple Analysis

One can argue that viscous effects will not be important if the thickness of the tangential boundary layer in the clearance region, as shown by the shaded region in Figure B.1, is much smaller than the clearance. As concluded by many investigators (see Senoo, 1958, [46]; Belik, 1977, [5]; Graham, 1985, [17]; Moore and Tilton, 1988, [39]), the boundary layer in the gap is laminar in nature. A conservative estimate for the thickness of the boundary layer in the gap region is thus approximately the thickness of a laminar boundary layer over a flat plate. (The favorable pressure gradient in the gap region will tend to make the boundary layer thinner than that for a flat plate.) Based on this approximation, the displacement thickness, at a distance y from the gap entrance, can be written (to one significant figure) as:

$$\delta^* = 2\sqrt{\frac{\nu y}{v_c}} \tag{B.1}$$

where v_c is the clearance flow velocity. At the gap exit, the displacement thickness is

$$\delta^* = 2\sqrt{\frac{\nu h}{v_c}} \tag{B.2}$$

where h is the blade thickness. This can be written as

$$\frac{\delta^*}{\tau} = \frac{2}{\tau}\sqrt{\frac{\nu h}{v_c}} = 2\sqrt{\frac{\nu}{V_1 c}}\sqrt{\frac{V_1}{v_c}}\sqrt{\frac{c^2}{\tau^2}\frac{h}{c}} \tag{B.3}$$

We define a blade loading coefficient as

$$\Delta C_p = \frac{\Delta p}{\rho V_1^2/2} \tag{B.4}$$

where Δp is the pressure difference across blade and V_1 is the inlet relative velocity. From the above definition and Eq. (5.11), we have

$$\frac{v_c}{V_1} = \frac{\Delta C_p}{2} \tag{B.5}$$

Eq. (B.3) then becomes

$$\frac{\delta^*}{\tau} = \frac{2}{\sqrt{Re}} \sqrt{\frac{2}{\Delta C_p}} \frac{c}{\tau} \sqrt{\frac{h}{c}} \tag{B.6}$$

The clearance flow is mainly inviscid if

$$\frac{2}{\sqrt{Re}} \sqrt{\frac{2}{\Delta C_p}} \frac{c}{\tau} \sqrt{\frac{h}{c}} \ll 1 \tag{B.7}$$

More precisely, the viscous effects will not be significant if the boundary layer thickness is, say, an order of magnitude less than the clearance,

$$Inviscid: \quad \frac{2}{\sqrt{Re}} \sqrt{\frac{2}{\Delta C_p}} \frac{c}{\tau} \sqrt{\frac{h}{c}} \leq 0.1 \tag{B.8}$$

and the viscous effects will be dominant if the two are of the same order of magnitudes, i.e.

$$Viscous: \quad \frac{2}{\sqrt{Re}} \sqrt{\frac{2}{\Delta C_p}} \frac{c}{\tau} \sqrt{\frac{h}{c}} \simeq 1 \tag{B.9}$$

For a modern compressor, $Re \simeq 5 \cdot 10^5$, $\Delta C_p \simeq .5$, $h/c \simeq .05$, and the calculated δ^*/τ from Eq. (B.7) is roughly ten percent for a clearance to chord ratio of one percent. The clearance flow in a compressor can be regarded as mainly inviscid.

We now compare our results to Rains' correlation. Based on his experimental studies, Rains (1954, [43]) presented a semi-empirical correlation criterion for the effects of viscosity on clearance flow in a turbomachine. This can be written as:

$$Inviscid: \quad \frac{1}{\sqrt{Re}} \frac{c}{\tau} \sqrt{\frac{h}{c}} \leq .09$$

$$Viscous: \quad \frac{1}{\sqrt{Re}} \frac{c}{\tau} \sqrt{\frac{h}{c}} \geq .41$$

Applying Eqs. (B.8) and (B.9) based on the parameters used in the experiment, the results were found to be

$$Inviscid: \quad \frac{1}{\sqrt{Re}} \frac{c}{\tau} \sqrt{\frac{h}{c}} \leq .03$$

$$Viscous: \quad \frac{1}{\sqrt{Re}} \frac{c}{\tau} \sqrt{\frac{h}{c}} \geq .26$$

These agree with the experimental results of Rains, although the former is bit more conservative than the latter.

In summary, a simple analysis has been carried out to assess whether viscous effects are important in the clearance flow. The results show that the clearance flow is basically inviscid and this is supported by many other investigations. The theory also gives similar results to those of Rains, which is a special case of the analysis.

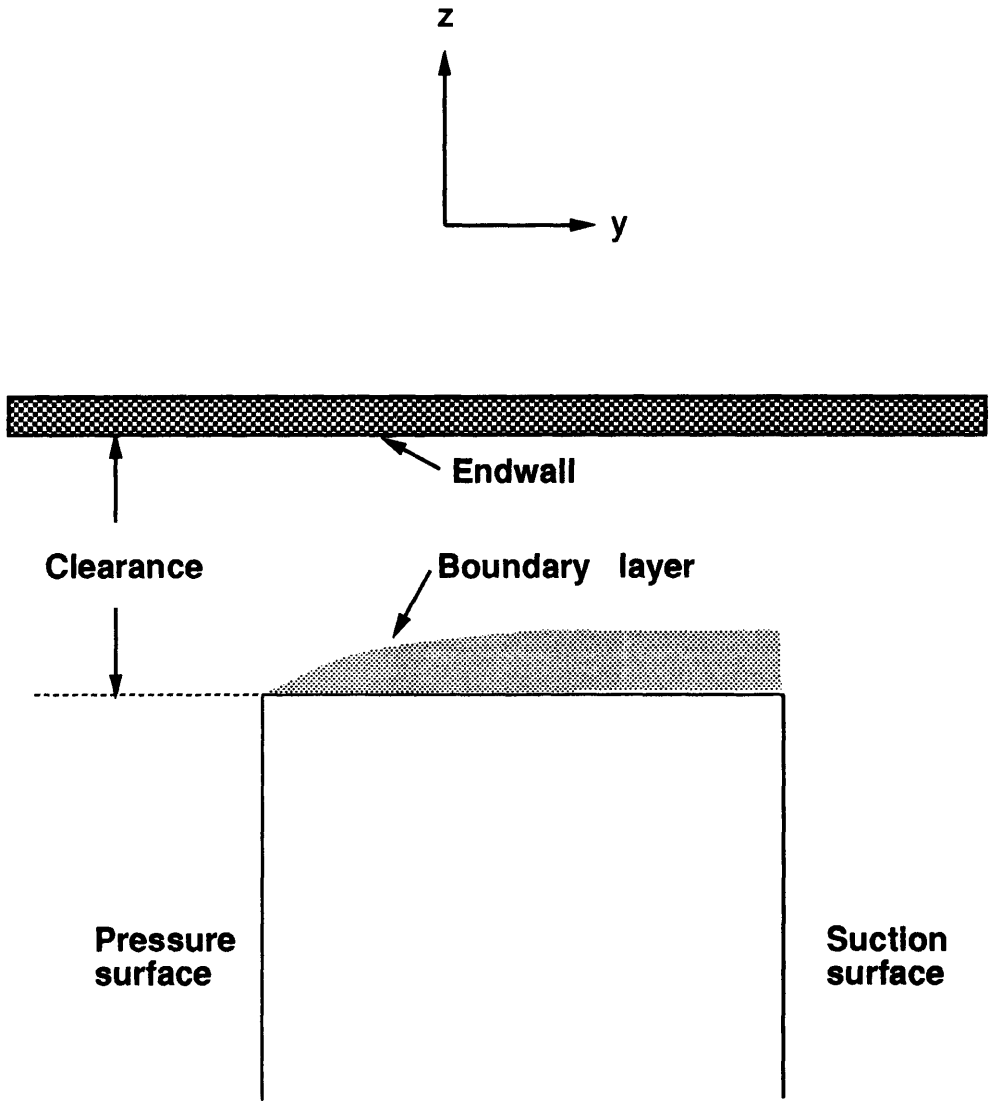

Figure B.1: Schematic of a boundary layer in clearance region

Appendix C

Radial Motion of Tip Vortex Center for Large t^*

We now examine the radial motion of the center of a clearance vortex inside blade passage when $t^* \gg 1$. Consider the clearance vortex shed from blade tip as illustration in Fig. C.1. Also shown in the figure is the image of the clearance vortex needed to satisfy the kinematic boundary conditions at the wall. The magnitude of Kelvin impulse of this vortex pair plus the bound vortex sheet, i.e. the blade, is given by:

$$I = 2\rho \int_0^{H-\tau} \gamma \, z \;\; dz + 2\rho \int_0^{\epsilon_{max}} \gamma \, z \, d\epsilon \tag{C.1}$$

where H is passage height, γ is strength of the vortex sheets, and ϵ is the intrinsic coordinate along the shed vortex sheet. Eq. (C.1) can be written as

$$I = 2\rho(\Gamma_b \, z_b + \Gamma_s \, z_s) \tag{C.2}$$

where Γ_b and Γ_s are, respectively, the circulation of the bound and shed vortex sheet, and z_b, and z_s are, respectively, the centroid of vorticity of the bound and shed vortex sheet. Note that $z_s = H - z_v$.

Since the rate of change of the Kelvin impulse is equal to the force exerted on the flow, differentiating Eq. (C.2) with respect to time t gives:

$$\frac{d(\Gamma_b z_b)}{dt} + \frac{d(\Gamma_s z_s)}{dt} = \frac{F_b}{\rho} \tag{C.3}$$

where F_b is the total force on the blade (per unit chord).

The radial motion of the shed vortex centroid (z_s) for large t^* is now examined. For $t^* \gg 1$, Γ_b and z_b can be treated as constants so that Eq. (C.3) becomes:

$$\frac{d(\Gamma_s z_s)}{dt} = \frac{F_b}{\rho} \tag{C.4}$$

and also from Eq. (2.37)

$$\frac{\Delta p}{\rho} = (\gamma \overline{w})_{tip} = Const. \tag{C.5}$$

where γ is the strength of the bound vortex sheet and $\overline{w}$ is the average velocity, both evaluated at blade tip. In addition, the rate of the change of the shed circulation remains constant for $t^* \gg 1$, i.e.

$$\frac{d\Gamma_s}{dt} = (\gamma \overline{w})_{tip} = Const. \tag{C.6}$$

Integrating this gives

$$\Gamma_s = (\gamma \overline{w})_{tip}\, t + C_1 \tag{C.7}$$

, where C_1 is an integration constant. Substituting Eqs. (C.6) and (C.7) into Eq. (C.4) one has

$$z_s + [t + \frac{C_1}{(\gamma \overline{w})_{tip}}]\frac{dz_s}{dt} = \frac{F_b}{\rho(\gamma \overline{w})_{tip}} \tag{C.8}$$

From Eqs. (5.19) , (5.20), (5.23), and (C.5), it is found that

$$z_s + (t + C_2)\frac{dz_s}{dt} = H - (1 + k)\tau \tag{C.9}$$

where, for simplicity, we have made the following substitution:

$$C_2 = \frac{C_1}{(\gamma \overline{w})_{tip}}$$

We note that, under the approximations made in getting Eqs. (C.9), the result will be only qualitative rather than quantitative. However, it is sufficient for the purpose of this study. Eq. (C.9), a simple first order differential equation, can easily be solved and the result is found to be

$$z_v^* = 1 + k + \frac{C_3}{t^* + C_4} \tag{C.10}$$

where C_3 andC_4 are constants. For $t^* \gg 1$, we have

$$z_v^* \simeq Const. \tag{C.11}$$

This is the desired result, which indicates that the centroid of the shed vortex sheet stays (approximately) at a constant radial location when $t^* \gg 1$. This conclusion is also true for the centroid of the vortex core since the two have the same functional dependence on time t^*.

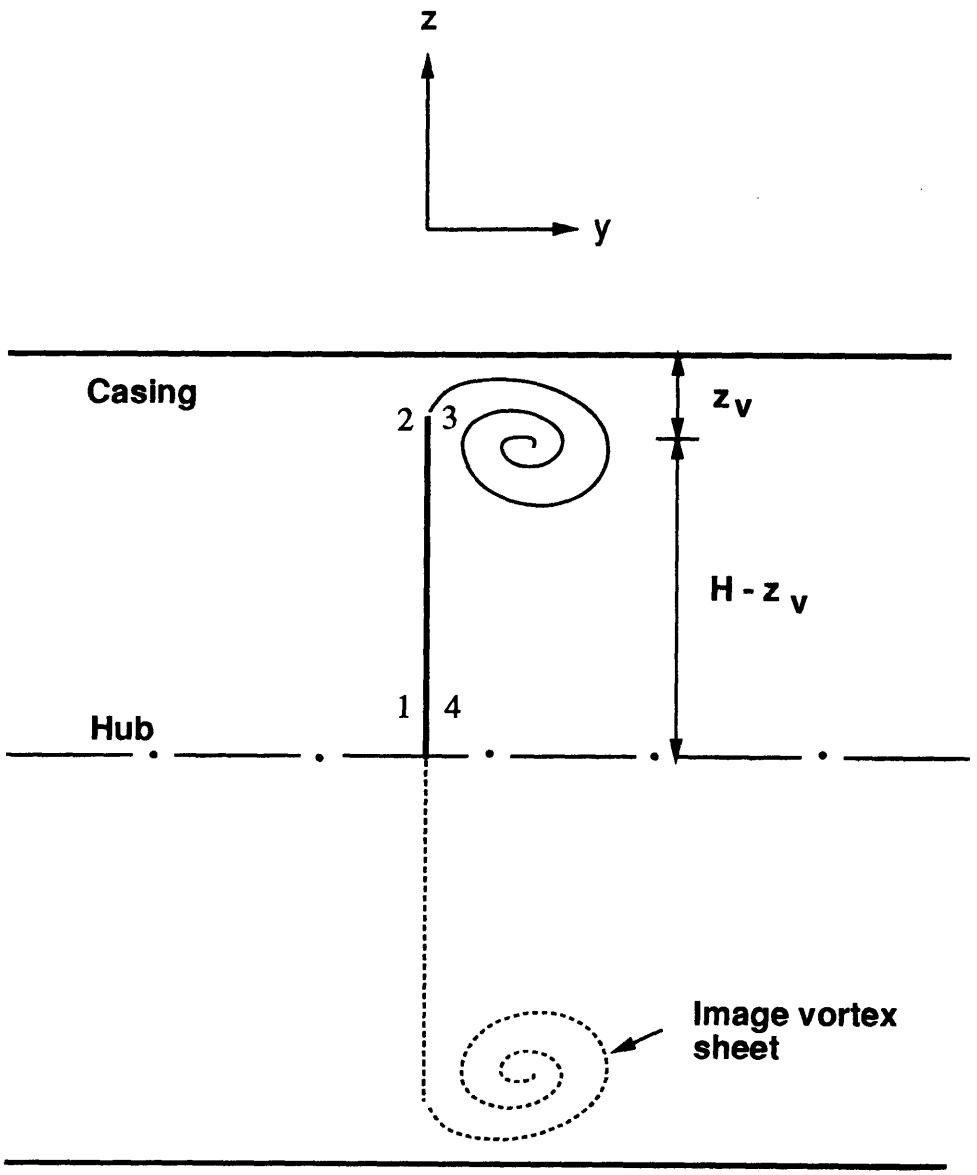

Figure C.1: Illustration of a vortex sheet and its image in a blade passage

Appendix D

Convection Velocity of A Point Vortex - Routh's Correction

Consider a point vortex located at Φ_0 in the physical plane and Ξ_0 in the transformed plane. The conformal transformation can be written as

$$\Phi = \Phi(\Xi) \tag{D.1}$$

The induced (complex) velocity at the vortex (Φ_0) in the physical plane is

$$Q(\Phi_0) = [\frac{dF(\Phi)}{d\Phi} - \frac{i\Gamma_0}{2\pi\ (\Phi - \Phi_0)}] \tag{D.2}$$

, evaluated at $\Phi = \Phi_0$, where F is the complex potential of the flow. In Ξ plane, the complex potential can be written as

$$F(\Xi) = F'(\Xi) + \frac{i\Gamma_0}{2\pi}\ln(\Xi - \Xi_0) \tag{D.3}$$

, where F' is complex potential of the flow excluding the point vortex. Differentiating the complex potential, one has

$$\frac{dF(\Phi)}{d\Phi} = \frac{dF(\Xi)}{d\Xi}\frac{d\Xi}{d\Phi} \tag{D.4}$$

From Eqs. (D.3) and (D.4), one has

$$\frac{dF(\Phi)}{d\Phi} = [\frac{dF'(\Xi)}{d\Xi} + \frac{i\Gamma_0}{2\pi\ (\Xi - \Xi_0)}]\frac{d\Xi}{d\Phi} \tag{D.5}$$

Since the vortex induced no velocity at its center, the complex velocity of the vortex in the transformed plane is

$$Q(\Xi_0) = \frac{dF'(\Xi)}{d\Xi} \tag{D.6}$$

Substituting Eqs. (D.5) and (D.6) into (D.2), one has

$$Q(\Phi_0) = Q(\Xi)\,\frac{d\Xi}{d\Phi} + \frac{i\Gamma_0}{2\pi}\left(\frac{1}{\Xi - \Xi_0}\frac{d\Xi}{d\Phi} - \frac{1}{\Phi - \Phi_0}\right) \tag{D.7}$$

evaluated at $\Phi = \Phi_0$ and $\Xi = \Xi_0$ The first term on the right hand side of Eq. (D.7) represents a direct transformation of the complex velocity of a vortex in the Ξ (transformed) plane to the Φ (physical) plane and the second term is a correction, called Routh's rule, to account for singular behavior of the velocity of a point vortex due to conformal mapping. To calculate the correction, one can expand

$$\Xi - \Xi_0 \simeq \frac{d\Xi}{d\Phi}\,(\Phi - \Phi_0) + \frac{1}{2}\frac{d^2\Xi}{d\Phi^2}\,(\Phi - \Phi_0)^2 \tag{D.8}$$

The correction term is then

$$-\frac{i\Gamma_0}{4\pi}\,\frac{d^2\Xi}{d\Phi^2}\,/\frac{d\Xi}{d\Phi} \tag{D.9}$$

Appendix E

Leakage Flow Approach

E.1 Vortex Trajectory and Similarity Scaling

Clearance flow was examined by Rains (1954, [43]) based on a leakage flow approach, which is discussed in the text. We now use this approach to examine the behavior of clearance flow and compare the results to the vortex calculation.

It is assumed that main stream velocities on suction side and pressure side of a blade are given by $V_1 + u'$ and $V_1 - u'$, respectively, as shown in the upper part of Fig. E.1, where V_1 is the relative inlet velocity and u' is the velocity perturbation in the streamwise direction. Because clearance flow induces a velocity v_t[1] normal to the pressure side velocity, $V_1 - u'$, resultant velocity of the clearance flow is thus the vector sum of these two velocities. On the suction side, because total and static pressure in the clearance flow are identical to those in the main stream, the clearance flow velocity has a magnitude equal to $V_1 + u'$ and an angle β with the main stream, which is shown in the lower part of the figure. Rains (1954, [43]) showed

$$\tan\frac{\beta}{2} = \frac{v_t}{2\,V_1} \tag{E.1}$$

[1]Note that v_t is the jet velocity and is different from v_c, which is the tangential component of cross flow velocity averaged over clearance.

A vortex sheet is thus shed off at the tip. The convection velocity of the vortex sheet, denoted by V_m, is the vector mean velocity of the clearance flow velocity and the suction side velocity as shown in the lower part of the figure. At time t the vortex sheet thus moves a distance equal to $V_m \sin(\beta/2)\, t$ normal to the blade, and the centroid of the vortex sheet thus moves half of that distance, i.e.

$$y_v = \frac{1}{2} V_m \sin \frac{\beta}{2} t \tag{E.2}$$

which can also be written as:

$$y_v = \frac{v_t}{4} t \tag{E.3}$$

Because $v_t = \sqrt{2\Delta p/\rho}$, one has

$$y_v = \frac{1}{4}\sqrt{\frac{2\Delta p}{\rho}}\, t \tag{E.4}$$

Dividing this by clearance τ, it can be shown that

$$y_v^* = \frac{\sqrt{2}}{4} t^* \simeq 0.354\, t^* \tag{E.5}$$

Two flow features are noted from the analysis. First the vortex trajectory does not vary with clearance as indicated in Eq. (E.4), as concluded from the vortex calculation. In addition, as shown in Eq. (E.5), there exists a similarity parameter t^* for the clearance flow and the non-dimensional vortex location y_v^* depends only this similarity parameter, as concluded from the similarity analysis in Chapter 2. The leakage flow analysis also shows that the ratio of y_v^*/t^* is about .354, which agrees well with the value (.365) from the vortex calculation.

Downstream of the trailing edge, there is no vorticity shed off at the tip and the vortex sheet and its centroid thus move with the same velocity $\frac{v_t}{2}$. Since the cross-flow plane velocity of the centroid downstream of the trailing edge is twice as much as that in blade passage, there will be a change in the vortex core trajectory at the trailing edge, which agrees with the results in Chapter 3.

E.2 Leakage Flow Rate

Clearance mass flow $\dot{m}_c$ is given by Eq. (5.10)

$$\dot{m}_c = \rho \, v_c \, \tau \tag{E.6}$$

where v_c is the tangential component of cross flow velocity averaged over clearance. Based on the leakage flow approach, it can be shown that

$$v_c = \xi \, \sqrt{2} \, \sqrt{\frac{p_1 - p_2}{\rho}} \tag{E.7}$$

where ξ is the contraction factor equal to $\frac{\pi}{\pi + 2}$, p_1 is the static pressure on the pressure surface away from tip, and p_2 is the static pressure at the vena contracta, which are shown in Fig. E.2, so that

$$v_c \simeq 0.86 \, \sqrt{\frac{p_1 - p_2}{\rho}} \tag{E.8}$$

From the vortex calculation,

$$v_c \simeq 1.0 \, \sqrt{\frac{p_1 - p_3}{\rho}} \tag{E.9}$$

where p_3 is the static pressure on the suction surface away from the tip as shown in the figure.

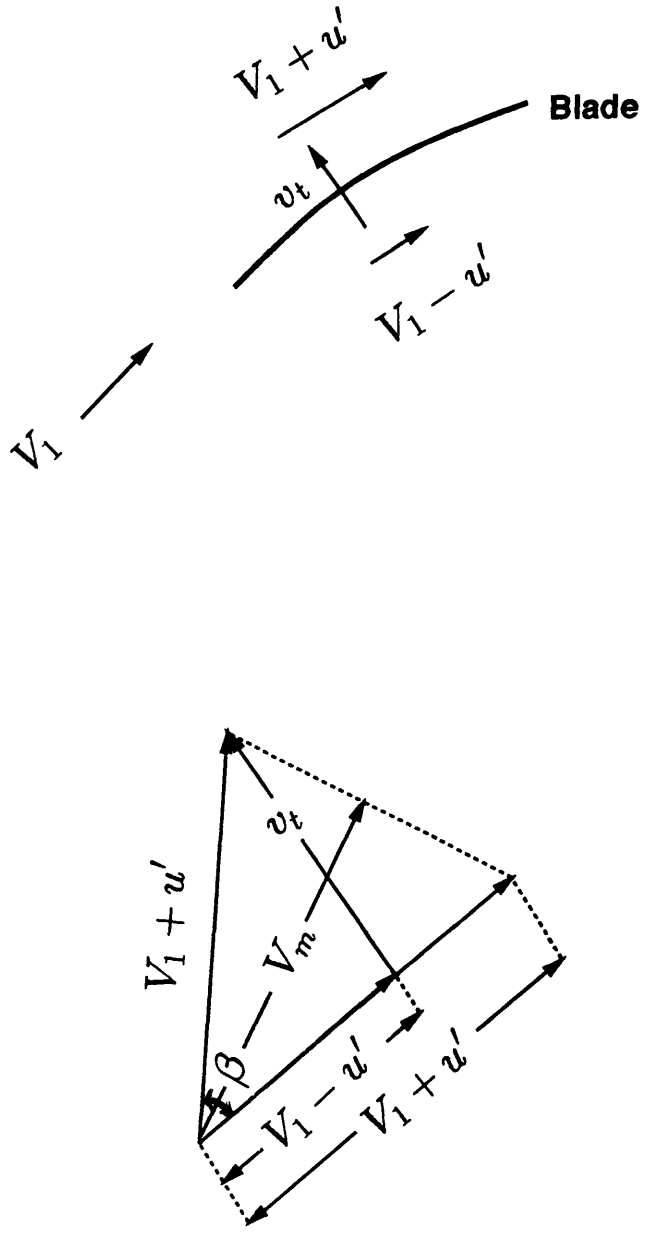

Figure E.1: Schematic of clearance flow (Leakage flow model)

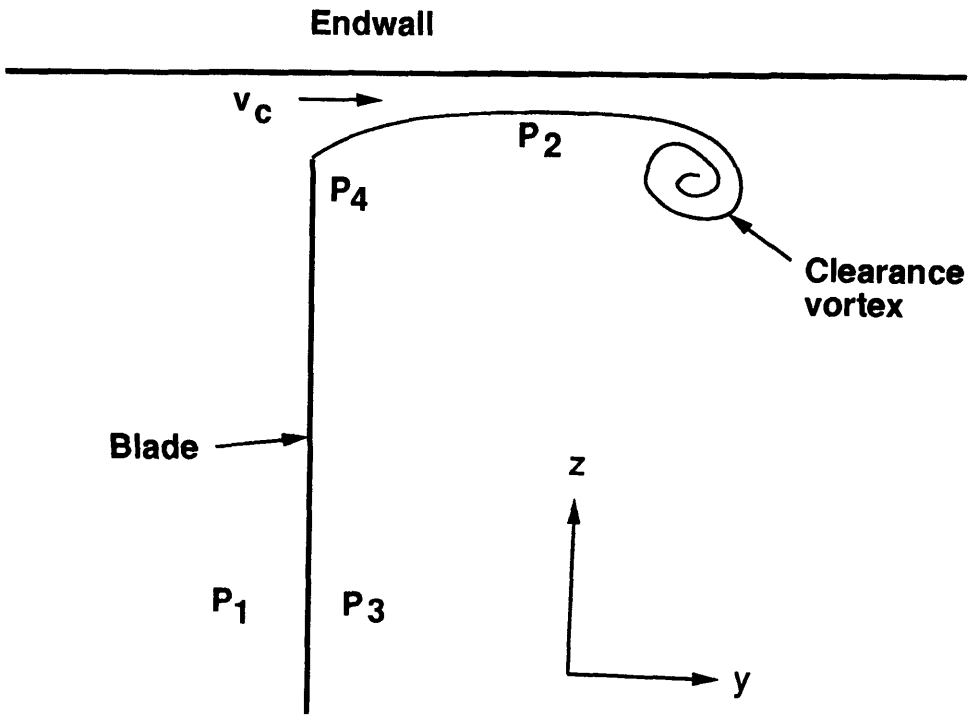

Figure E.2: Illustration of a clearance jet in a cross flow plane

Appendix F

Radial Motion of Tip Vortex After Trailing Edge

Consider a number of point vortices moving by their own induced velocities in a channel as shown in Fig. F.1. This can be represented by a vortex system and its appropriate images as given in Fig. F.2. Specifying the situation to be periodic with period $2H$, we examine only the vortices which lie between z = $\pm H$.

The Kelvin impulse of a vortex pair is given by

$$I_i = \rho \Gamma_i d_i \tag{F.1}$$

where Γ_i is the circulation of the point vortex and d_i is the distance between the centers of the vortex pair. The impulse of the N vortex pairs between z = $\pm H$ is:

$$I = \sum_{i=1}^{N} \rho \, \Gamma_i \, d_i \tag{F.2}$$

There is no force on the vortices so that the total impulse is constant. Also in the region downstream of the trailing edge, the total circulation (of the vortices between $z = o$ and $z = H$) is conserved, i.e.

$$\Gamma = \sum_{i=1}^{N} \Gamma_i = Const. \tag{F.3}$$

Combining Eq. (F.2) and (F.3), we have

$$\frac{\sum_{i=1}^{N} \Gamma_i \, d_i}{\sum_{i=1}^{N} \Gamma_i} = Const. = \overline{d} \tag{F.4}$$

Since $\overline{d} = 2z_c$, the centroid of the vortices , z_c, remains at a fixed radial distance from the wall.

The conclusion also holds for a vortex sheet. The derivation is similar and the result is

$$\frac{\int_0^{\epsilon_{max}} z\ \gamma\ d\epsilon}{\int_0^{\epsilon_{max}} \gamma\ d\epsilon} = Const. \tag{F.5}$$

where γ = strength of the vortex sheet, and ϵ is the intrinsic coordinate along the sheet.

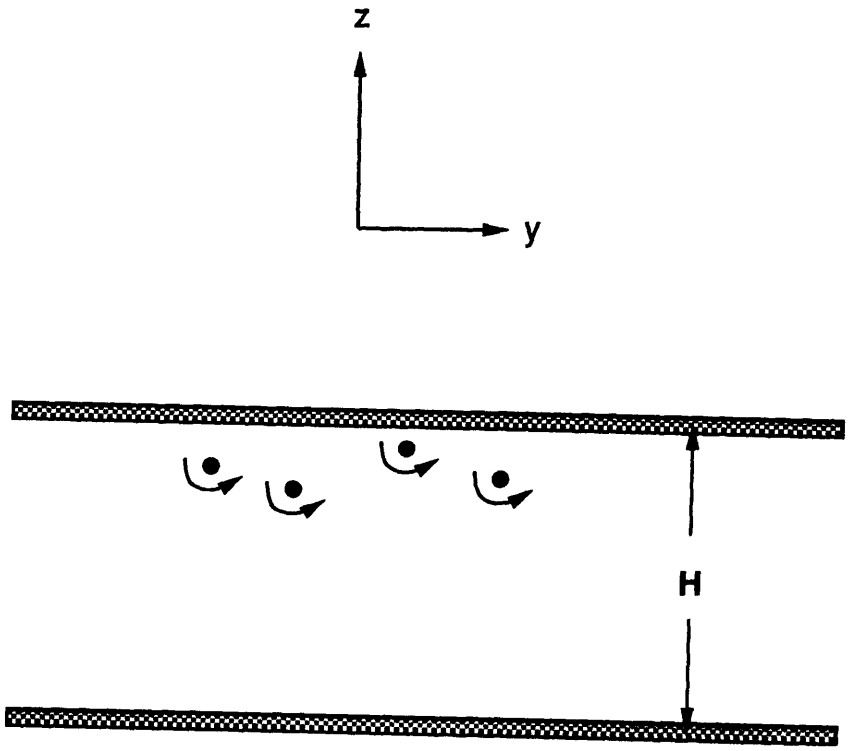

Figure F.1: A number of vortices in a channel

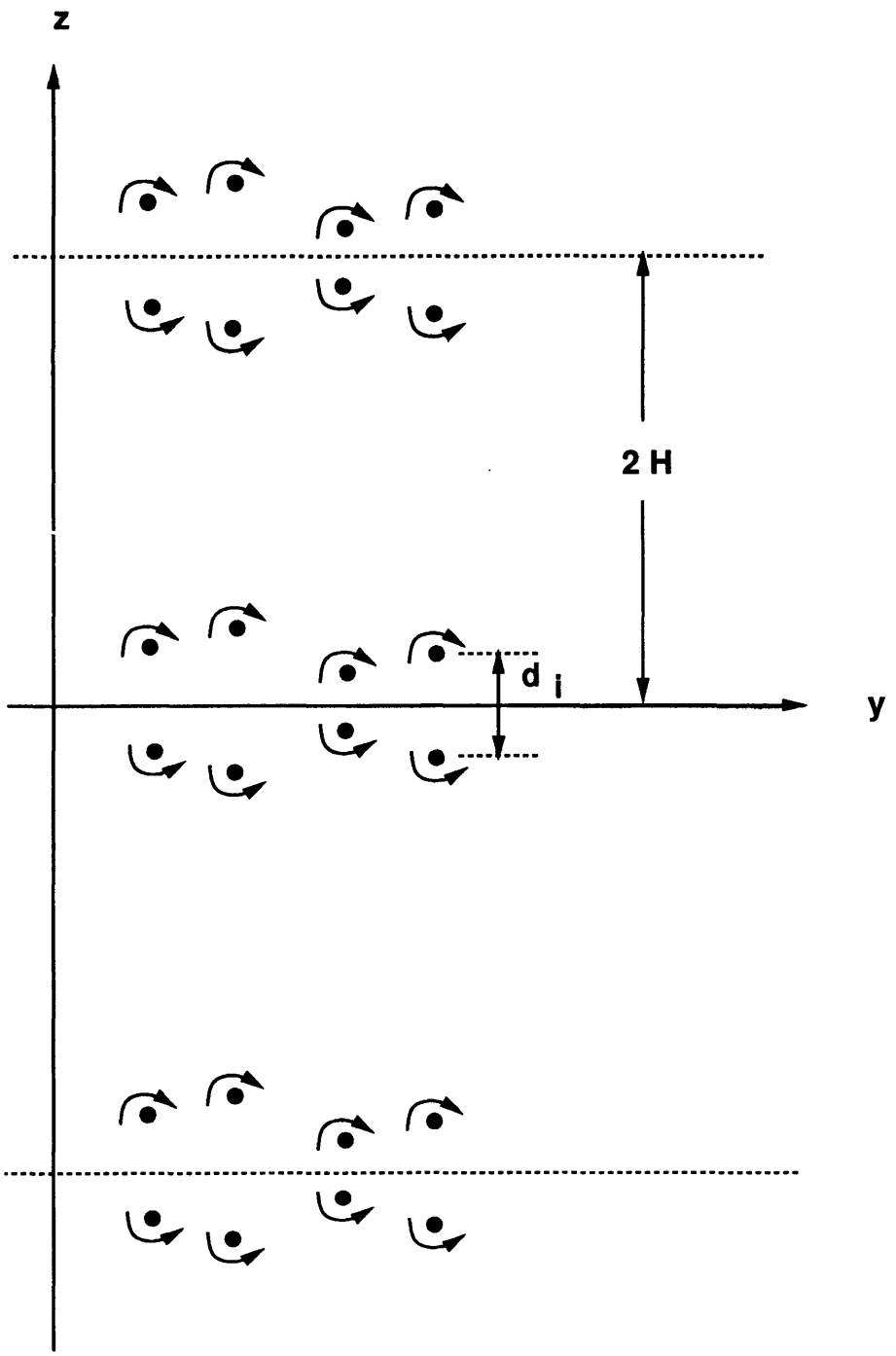

Figure F.2: Vortices and their images

Appendix G

Cross Flow Plane Mach Number

We now examine the cross flow Mach number as a means of assessing whether compressibility effect would be expected to be important. Consider the clearance flow of a rotor with mid-span relative inlet velocity, V_1, and Mach number, M_1. The cross flow Mach number, denoted by M_c, is

$$M_c^2 = \frac{v_c^2}{a^2} \tag{G.1}$$

where v_c is the cross-flow velocity in the clearance and a is the speed of sound. This can be written

$$M_c^2 = \frac{v_c^2}{V_1^2}\,\frac{V_1^2}{a_1^2}\,\frac{a_1^2}{a^2} \tag{G.2}$$

From conservation of energy,

$$a^2 + \frac{\gamma-1}{2}[(V_1+u')^2 + v_c^2] = a_1^2 + \frac{\gamma-1}{2}V_1^2 \tag{G.3}$$

where u' is the velocity perturbation in the streamwise direction and γ is the specific heat ratio. The above equation can be written as:

$$\frac{a^2}{a_1^2} = 1 - \frac{\gamma-1}{2}M_1^2(2\frac{u'}{V_1} + \frac{v_c^2}{V_1^2}) \tag{G.4}$$

From Eqs. (G.2) and (G.4), the cross flow Mach number is found to be, after neglecting higher order terms,

$$M_c^2 = \frac{v_c^2}{V_1^2}M_1^2 \tag{G.5}$$

For the clearance flow, one has, from Eq. (5.11),

$$\frac{\Delta p}{\rho} = v_c^2 \tag{G.6}$$

, where Δp is the mid-span blade loading. Note the blade loading coefficient is defined as

$$\Delta C_p = \frac{\Delta p}{\rho V_1^2/2} \tag{G.7}$$

From Eqs. (G.5), and (G.6) and (G.7), the clearance flow Mach number becomes:

$$\frac{M_c}{M_1} = (\frac{\Delta C_p}{2})^{1/2} \tag{G.8}$$

For a subsonic compressor, ΔC_p is in general less than 0.5 and M_1 is less than unity so that $M_c < 0.5$. A clearance flow can be treated as incompressible.

The cross flow Mach number in a supersonic stage is also of interest based on data from a highly loaded transonic stage (see Sulam, Keenan, and Flynn, [54]). Tip speed of the rotor is 1600 ft/sec with constant spanwise total pressure ratio of 2.0. Relative inlet Mach numbers are 1.6 at the tip and supersonic over nearly the entire span. We have calculated ΔC_p based on the experimental results and the cross flow Mach numbers from Eq. (G.8). The results showed that the cross-flow Mach numbers were less than 0.57 from design point up to before stall at design speed. This indicates that the compressibility effect may not be important even for transonic and supersonic compressors.

To study the compressibility effect a bit further, the cross flow Mach number is related to the stage pressure ratio because it is more available than the blade loading coefficient ΔC_p. First, define a pressure rise coefficient of a rotor as:

$$C_p^* = \frac{p_2 - p_1}{\rho V_1^2/2} \tag{G.9}$$

, where p_1 and p_2 are, respectively, the inlet and exit static pressure of the rotor. Eq. (G.9) can be written as

$$\frac{p_2}{p_1} = 1 + \frac{\gamma M_1^2}{2} C_p^* \tag{G.10}$$

Assume the same pressure ratio holds for the stator, the stage static pressure ratio is

$$\frac{p_3}{p_1} = (1 + \frac{\gamma M_1^2}{2} C_p^*)^2 \tag{G.11}$$

, where p_3 is the stator exit static pressure. The stage total pressure ratio, π_s, is

$$\pi_s = \frac{p_{t3}}{p_{t1}} = \frac{p_3}{p_1} (\frac{1 + \frac{\gamma-1}{2} M_{1abs}^2}{1 + \frac{\gamma-1}{2} M_{3abs}^2})^{\gamma/(\gamma-1)} \tag{G.12}$$

, where M_{1abs} is the rotor inlet absolute Mach number and M_{3abs} is the stator exit absolute Mach number. For repeating stages, $M_{1abs} \simeq M_{3abs}$, it then follows that

$$\pi_s = \frac{p_3}{p_1} \tag{G.13}$$

Note that even when, say, $M_{1abs} = 0.6$ and $M_{3abs} = 0.5$, the error in Eq. (G.13) is less then 10 %. Substituting Eq. (G.11) into (G.13) gives

$$\pi_s = (1 + \frac{\gamma M_1^2}{2} C_p^*)^2 \tag{G.14}$$

or, after rearranging,

$$C_p^* = \frac{2}{\gamma M_1^2} \ (\sqrt{\pi_s} - 1) \tag{G.15}$$

From Eqs. (G.8) and (G.15) the cross flow Mach number takes the following form:

$$M_c^2 = \frac{\sqrt{\pi_s} - 1}{\gamma} \frac{\Delta C_p}{C_p^*} \tag{G.16}$$

For most modern compressors, C_p^* lies between 0.3 and .45 (Wisler, 1985, [60]). Therefore ΔC_p and C_p^* are about the same values and Eq. (G.16) can be simplified as:

$$M_c^2 \simeq \frac{\sqrt{\pi_s} - 1}{\gamma} \tag{G.17}$$

The cross flow Mach number can be computed once the stage pressure is known. Calculation has been carried out for both fan and core compressor stages of current aircraft engines such as J79, E^3, F100, etc. The computed clearance flow Mach numbers are shown in Fig. G.1 for fans and Fig. G.2 for compressors. From the figures, the computed clearance flow Mach numbers are less than 0.5 for fans and 0.4 for compressors. The results thus indicate that the compressibility effect will not be significant in both fans and compressors.

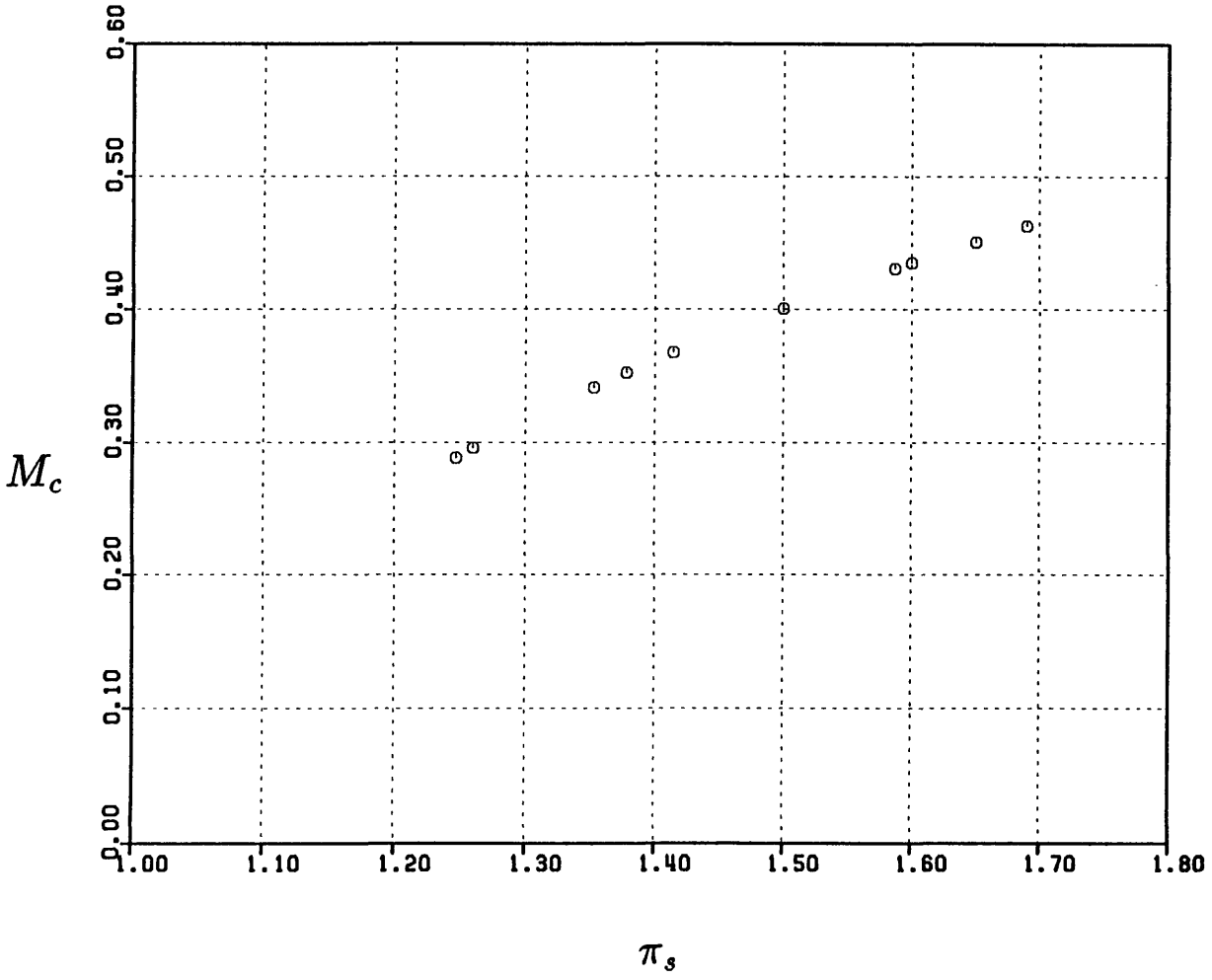

Figure G.1: Computed clearance flow Mach number - Fans

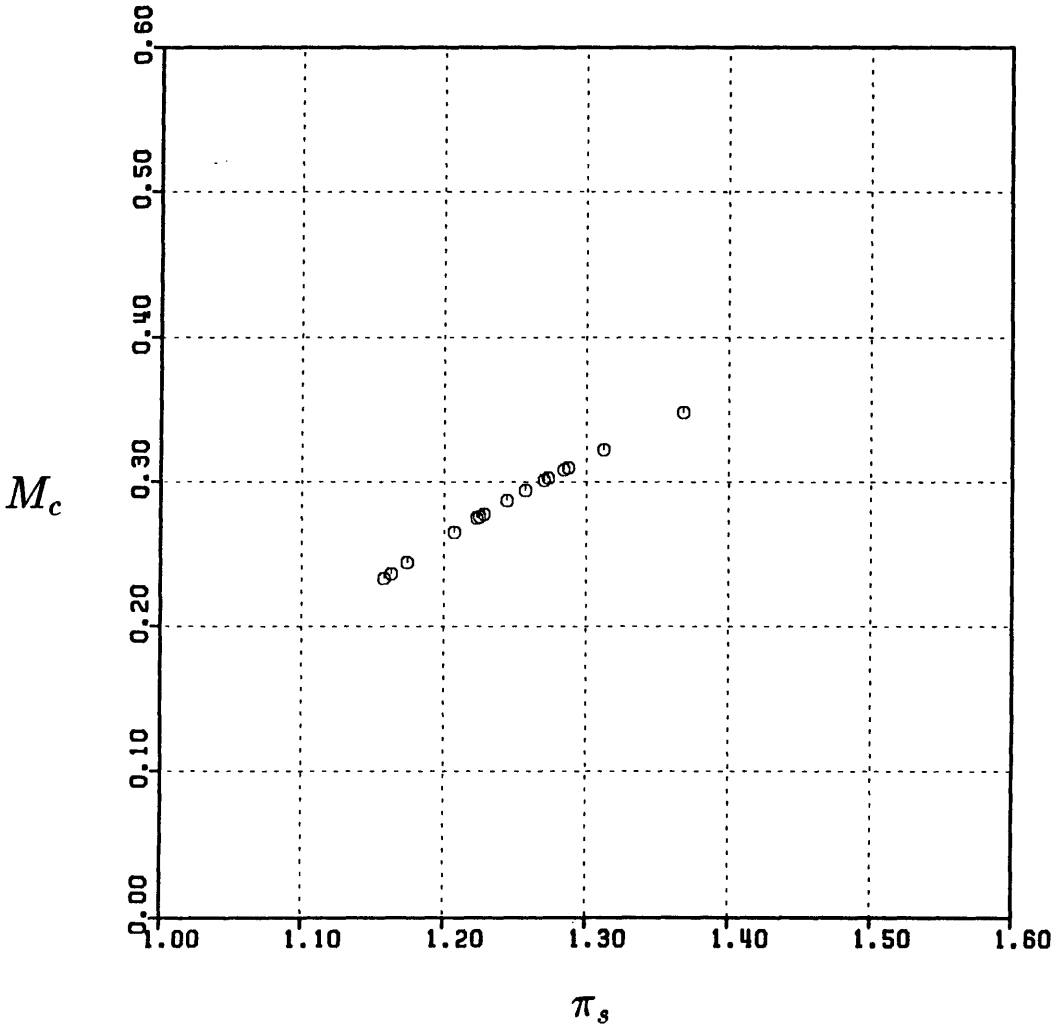

Figure G.2: Computed clearance flow Mach number - Compressors

Appendix H

Effects of Secondary Flow

Consider the upstream vorticity due to inlet casing boundary layer as shown in Figure H.1. The exit streamwise vorticity ω_{s2} consists of two parts. The first part is from the inlet streamwise vorticity ω_{s2} and is given by

$$\omega'_{s2} = -\omega_{s1} \frac{V_2}{V_1} = -\omega_{s1} \frac{\cos(\beta_1^\circ)}{\cos(\beta_2^\circ)} \tag{H.1}$$

The second part is from turning of the inlet normal vorticity ω_{n1} and is given approximately by

$$\omega''_{s2} = 2\theta^\circ \, \omega_{n1} \tag{H.2}$$

, where θ° is camber angle. The total streamwise vorticity at the exit is thus given by

$$\omega_{s2} = \omega'_{s2} + \omega''_{s2} = \omega_1 \cos(\beta_1^\circ) \, (2\theta^\circ - \frac{\sin(\beta_1^\circ)}{\cos(\beta_2^\circ)}) \tag{H.3}$$

and the governing equation of the secondary flow at the exit is

$$\nabla^2 \Psi = -\omega_{s2} \tag{H.4}$$

where Ψ is the stream function. This equation was solved by a finite-difference analogue with a well known successive over relaxation (SOR) scheme. The details of the method is then omitted here.

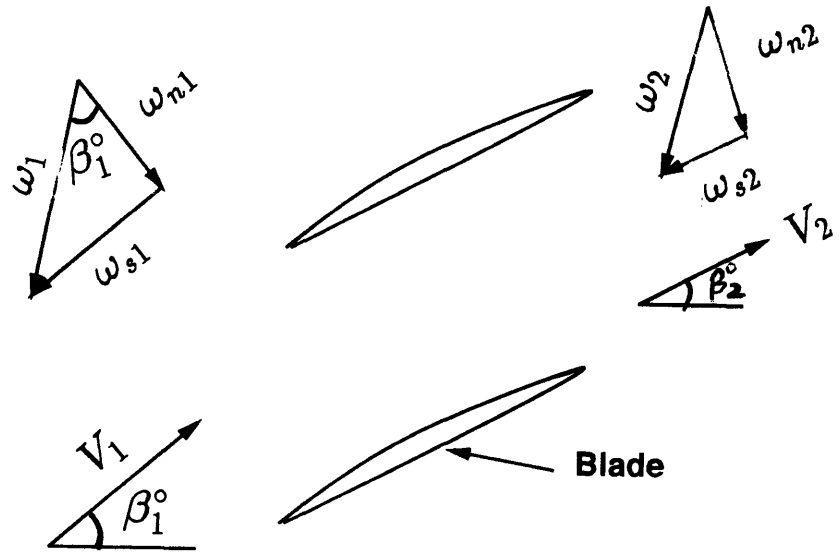

Figure H.1: Schematic of streamwise vorticity

Appendix I

Midspan Flow Perturbations due to Clearance

The effect of clearance on the spanwise mass flow redistribution is examined. An analysis based on lifting line consideration has been carried out. It shows that, away from the clearance region, the flow perturbations due to clearance are small and hence the flow coefficient and the loss at midspan can be treated as constant, i.e. indepentent of clearance.

I.1 Lifting Line Consideration

As stated, we examine the flow perturbations using a lifting line approach. First consider a cascade of blades with span b, pitch s circulation Γ, and tip clearance τ, replaced by a series of bound and trailing tip vortices. The perturbations to the flow along the lifting lines for this vortex system, shown in Fig. I.1, was examined by Lakshminarayana and Horlock (1965, [30]) and the result is

$$\Delta V = \frac{\Gamma}{4s} \left(\frac{\coth^2(\pi z/s) - 1}{\coth(\pi z/s) + \coth(2\pi\tau/s)} \right) \tag{I.1}$$

where ΔV is the velocity perturbation and z is the spanwise distance measured from blade tip. The ratio of the velocity perturbation inside clearance region, say $z = -\tau_{,,}$

to that at mid span, say $z = s/2$, can be found from Eq. (I.1) to be

$$\frac{\Delta V_{midspan}}{\Delta V_{endwall}} = \left(\frac{\coth^2(\pi/2) - 1}{\coth^2(\pi\tau/s) - 1}\right) \left(\frac{\coth(-\pi\tau/s) + \coth(2\pi\tau/s)}{\coth(\pi/2) + \coth(2\pi\tau/s)}\right) \tag{I.2}$$

Using Taylor's expansion, after some algebra, one has

$$\left|\frac{\Delta V_{midspan}}{\Delta V_{endwall}}\right| \simeq \frac{\sinh^2(\pi\tau/s)}{\sinh^2(\pi/2)} \tag{I.3}$$

i.e.

$$\left|\frac{\Delta V_{midspan}}{\Delta V_{endwall}}\right| \sim \left(\frac{\tau}{s}\right)^2 \tag{I.4}$$

Since τ/s is of order 10^{-2}, one can thus conclude that the mass flow (and the loss) at midspan can be treated as constant and independent of clearance.

I.2 Actuator Disc Approximation

It is of interest to see what happens to the previous results if $s \to 0$, i.e. in the limit of actuator disc approximation. In this approximation, the number of blades increases so that $s \to 0$, with $c/s = \text{const}$. The lift lines stack to form vortex sheets with strength γ. The velocity perturbation in the endwall region is then given by

$$\Delta V = \gamma, \quad \gamma \sim \frac{\Gamma}{s}$$

so the axial velocity perturbation in the endwall region is of order

$$(\Delta C_x)_{endwall} \sim \frac{\Gamma}{s}$$

For constant mass flow, the change in averaged axial velocity outside the gap is

$$(\Delta C_x)_{midspan} \sim \frac{\Gamma}{s}\,\frac{s\,\tau}{b\,s}$$

i.e.

$$(\Delta C_x)_{midspan} \sim \frac{\Gamma\,\tau}{s\,b}$$

so that

$$\left|\frac{\Delta V_{midspan}}{\Delta V_{endwall}}\right| \sim \left(\frac{\tau}{b}\right) \sim \left(\frac{\tau}{s}\right) \tag{I.5}$$

which is different from the previous result. Note that $\Gamma \sim c\ C_x$ one has

$$\frac{(\Delta C_x)_{midspan}}{C_x} \sim \frac{c}{s}\ (\frac{\tau}{b}) \tag{I.6}$$

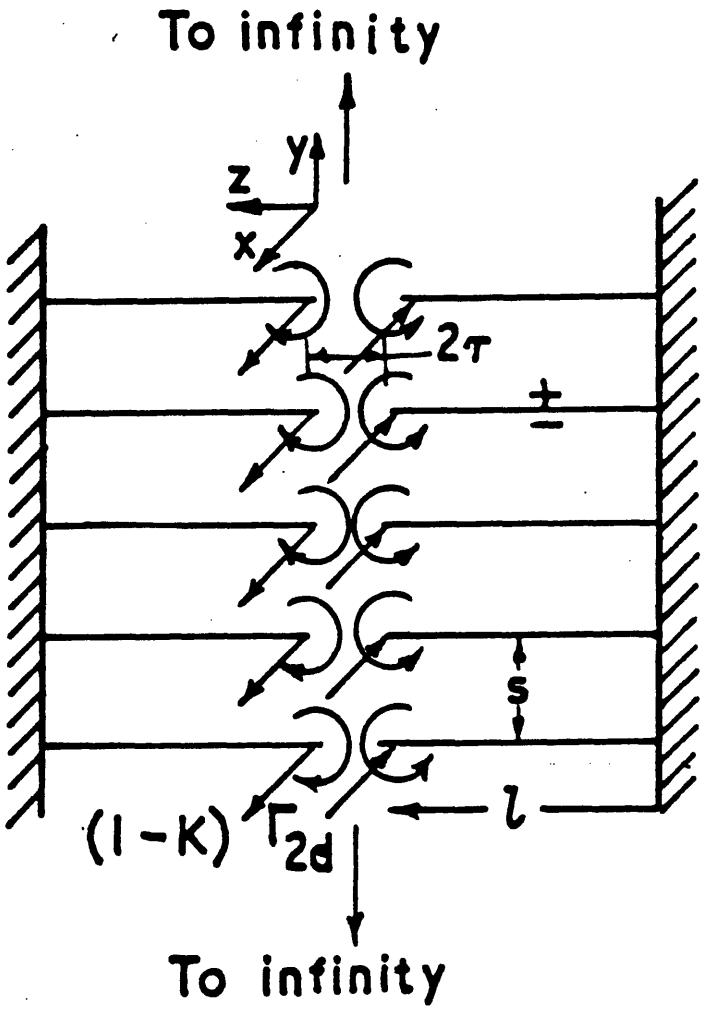

Figure I.1: Schematic of vortex system in a casacde (from Lakshminarayana and Horlock (1965))

Appendix J

Energy and Momentum Views of Clearance Losses

Consider free stream and leakage flow on the suction side of a blade as shown in Fig. J.1. With clearance, the flow in the clearance region has velocity V_s, same as the free stream velocity on the suction side, but with different direction. In this case, total mechanical energy, and mechanical energy and momentum associated with the streamwise and crossflow velocity are

- Total M.E. : $(\dot{m} + \dot{m}_c)\frac{V_s^2}{2}$
- Streamwise M.E. : $\dot{m}\frac{V_s^2}{2} + \dot{m}_c\frac{V_p^2}{2}$
- Crossflow M.E. : $\dot{m}_c\frac{V_c^2}{2}$
- Streamwise Mom. $\dot{m}V_s + \dot{m}_cV_p$
- Crossflow Mom. $\dot{m}_cV_c$

where $\dot{m}$ is the free stream mass flow, $\dot{m}_c$ is the leakage flow, V_s and V_p are the suction side and pressure side velocity, and V_c is the crossflow velocity.

Without clearance, as shown in Fig. J.2, the flow in the previous clearance region (shaded area) and free stream have the same velocity, both in magnitude and direction so that

- Total M.E. : $(\dot{m} + \dot{m}_c)\frac{V_s^2}{2}$
- Streamwise M.E. : $(\dot{m} + \dot{m}_c)\frac{V_s^2}{2}$
- Crossflow M.E. : zero
- Streamwise Mom. $(\dot{m} + \dot{m}_c)V_s$
- Crossflow Mom. zero

The momentum view of Senoo considers the change in the streamwise momentum between these two cases, i.e. $\dot{m}_c(V_s - V_p)$ and the resulting change in work (i.e. loss) is thus given by

$$\dot{m}_c(V_s - V_p)V_{mean}$$

where V_{mean} is an averaged streamwise velocity. Since the streamwise component of velocity in the clearance flow changes from V_s (zero clearance) to V_p (with clearance), the average velocity is then $(V_s + V_p)/2$ and the work difference is then

$$\dot{m}_c\frac{V_s^2 - V_p^2}{2}$$

The energy view considers the loss as the change in the crossflow energy between these two cases, i.e.

$$\dot{m}_c\frac{V_c^2}{2}$$

But

$$V_c^2 = V_s^2 - V_p^2$$

the momentum and the energy view thus give the same loss.

In the momentum approach, the loss is assumed to be the difference in streamwise kinetic energy, whereas it is the difference in crossflow energy in the energy approach. Since the total energy remains the same , these two approaches will give the same results.

One can also look at the change in the cross flow momentum, which is

$$\dot{m}_c(V_c)V'_{mean}$$

where V'_{mean} is an averaged crossflow velocity. Since the crossflow component of velocity in the clearance flow changes from zero (zero clearance) to V_c (with clearance), the average velocity is then $V_c/2$ and the work difference in the crossflow with and without clearance is

$$\dot{m}_c\frac{V_c^2}{2}$$

which is identical to the results based on the energy view, i.e. the momentum and energy view points to the crossflow give the same loss as they should.

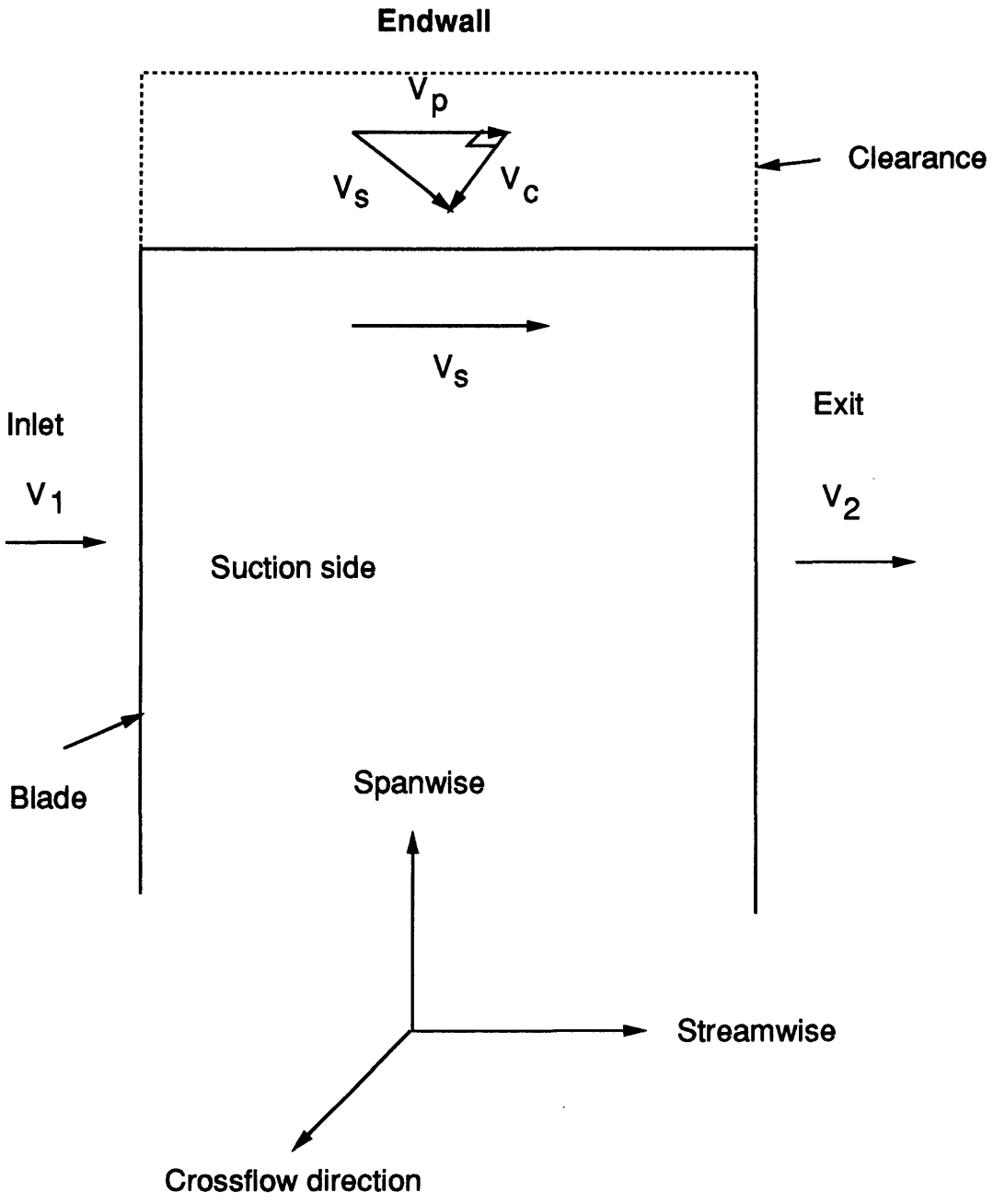

Figure J.1: Schematic of fluid velocity on blade suction side with clearance

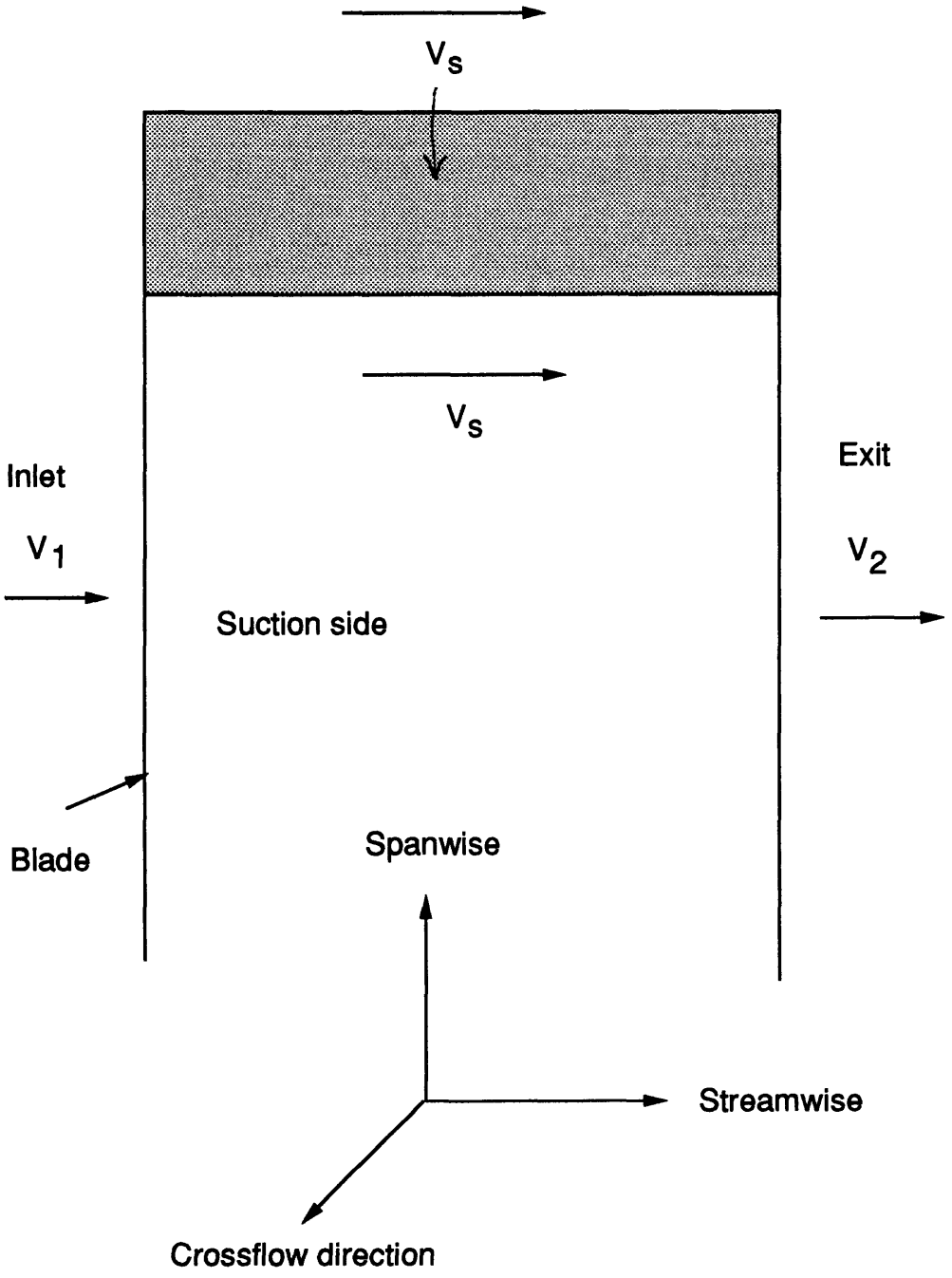

Figure J.2: Schematic of fluid velocity on blade suction side without clearance

Appendix K

Derivation of Efficiency Reduction due to Clearance in A Turbine

The efficiency of a turbine is given by

$$\eta_t = \frac{L}{\dot{m} C_p T_{t1} [1 - \pi_t^{(\gamma-1)/\gamma}]} \tag{K.1}$$

, which can be written as

$$\eta_t = \eta_t(L(\pi_t, \tau), \dot{m}(\pi_t, \tau))$$

Under constant π_t, one has

$$\frac{\Delta\eta_t}{\eta_t} = \frac{1}{L}\frac{\partial L}{\partial \tau}|_{\pi_t} \Delta\tau - \frac{1}{\dot{m}}\frac{\partial \dot{m}}{\partial \tau}|_{\pi_t} \Delta\tau \tag{K.2}$$

From conservation of energy,

$$\dot{m} C_p T_{t1}(1 - \pi_t^{(\gamma-1)/\gamma}) = L + Losses \tag{K.3}$$

Differentiating this w.r.t. the clearance,τ, gives

$$\frac{\partial L}{\partial \tau}|_{\pi_t} = \frac{\partial \dot{m}}{\partial \tau}|_{\pi_t} C_p T_{t1}(1 - \pi_t^{(\gamma-1)/\gamma}) - \frac{\partial Losses}{\partial \tau}|_{\pi_t} \tag{K.4}$$

Assuming the change in total losses with clearance is from the change in the clearance loss only, it is found that

$$\frac{\partial Losses}{\partial \tau}|_{\pi_t} = \Pi \left(\frac{\dot{m} U_t^2}{2H} + \frac{\tau U_t^2}{2H}\frac{\partial \dot{m}}{\partial \tau}|_{\pi_t}\right) \tag{K.5}$$

,where

$$\Pi \equiv \frac{8\sqrt{2}}{5} A\, G\, \zeta\, \phi^2 \left(\frac{c^0}{c}\right) \sqrt{\frac{s}{c}}$$

Putting Eqs. (K.4) and (K.5) into Eq. (K.2), the result is written

$$\frac{\Delta\eta_t}{\eta_t} = \frac{1-\eta_t}{\eta_t} \frac{1}{\dot{m}} \frac{\partial \dot{m}}{\partial \tau}\Big|_{\pi_t} \Delta\tau - \frac{\Pi \dot{m} U_t^2}{2L}\left(\frac{\Delta\tau}{H} + \frac{\tau}{H}\frac{1}{\dot{m}}\frac{\partial \dot{m}}{\partial \tau}\Big|_{\pi_t} \Delta\tau\right) \tag{K.6}$$

The variation of efficiency with clearance can be obtained. Neglecting higher order terms, the result takes the form

$$\frac{\Delta\eta_t}{\eta_t} = -\frac{8\sqrt{2}}{5}\frac{AG}{B}\,\zeta\,\phi^2 \left(\frac{c_t}{c_m}\right)\sqrt{\frac{s_m}{c_m}}\left(\frac{\Delta\tau}{H}\right) \tag{K.7}$$

Appendix L

Effect of Flow Reattachment on Clearance Loss

L.1 Non-Reattached Clearance Flow

Consider a clearance flow in a cross flow plane as illustrated in Fig. L.1. At the gap exit one has

$$p_2 = p_0 - \frac{1}{2}\rho v_2^2 \tag{L.1}$$

and the leakage mass flow

$$\dot{m}_{c1} = \xi\tau\rho v_2 \tag{L.2}$$

, where p_0 is the static pressure at mid span near pressure surface, p_2 is the static pressure at the tip of suction surface, and ξ is the contraction factor given by

$$\xi = \frac{\pi}{\pi + 2} \tag{L.3}$$

If the leakage jet is fully mixed at station 3 as shown in the figure, the decrease of total pressure can be found to be

$$\Delta p_t = \frac{1}{2}\rho v_2^2(1 - \frac{\xi\tau}{H})^2 \tag{L.4}$$

and the loss of flux of energy is

$$\Delta E_1 = \dot{m}_{c1}\frac{\Delta p_t}{\rho} = \frac{1}{2}\xi\tau\rho v_2^3(1 - \frac{\xi\tau}{H})^2 \tag{L.5}$$

From Eqs. (L.1) and (L.5), one has

$$\Delta E_1 = \frac{1}{2}\xi\tau\rho[\frac{2(p_0 - p_2)}{\rho}]^{3/2}(1 - \frac{\xi\tau}{H})^2 \tag{L.6}$$

L.2 Reattached Clearance Flow

We now examine the mixing losses for a reattached clearance flow. Assuming after the vena contracta the clearance jet re-attaches at blade tip and is fully mixed out before leaving the gap as indicated in Fig. L.2, the mixing losses occurred inside the gap can be calculated as follows.

Between station 0 and 1 the flow is inviscid so that

$$p_1 = p_0 - \frac{1}{2}\rho v_1^2 \tag{L.7}$$

Because of mixing in the gap, the static pressure at the exit is

$$p_2 = p_1 + \rho v_1^2 \xi(1 - \xi) \tag{L.8}$$

Putting Eq. (L.7) into Eq. (L.8) , the result takes the following form:

$$v_1 = \frac{1}{\sqrt{1 - 2\xi + 2\xi^2}}\sqrt{\frac{2(p_0 - p_2)}{\rho}} \tag{L.9}$$

The leakage mass flow can be written

$$\dot{m}_{c2} = \rho\xi\tau\frac{1}{1 - 2\xi + 2\xi^2}\sqrt{\frac{2(p_0 - p_2)}{\rho}} \tag{L.10}$$

The loss of total pressure due to mixing inside the gap is

$$p_{t1} - p_{t2} = \frac{1}{2}\rho v_1^2(1 - \xi)^2 \tag{L.11}$$

To calculate the mixing losses outside the gap, it is assumed that the uniform flow at the gap exit is mixed out again downstream, say at station 3, as shown in Fig. L.2. The total pressure loss due to the latter mixing is

$$p_{t2} - p_{t3} = \frac{1}{2}\rho v_2^2(1 - \frac{\tau}{H})^2 \tag{L.12}$$

The overall loss in total pressure can be written

$$p_{t1} - p_{t3} = \frac{1}{2}\rho v_1^2[(1-\xi)^2 + \xi^2(1-\frac{\tau}{H})^2] \tag{L.13}$$

and

$$\Delta E_2 = \frac{1}{2}\xi\tau\rho[\frac{2(p_0 - p_2)}{\rho}]^{3/2}\frac{(1-\xi)^2 + \xi^2(1-\tau/H)^2}{(1-2\xi+2\xi^2)^{3/2}} \tag{L.14}$$

The change in leakage mass flow and mixing losses from the flow reattachment can now be determined. Assuming the driving force of the clearance flow, $p_0 - p_2$, is the same in both cases, one can obtain

$$\frac{\dot{m}_{c2}}{\dot{m}_{c1}} = \frac{1}{\sqrt{1-2\xi+2\xi^2}} \tag{L.15}$$

and

$$\frac{\Delta E_2}{\Delta E_1} = \frac{(1-\xi)^2 + \xi^2(1-\tau/H)^2}{(1-\xi\tau/H)^2(1-2\xi+2\xi^2)^{3/2}} \tag{L.16}$$

Substituting in ξ from Eq. (L.3) and neglecting τ/H, one has

$$\frac{\dot{m}_{c1}}{\dot{m}_{c2}} \simeq \frac{\Delta E_2}{\Delta E_1} \simeq 1.38 \tag{L.17}$$

The leakage mass flow and mixing losses are thus about 38 % larger due to the flow reattachment.

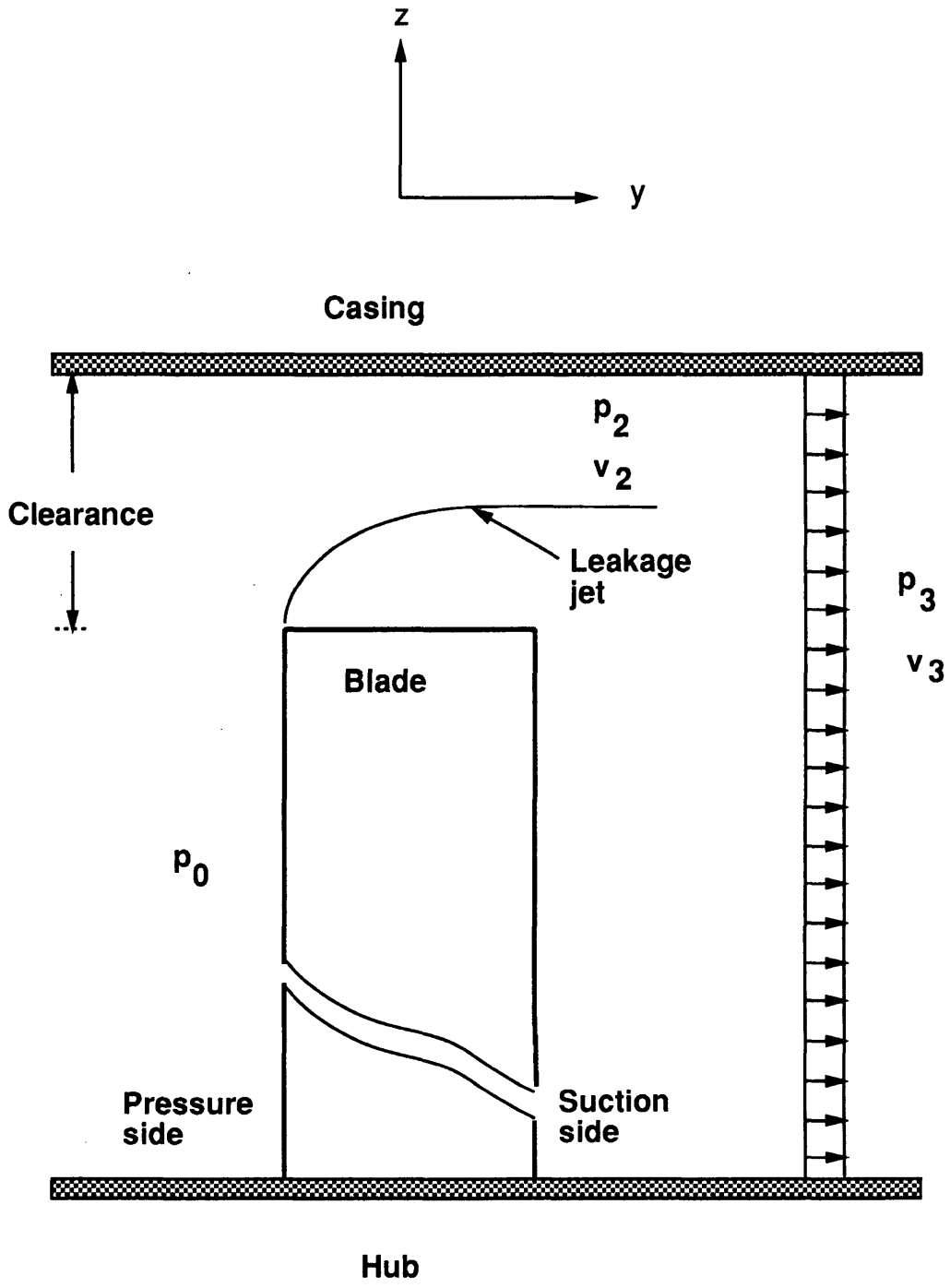

Figure L.1: A non-reattached clearance flow on a cross flow plane

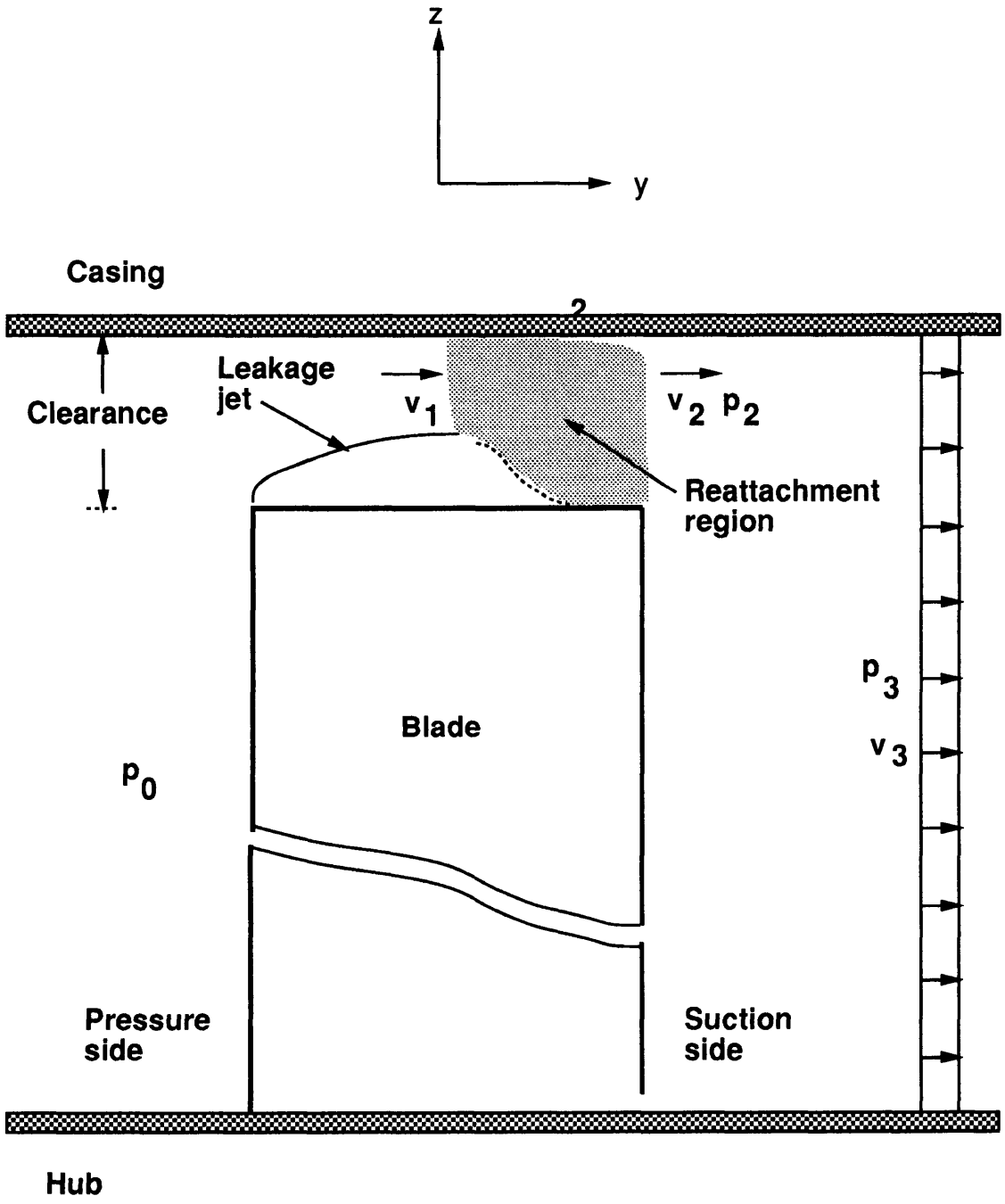

Figure L.2: A reattached clearance flow on a cross flow plane

Appendix M

Effect of Rankine Vortex on Pressure Rise in A Diffuser

The purpose of this study is to provide physical insight into how the pressure rise will be affected by the presence of a (clearance) vortex and to understand parametric trends as well.

The fluid mechanic model used consists of an axial flow with swirl through a cylindrical tube, which undergoes an area change, as illustrated in Fig. M.1. The flow is assumed inviscid and axisymmetric throughout. In addition, swirl distribution of the fluid is taken as solid body rotation from centerline to some radius (inner flow) and as free vortex flow from that radius to the wall (outer flow) with no discontinuity at the interface. The inner flow is a vortex tube , which can be termed as a Rankine vortex. Upstream of the transition, axial velocities in the inner and outer flows are assumed uniform, however, the two velocities can be different. Finally, radial component of velocity is assumed zero upstream and downstream of the transition.

The flow upstream is then given by:

$$u = U_1, \;\; v = \Omega\, r \;, w = 0; \;\; 0 \leq r \leq r_1 \;; \tag{M.1}$$

$$u = U_3, \;\; v = \frac{\Omega\, r_1^2}{r}, \;\; w = 0; \;\; r_1 \leq r \leq r_3 \tag{M.2}$$

where u, v, and w are, respectively, the axial, tangential, and radial components of the

velocity, U_1 and U_3 are constants, r_1 is the radius of the vortex tube, r_3 is the radius of the wall upstream, and Ω is a constant.

On the downstream side, the axial velocity is uniform outside the vortex tube. However, it will vary with radius inside the vortex tube, as illustrated in the figure. This non-uniformity in the axial velocity profile has been examined and explained by Batchelor (1967, [4]) and the explanation is given briefly as follows. Due to the area change, there is a change in the shape of the vortex-lines (in the vortex tube) downstream, which induces a azimuthal component of vorticity and therefore a non-uniform axial velocity in the vortex downstream. The axial velocity is minimum at the axis, as shown in the figure. The flow downstream can be shown to be

$$\frac{u(r)}{U_1} = 1 + \frac{k'r}{2}\left(\frac{r_1^2}{r^2} - 1\right)\frac{J_0(k'r)}{J_1(k'r_2)} \quad , w = 0; \;\; 0 \le r \le r_2 \tag{M.3}$$

$$u = U_4, \;\; v = \frac{\Omega\, r_1^2}{r}, \;\; w = 0; \;\; r_2 \le r \le r_4 \tag{M.4}$$

where $U_1 = 4$ is a constant, $k' = 2\Omega/U_1$, J_o and J_1 are Bessel functions, and r_2 and r_4 are, respectively, the radius of the vortex tube and the wall, downstream. The flow downstream will be determined if area ratio r_4^2/r_3^2 is given. The unknowns are U_4 and r_2, which can be determined from two constraints: 1) the conservation of mass flow between the wall and the interface , and 2) same total pressure difference at the interface upstream and downstream, i.e. $p_{t1} - p_{t3} = p_{t2} - p_{t4}$.

For a vortex tube with area $r_1^2/r_3^2 = 0.3$, and the same axial velocity as the outer flow, i.e. $U_1 = U_3$, the calculated pressure rise at the wall between the upstream and downstream side against the area ratio r_4^2/r_3^2 is given in Fig. M.2 for four different values of inlet swirl, i.e. .25, .5, .75 ,and 1.0. The pressure rise is normalized by $\frac{1}{2}\rho U_3^2$ and the inlet swirl is defined as $v(r_1)/U_3$. Also shown in the figure (solid line) is the pressure rise in an ideal diffuser, i.e. a diffuser without any inlet swirl.

Several interesting features of the flow can be seen from the figure. First, the existence of a Rankine vortex can greatly affect the behavior of the pressure rise char-

acteristics of the diffuser. It will reduce the pressure rise: the stronger the swirl is, the smaller the pressure rise at wall becomes. This behavior can be explained in terms of radial shift of the interface with swirl. Consider the case in which there is no swirl and $U_1 = U_3$ so that the axial velocity downstream is uniform from the axis to the wall. The interface is located at a radius r_1, upstream, and is located at a radius, say r_2^*, downstream. With swirl, due to the above-discussed non-uniformity in the axial velocity downstream, the axial velocity right below the interface would be higher than that right above it if the interface were still located at r_2^*. Since the total pressure is constant along the interface, this means the static pressure right below the interface would be higher than that right above it. To balance the pressure difference, the interface downstream has to move radially outwards. As a consequence, the pressure rise on the wall will be smaller than the zero swirl case. In addition, the non-uniformity becomes much more severe as swirl increases so that the interface moves further away from the axis and the pressure rise at wall becomes smaller, as can be seen from the figure.

A more striking feature of the flow is that the pressure rise initially increase with the area ratio. However, it reaches a maximum at a critical area ratio and then starts to fall off with an increase in area ratio [1]. This peaking-over phenomenon is a consequence of the above-discussed increasing vortex area with swirl on the downstream side, which can be seen in Fig. M.3. Plotted in the figure are the normalized radius of the wall (r_4/r_1) and the interface (r_2/r_1) as well as the (normalized) area between them, $(r_4^2 - r_2^2)/r_1^2$, as a function of the area ratio. The result shows that, because of an considerable increase in the size of the vortex tube downstream, the area of the outer flow, although initially increases with the area ratio, gets to a maximum and then decreases with increasing area ratio. The static pressure rise on the wall thus peaks over as seen in Fig. M.2.

In addition, since the vortex tube downstream grows with the swirl, the wall pressure rise peaks over at a smaller area ratio as the inlet swirl becomes stronger. Static pressure

[1] For the smallest swirl, $v(r_1)/U_3 = .25$, the critical area is roughly 8.0 so that the peak-over behavior can not be seen in the figure.

rise at the interface is given in Fig. M.4 , which shows similar behavior.

It should be pointed out that the calculation has been carried out up a cut-off area ratio at which reversed flow start to exist on the axis, where the minimum axial velocity takes place. The solution is no longer valid and the vortex tube may break down before the area ratio reaches the cut-off value. The vortex breakdown is a very complex phenomenon, which is still not well understood, and will not be discussed here. For reference, the calculated axial velocities on the axis for the various values of swirl (.25,.50,.75, and 1.0) are shown in Fig. M.5 with $r_1^2/r_3^2 = 0.3$ and $U_1 = U_3$.

To see the effect of the size of the vortex tube on the wall pressure rise, calculation has been carried out for four different values of r_1^2/r_3^2, i.e. 0.1, 0.3, 0.5, and 0.9, with constant swirl $v(r_1)/U_3 = 1$ and $U_1/U_3 = 1$. The calculation results show that the pressure rise peaks over at a smaller area ratio for a smaller vortex size, which can be seen in Fig. M.6. The results also show that the pressure rise capability increases with cross-section area of the vortex.

We have also examined the effect of different axial velocities in the inner and outer flows on the wall pressure rise. Fig. M.7 shows the result for $U_1/U_3 = .9$, 1.0, and 1.1. It indicates that, for a given area ratio, the axial velocity defect in the vortex tube will reduce the wall pressure rise. In addition, the pressure rise ends at a smaller area ratio for smaller U_1 at which reversed flow occurs earlier. So far, the most interesting results of the calculation is that the pressure rise can peak over with a Rankine vortex in a diffuser. Other features that are of interest are that the axial velocity in the vortex becomes smaller as the area ratio increases, becoming zero at the cutoff area ratio and that, as with a simple wake flow, an axial velocity defect in the vortex degrades the pressure rise capability.

As mentioned in the beginning of the analysis, the purpose of the effort is to provide physical insight into how the pressure rise in a compressor would be affected by the presence of a (clearance) vortex and to understand parametric trends. Suggestions from this study for a compressor can be summarized as follows:

- The clearance vortex can play a large role in the pressure rise of a compressor.
- As flow coefficient decreases, the clearance vortex grows both in size and strength (circulation) and, as a consequence, the pressure rise will be smaller.
- The peaking-over of the compressor characteristic *may* be due to not only the viscous effect, i.e. the growth in the endwall boundary layers, but also a inviscid phenomenon, i.e. due to the interaction between the clearance vortex and surrounding flow.
- Vortex breakdown *may* play a role in the discontinuity in a compressor pressure rise characteristics, i.e. the stall phenomenon.

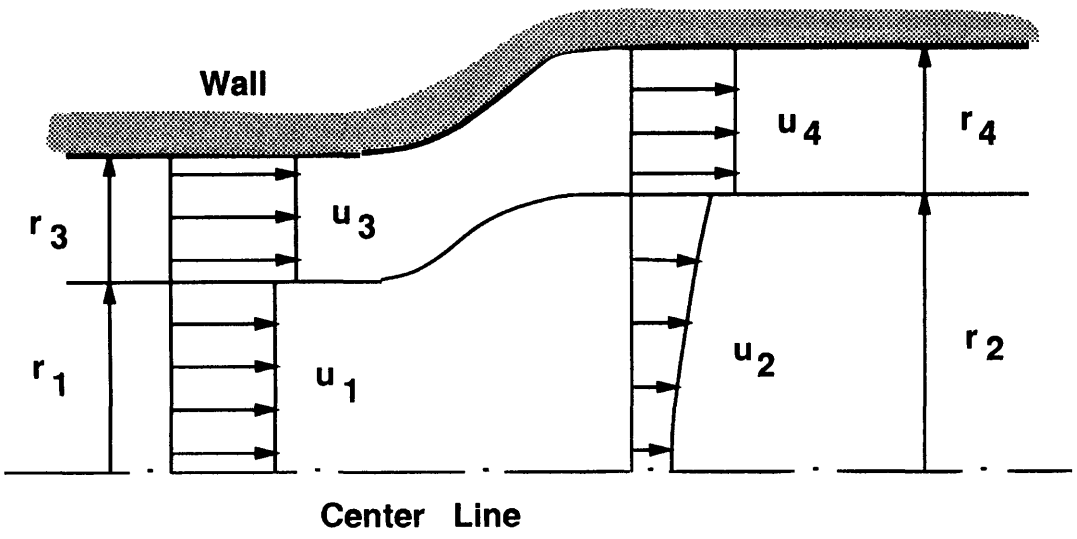

Figure M.1: A Rankine vortex in a diffuser with swirl

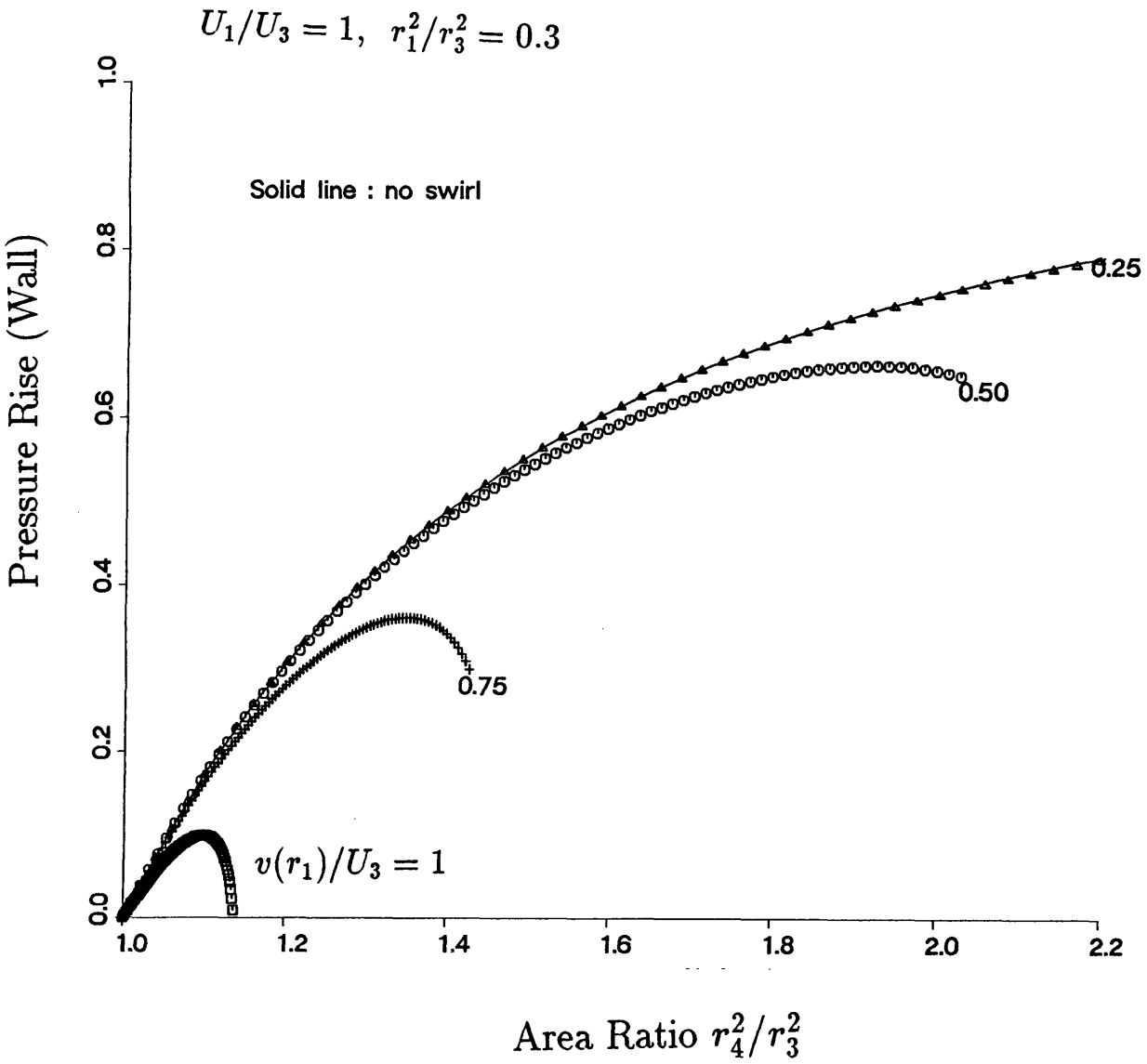

Figure M.2: Wall pressure rise vs. area ratio for different values of swirl

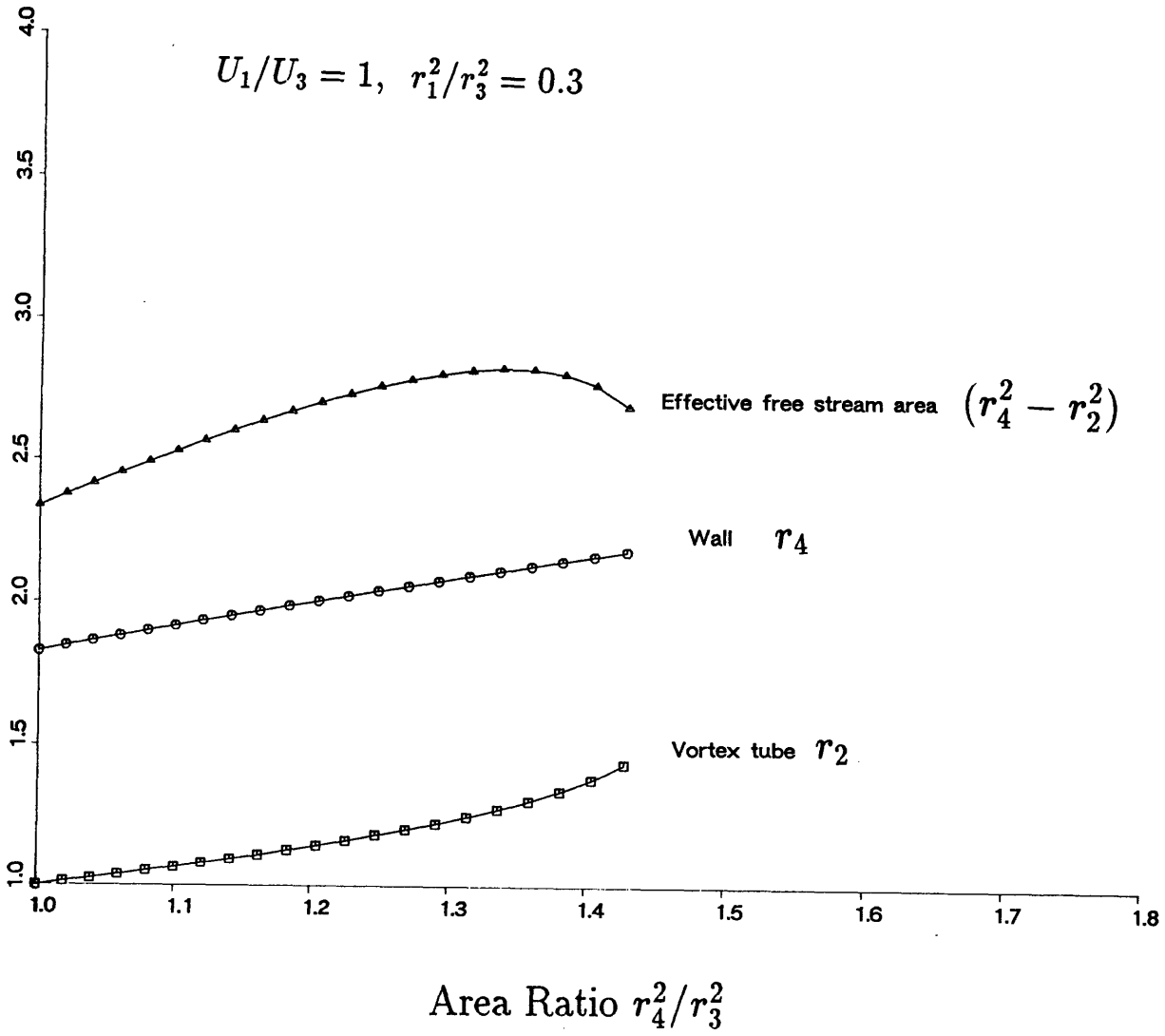

Figure M.3: Radius of a vortex tube and area of outer flow vs. area ratio

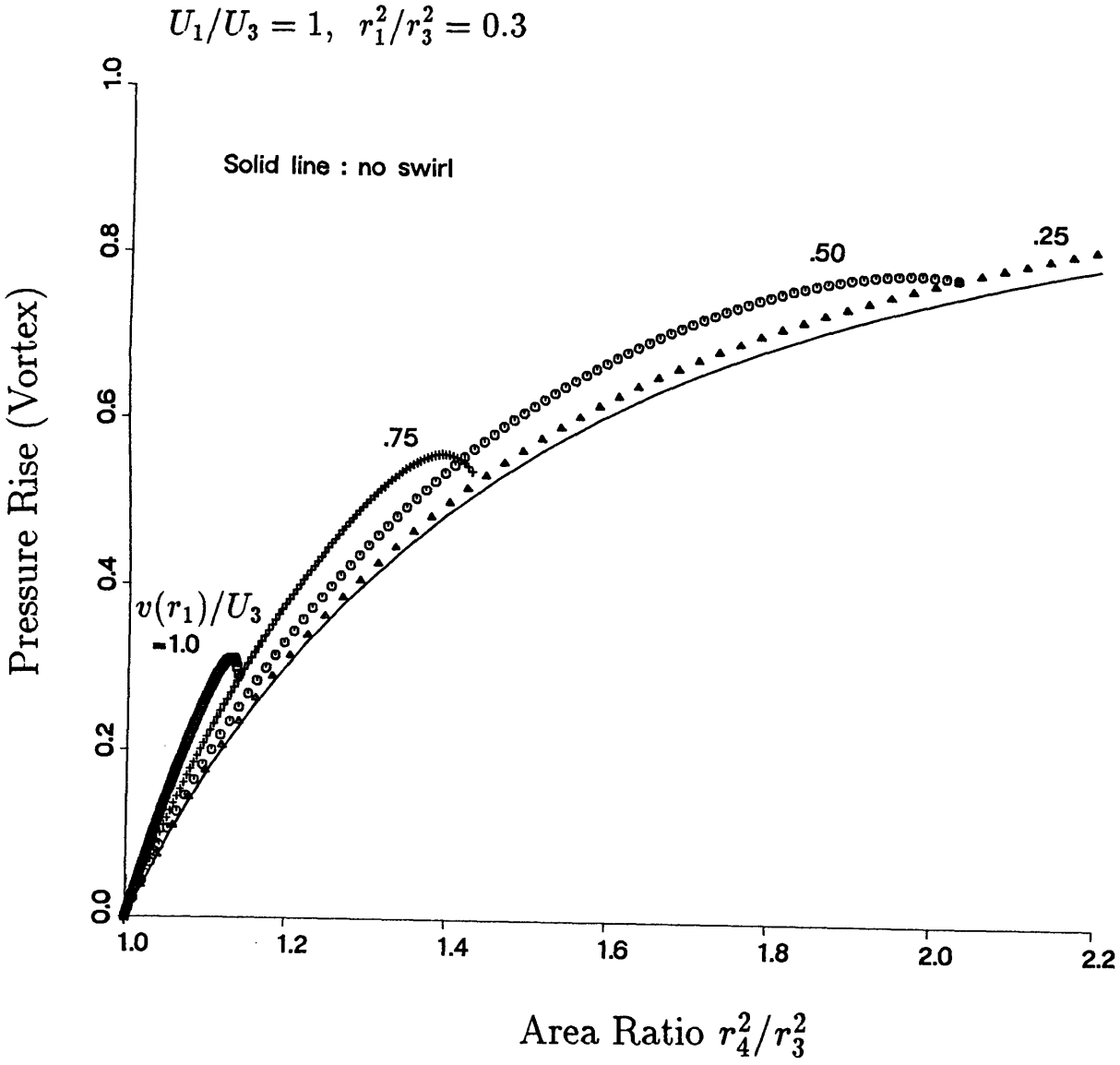

Figure M.4: Interface pressure rise vs. area ratio for different values of swirl

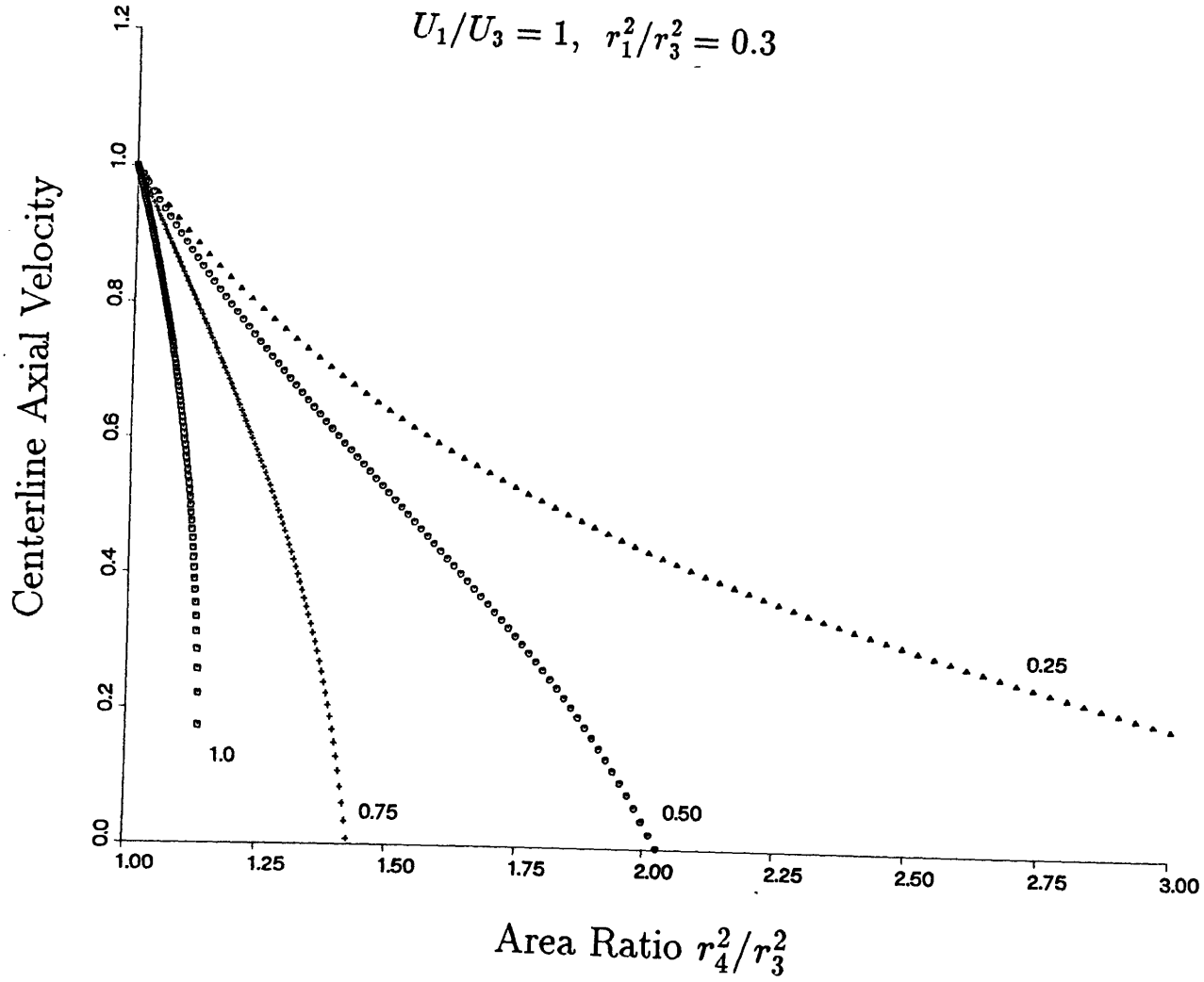

Figure M.5: Center-line axial velocity vs. area ratio for different values of swirl

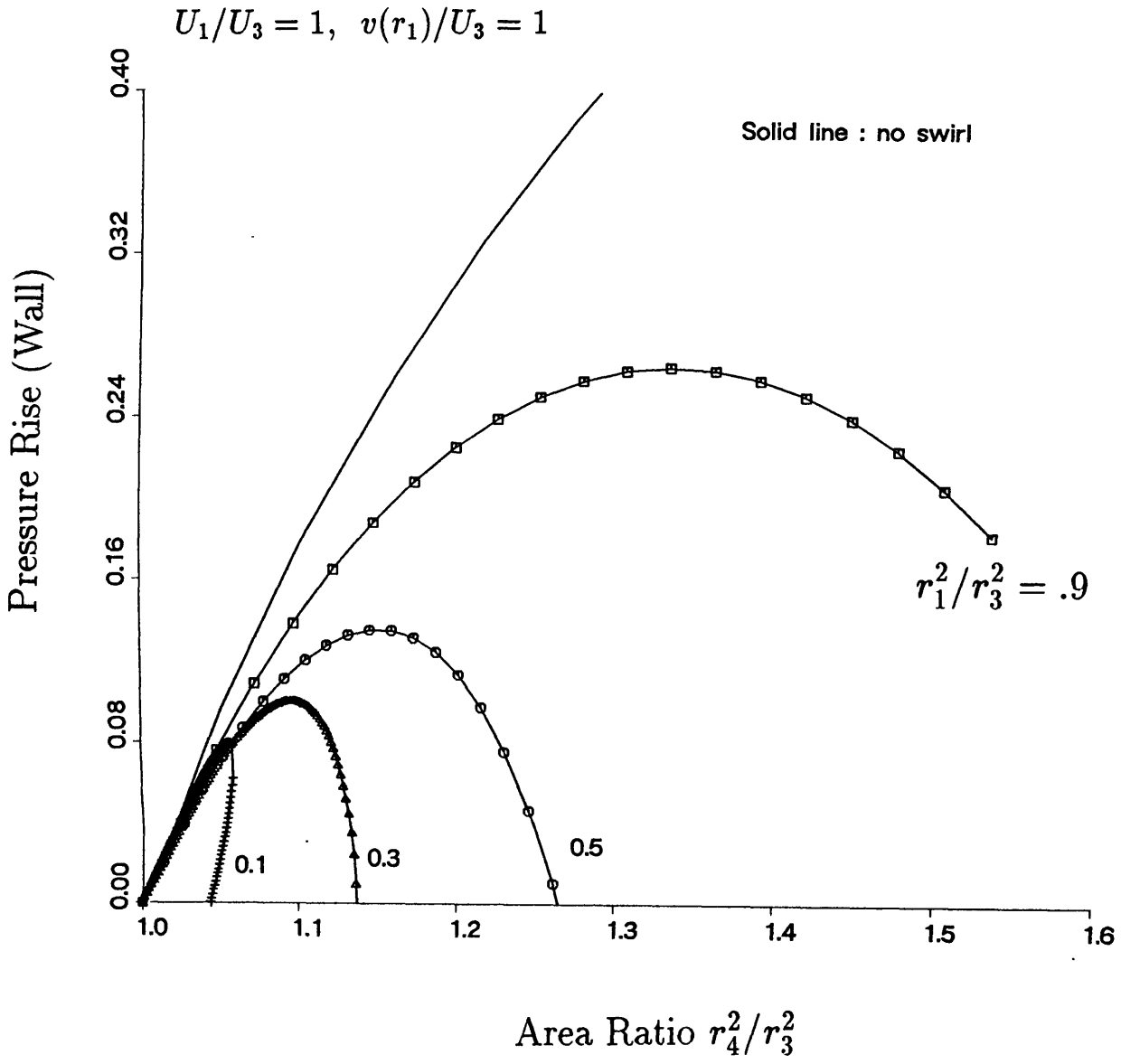

Figure M.6: Wall pressure rise vs. area ratio for different values of vortex size

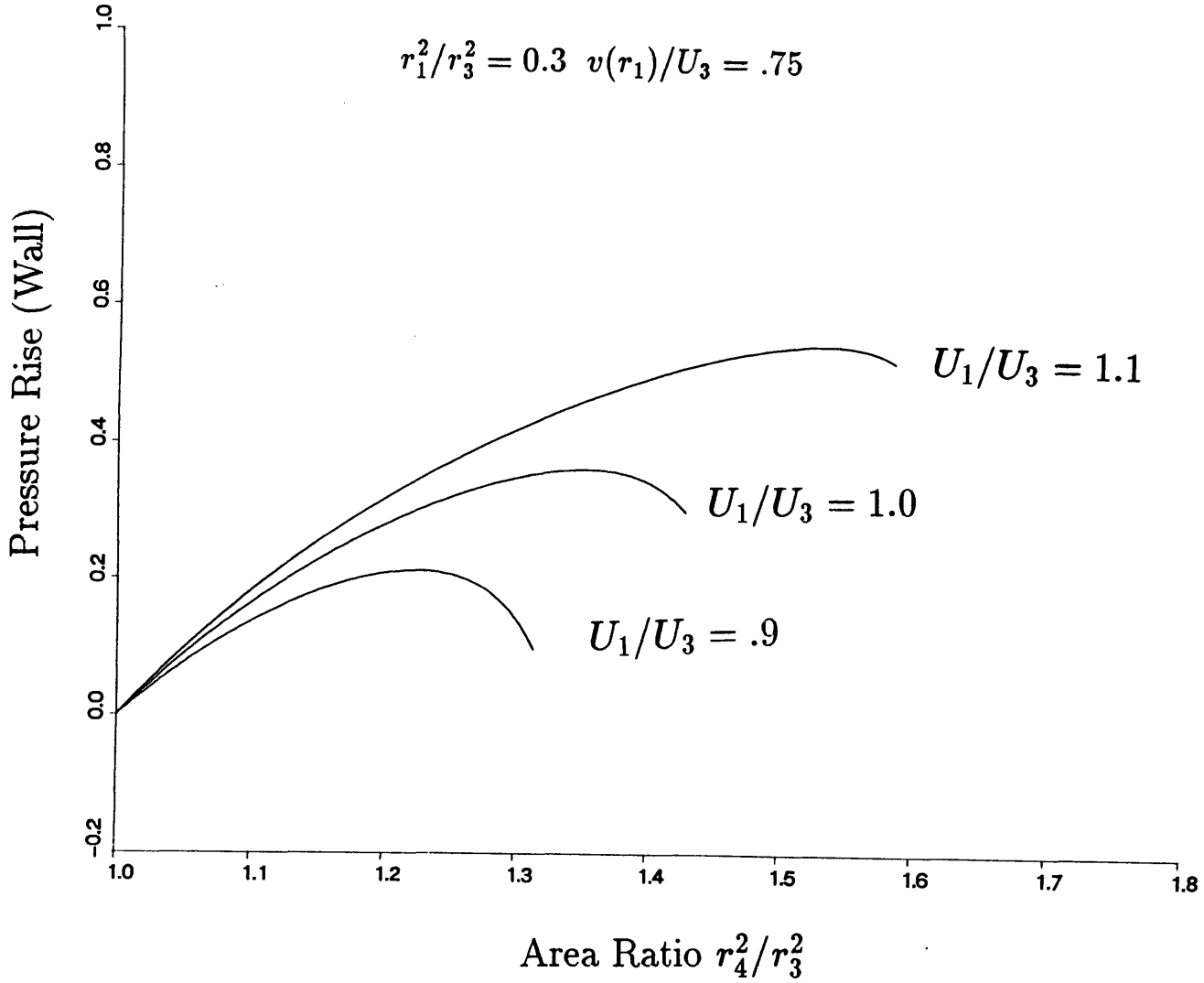

Figure M.7: Effect of axial velocity defect on pressure rise

Bibliography

[1] Adamczyk, J.J., Celestina, M.L., and Greitzer, E.M. . *The Role of Tip Clearance in High-Speed Fan Stall.* to appear, 1990.

[2] Adamczyk, J.J., et al. *Simulation of Three-Dimensional Viscous Flow Within a Multistage Turbine.* ASME Papre No. 89-GT-152, 1989.

[3] Balsa, T.F., and Mellor, G.L. *The Simulation of Axial Compressor Performance Using an Annulus Wall Boundary Layer Theory.* J. of Engineering for Power, Vol. 97, pp.305-318, 1975.

[4] Batchelor, G.K. *An Introduction to Fluid Mechanics.* Cambridge University Press, 1967.

[5] Belik, L. *Three Dimensional and Relaminarization Effects in Turbine Blade Cascade - An Experimental Study.* Proceedings of 1977 Joint JSME/ASME Gas Turbine Congress, pp. 310-310, 1977.

[6] Booth, T.C. *Importance of Tip Clearance Flows in Turbine Design.* Von Karman Institute Lecture Series 1985-05 on *Tip Clearance Effects in Axial Turbomachinery,* 1985.

[7] Booth, T.C., Dodge, P.R., and Hepworth H.K. *Rotor-Tip Leakage : Part 1-Basic Methodology.* ASME Transactions, J. of Engineering for Power, V104, 1982.

[8] Chen, G.T., Greitzer, E.M., Tan, C.S., and Marble, F.E. . *Similarity Analysis of Compressor Tip Clearance Flow Structure.* ASME Paper 90-GT-153, 1990.

[9] Crook, A.J. *Numerical Investigation of Endwall/Casing Treatment Flow Phenomena.* M.S. Thesis, Department of Aeronautics and Astronautics, MIT, 1989.

[10] Cumpsty, N.A. *Compressor Aerodynamics.* Longman Scientific and Technical Publications, 1989.

[11] Dawes, W.N. *A Numerical Analysis of the Three-Dimensional Viscous Flow in a Transonic Compressor Rotor and Comparison With Experiment.* ASME J. of Turbomachinery, Vol. 109, pp. 83-90, 1987.

[12] De Ruyck, J., and Hirch, C. *Investigation of an Axial Compressor End-Wall Boundary Layer Prediction Method.* ASME Paper No. 80-GT-53, 1980.

[13] Dean, R.C. Jr. *The Influence of Tip Clearance on Boundary-Layer Flow in a Rectilinear Cascade.* MIT, Gas Turbine Lab., Report No. 27-3, 1954.

[14] Dishart, P.T., and Moore, J. . *Tip Leakage Losses in a linear Turbine Cascade.* ASME No. 89-GT-56, 1985.

[15] Evans, R.A., and Bloor, M.I.G. *The Starting Mechanism of Wave-Induced Flow Through a Sharp-Edged Orifice.* J. Fluid Mechanics, Vol. 82, 1977.

[16] Farokhi, S. *Analysis of Rotor Tip Clearance Loss in Axial-Flow Turbines.* J. Propulsion Vol. 4, No. 5, 1987.

[17] Graham, J.A.H. *Investigation of a Tip Clearance Cascade in a Water Analogy Rig.* ASME Paper No 85-IGT-65, 1985.

[18] Haas, J.E., and Kofskey, M.G. *Effect of Rotor Tip Clearance and Configuration on Overall Performance of A 12.77-Centimeter Tip Diameter Axial-Flow Turbine.* ASME Paper No. 79-GT-42, 1979.

[19] Hah, C. *A Numerical Modelling of Endwall and Tip Clearance Flow of an Isolated Compressor Rotor.* ASME J. Eng. for Power, Vol. 108, pp. 15-21, 1986.

[20] Herzig, H.Z., Hansen, A.G., and Costello, G.R. *A Visualization Study Secondary Flow in Cascade.* NACA Report 1163, 1953.

[21] Holeski, D.E., and Futral, S.M. *Effect of Rotor Tip Clearance on The Performance of a 5-inch Single-Stage Axial-Flow Turbine.* NASA TM X-1757, 1969.

[22] Horlock, J.H. *Axial Flow Compressors.* Robert E. Krieger Publishing Company, Huntington, New York, 1973.

[23] Inoue, M., and Kuroumaru, M. *Structure of Tip Clearance Flow in an Isolated Axial Compressor Rotor.* ASME Paper No 88-GT-251, 1988.

[24] Inoue, M., Kuroumaru, M., and Fukuhara, M. *Behavior of Tip Leakage Flow Behind an Axial Compressor Rotor.* ASME Journal of Engineering for Gas Turbines and Power, Vol. 108, pp. 7-13, 1986.

[25] Jefferson, J.L., and Turner, R.C. *Some Shrounding and Tip Clearance Effects in Axial Flow Compressors.* International Ship Building Research Progress, Vol 5, No 42, 1958.

[26] Johnson, M.C. *The Effects of Hub Treatment on Compressor Endwall Flowfields.* M.S. Thesis, Department of Aeronautics and Astronautics, MIT, 1985.

[27] Kock, C.C., and Smith, L.H. Jr. *Loss Sources and Magnitude in Axial-Flow Compressors.* ASME J. of Eng. for Power, Vol. 98, pp. 411- 424, 1976.

[28] Kofskey, M.G., and Nusbaum, W.J. *Performance Evaluation of A Two-Stage Axial-Flow Turbine for Two Values of Tip Clearance.* NASA TN D-4388, 1968.

[29] Lakshminarayana, B. *Method for Predicting the Tip Clearance Effects in Axial Flow Turbomachinery,.* ASME Journal of Basic Engineering, Vol. D92, pp. 467-482, 1970.

[30] Lakshminarayana, B., and Horlock, J.H. *Leakage and Secondary Flows in Compressor Cascades.* ARC R & M No. 3483, 1965.

[31] Lakshminarayana, B., and Murthy, K.N.S. *Laser-Doppler Velocimeter Measurement of Annulus Wall Boundary Development in a Compressor Rotor.* Journal of Turbomachinery, Vol. 110, pp.377-385, 1988.

[32] Lakshminarayana, B., Sitaram, N., and Zhang, J. *End-Wall and Profile Losses in a Low-Speed Axial Flow Compressor Rotor.* ASME Paper No. 85-GT-174, 1985.

[33] Lamb, H. *Hydrodynamics.* 6th Edition, Dover Publications, New York, 1932.

[34] Lee, N.K.W. Private Communication, 1989.

[35] Leonard, A. *Vortex Methods for Flow Simulation.* J. Computational Physics, Vol. 37, pp. 289-335, 1980.

[36] Ludwing, L.P. *Gas Path Sealing in Turbine Engines.* AGARD Conference Proceedings No. 237 on *Seal Technology in Gas Turbines Engines*, 1978.

[37] Martinez-Sanchez, M., and Gauthier, R.P. *Blade Scale Effects of Tip Leakage.* Gas Turbine Lab. Report No. 202, MIT, 1990.

[38] Mayle, R.E., and Metzger, D.E. *Heat Transfer at The Tip of An Unshrouded Turbine Blade.* Heat Transfer, Munich, Vol. 3, 1982.

[39] Moore, J., and Tilton, J.S. *Tip Leakage Flow in a Linear Turbine Cascade,.* ASME J. Turbomachinery, Vol.110, pp. 301-309, 1988.

[40] Morphis, G., and Bindon, J.P. *The Effects of Relative Motion, Blade Edge Radius and Gap Size on the Blade Tip Pressure Distribution in an Annular Turbine Cascade With Clearance.* ASME Paper No 88-GT-256, 1988.

[41] Perry, A.E., and Tan, D.K.M. *Simple Three-Dimensional Vortex Motions in Co-Flowing Jets.* J. of Fluid Mechanics, Vol. 141, pp.197-231, 1980.

[42] Pouagare, M., and Delaney, R.A. *Study of 3-D Viscous Flows in Axial Compressor Cascade Including Tip Leakage Effects Using a Simple Based Algorithm.* ASME J. of Turbomachinery, Vol. 108, pp. 51-58, 1986.

[43] Rains D.A. *Tip Clearance Flow in Axial Flow Compressors and Pumps.* California Institute of Technology, Hydrodynamics and Mechanical Engineering Laboratories Report, No.5, 1954.

[44] Sarpkaya, T. *Computational Methods With Vortices - The 1988 Freeman Scholar Lecture.* J. of Fluids Engineering, Vol. 111, pp. 5-52, 1989.

[45] Schmidt, M.J.P., Agnew, B., and Elder, R.L. *Tip Clearance Flows - Part Two, Study of Various Models and Comparison with Test Results.* AIAA, ISABE 87-7035, 1987.

[46] Senoo, Y. *The Boundary Layer on the Endwall of a Turbine Nozzle Cascade.* ASME Journal of Engineering for Power, Vol. 80., 1958.

[47] Senoo, Y. *Mechanics on the Tip Clearance Loss of Impeller Blades.* ASME Paper No. 90-GT-37, 1990.

[48] Senoo, Y., and Ishida, M. *Pressure Loss Due to the Tip Clearance of Impeller Blades in Centrifugal and Axial Blowers.* ASME Journal of Engineering for Gas Turbine and Power, Vol. 108, pp.32-37, 1986.

[49] Sjolander, S.A., and Amrud, K.K. *Effects of Tip Clearance on Blade Loading in a Planer Cascade of Turbine Blades.* ASME Paper 86-GT-245, 1986.

[50] Smith, G.D.J. *Casing Treatment in Axial Compressors.* Ph.D. Thesis, Engineering Department, University of Cambridge, 1980.

[51] Spencer, E.A. *The Performance of an Axial Flow Pump.* Proceedings of the Institute of Mechanical Engineers, Vol. 170, No. 25, 1956.

[52] Storer, J.A. personal communication, 1990.

[53] Storer, J.A., and Cumpsty, N.A. *Tip Leakage FLow in Axial Compressors.* presented at 1990 ASME Gas Turbine Conference, 1990.

[54] Sulam, D.H., Keenan, M.J., and Flynn, J.T. *Single-Stage Evaluation of Highly-Loaded High-Mach Number Compressor Stages, Part two: Data and Performance Multiple-Circular-Arc Rotor.* NASA CR-72694 (or PWA-3772).

[55] Szanca, E.M., Bebning, F.P., and Scbum, H.J. *Research Turbine for High-Temperature Core Engine Application, Part Two - Effect of Rotor Tip Clearance on Overall Performance.* NASA TN D-7639, 1974.

[56] Takata, H. Personal Communication, 1988.

[57] Vavra, M.H. *Aerothermodynamics and Flow in Turbomachines.* John Wiley, Inc., 1960.

[58] Ware, T.C., Kobayashi, R.J., and Jackson, R.J. *High-Tip Speed, Low Loading Transonic Fan Stage, Part Two: Final Report.* NASA CR-121263, 1973.

[59] Wisler, D.C. *Loss Reduction in Axial-Flow Compressors Through Low-Speed Model Testing.* ASME Paper 84-GT-184, 1984.

[60] Wisler, D.C. *Aerodynamic Effects of Tip Clearance, Shrouds, Leakage Flow, Casing Treatment and Trenching in Compressor Design.* Von Karman Institute Lecture Series 1985-05 on *Tip Clearance Effects in Axial Turbomachinery*, 1985.

[61] Yokoyama, E. *Comparative Study of Tip Clearance Effects in Compressor and Turbines.* Gas Turbine Lab. Report No. 63, MIT, 1961.

[62] Zhang, J. *An Experimental, Analytical, and Computational Investigation of Turbomachinery Rotor Flow Fields.* Ph.D. Thesis, Department of Aeronautical Engineering, Pennsylvania State University, 1988.